Magnetic Resonance Imaging and Electron Beam Computed Tomography of the Coronary Arteries

Magnetische Resonantie Beeldvorming en Electronen Bundel Computer Tomografie van de Coronaire Arteriën

ISBN 90-73235-80-4

Optima Grafische Communicatie
P.O. Box 84118
3009 CC Rotterdam
The Netherlands

Magnetic Resonance Imaging and Electron Beam Computed Tomography of the Coronary Arteries

Magnetische Resonantie Beeldvorming en Electronen Bundel Computer Tomografie van de Coronaire Arteriën

Proefschrift

ter verkrijging van de graad van doctor aan de
Erasmus Universiteit Rotterdam op gezag van de
Rector Magnificus Prof.dr.ir. J.H. van Bemmel
en volgens besluit van het College voor Promoties

De openbare verdediging zal plaatsvinden op
woensdag 6 december 2000 om 13.45 uur

door

Robert-Jan Matthijs van Geuns

geboren te Son en Breugel

Promotiecommissie

Promotor:	Prof.dr. P.W. Serruys
Overige leden :	Prof.dr. L. Jordaens
	Prof.dr. E.E. van der Wall
	Prof.dr. A.C. van Rossum
Copromotoren :	Dr. P.J. de Feyter
	Dr. M. Oudkerk

Financial support by the Netherlands Heart Foundation for the publication of this thesis is gratefully acknowledged.

aan Madeleine en onze kinderen

Contents

Foreword 11

Part 1 Magnetic Resonance Imaging

Chapter 1 Basic principles of magnetic resonance imaging. 17
Progress in Cardiovascular Disease 1999;42(2):149-156

Chapter 2 Magnetic resonance imaging of the coronary arteries: 27
Techniques and results.
Progress in Cardiovascular Disease 1999;42(2):156-166

Chapter 3 Magnetic resonance imaging of the coronary arteries: 41
Advanced imaging concepts.
Eur Radiology 2000;10:12-35

Chapter 4 Magnetic resonance imaging of the coronary arteries: 77
Imaging planes and resulting images in two-dimensional imaging.
Coronary Artery Disease 1999;10(7):525-531

Chapter 5 Magnetic resonance imaging of the coronary arteries: 85
Anatomy of coronary arteries and veins in three-dimensional imaging.
Coronary Artery Disease 1999;10:261-267

Chapter 6 Magnetic resonance imaging of the coronary arteries: clinical results 95
from three-dimensional evaluation of a respiratory gated technique.
Heart 1999;82:515-519

Chapter 7 Breath-hold coronary MR angiography with volume targeted imaging. 105
Radiology 1998;209:209-219

Chapter 8 VCATS: Volume coronary angiography using targeted scans. 125
A new strategy in MR coronary angiography.
Int J of Cardiac Imaging, accepted

Chapter 9 Quantitative analysis of coronary artery lumen definition for 133
breath-hold and free-breathing retrospective respiratory gated
magnetic resonance coronary angiography.
Submitted

Chapter 10 MR coronary angiography with breath-hold targeted volumes: 145
Preliminary clinical results.
Radiology 2000;217:270-277

Chapter 11 Magnetic resonance angiography of single and sequential venous 159
bypass grafts: Assessment of patency over the entire length of the graft.
Submitted

Chapter 12 Improvements in magnetic resonance imaging of the coronary 169
arteries with a clinical available intravascular contrast agent.
Submitted

Part 2 Electron Beam Computed Tomography

Chapter 13 Intravenous coronary angiography using electron beam computed tomography. 181
Progress in Cardiovascular Disease 1999;42:139-148

Chapter 14 In vivo assessment of three-dimensional coronary anatomy using electron beam computed tomography after intravenous contrast administration. 195
Heart 1999;82:523-525

Chapter 15 Intravenous coronary angiography by electron beam computed tomography: A clinical evaluation. 201
Circulation 1998;98:2509-12

Chapter 16 Coronary artery fly-through using electron beam computed tomography. 209
Circulation 2000;102:e6-e10

Part 3 MRI versus EBT for non-invasive coronary angiography

Chapter 17 Non-invasive coronary imaging: A comparison between MRI and EBT. 219
Submitted

Part 4 Supplement on MRI of the Thoracic Arteries

Chapter 18 Technical aspects of magnetic resonance imaging for thoracic aorta disease. 231
Submitted

Chapter 19 Contrast enhanced three-dimensional magnetic resonance angiography in congenital and acquired disease of the great thoracic vessels. 243
Submitted

Part 5 Discussion, Conclusions and Summary

Chapter 20 General discussion and conclusions. 257

Chapter 21 Summary. 267

Samenvatting 271

Dankwoord 275

Publications 279

Curriculum vitae 283

Stellingen 285

Foreword

FOREWORD

Since it's introduction selective coronary angiography has become the most essential diagnostic tool in the management of patients with coronary artery disease. Conventional selective coronary angiography is available worldwide and provides a rapid and accurate delineation of the coronary anatomy of the entire coronary artery tree.[1,2] Presently selective coronary angiography is a prelude to revascularization procedures as coronary artery bypass graft surgery (CABG) or percutanous transcatheter coronary angioplasty (PTCA) and seems irreplaceable.[3]

However, conventional selective coronary angiography is not ideal because of the arterial puncture, the use of X-rays, the high costs and a small risk of serious complications. This has inspired the development of non-invasive imaging modalities to visualize the coronary arteries. Conventional selective coronary angiography has been limited mainly to symptomatic patients. Successful development of non-invasive coronary imaging techniques will allow early preclinical assessment, repeated asssesments in symptomatic patients and the applicitation as a research tool to follow early and late coronary artery disease processes. The major challenges for non-invasive imaging modalities are: the relative small vessel size, the complex three-dimensional trajectory, cardiac and respiratory motion. Magnetic resonance imaging (MRI) and Electron beam computed tomography (EBT) are presently the two major alternatives to selective coronary angiography.[4,5] The goal of this thesis is to study the possibilities and limitations of both techniques and compare the clinical results for the detection of coronary artery disease.

The first part of this thesis deals with ECG-triggered MRI of the coronary arteries. In this part present MRI techniques are described and new protocols are introduced. The value of these protocols was studied in patients with coronary artery stenosis and coronary artery bypass grafts. The last chapter in this part studies the effect of a clinical available partially intravascular MR contrast agent on magnetic resonance coronary angiography. Part two focuses on the development of EBT for coronary angiography. The first chapter in this part describes the technique of non-invasive coronary angiography with electron beam computed tomography using intravenous contrast agent administration. This chapter is followed by two clinical studies with EBT. The last chapter in this part introduces virtual angioscopy as the future in post-processing of three-dimensional datasets obtained with EBT. In the third part of this thesis the capability of both techniques to visualize the coronary arteries non-invasively and the diagnostic value to detect coronary artery stenoses are compared. Part 4 is a supplement on non-ECG-triggered magnetic resonance angiography of the thoracic arteries, which demonstrates the advantages of contrast agents for these sequences. While in ECG-triggered magnetic resonance *coronary* angiography contrast agent has been less effective. Chapter 20 summarizes this thesis in relation to the evaluation of patients with atherosclerotic disease and provides a view on the future of cardiovascular imaging.

REFERENCES

1. Sones FJ, Shirey E. Cine coronary angiography. Mod Concepts Cardiovasc Dis. 1962;31:735-738.
2. Judkins MP. Selective coronary arteriography. I. A percutaneous transfemoral technic. Radiology. 1967;89:815-24.
3. Ross JR, Brandenburg RO, Dinsmore RE. Guidelines for coronary angiography. A report of the American College of Cardiology/American Heart Association Task Force on Assessment of

Diagnostic and Therapeutic Cardiovascular Procedures (Subcommittee on Coronary Angiography). Circulation. 1987;76:963A-977A.

4. Manning WJ, Li W, Edelman RR. A preliminary report comparing magnetic resonance coronary angiography with conventional angiography. N Engl J Med. 1993;328:828-32.
5. Moshage WE, Achenbach S, Seese B, et al. Coronary artery stenoses: three-dimensional imaging with electrocardiographically triggered, contrast agent-enhanced, electron-beam CT. Radiology. 1995;196:707-14.

Part 1

Magnetic Resonance Imaging

Chapter 1

Basic Principles of Magnetic Resonance Imaging

R.J.M. van Geuns, P.A. Wielopolski, H.G. de Bruin, B.J.W.M. Rensing,

P.M.A. van Ooijen, M. Hulshoff, M. Oudkerk, P.J. de Feyter.

Published in Progress in Cardiovascular Disease 1999;42(2):149-156

ABSTRACT

Magnetic Resonance Imaging (MRI) is a noninvasive imaging technique that is becoming more and more important in clinical cardiology. Physicians should understand the basic principles of MRI before reliable use in practice is possible. Therefore, we will give an introduction to basic MRI principles necessary to understand the difficulties of cardiac MRI. First the generation of a signal by the combination of a strong magnetic field, radiofrequency pulses, and temporary changes in the magnetic field is explained. Then, the processes of localization of different points in an image, resolution and signal-to-noise ratio are highlighted. Finally, the influence of tissue characteristics such as T_1 and T_2, on the contrast of an image are discussed.

INTRODUCTION

Magnetic Resonance (MR) imaging is an exciting diagnostic imaging tool that uses strong magnets and low-energy radiofrequency signals (such as those found in radios and televisions) to gather information from certain atomic nuclei within the body. Therefore, MR does not require ionizing radiation to obtain images. Several textbooks on magnetic resonance imaging (MRI) give excellent overviews of the basic concepts of MR physics.[1-4] Therefore, in this paper we restrict ourselves to summarizing these basic physics concepts and refer the reader to the textbooks for a more detailed description.

THE SOURCE OF THE MR SIGNAL

A correct description of what happens when tissue is subjected to a magnetic field relies on quantum mechanics. Fortunately, all the theory necessary for MRI can be based on a simple classical model in which certain nuclei that spin around their own axis behave like small magnets. For clinical imaging, hydrogen is the most frequently used nucleus, but other possible nuclei are carbon-13, sodium and phosphorus. Under normal circumstances these tiny magnets are randomly distributed in space, the magnetic moments cancel each other out, and thus the net magnetic vector is zero (Figure 1A). However, when the patient is submitted to a strong external magnetic field (B_0) the nuclei adopt one of two possible orientations: parallel or antiparallel to the external field (Figure 1B). Parallel alignment is the lower energy state and is thus the preferred alignment, whereas antiparallel alignment is the higher energy state. The energy difference between the two states is very small: the population ratio is approximately 100,000 to 100,006. A net magnetization vector (Mz) aligned to the external magnet results from the difference between the two populations. Individual nuclei do not actually line up with the magnetic field but wobble or precess around the direction of the external field (Figure 2A). The frequency of this precession is given by the Larmor equation:

$$F = \gamma B_0/2\pi$$

Where F is the precessional frequency, B_0 is the strength of magnetic field and γ is the gyromagnetic ratio of the nucleus.
This frequency is also called the Larmor frequency. In the frequently used commercial systems of 1.5 Tesla (T), the Larmor frequency will be 63.75 MHz for hydrogen. It is of note that the phase of precession around the axis of the magnetic field is different for each individual nucleus (Figure 2B).

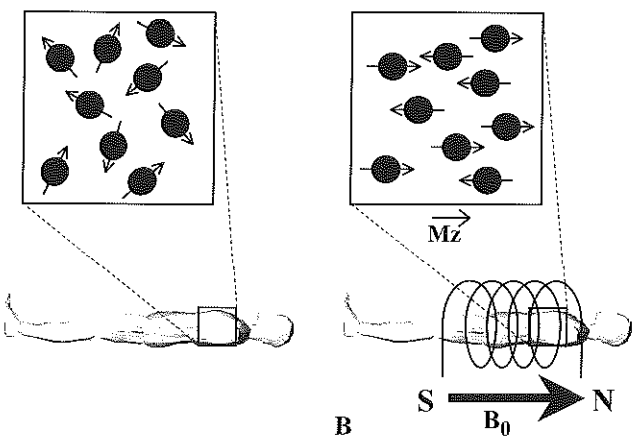

Figure 1. A. *Without a magnetic field the magnetic moments of the nuclei are distributed at random and thus the net magnetization factor is zero.* ***B.*** *When there is a strong external magnetic field the spinning nuclei align parallel or antiparallel to the external field (B_0) with a few more parallel than antiparallel. This results in a net magnetization vector (Mz) parallel to the external magnetic field.*

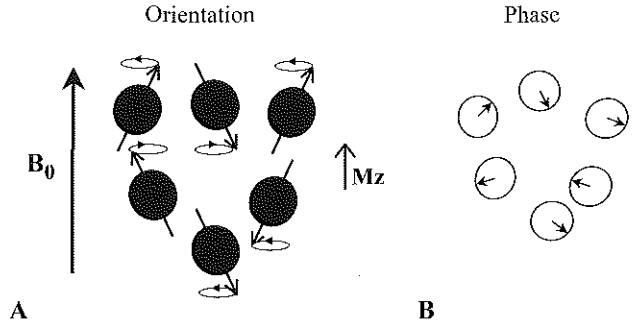

Figure 2. A. *In more detail the individual nuclei spin around their own axis and wobble or precess around the direction of the external field (Bo).* ***B.*** *The phase of the precession around the axis of the external magnetic field is different for each individual nucleus.*

EXCITATION

The net magnetization vector from the nuclei inside the magnet in its equilibrium state is static and does not produce a measurable signal. To obtain information from the spins, the direction of the net magnetization vector has to be altered. For this the precessing spins are excited by applying energy, in the form of radiofrequency (RF) energy pulses of exactly the Larmor frequency (resonance frequency). When an RF signal is given at the resonance frequency into the patient, two phenomena occur: first, enough protons absorb energy to jump from the parallel state to the higher level of the antiparallel state, and second, the spins are "whipped" to precess in phase. The effect of all this is that the net magnetization (Mz) flips 90° from the positive z-axis to transverse plane (Figure 3). The net magnetization in the transverse plane rotates around B_0 at the Larmor frequency. This rotating transverse magnetization can be measured, because it will induce an alternating current (AC) in the receiver coil placed around the patient.

RETURN TO EQUILIBRIUM

After the RF frequency transmitter is switched off, the equilibrium state will be sought (high energy back to low energy). This means that the magnetization decays over time, which is represented by a decreasing magnitude of Mz in the transverse plane. Consequently, the induced signal in the receiver coil will decrease in time. This decreasing signal is called the free induction decay (FID)(Figure 4). The time required for the signal to return to equilibrium is the relaxation time.

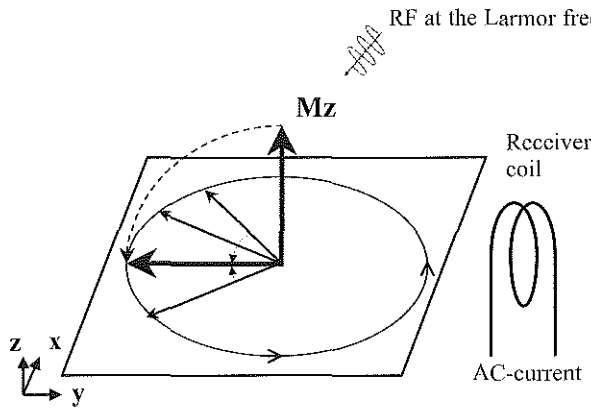

Figure 3. *When the spins are exited with a RF pulse of exactly the Larmor frequency, the net magnetization flips 90° and the spins are "whipped" to precess in phase. The rotating net magnetization vector induces an AC in a receiver coil.*

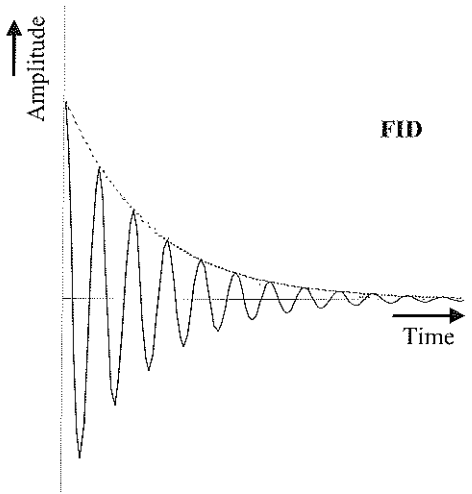

Figure 4. *The received signal detected by the receiver coil, the FID, decreases over time, when the net magnetization vector returns to its original orientation.*

Two relaxation processes exist: transverse relaxation and longitudinal relaxation. Both processes are independent. The process of realignment to the external magnetic field is called the longitudinal relaxation process (Figure 5). It is characterized by the T_1, relaxation time. The T_1 relaxation time is defined as the time required for the system to recover to 63% of its equilibrium value after it has been exposed to a 90° RF pulse (Figure 6). Various human tissues have different T_1 values (Table 1).

The second process of relaxation, the transverse relaxation, depends on the spins precessing around the magnetization vector. Initially, after the excitation by the RF pulse, the spins precess completely in phase. However, as time passes, the observed signal starts to decrease because the spins begin to dephase due to small differences in the Larmor frequency induced by random local magnetic inhomogeneities, due to spin-spin interaction and inhomogeneity of the main static magnetic field B_0. This process is called the transverse relaxation or spin-spin relaxation and is characterized by the T_2 relaxation time (Figure 5). The T_2 relaxation time is the time it takes for dephasing to decay the signal to 37% of its original value (Figure 6). The T_2 time from various tissues is different, but the T_2 time is always shorter than the T_1 time.

SPATIAL ENCODING

To create an image, the MR signal from the H-protons has to contain information about where these H-protons are positioned in the patient. This is done in three steps: slice selection, frequency encoding, and phase encoding.

To select an imaging slice through the body, a magnetic gradient (for example 25 milliT/m) is added along the main magnetic field in the caudal to cranial direction. Because the frequency of precession, and

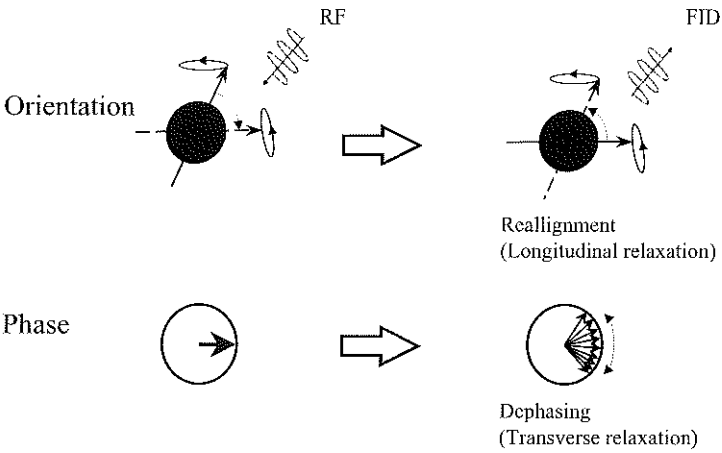

Figure 5. *During relaxation, two processes exist: longitudinal relaxation and transverse relaxation. Longitudinal relaxation (upper row) is the realignment of the net magnetization to the external magnetic field. Transverse relaxation is the dephasing of the precessing spins (lower row).*

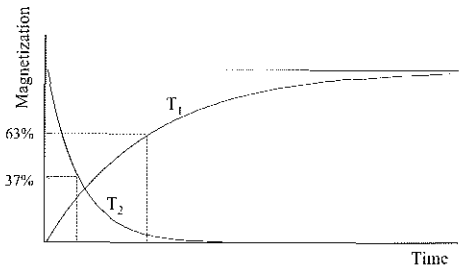

Figure 6. *Longitudinal relaxation is characterized by the T_1 relaxation time, which is the time to recover 63% of the original net magnetization vector. Transverse relaxation is characterized by the T_2 time, which is the time it takes to decay the signal to 37% of the original signal.*

Table 1. T_1 and T_2 value of different tissues at 1.5T

Tissue	T_1 (msec)	T_2 (msec)
Skeletal muscle	870	47
Myocardium	600	40
Liver	490	43
Fat	260	84
Arterial blood	1,210	35
Venous blood	1,210	250

thus the frequency at which the spins can be excited, is dependent on the local strength of the magnetic field, a narrow band of frequencies will only excite a thin slice (3 to 8 mm) of spins through the body (Figure 7). With a change in the excitation frequency another parallel slice can be acquired later. To obtain slices in other directions, for example vertical slices, the direction of gradients for the slice encoding are altered to an anterior-posterior gradient. By using combinations of gradients in all three directions, it is possible to acquire a slice in any arbitrary direction through the body.

The frequency and phase encoding are used to obtain information for the individual points within a slice, the picture elements or pixels. For the phase encoding, a short temporary change in the magnetic field is applied between the RF excitation pulse and the readout of the signal. This change in the magnetic field will influence the frequency of precessing, resulting in a shift in the phase of precessing of the spins dependent on the duration of this gradient switch. By repeating this process with different duration of the temporary gradients, signals with a different phase encoding are acquired (Figure 8).

The frequency encoding is used to differentiate pixels with the same phase encoding. A magnetic gradient during readout of the signal results in a specific shift of the resonance frequency, likewise the effect of the

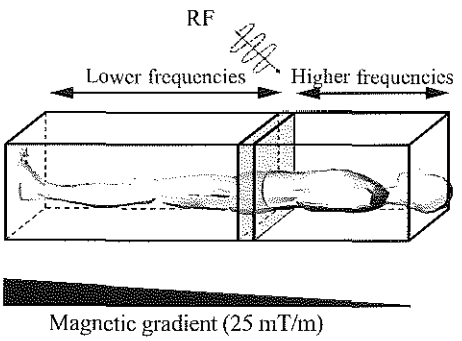

Figure 7. *A single slice through the body is selected in MRI by superimposing a small magnetic gradient on the main magnetic field in cranial-caudal direction. A RF pulse will only exited the spins, where the RF pulse matches the local precessing frequency determined by the Larmor equation.*

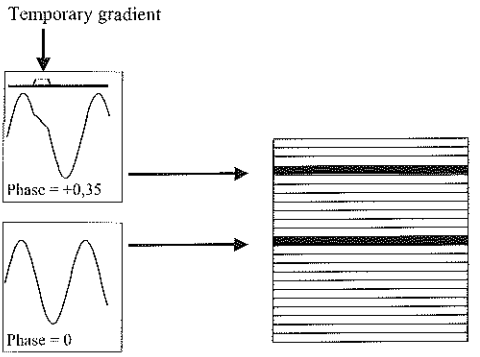

Figure 8. *During phase encoding a temporary gradient is applied. The change in the magnetic field will influence the precessing frequency, after the gradient is switched off, the spins will precess with the original frequency, but a small change in the phase of precessing will remain. The process has to be repeated to acquired multiple AC signals with different phase encodings.*

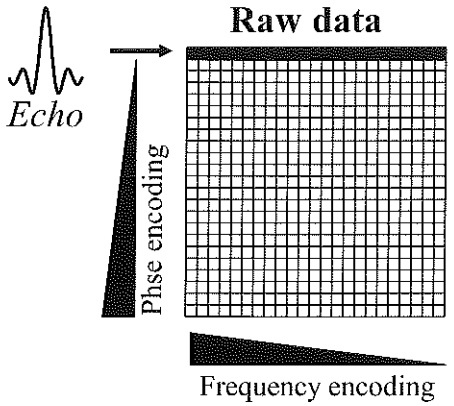

Figure 9. Frequency encoding, with a gradient during readout of the AC signal, is used to differentiate pixels with the same phase encoding.

slice-encoding gradient, for pixels with the same phase shift (Figure 9).

Combining phase and frequency information allows the creation of a grid in which each pixel has a defined combination of phase and frequency codes (Figure 9). This grid of raw data is called the K-space. With a Fast Fourier Transform, the raw data, that represents an amplitude as a function of time, are transformed into a curve that represents an amplitude as function of the frequency (Figure 10). The amplitude of each frequency represent the intensity of each pixel. The Fourier transform is performed in both the frequency and phase encoding direction.

Important to realize is that the imaging time for a single image depends on the number of image lines desired, which is directly related to the number of signals with different phase shift that have to be acquired. For example, for an image of 256 × 256 pixels, or 256 image lines, 256 signals have to be acquired.

THE ECHO SIGNAL, SPIN-ECHO IMAGING

There are several reasons why the FID signal is not used for clinical imaging. First there is a certain time necessary to perform the spatial encoding, even with present ultrafast MR scanners this can not be performed before the FID declines. Second, the creation of a second AC signal gives opportunities to modify the contrast in the images depending on the T_1 and T_2 values of the tissues.

To evoke a second AC signal, a second RF pulse is applied which flips the spin by 180°, and also reverses the dephasing process (Figure 11). As the spins rephase, the amplitude of the AC signal increases and this signal, called the echo signal, is measured at its maximum (time of echo = TE).

MR techniques using the combination of a 90° and a 180° RF pulse to generate an echo signal are called spin-echo sequences.

CONTRAST

MRI has the potential to visualize the dif-

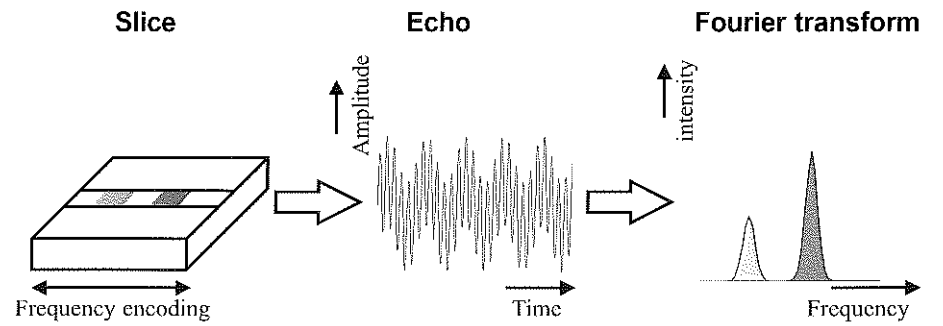

Figure 10. A hypothetical AC signal of a single image with two pixels with a different proton density will result in a AC signal, with interference pattern of 2 sinusoidal AC currents. A Fast Fourier Transform extracts the different frequencies and their amplitude from the echo signal. The amplitude of each frequency represents the proton density in each pixel.

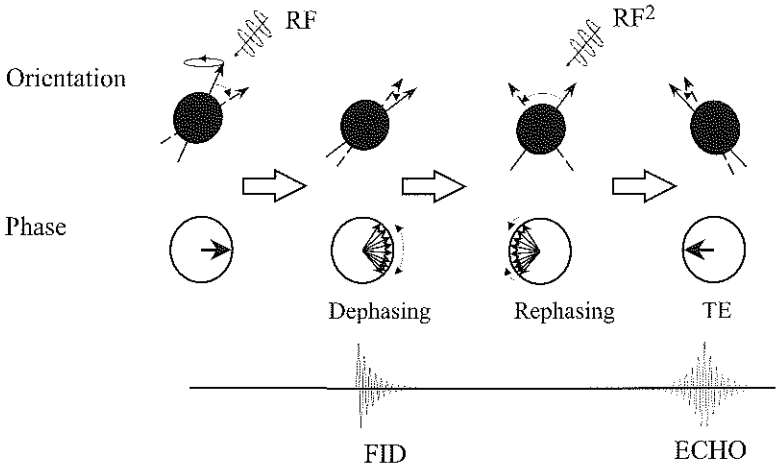

Figure 11. *Due to dephasing, the FID signal rapidly decreases before the longitudinal magnetization returns to zero. A second RF pulses (RF2), which flips the spins by 180°, also reverses the dephasing process. When the spins are in phase again, a second AC signal, the echo signal, arises. The interval between the first RF pulse and the echo signal is called the time of echo (TE).*

ference in T_1 and T_2 of different tissues. Using these differences, contrast between different soft tissues in MRI is superb compared with x-ray computer tomography. If the time for the next repetition of RF pulses (time of repetition = TR) is shorter than the time necessary for total longitudinal relaxation, the contrast in the image will be mainly influenced by the difference in T1 value of the tissues (Figure 12). Using a long TR and a long TE, the contrast will be dependent on T_2 differences. A combination

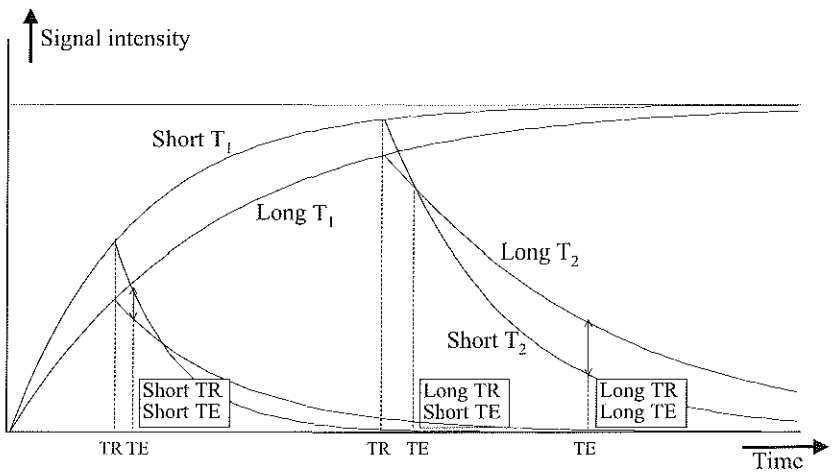

Figure 12. *Contrast between different tissues. Two tissues each with a different T_1 and T_2 value have different signal intensity dependent on the time. The contribution of T_1 to the signal intensity of a pixel is dependent on the TR used, indicated in the figure for a short and a long TR. From these points, the signal intensity decays along the T_2 curve. Using a short TR and TE, the signal intensity and contrast will be mainly be influenced by the differences in T_1 value of the tissues (T_1 weighted imaging). A combination of a long TR and a short TE will result in contrast dependent on the proton density, whereas a long TR and a long TE will pronounce difference in T_2 value (T_2 weighted imaging).*

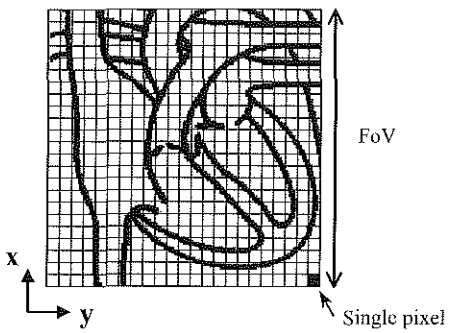

Figure 13. In MR imaging, resolution is determined by the pixel size, which is dependent on the number of lines in the x and y direction used in the matrix and the FoV covered with this matrix. Pixel size = FoV (x)/ N0. lines (x) × FoV (y)/ N0. lines (y)

of a long TR with a short TE will not be dependent on T_1 or T_2, but only on the proton density of the tissue.

RESOLUTION

In digitized imaging, such as MRI, pictures are composed of a matrix of elements, called picture elements or pixels. The image represents the field of view (FoV). The image matrix defines the number of pixels used to construct an image that is determined by the number of frequency encodings (128 or 256 on the x-axis) and the number of phase-encoding steps used (128 or 256 on the y-axis) for a certain FoV (Figure 13). Therefore, the FoV, the matrix size used, and the slice thickness determine the volume of each pixel.

In practice the resolution is not determined by the pixel size (the smaller, the higher the resolution), but the signal-to-noise ratio is the limiting factor, if the pixels become to small and do not contain enough spinning protons to produce a measurable signal the resolution is in practice impossible.

SUMMARY

To obtain a single MR image, a complex combination of RF pulses and magnetic gradient switches have to be applied. In spin-echo imaging, two RF pulses combined with gradient switches in three directions result in one echo signal with spatial information. For an electrocardiogramtriggered cardiac image, in each heartbeat one combination is completed and thus one echo is acquired (Figure 14). To complete a single image of 256 lines, 256 echos with different phase

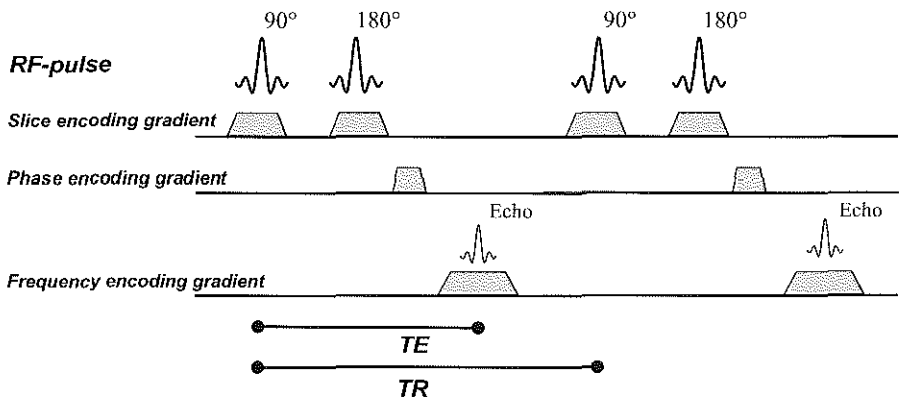

Figure 14. Example of a spin-echo sequence. An echo signal is evoked after a 90° and a 180° RF pulse. Spatial encoding of the echo signal is performed with gradient switches in three directions. The slice selection gradient is present during RF excitation, which will now only excite a thin slice through the body. The phase-encoding gradient is shortly present between the excitation and the sampling of the echo signal. Finally, the frequency-encoding gradient is activated during the echo acquisition. This combination of RF pulses and gradient switches is repeated 128 or 256 heartbeats with different phase-encoding steps. Imaging time will be approximately 3 to 4 minutes for a single cardiac triggered image.

encodings need to be sampled; therefore, imaging time, for a single spin-echo image, will be 256 heartbeats, which takes in most patients between 3 and 4 minutes.

REFERENCES

1. Stark DD, Bradley WG. Magnetic Resonance Imaging. St. Louis: Mosby-Year Book, 1992.
2. Rinck P. Magnetic Resonance in Medicine. Oxford: Blackwell Scientific Publications, 1993.
3. Heiken JP, Brown JJ. Manual of Clinical Magnetic Resonance Imaging. New York: Raven Press, 1991.
4. Rayan SS. MRI: A conceptual overview. Berlin: Springer, 1997.

Chapter 2

Magnetic Resonance Imaging of the Coronary Arteries: Techniques and Results

R.J.M. van Geuns, P.A. Wielopolski, H.G. de Bruin,

B.J.W.M. Rensing, P.M.A. van Ooijen, M. Hulshoff,

M. Oudkerk, P.J. de Feyter.

Published in Progress in Cardiovascular Disease 1999;42(2):156-166

ABSTRACT

Recently a new noninvasive imaging technique, Magnetic Resonance Imaging (MRI) has been developed that has the potential to assess the coronary arteries. MRI of the coronary arteries is a challenging task because of the motion of the vessels during cardiac contraction and the motion of the heart with respiration. Several two-dimensional and three-dimensional acquisition techniques have been developed to overcome these problems. In this article we will describe different conventional MR techniques such as spin-echo and gradient-echo. Also, we will describe new developments in MRI as ultrafast breathhold techniques using echo planar imaging or targeted volume scanning. Other new developments are respiratory gating techniques with or without respiratory motion correction. Finally, we will review the results of these techniques in the detection of coronary artery bypass grafts patency, coronary artery stenosis, and the evaluation of coronary artery anomalies.

INTRODUCTION

Since the introduction in 1959 of contrast-enhanced coronary angiography, the technique has been until now the indisputable standard of reference for the diagnosis of coronary artery disease. Nonetheless, cardiac catheterization is an invasive and expensive procedure with a (small) risk of morbidity and mortality. Recently, a new noninvasive imaging technique, magnetic resonance (MR), has been developed that has the potential to assess the coronary arteries. In this article we will give an introduction to MR coronary imaging techniques and review the first clinical results.

Since the introduction of magnetic resonance imaging (MRI), a truly noninvasive technique not associated with radiation is available for clinical use. MRI of the coronary arteries is a challenging task because of motion of the vessels during cardiac contraction and the motion of the heart with respiration. Also, the complexity of the anatomy in three directions hampers MR imaging. Electrocardiogram (ECG) triggering with data collection during mid to late diastole minimizes blur from coronary artery motion during cardiac contraction. To reduce respiratory motion, imaging can be performed with breath holding or with respiratory gated techniques. The complex coronary anatomy can be studied with two-dimensional (2D) or three-dimensional (3D) acquisition techniques.

In this article, we will describe different conventional MR techniques such as spin-echo (SE) imaging, which was the first used to visualize proximal coronary arteries and coronary artery bypass grafts, and gradient-echo (GE) imaging, introduced later to speed up image acquisition that now is frequently employed for coronary imaging. Also, we will discuss the differences between 2D and 3D techniques and describe new developments in MRI as ultrafast breath-hold techniques and respiratory gated techniques.

CHALLENGES OF MR CORONARY IMAGING

Recently, MRI has been used to visualize the coronary arteries. However, when performing MR coronary imaging many challenges, which specifically pertain to coronary imaging, should be met (Table 1).

First, there is the formidable problem of cardiac motion causing blurring of the images. Cardiac imaging with acquisition of, eg, more than 50 images per second (possible with conventional x-ray coronary angiography techniques) during cardiac diastole would result in a nearly motion-free imaging, but unfortunately such ultrafast MR acquisition techniques are not available. Another approach is therefore necessary that consists of the use of two interrelated components: (1) triggering on the electrocardiogram (ECG) signal so that the acquisition of images can be achieved in a predetermined phase of the heart cycle, and (2) choosing a time window within the cardiac cycle where cardiac motion is minimal or absent. This window is usually in mid to late diastole and lasts for 100 to 150 ms. Therefore, ultrafast acquisition techniques are necessary to acquire motion-free images during this short time window in the cardiac cycle.

Second, respiratory motion causing blurring of the images. Basically, two techniques have been used to overcome respiratory motion: breath holding and respiratory gating techniques. Breath holding is possible during 20 seconds in the majority of the patients. With a heart rhythm of 60 beats per minute, this permits data acquisition during 20 consec-

Table 1. Challenges in MRI of the Coronary Arteries

1.	Cardiac motion
2.	Respiratory motion
3.	Complex anatomy
4.	Epicardial fat

utive heartbeats in a single breath hold. With fast techniques, described later in the article, it is possible to collect one image in one breath hold. Respiratory gating techniques make use of a navigator technique, which monitors the movement of the diaphragm during respiration. Acquisition takes place during a predetermined small window of diaphragm movement, assuring data collection at a nearly identical diaphragm level.

Third, there is the issue of the complex anatomy. MR imaging can be accomplished with 2D imaging (slice acquisition) or with 3D imaging (volume acquisition) techniques. The tortuosity and complex course of the epicardial coronary vessels makes it difficult or often impossible to "catch" the entire coronary tree in one thin (3 to 4 mm) monoplanar slice obtained with 2D techniques. Acquisition of 2 or more contiguous slices should solve this problem. Three-dimensional imaging containing longer segments of the coronary arteries in one acquisition definitely eliminates this problem. If the data are acquired transversally over the whole volume of the heart, imaging can be operator independent, and all required imaging planes can be reconstructed off-line. Another advantage of 3D imaging is the higher signal-to-noise ratio. Disadvantages of 3D imaging are the longer scanning time, the increased likelihood of motion artifacts, and less inflow in the volume of fresh unsaturated blood.

Fourth, fat gives off a bright MR signal in several techniques, which may interfere with the signal of blood within the coronary arteries. To improve contrast between coronary blood and surrounding pericardial fat, the signal from fat must be suppressed. This is achieved by application, before the acquisition pulse, of a strong radiofrequency (RF) pulse that selectively saturates the magnetization of fat-bound hydrogen atoms but does not affect water-bound hydrogen atoms. Fat suppression is an essential component in the technique of MR coronary imaging.

SE IMAGING OR BLACK BLOOD IMAGING

SE imaging was the first clinically used MR technique. After excitation by a RF pulse, a second RF pulse is applied to rephase the spinning atoms which will form the echo signal after a certain time. Because there is a certain time between the two RF pulses, moving blood will be out of the imaging plane when the second RF pulse is applied. Moving blood will thus produce no echo signal and hence be black in the image. Slow-moving blood can be excited by both RF pulses, thus producing an echo-signal, and hence be gray or white in the image. The next signal can only be acquired after the atoms have returned to their original position, depending on tissue characteristics, in cardiac imaging usually on the next heartbeat. For an image with 256 lines, 256 heartbeats, approximately 3 minutes are necessary. With this technique it has been possible to visualize the proximal coronary arteries[1,2]

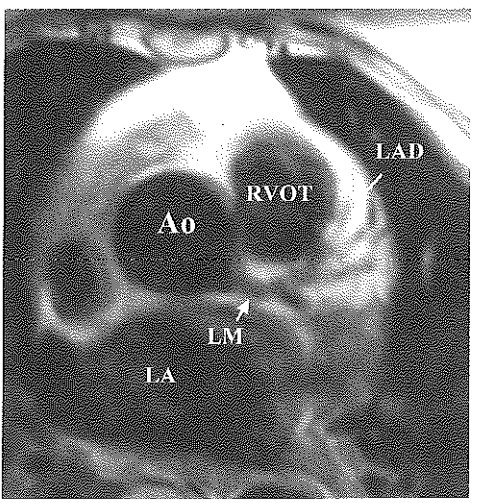

Figure 1. *Axial SE of the proximal coronary arteries. Cardiac motion is suppressed by ECG triggering, but blur exists due to the respiratory motion during the long scanning time. Ao, Aorta; RVOT, right ventricular outflow tract; LA, left atrium; LM, left main; LAD, left anterior descending coronary artery.*

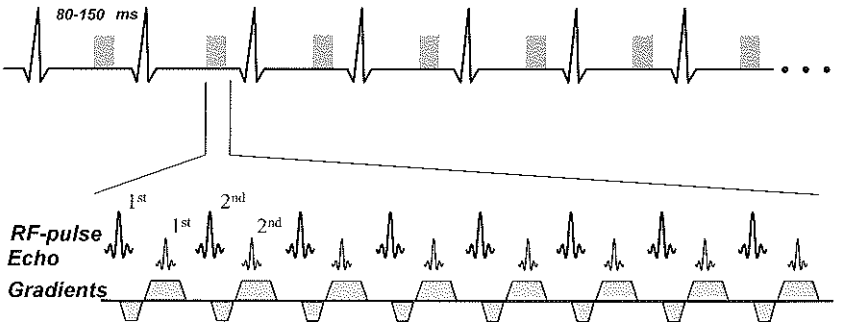

Figure 2. Diagram of a segmented GE technique. From a RF pulse, an echo signal can be retrieved by a 180° switch of the gradient system. Within a window of 80 to 150ms during mid to late diastole, 8 echoes are acquired, completing an image with 128 lines in 16 heartbeats, allowing cardiac triggered breath-hold imaging.

(Figure 1) and coronary artery bypass grafts. However, due to the relatively long acquisition time, Paulin et al[1] concluded that, due to significant motion artifacts, SE imaging was unsatisfactory for diagnosis of coronary atherosclerotic disease.

2D GE IMAGING OR BRIGHT BLOOD IMAGING

In GE imaging, the echo signal is produced by a single RF pulse followed by a 180° switch of the magnetic gradients instead of a second RF pulse. For coronary imaging, Edelman et al[3] acquired 8 echoes within a window of 120 ms per RR interval (Figure 2). The information for a single image with 128 lines can now be acquired in 16 heartbeats. The majority of the patients are able to withhold their breath for 16 to 25 s, and therefore data for one image can be acquired within one breath hold. They were able to obtain a resolution of 1.8 × 0.9 mm, whereas the slice thickness is 4 mm. This sequence is frequently referred to as segmented 2D GE imaging.

The gradient switch will rephase all the atoms that have been excited by the RF pulse, even moving blood, showing the coronaries bright in distinction to SE imaging. Only turbulent blood flow will dephase before the echo signal is acquired and be less bright or even black in the image, therefore presenting as a distinct signal void. This has been one of the most important ways to detect significant coronary artery stenosis given the limited resolution that can be achieved with current technology.

The 2D slices can be angulated to evaluate different segments of the coronary artery tree, but even then it is not always possible to cover the complete artery (Figure 3). In this example is clearly shown that the prox-

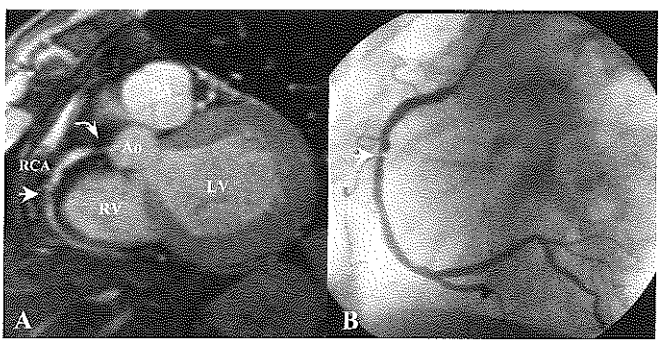

***Figure 3. (A)** Example of a 2D segmented GE image with signal loss (strait arrow) occurring just beyond a stenosis in the right coronary artery (RCA). Note that the very proximal segment of the RCA runs out of the imaging plane (curved arrow), which suggests the presence of a significant stenosis. **(B)** Corresponding conventional coronary angiogram. Ao, Aorta; PA, pulmonary artery; LV, left ventricle; RV, right ventricle.*

imal part of the right coronary artery (RCA) runs out of the imaging plane, illustrating the necessity of multiple contiguous images to review longer segments of the coronary arteries. This requires multiple breath holds to visualize one entire segment. Inconsistent breath holding can introduce important misregistration artifacts, suggesting the false presence of a stenosis or even a total occlusion. Different angulations are necessary to visualize all the proximal and mid segments of the right and left coronary artery system, so that a total examination takes 45 to 60 minutes. Using this elaborate technique, Manning et al identified the left main in 24 of the 25 (92%) healthy subjects.[4] The left anterior descending coronary artery (LAD) was identified in 100% of the subjects over a length of 28 to 93mm (average 44 mm), the circumflex coronary artery (LCX) in 76% (9 to 42 mm, average 25 mm), and the right coronary artery (RCA) also in 100% of the subjects (length 24 to 122 mm, average 58 mm). In conclusion, it appears that with the 2D imaging technique, images can be obtained with adequate quality and minimal or no cardiac or respiratory motion artifacts in the majority of the cases. However, the overall robustness and reliability of the visualization of the complex 3D anatomy of the coronary arteries is not sufficient, mainly because of the collection of data during several breath holds. This has restricted its clinical utility.

3D GE IMAGING WITH RESPIRATORY GATING

Three-dimensional MRI requires the acquisition of more echo signals to complete the data for the desired volume. This considerably lengthens the acquisition time beyond breath-holding possibilities using conventional MR systems. To minimize respiratory blurring, Li et al[5] used averaging of multiple acquisitions, but images still remained too much blurred[6] for clinical use.

To improve the image quality of 3D GE imaging, respiratory gating can be used. Initial attempts with a belt around the abdomen did not give reliable results. Respiratory gating by measuring the diaphragm movement with a MR technique (MR-navigator) is much more reliable.[7] A diamond-shaped region of tissue through the dome of the right hemidiaphragm is selectively imaged (Figure 4A). All the data are frequently resampled to be sure that expiration data are acquired, in general, depending on the respiration frequency, 5 or 6 times. Retrospectively, a special algorithm selects only the data from expiration to generate the image (Figure 4B).[8] A volume of 32-mm thickness with a resolution of 1.9 × 1.25 mm requires 10- to 12- minute acquisition time. However, to image the whole heart 3 or 4

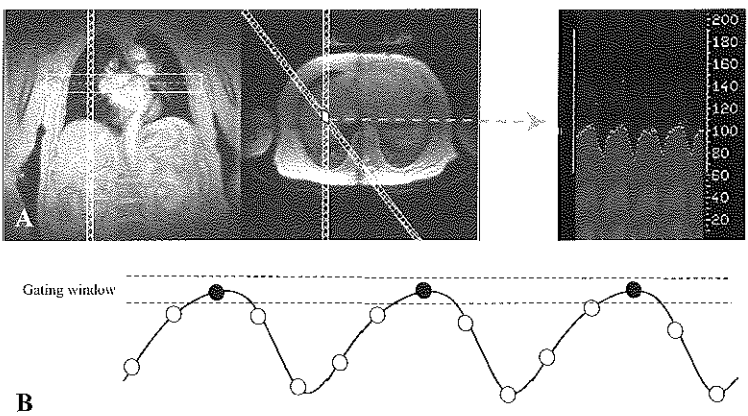

Figure 4. (A) Respiratory gating with a MR-navigator technique. A diamond-shaped column through the dome of the right hemidiaphragm is selectively imaged. (B) Analysis of navigator data is performed to retrospectively select data from a gating window within end expiration.

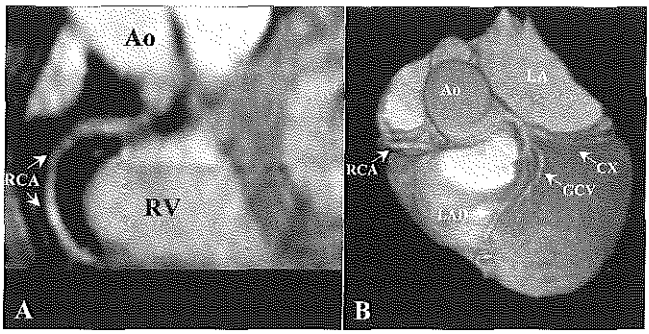

Figure 5. *(A) Reconstruction of an image from a 3D-navigator technique along the right coronary artery (RCA).* ***(B)*** *Three-dimensional representation with a volume-rendering technique of a 3D-navigator dataset. Ao, aorta; RV, right ventricle; LAD, left anterior descending; CX, circumflex coronary artery; GCV, great cardiac vein, LA, left atrium. The auricle of the left atrium is manually removed from the data set.*

volumes are needed so that the total imaging time counts up to 40 to 50 minutes. Postprocessing of these datasets allows reconstruction of images along the coronary arteries (multiplanar reconstruction [MPR]) with resulting images being comparable with 2D GE imaging (Figure 5A), and 3D impression using dedicated software (volume rendering techniques) to produce images comparable to anatomical atlases (Figure 5B). The results from several clinical studies will be discussed later.

Modification of the navigator technique allows correcting for the occurrence of shift of the coronary arteries caused by respiratory motion.[9,10] The extent of the shift of coronary arteries with the respiration has been studied by Wang et al.[11] The shift of the proximal coronary arteries in craniocaudal direction was 60% of the diaphragm movement and the shift of the apex was 90% of the diaphragm displacement. Danias et al[12] studied volunteers and showed that the same image quality can be obtained as with breath-hold imaging if they applied this correction on the navigator technique. However, only a relatively disappointing 33% reduction in acquisition time compared to navigator gating alone was achieved. This means that for imaging of the total heart the image acquisition time is decreased from 40 to 50 minutes to 30 minutes.

3D IMAGING WITH ECHO-PLANAR TECHNIQUES

Since the development of the earlier fast MRI techniques as the 2D GE imaging, MRI hardware has improved and new ultrafast sequences have been created. One of the new possibilities is echo-planar imaging (EPI).[13] With this technique, following one RF pulse, multiple readouts can be sampled during the echo by using ultrafast gradient switches. If 4 readouts are performed on one RF pulse, with 14 RF pulses, 56 image lines can be acquired (Figure 6) in a window of 150 ms. The speed of this acquisition is enormous, and it is even possible to acquire a 3D volume of the entire coronary artery tree within one breath hold.[14,15] Figure 7A illus-

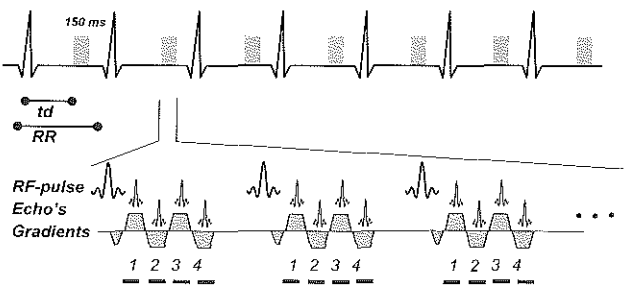

Figure 6. *Diagram of a segmented multishot EPI GE technique. Following one RF pulse 4 echoes are retrieved by ultrafast gradient switches. Within a time window of 150 ms per heartbeat 14 RF pulses are given, so that 56 echoes can be collected. A 3D-data set of the entire coronary artery can thus be acquired in one breath hold.*

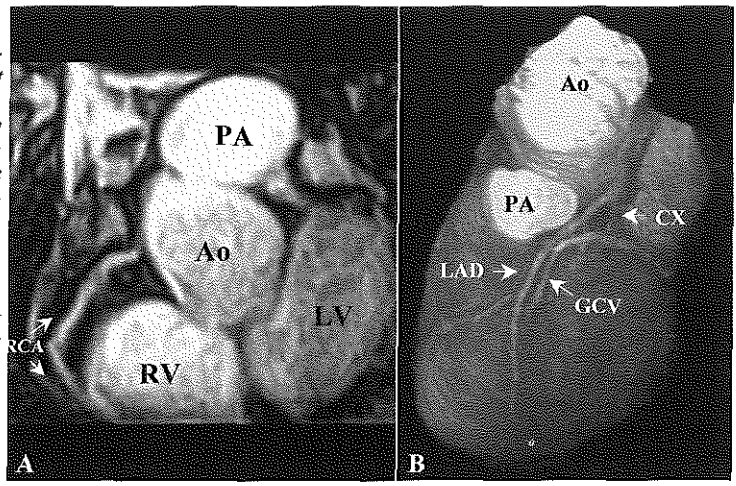

Figure 7. *(A) Reconstruction along the right coronary artery (RCA) from a single breath hold 3D EPI scan.* ***(B)*** *Volume rendering of the same data set. Left cranial view. RV, right ventricle; LV, left ventricle; Ao, aorta; PA, pulmonary artery; LAD, left anterior descending artery; CX, circumflex coronary artery; GCV, great cardiac vein.*

trates a reconstruction along the RCA from a 3D EPI dataset, and Figure 7B illustrates a volume rendering of the left coronary system. The coronary arteries can easily be visualized in the majority of the patients, but image quality is not consistent enough for use in clinical practice.

3D GE IMAGING WITHIN A BREATH HOLD

With the development of high-power gradient systems, it is possible to scan up to 21 image lines within a time window of 110 ms during every heart beat with conventional GE techniques. We used these possibilities to develop a 3D GE scan that covers a small volume of 24-mm thickness in one breath hold and that has some advantages over earlier techniques. Unlike the breath-hold EPI technique, which can only acquire axial data, this technique can angulate the volume in any desired direction. Because of the complex course of the coronary arteries, it is impossible to cover the entire coronary tree in one small volume. However the entire coronary tree can be divided into different segments, each with a particular volume along a particular direction. Thus, different scans are selected for the different segments of the coronary tree. With this approach, called volume coronary angiography using targeted scans (VCATS),[16] we first use a single breath-hold 3D-EPI scan to cover the total heart volume. This 3D scan is used as a localizer to

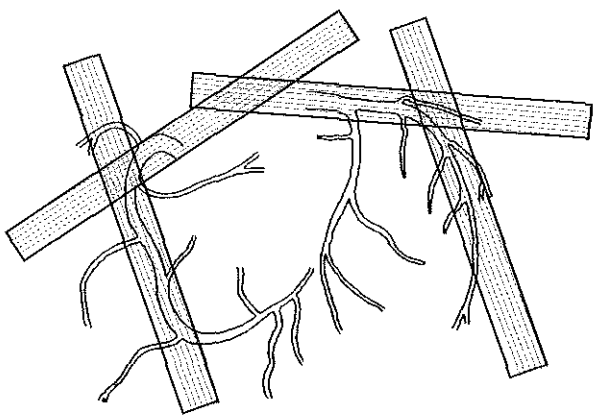

Figure 8. *Different targeted volumes are used for detailed examination of selected coronary artery segments. This is called VCATS. Displayed are four examples of possible angulations for different segments.*

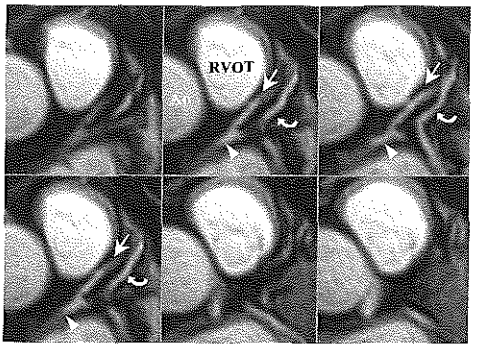

Figure 9. *Six contiguous slices from a 3D targeted volume for the left coronary artery obtained in one breath hold. Arrowheads, left main; straight arrows, left anterior descending; curved arrows, great cardiac vein. Ao, aorta; RVOT, right ventricular outflow tract.*

target the smaller volume scans, which are optimal for each individual coronary segment (Figure 8).

Imaging a segment of a coronary artery in one breath hold eliminates the problems of inconsistent breath holding, introducing artifacts in breath-hold 2D-GE imaging. With this technique it is possible to image a coronary artery segment with a resolution of 1.9 × 1.25 × 1.5 mm within 21 heartbeats. Figure 9 is an example from a transversal data set positioned at the left main and proximal anterior descending coronary artery. Figure 10 is an illustration of an angulated volume along the right coronary artery. In general, 7 targeted volumes are sufficient to visualize the important coronary artery segments (Table 2). In an initial study using VCATS, we showed that visualization of more than 90% of the proximal coronary artery segments and proximal coronary artery stenosis[17] was possible. This technique follows the course of the coronary arteries better, and may reduce false-positive diagnosis of a severe stenosis due to running out of the imaging plane of a coronary artery.

Table 2. Standard 7 Targeted Volumes Covering the Major Coronary Artery Branches

Volume	Coronary segment evaluated
1	Plane along LM, proximal LCX and proximal LAD (segments 5,6,7,11)
2	Plane of proximal RCA (segment 1)
3	Plane along distal RCA (segments 3,4)
4	Plane through aortic root and proximal RCA and LM (segments 1,5,6)
5	Plane along LCX (segment 11,12,13)
6	Plane along distal LAD (segments 8,9)
7	Plane along RCA (segment 2)

Abbreviations: LM, left main, LCX, left circumflex; RCA, right coronary artery; LAD, left anterior descending.

CLINICAL RESULTS

The SE technique was the first to be used for clinical studies of the patency of coronary artery bypass grafts. With the faster GE techniques, the evaluation of coronary artery anomalies and stenosis has been attempted.

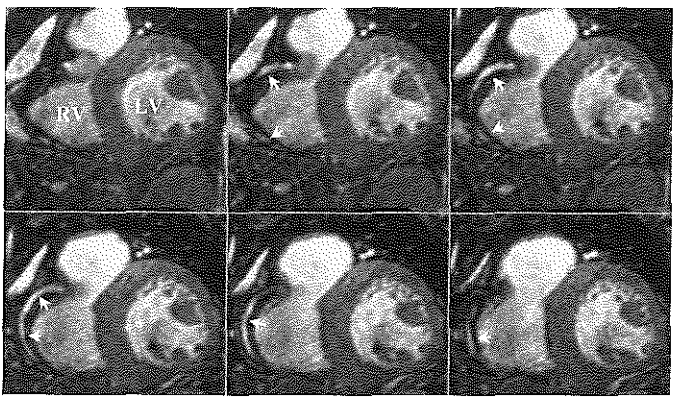

Figure 10. *Six slices obtained from a targeted volume along the right coronary artery (straight arrows). It is clearly shown that, due to the complex course of the coronary artery, the different segments of the artery are only visualized in particular slices and "disappear" in other slices. RV, right ventricle; LV, left ventricle.*

Table 3. Sensitivity, Specificity, and Accuracy of Various Techniques in the Assesment of Coronary Artery Bypass Graft Patency by MRI

Author	Technique	Grafts	Patency	Sens	Spec	Accuracy
White	Spin-echo	72	69%	86%	59%	78%
Rubinstein	Spin-echo	47	62%	90%	72%	83%
Jenkins	Spin-echo	41	63%	89%	73%	83%
Frija	Spin-echo	52	83%	98%	78%	94%
Galjee	Spin-echo	98	74%	98%	85%	96%
White	Gradient-echo	28	50%	93%	86%	89%
Aurigemma	Gradient-echo	45	73%	88%	100%	91%
Galjee	Gradient-echo	98	74%	98%	88%	96%

Abbreviations: Grafts, number of grafts evaluated; Patency, percentage of patent grafts; SE, spin-echo imaging; GE, gradient-echo imaging.

Coronary Artery Bypass Grafts

Saphenous vein and internal mammary artery bypass grafts are easier to image than coronary arteries using conventional MR imaging techniques due to their larger size (5 to 10 mm in diameter) and lesser mobility associated with cardiac and respiration motion. The first study was published by White et al[18] in 1987. They used a conventional SE sequence to assess bypass graft patency and achieved a sensitivity of 86% and a specificity of 59%. With increasing experience and faster sequences, such as GE, results improved (Table 3).[19-23] However, these examinations only provide information on bypass patency and no information about graft patency distal to the first coronary anastomosis or nonoccluding stenoses within the graft, limiting the application in clinical practice. Major obstacles to bypass graft imaging are the local image artifacts associated with metallic haemostatic clips, sternal wires, and graft markers. Although internal mammary artery grafts can also be visualized, so far this has been only studied in limited numbers of patients due to the abundant image artifacts related to the presence of hemostatic clips

Coronary Artery Anomalies

Among adults referred for contrast x-ray coronary angiography, anomalous origins of the coronary arteries are found in 0.6% to 1.2% of the patients.[24] Fortunately, the majority of these anomalies are clinically benign. However, origin of the left coronary artery from the contralateral side, with subsequent course posterior to the pulmonary artery and anterior to the ascending aorta is associated with sudden death.[25,26] MRI is an ideal technique to evaluate such patients. In two-blinded studies with 2D-GE sequences involving 35 patients with anomalous aortic origins of the coronary arteries, magnetic resonance coronary angiography identified the anomalous coronary artery course in 97% of the cases.[27,28] It may be concluded that MR coronary angiography may be used as a screening tool in young patients with unexplained arrhythmias or syncope during exercise.

Table 4. Detection of Coronary Artery Stenosis in Different Vessels by Breath Hold 2D GE MRI

Coronary	No. with disease	Sens (%)	Spec (%)	PV+ (%)	PV- (%)
Left Main	2 (5%)	100	100	100	100
LAD	23 (64%)	87	92	95	80
LCX	7 (20%)	71	90	63	93
RCA	20 (53%)	100	78	83	100
All vessels	52 (53%)	90	92	85	95
All patients	29 (74%)	97	70	90	88

Data on 39 patients from Manning et al.[29]
Abbreviations: PV+, positive predictive value; PV-, negative predictive value

Table 5. Detection of Coronary Artery Stenosis With Breath hold 2D GE MRI

Author	All vessels Sensitivity (%)	All vessels Specificity (%)
Manning, 1993	90%	92%
Duerinckx, 1994	63%	71%
Post, 1997	63%	89%
Pennell, 1996	85%	95%

Table 6. Detection of Coronary Artery Stenosis With a 3D Respiratory Gated GE MRI

Author	N	Lesions	Sens (%)	Spec (%)
Post, 1996	20	21	38	95
Müller, 1997	30	54	83	94
Kessler, 1997	73	43	65	n.a.
Woodard, 1998	10	10	73	n.a.
Sandstede, 1999	30	37	81	89
Van Geuns, 1999	29	26	50	91
Huber, 1999	70	53	73	50

Abbreviations: 3D-NAV, 3D respiratory gated (navigator) MR technique; N, number of patients; Lesions, number of significant (>50%) lesions; n/a, not available.

Coronary Artery Stenosis

Manning et al published in 1993 the first study on 39 patients referred for elective coronary angiography.[29] In this study they used the segmented 2D GE technique with fat suppression. In a blinded analysis, sensitivity and specificity of the 2D MR technique for the detection of significant stenosis (greater than 50% diameter reduction) on conventional contrast x-ray angiography were 90% and 92%, respectively, positive and negative predictive values were 0.85 and 0.95, respectively. Data for individual vessels and patients are shown in table 4. Using similar techniques Pennell,[30] Duerinckx,[31] and Post[32] were not able to confirm these surprisingly good results. These studies demonstrated a sensitivity varying from 63% to 85% (Table 5). The differences of the results can be partially explained by bias due to different patient selection criteria, but it also reflects the present lack of robustness of the 2D GE imaging technique. In its present state 2D GE MRI cannot yet be considered a reliable alternative to conventional angiography for imaging of coronary artery stenoses.

Table 7. Characteristics of Different MR Techniques for Imaging of the Coronary Arteries

	SE	2D GE	3D GE-NAV	3D GE-EPI	3D GE-BH
Imaging lines per heartbeat	1	8	8	56	21
Acquisition time	Minutes	Sec	Minutes	Sec	Sec
S/N	+++	++	++	+	++
Operator dependency	++	+	++	+++	+
Post-processing as 3D-reconstrutions	+	+	+++	+++	++
Inconsistent breath holding artifacts	0	##	0	0	#
Non-breath holding artifacts	0	#	0	##	##
Blur from respiratory motion	##	0	#	0	0
Practical resolution limited by:	Respiratory movement	BH-time	Residual movement (gating window)	S/N and BH-time	BH-time

Abbreviations: SE, spin-echo imaging; 3D GE-NAV, 3D GE imaging with respiratory gating (Navigator); 3D GE-EPI, 3D GE with EPI; 3D GE-BH, 3D GE imaging with targeted volumes in a single breathhold; S/N, signal-to-noise ratio; BH, breath hold; +++, best; ++, acceptable; +, minimal; ##, frequently present; #, some times present; 0, not applicable

Three-dimensional respiratory-gated techniques have also been used for patient studies. The specificity is high (94% to 95%) for most studies, but sensitivity varies for 38% to 83% (table 6).[33-39] Image quality is negatively affected by residual respiratory blur and irregular respiration patterns or involuntary patient motion during the relatively long acquisition time. An additional problem with MRI results from the imaging of veins, which can easily be mistaken for arteries, and imaging of the pericardial sac causing misjudgment.[40]

CONCLUSIONS

MR imaging of the coronary arteries is a challenging task, and many problems still have to be overcome. Several techniques have been introduced, each with its own characteristics (Table 7). SE imaging, as the first and slowest technique, has only been successful in the detection of patency of coronary artery bypass grafts. With the introduction of GE imaging, the number of signals acquired with in one heartbeat increased, which shortens the imaging time to one breath hold for one image. This technique has shown to be able to detect coronary artery anomalies and patency of coronary artery bypass grafts, but seems inadequate for the detection of coronary artery or bypass graft stenosis. Finally, several 3D imaging, respiratory-gated imaging (with or without respiratory correction) and ultra-fast breath-hold techniques have been introduced. The value of these techniques has still to be established.

REFERENCES

1. Paulin S, von Schulthess GK, Fossel E, et al. MR imaging of the aortic root and proximal coronary arteries. AJR Am J Roentgenol. 1987;148:665-70.
2. Alfidi RJ, Masaryk TJ, Haacke EM, et al. MR angiography of peripheral, carotid, and coronary arteries. AJR Am J Roentgenol. 1987;149:1097-109.
3. Edelman RR, Manning WJ, Burstein D, et al. Coronary arteries: breath-hold MR angiography. Radiology. 1991;181:641-3.
4. Manning WJ, Li W, Boyle NG, et al. Fat-suppressed breath-hold magnetic resonance coronary angiography. Circulation. 1993;87:94-104.
5. Li D, Paschal CB, Haacke EM, et al. Coronary arteries: three-dimensional MR imaging with fat saturation and magnetization transfer contrast. Radiology. 1993;187:401-6.
6. Wang Y, Grist TM, Korosec FR, et al. Respiratory blur in 3D coronary MR imaging. Magn Reson Med. 1995;33:541-8.
7. Li D, Kaushikkar S, Haacke EM, et al. Coronary arteries: three-dimensional MR imaging with retrospective respiratory gating. Radiology. 1996;201:857-63.
8. Hofman MB, Paschal CB, Li D, et al. MRI of coronary arteries: 2D breath-hold vs 3D respiratory-gated acquisition. J Comput Assist Tomogr. 1995;19:56-62.
9. Stuber M, Botnar RM, Danias PG, et al. Double-oblique free-breathing high resolution three-dimensional coronary magnetic resonance angiography. J Am Coll Cardiol. 1999;34:524-31.
10. Botnar RM, Stuber M, Danias PG, et al. Improved coronary artery definition with T2-weighted, free-breathing, three-dimensional coronary MRA. Circulation. 1999;99:3139-48.
11. Wang Y, Riederer SJ, Ehman RL. Respiratory motion of the heart: kinematics and the implications for the spatial resolution in coronary imaging. Magn Reson Med. 1995;33:713-9.
12. Danias PG, McConnell MV, Khasgiwala VC, et al. Prospective navigator correction of image position for coronary MR angiography. Radiology. 1997;203:733-6.
13. Edelman RR, Wielopolski P, Schmitt F. Echo-planar MR imaging. Radiology. 1994;192:600-12.
14. Wielopolski PA, Manning WJ, Edelman RR. Single breath-hold volumetric imaging of the heart using magnetization-prepared 3-dimensional segmented echo planar imaging. J Magn Reson Imaging. 1995;5:403-9.
15. Wielopolski P, Oudkerk M, de Bruin H, et

al. Breath-hold 3D MR Coronary Angiography (Abstract). Radiology. 1996;210(P):273.
16. Wielopolski P, vanGeuns R, deFeyter P, et al. Breath-hold Coronary MR Angiography with Volume Targeted Imaging. Radiology. 1998;209:209-219.
17. van Geuns RJM, Wielopolski PA, Rensing B, et al. Clinical Evaluation of Breath-hold MR Coronary Angiography using Targeted Volumes (Abstract). Procedings of the International Society for Magnetic Resonance in Medicine. 1998.
18. White RD, Caputo GR, Mark AS, et al. Coronary artery bypass graft patency: non-invasive evaluation with MR imaging. Radiology. 1987;164:681-6.
19. Rubinstein RI, Askenase AD, Thickman D, et al. Magnetic resonance imaging to evaluate patency of aortocoronary bypass grafts. Circulation. 1987;76:786-91.
20. Jenkins JP, Love HG, Foster CJ, et al. Detection of coronary artery bypass graft patency as assessed by magnetic resonance imaging. Br J Radiol. 1988;61:2-4.
21. Frija G, Schouman-Claeys E, Lacombe P, et al. A study of coronary artery bypass graft patency using MR imaging. J Comput Assist Tomogr. 1989;13:226-32.
22. Galjee MA, van Rossum AC, Doesburg T, et al. Value of magnetic resonance imaging in assessing patency and function of coronary artery bypass grafts. An angiographically controlled study. Circulation. 1996;93:660-6.
23. White RD, Pflugfelder PW, Lipton MJ, et al. Coronary artery bypass grafts: evaluation of patency with cine MR imaging. AJR Am J Roentgenol. 1988;150:1271-4.
24. Kimbiris D, Iskandrian AS, Segal BL, et al. Anomalous aortic origin of coronary arteries. Circulation. 1978;58:606-15.
25. Chaitman BR, Lesperance J, Saltiel J, et al. Clinical, angiographic, and hemodynamic findings in patients with anomalous origin of the coronary arteries. Circulation. 1976;53:122-31.
26. Levin DC, Fellows KE, Abrams HL. Hemodynamically significant primary anomalies of the coronary arteries. Angiographic aspects. Circulation. 1978;58:25-34.
27. McConnell MV, Ganz P, Selwyn AP, et al. Identification of anomalous coronary arteries and their anatomic course by magnetic resonance coronary angiography. Circulation. 1995;92:3158-62.
28. Post JC, van Rossum AC, Bronzwaer JG, et al. Magnetic resonance angiography of anomalous coronary arteries. A new gold standard for delineating the proximal course? Circulation. 1995;92:3163-71.
29. Manning WJ, Li W, Edelman RR. A preliminary report comparing magnetic resonance coronary angiography with conventional angiography. N Engl J Med. 1993;328:828-32.
30. Pennell DJ, Bogren HG, Keegan J, et al. Assessment of coronary artery stenosis by magnetic resonance imaging. Heart. 1996;75:127-33.
31. Duerinckx AJ, Urman MK. Two-dimensional coronary MR angiography: analysis of initial clinical results. Radiology. 1994;193:731-8.
32. Post JC, van Rossum AC, Hofman MB, et al. Clinical utility of two-dimensional magnetic resonance angiography in detecting coronary artery disease. Eur Heart J. 1997;18:426-33.
33. Post JC, van Rossum AC, Hofman MB, et al. Three-dimensional respiratory-gated MR angiography of coronary arteries: comparison with conventional coronary angiography. AJR Am J Roentgenol. 1996;166:1399-404.
34. Muller MF, Fleisch M, Kroeker R, et al. Proximal coronary artery stenosis: three-dimensional MRI with fat saturation and navigator echo. J Magn Reson Imaging. 1997;7:644-51.
35. Woodard PK, Li D, Haacke EM, et al. Detection of coronary stenoses on source and projection images using three-dimensional MR angiography with retrospective respiratory gating: preliminary experience. AJR Am J Roentgenol. 1998;170:883-8.
36. Kessler W, Achenbach S, Moshage W, et al. Usefulness of respiratory gated magnetic resonance coronary angiography in assessing narrowings > or = 50% in diameter in native coronary arteries and in aortocoronary bypass conduits. Am J Cardiol. 1997;80:989-93.
37. Sandstede JJ, Pabst T, Beer M, et al. Three-dimensional MR coronary angiography

using the navigator technique compared with conventional coronary angiography. AJR Am J Roentgenol. 1999;172:135-9.
38. van Geuns RJ, de Bruin HG, Rensing BJ, et al. Magnetic resonance imaging of the coronary arteries: clinical results from three dimensional evaluation of a respiratory gated technique. Heart. 1999;82:515-9.
39. Huber A, Nikolaou K, Gonschior P, et al. Navigator echo-based respiratory gating for three-dimensional MR coronary angiography: results from healthy volunteers and patients with proximal coronary artery stenoses. AJR Am J Roentgenol. 1999;173:95-101.
40. Duerinckx AJ, Atkinson DP, Mintorovitch J, et al. Two-dimensional coronary MRA: limitations and artifacts. Eur Radiol. 1996;6:312-25.

Chapter 3

Magnetic Resonance Imaging of the Coronary Arteries: Advanced Imaging Concepts

P.A. Wielopolski, R.J.M. van Geuns, P.J. de Feyter,

M. Oudkerk

Published in Eur. Radiology 2000;10:12-35 as "Coronary Arteries"

ABSTRACT

Coronary angiography (CA) is presently considered the gold standard for the assessment of the coronary arteries. However, the presence of ionizing radiation, its invasiveness and the small associated risk of morbidity prompted long ago the development of more patient-friendly imaging modalities. A promising technique, magnetic resonance imaging (MRI), has been regarded as the major modality in the coming decade. Although still in its infancy qualitatively, its flexibility and non-invasiveness opens the door for a comprehensive evaluation of the heart and the coronary arteries in one single sitting with high anatomical definition and excellent soft tissue contrast capabilities, double-oblique tomographic sections and the possibility to quantify an innumerable number of cardiovascular physiological parameters. Numerous ideas have been assessed, comprising breath-hold and free-breathing two-dimensional and three-dimensional measurements. New ongoing trials with intravascular contrast agents may provide for all these techniques the long-awaited essential boost for reliable magnetic resonance coronary angiography (MRCA). Introduction of parallel MRI acquisition techniques, such as simultaneous acquisition of spatial harmonics (SMASH) and sensitivity encoding (SENSE) may provide the speed enhancement required to shorten imaging time for all techniques explored to date.

INTRODUCTION

Despite its indisputable standard of reference for the detection of coronary artery stenosis, conventional coronary angiography (CA) is expensive, requires ionizing radiation and its invasiveness poses risks of major complications that can lead to stroke and death. In response, several imaging methodologies have been investigated to help assess, directly or indirectly, the state of the coronary circulation and determine the severity of a coronary lesion with lesser risks while providing a less costly and safer alternative to patient screening and follow-up. Localizing coronary lesions and their possible impact is key to how disease management can carry through in a given cardiac patient. Although several non-invasive imaging modalities have been available clinically that can provide this information, MRI deserves special attention. Magnetic resonance imaging is devoid of harmful radiation exposure ensuring study repeatability and it can deliver high-resolution images with superb contrast characteristics in any desired orientation, especially suitable to study the coronary anatomy. The technique can also furnish functional parameters to complement the evaluation of a detected coronary lesion (e. g., through myocardial motion analysis and perfusion mapping during rest and stress tests). With clear advantages over other techniques, MRI could broaden enormously the scope in the assessment of cardiovascular diseases in preventive medicine if reliable patient screening could be performed before symptoms of coronary artery disease appear that would require immediate catheterization. In this review we put in perspective and generalize on all magnetic resonance coronary angiographic (MRCA) techniques that have been investigated to date. To accomplish this, an outlook on basic scanning concepts and possibilities already explored for MRCA is presented. We generalize on the potential impact of hardware and software advances on newer 'dedicated cardiovascular' MRI units on current MRCA concepts, the commercial appearance of intravascular contrast agents and novel acquisition strategies that all together may reduce dramatically the imaging time for 'the integrated assessment' of the heart and coronary arteries in the near future.

CHALLENGES TO TOMOGRAPHIC IMAGING: THE SUCCESS OF CONVENTIONAL CORONARY ANGIOGRAPHY

Native coronary arteries not only have a small caliber, ranging between 2 and 5 mm, but their path over the heart is generally tortuous and they are subjected to the pumping action of the heart and respiration. The coronary vessels mostly curve around the wall of the cardiac ventricles, making it difficult to find a single tomographic imaging plane that can encase entirely a coronary branch.

The success of CA for the assessment of the coronary arteries is based on simple facts. Conventional CA is photographic in nature, enjoying exquisite temporal resolution with a frame rate reaching 60 frames per second and high in-plane spatial resolution, of the order of 0.1×0.1 mm^2 for current digital imaging systems. But most adequate to CA is the use of selective contrast injections, targeting directly left and right coronary artery trees. Therefore, CA can render projection images of the entire coronary path over the heart without the interference of cardiac chambers and myocardium. Additionally, the fluoroscopic nature of CA provides information on the dynamics of the contrast media injected, giving an intuitive indication to the coronary artery flow patterns during cine review. This can be considered a real asset for CA, still to be seen applied to tomographic imaging techniques.

The aforementioned characteristics of CA impose large constraints on any non-invasive

tomographic technique; therefore, no other imaging modality can fully integrate all the versatility provided by CA, lacking spatial resolution, acquisition speed, or coverage. Magnetic resonance imaging is no exception to the rule, temporal and spatial resolution being mutually exclusive parameters. In addition, with non-invasiveness the current strength of MRI, selective injection of contrast agents is not a viable option for selective MRCA, making projection imaging, in essence, not possible unless tagging techniques with subtraction are used. Since MRI can be regarded relatively slowly when high-resolution images are attempted (image resolution is difficult to attain in a single-shot technique with temporal resolution < 60 ms), a composite raw data set must be formed over several heart cycles, making it susceptible to cardiac motion and arrythmias. Another consideration that must be present is that image resolution is also susceptible to respiratory motion.

MR IMAGING TECHNIQUES: SPIN ECHOES AND GRADIENT-RECALLED ECHOES

Two different techniques can be applied to view the coronary arteries. Spin echo (SE) scans and variants (turboSE, fast-SE) can produce excellent anatomical images of the heart and great vessels with images in which signal suppression in blood-filled compartments is typical in providing improved contrast. Spin-echo-based techniques are regarded as 'black-blood' techniques and are ideal to observe the vessel lumen and, eventually, vessel walls if the signal-to-noise ratio (SNR) and resolution is sufficient. On the contrary, gradient-recalled echo (GRE)-based techniques provide, in general, the opposite contrast by making use of the signal enhancement possible from inflow of non-saturated blood to the region of interest to produce 'bright-blood' images. Additionally, GRE techniques are amenable to both two-dimensional (2D) and three-dimensional (3D) imaging formats.

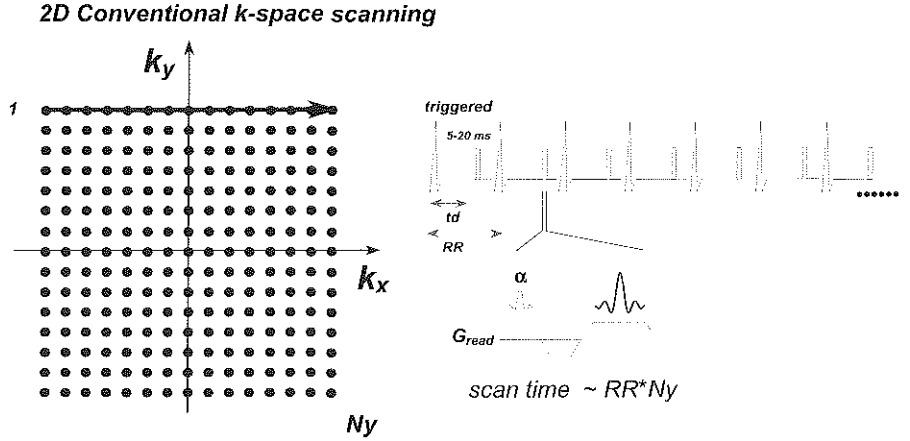

Figure 1. *Conventional 2D k-space encoding. One single line of k-space is acquired per heartbeat (shown for a GRE readout). Imaging time equals the number of in-plane phase-encoding lines selected. Temporal resolution is excellent, with each readout accomplished in several milliseconds. In the example, 15 heartbeats are needed to cover the entire k-space matrix. k_x frequency encoding; k_y phase encoding; N_y number of in-plane phase-encoding steps; td delay to acquisition; RR cardiac period; G_{read} readout gradient waveform.*

TECHNIQUE EVOLUTION: FROM SLOW TO ULTRAFAST

To eliminate cardiac motion interference in image resolution (blurring and ghosting removal) it is necessary to synchronize the image acquisition to a specific phase of the cardiac cycle. This is achieved by triggering the acquisition to the acquired ECG signal by a physiological monitoring unit. Both ECG-triggered SE and GRE techniques as conceived over a decade ago are extremely slow for cardiac imaging. A single line of data was acquired per cardiac phase and required as many heartbeats as in-plane phase-encoding lines to achieve a desired resolution (assuming a 2D scan with a single average; see Figure 1). Because repetition times (TR) could be shortened to several milliseconds with GRE techniques, such as with turbo FLASH scanning,[1-3] heart motion could be frozen by scanning all in-plane phase encodes in less than 300 ms after detecting the ECG signal with crude spatial resolution (e. g., TR = 3 ms, 64 × 128 matrix, 6.4 × 3.2-mm^2 in-plane resolution). A compromise between spatial and temporal resolution was offered soon enough with 2D segmented GRE,[4,5] a multi-shot modification collecting a reduced set of lines over multiple cardiac periods (Figure 2). For MRCA, advantage was taken that imaging could be performed during a small interval in mid-late diastole, a moment during which the heart could be considered fairly stationary (60-150 ms, depending on heart rate and coronary segment of interest).[6] A similar technique, multi-shot spiral imaging, was also conceived that reduced possible signal loss and flow misregistration from fast-moving blood in the coronary arteries (Figure 3).[7] Fast-SE techniques, the SE equivalent to the segmented GRE concept, have also found widespread applications in the thorax for assessing cardiac and coronary anatomy within comfortable breath-holds,[8] or with free-breathing techniques to augment patient comfort.[9] As mentioned previously, fast-SE variants have been targeted towards black-blood contrast, opposite to the bright blood appearance on GRE scans.

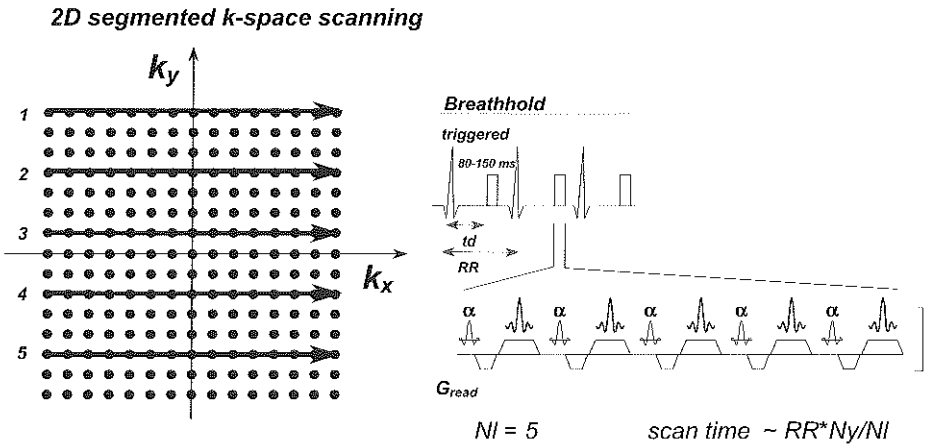

Figure 2. Segmented 2D k-space encoding. Taking advantage of the period the heart remains quiet during mid-late diastole, the acquisition window can be increased to encase several lines of k-space in an interleaved fashion (shown for a GRE readout). Time resolution is usually of the order of 50-150 ms depending on heart rate. Imaging time in heartbeats is equal to the number of phase-encoding lines divided by the number of lines collected per heartbeat. In the example, the entire k-space data is collected in three heartbeats. k_x frequency encoding; k_y phase encoding; NI number of lines scanned in acquisition window; N_y number of in-plane phase-encoding steps; td delay to acquisition; RR cardiac period; G_{read} readout gradient waveform

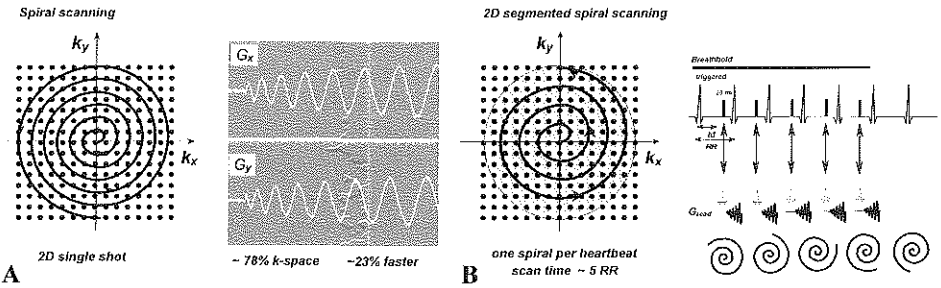

Figure 3 A, B. *Single-shot and segmented 2D spiral k-space encoding.* ***(A)*** *Spiral encoding process. In essence, the in-plane imaging gradients are oscillated in tandem (oscilloscope traces shown) to accomplish a spiral trajectory in k-space. Spiral permits a time savings of 23% over conventional spin-warp scanning.* ***(B)*** *To improve resolution k-space is covered with pieces of spiral trajectories that are rotated accordingly on every heartbeat to provide uniform coverage over k-space. This encoding strategy has very good flow properties but is susceptible to off-resonant effects (producing some blurring) that must be corrected before image presentation through post-processing and needs high-quality gradient hardware to obtain the desired trajectory. k_x frequency encoding; k_y phase-encoding; td delay to acquisition; RR cardiac period; G_{read} readout gradient waveform*

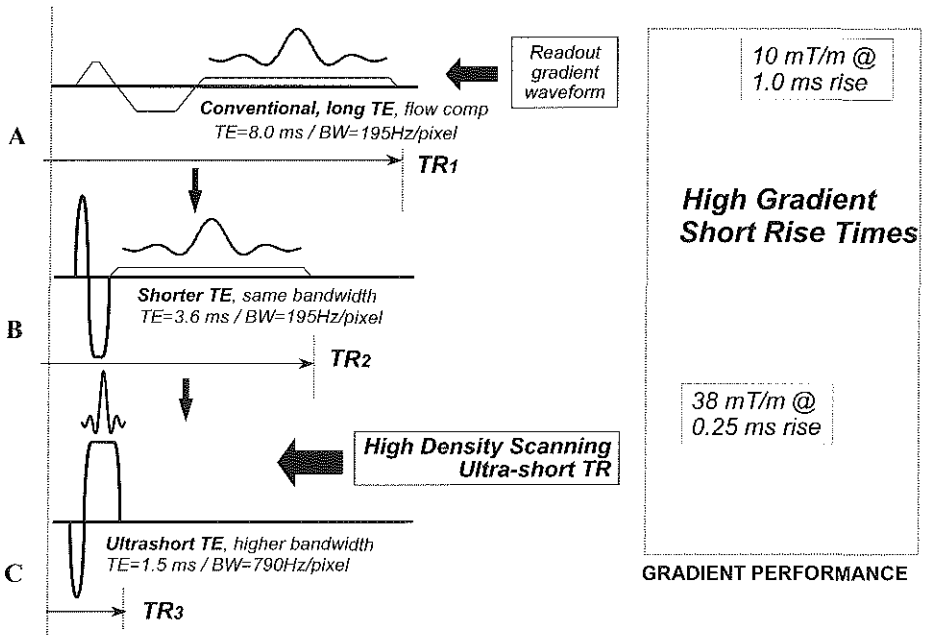

Figure 4 A-C. *Effects of improved gradient hardware on acquisition speed and readout bandwidth.* ***(A)*** *Example velocity compensated GRE waveform along the frequency-encoding direction calculated for an imaging system with a maximum gradient strength of 10 mT/m and a rise time of 1 ms.* ***(B)*** *Similar choice for imaging bandwidth as in A, but using stronger and faster imaging gradients permits a shorter TE with a gradient system using 38 mT/m and 0.25-ms rise time.* ***(C)*** *Using full gradient strength and speed, ultrashort TE is possible using high bandwidth acquisition conversely shortening also dramatically the time to acquire the MR signal. The repeat times possible, denoted by TR 1 , TR 2 , and TR 3 , respectively, can vary dramatically (TR 3 < <TR 2 < TR 1). Only for C can TR be made dramatically shorter because readout time is not time-consuming any more. In general, the RF excitation for c takes as long to execute as the readout time, making this solution more suitable for 3D imaging protocols to improve signal-to-noise ratio (SNR) at high bandwidth readouts. Values were computed for a 256 matrix scan at FOV = 200 mm and 64 points prior to the echo (1280 ms RF excitation)*

With improved gradient imaging hardware in newer MRI units (especially those called 'dedicated cardiac' MR scanners), stronger and faster imaging gradients can be used advantageously to speed up data acquisition, e.g to obtain better coverage with 3D scans by packing more data into that mid-late diastolic period with the heart standstill. Since gradient power has increased by more than 50 times within a decade (direct comparison of gradient-strength rise times), we can envision two distinctive ways to use this power to our advantage (Figure 4). In one case, the readout bandwidth can be maintained narrow while the proceeding gradients prior to signal readout can be scaled substantially in strength with reduced application times (compare Figure 4 a,b). Therefore, a shorter TE can be accomplished under the same SNR conditions, improving flow signal behavior, e. g., with velocity-compensated waveforms (Figure 5). Because higher readout gradients can be utilized during data acquisition, the readout bandwidth can be increased accordingly in order to sample the echo faster (Figure 4c). In this case, TE can be shortened dramatically with reduced sensitivity to flow dephasing and flow displacement. A penalty for using higher readout bandwidths is a reduction in the SNR available. The SNR is proportional to $BW^{-1/2}$, where BW indicates the acquisition bandwidth. An increase in acquisition bandwidth can be compensated by using a 3D scanning protocol. Three-dimensional acquisitions can cancel out the noise increase from broader bandwidth acquisitions by an additional factor of $(\text{partitions})^{1/2}$. Figure 5 illustrates phantom examples of the flow behavior improvement possible with high-performance gradients. These improvements are applicable to any GRE MRCA technique. For fast-SE acquisition schemes improvements are seen generally with shorter interecho spacings at constant readout bandwidth. The increasing availability of phased-array coil receivers to provide enhanced SNR over wide fields of view (FOV), e. g., panoramic array imaging, offer further reductions in TR and makes it practical to acquire more data lines per unit time with larger readout bandwidths. This SNR boost permits to augment the resolution per unit time and the possibility to

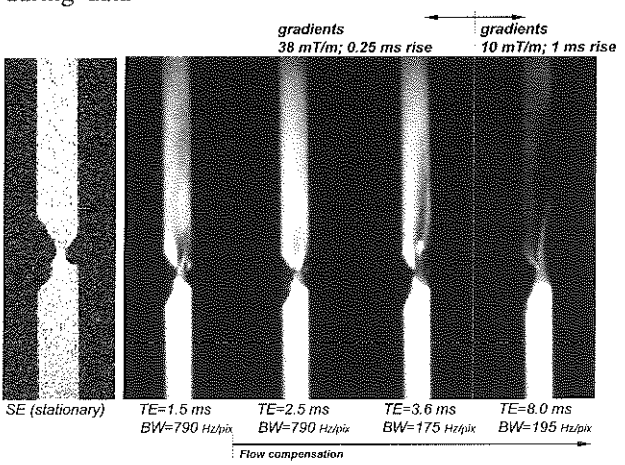

Figure 5. *Behavior of post-stenotic signal loss in a high-grade stenosis phantom with conventional (10 mT/m; 1-ms rise time) and high-performance (38 mT/m; 0.25-ms rise time) flow-compensated GRE sequences as a function of TE and readout bandwidth. The phantom consists of a straight tube with an irregular stenosis characterized by a 70% stenosis by area. Non-compensated high-performance GRE sequence at TE = 1.5 ms maintains the signal after the stenosis with just a slight attenuation. The best behavior is obtained with a fully flow compensated high-performance GRE sequence at TE = 2.5 ms. The post-stenotic signal loss is extreme with a conventional TE = 8.0 ms when compared with the high-performance equivalent at TE = 3.8 ms with comparable readout bandwidths. The stenosis area is only well depicted for the shortest TEs. The section thickness for all GRE sequence comparisons was 3 mm, and in-plane resolution 0.70 x 0.70 mm^2 . Flow direction is from bottom to top with a velocity of 95 cm/s. SE 2D spin-echo image, 2 mm, 0.35 x 0.35 mm^2 in-plane resolution; BWreadout bandwidth in Hz/pixel; TE echo time*

acquire breathhold 2D multislice and 3D cardiac examinations with more adequate coverage and spatial and temporal resolution. To fully utilize phased-array coil technology and the strength provided by the newest gradient hardware, 2D and 3D variants of the echo-planar imaging (EPI) technique can be considered for MRCA (Figure 6).[10] A suitable combination between GRE and EPI readouts can provide reduced sensitivity to field inhomogeneities (e. g., susceptibility artefacts from sternal wires) and a better compromise between resolution and acquisition speed for 2D MRCA.[11]

MRCA TECHNIQUES

SE-based techniques

The black-blood nature of cardiac-triggered SE techniques and fast-SE variants can demonstrate sections of coronary arteries fairly consistently. Occasionally, the proximal coronary arteries were appreciated in early days when blurring from respiration was not excessive, as illustrated in a study by Paulin et al. using conventional ECG-gated multislice multiphase SE.[12] With the introduction of k-space segmentation with fast-SE scans, studies can be accomplished in a comfortable breath-hold yielding excellent results for black-blood MRCA (Figure 7). McConnell et al. has further investigated the use of fast-SE scans with respiratory synchronized techniques to produce black-blood images with submillimeter resolution, aiming to improve the quantification of coronary artery stenosis and a first attempt to study the coronary artery wall.[9] With half-Fourier acquired single-shot turbo spin echo (HASTE), a singleshot modification of fast-SE cardiac anatomy has been studied with readout times of 300 ms,[13] providing the possibility to obtain rough shots of the coronary arteries and coronary artery bypass grafts (CABG), as demonstrated in Figure 8. Black-blood consistency in all fast-SE variants that have been used for cardiac studies use a black-blood preparation referred to as PRESTO.[14] This technique is very robust and uses a non-selective inversion rapidly fol-

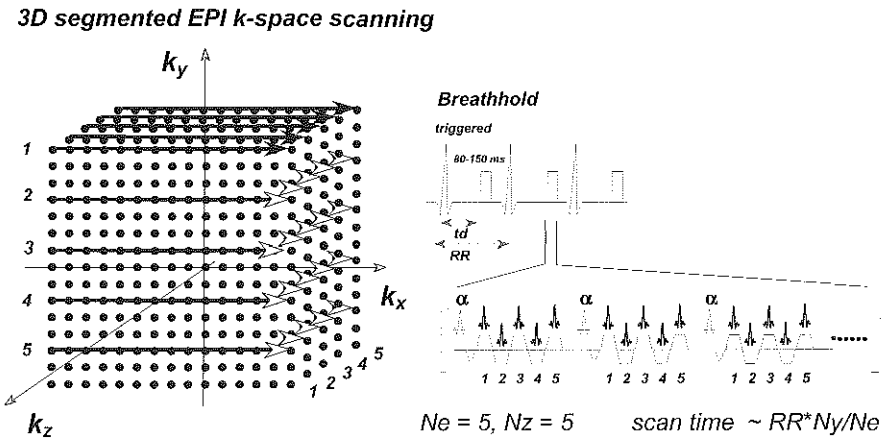

Figure 6. *Segmented 3D echo-planar imaging (EPI) k-space encoding. EPI permits to pack many readouts for each RF excitation (high-density readout) and a large number of lines can be collected within the allotted acquisition window per cardiac period. In this example, three heartbeats fill the entire 3D k-space matrix (15 × 15 × 5). Comparatively, scan time is the same as for the segmented 2D case depicted in Figure 2, because it is five times faster, collecting five slice-selection phase-encoding lines per RF excitation. k_X frequency encoding; k_Y phase encoding; N_Y number of in plane phase-encoding lines; N_E number of echoes per RF excitation; N_Z number of slice-selection phase-encoding steps; td delay to acquisition; RR cardiac period; G_{read} readout gradient waveform.*

lowed by a selective re-inversion. Using the inversion time of blood as inflow delay, blood that has moved into the imaging slice will have no signal and appear black. Fortunately, this inflow delay mostly coincides with mid-late diastole.

GRE techniques

Gradient-recalled-echo techniques provide greater flexibility for MRCA. Several variants have been explored using 2D and 3D scans combined with breath-hold and free-breathing measurements. It is sensitive to subdivide all MRCA techniques into three

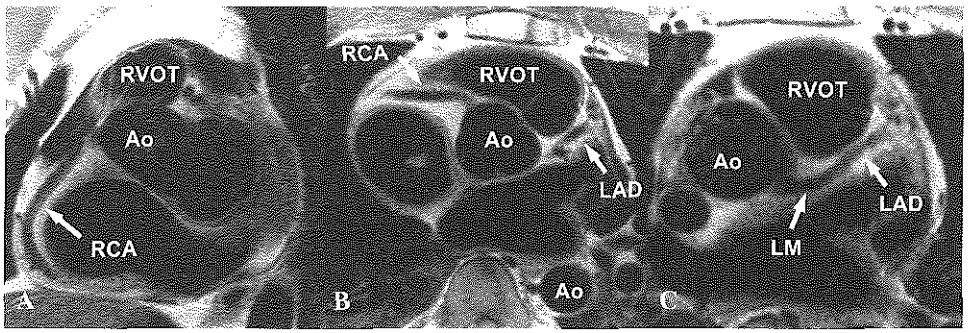

Figure 7 A-C. *Cardiac triggered, breath-hold 2D segmented blackblood fast SE.* ***(A)*** *Orientation along the RCA.* ***(B)*** *Orientation through the aortic root.* ***(C)*** *Orientation along LM and LAD. Every slice was collected in 22 heartbeats with a time resolution of 105 ms per shot (TE = 57 ms, interecho spacing = 7.12 ms, 15 lines/shot, 5 mm, 240 × 512 matrix, FOV = 285 × 380 mm²). RCA right coronary artery; LM left main; LAD left anterior descending; Ao aorta; RVOT right ventricular outflow track*

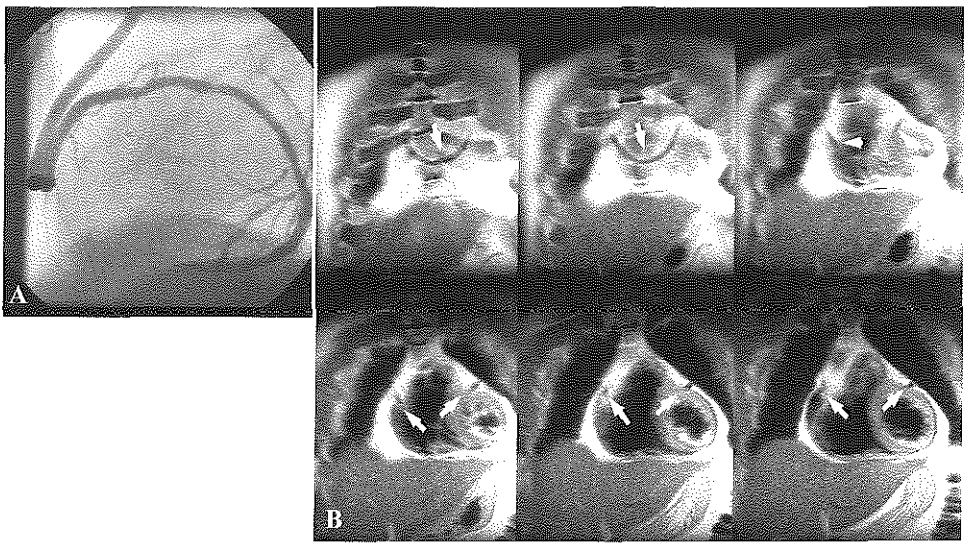

Figure 8.(A) *Cardiac triggered, free-breathing 2D single-shot blackblood fast SE (HASTE) technique for coronary bypass graft localization.* ***(B)*** *Conventional X-ray contrast angiogram of a 50-year-old patient with previous myocardial infarction and presently recurrent angina and with a venous jump graft from the aorta to the left anterior descending, diagonal, intermediate, and marginal branches, and the posterior descending artery. Six sections from 30 collected over 2 min during free-breathing. A single slice of the HASTE technique is acquired every three heartbeats with a time resolution of 395 ms per shot (TE = 30 ms, interecho spacing = 3.8 ms, 5-mm slice thickness, 1-mm overlap, 192 × 256 matrix, FOV = 350 × 350 mm 2). (see also Figs. 21, 22)*

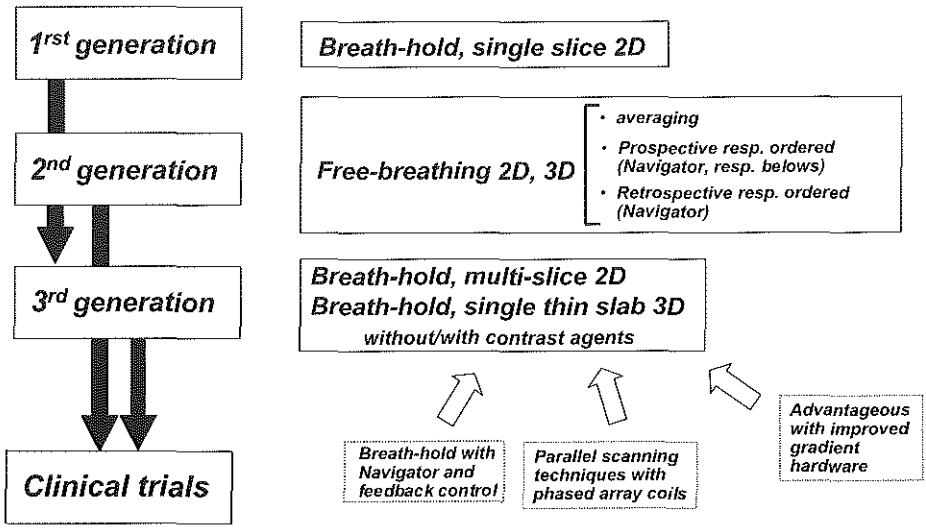

Figure 9. *Three 'bright-blood' magnetic resonance coronary angiography (MRCA) technique generations are identified. First-generation MRCA techniques comprise experiments and clinical trial results using the single-slice 2D segmented GRE and spiral scans. Second-generation identifies those MRCA techniques, generally 3D scans, that collect data during free breathing. Third-generation MRCA techniques exclusively aim for volume scans acquired within one or several breath-holds, preferably using high-perfor mance gradient systems and contrast agents. Hybrid setups may be applicable to breath-hold MRCA techniques by using some form of feedback control with navigator echoes to ensure the same diaphragm position for each breath-hold data collection (composite data sets/interslice registration). Clinical trials are still on their way for second- and third-generation techniques.*

technique 'generations', with a similar subdivision as suggested recently by Duerinckx (Figure 9).[15] The first-generation technique considers scans performed with 2D breathhold segmented GRE and spiral scanning. For the second generation four free-breathing strategies have been conceived: averaging multiple acquisitions[16,17] respiratory gating using respiratory bellows,[18] retrospectively respiratory navigator gated acquisition and reconstruction[19,20] and prospective real-time navigator respiratory data collection.[21-25] For the third-generation techniques we consider all breathhold MRCA scans that make use of high-performance gradients to cover either a large heart volume for localization or target with higher resolution a small volume along the coronary arteries.[10,26-28] Hybrid approaches using navigator echoes can be incorporated in first- and third-generation techniques to make it possible for data collection over multiple breath-holds using a respiratory feedback monitor (screen or indicator) to warn the patient to reproduce the same breath-hold position.[29] Another approach has also been applied in breath-hold 2D MRCA to correct only the reconstructed image location based on diaphragm position (or heart) to improve inter-slice correlation and aid in the review.[30,31] The feedback approach can improve SNR in composite data sets[32] and has been attempted for 3D imaging as well.[33,34] From all combinations possible, 2D breath-hold MRCA scans, 3D retrospective respiratory navigator gated MRCA and a preliminary assessment of prospective respiratory navigator MRCA and breath-hold 3D targeted-volume MRCA have been evaluated clinically (with patient populations ≥ 20; see Table 1). Three-dimensional prospective respiratory navigator MRCA scans are

being assessed in a multi-centre trail at this stage (W. Manning, pers. commun.). Other more exotic MRCA techniques further await clinical trials to determine their effectiveness (such as those using EPI methods and composite data collection in several breathholds using feedback strategies).

Coronary visualization: strategies

Coronary arteries are usually embedded in pericardial fat most of their course. Therefore, current bright-blood GRE MRCA techniques use some form of fat-suppression scheme to separate the signal from coronary artery lumen from surrounding perivascular fat. Proton-density weighting can be used to characterize the signal characteristics of all non-contrast enhanced GRE MRCA techniques. Coronary segments that run close or within the myocardium that are not surrounded with enough fat cannot be well appreciated and the contrast needs to be enhanced using some form of magnetization preparation (MP) scheme prior to data collection on every heartbeat. Two MP schemes have mainly been devised. The first one considers the application of magnetization transfer (MT) irradiation,[17,26] the second, a T2-weighted preparation.[35] Botnar et al. reported a contrast-to-noise ratio enhancement of 123% with T2 preparation.[36] The end result from these two MPs is similar; however, T2-weighted preparation can have additional advantages. With T2 preparation better differentiation between arteries and veins is possible by accentuating arterial and venous T2 differences by choosing an optimal TE as demonstrated by Brittain et al. (TE ~ 78 ms for $T2_{arteries}$ = 223 ms and $T2_{veins@20\%O2saturation}$ = 35 ms at 1.5 T, a signal ratio of approximately 6.5).[37] In addition, the contrast generated is independent of heart rate (for MT contrast, MT irradiation must otherwise be applied during all the time data is not acquired to make the contrast generation mechanism more heart rate independent). Both MT irradiation and T2-weighted MP decrease the signal from the coronary artery wall providing a more realistic measure of the coronary vessel diameter.[36] Another type of contrast that can be used for coronary artery visualization is that provided by T1-weighted GRE scans. Bright blood can only be achieved if contrast agents are added to the blood pool (extravascular or intravascular) that can shorten the T1 of blood considerably. In this case the T1 shortening should be such that the fat signal is dramatically suppressed for the TR and excitation flip angle considered.

First-generation MRCA: breath-hold 2D techniques

The breath-hold 2D fat-suppressed segmented GRE technique represents the first attempt to resolve the coronary arteries

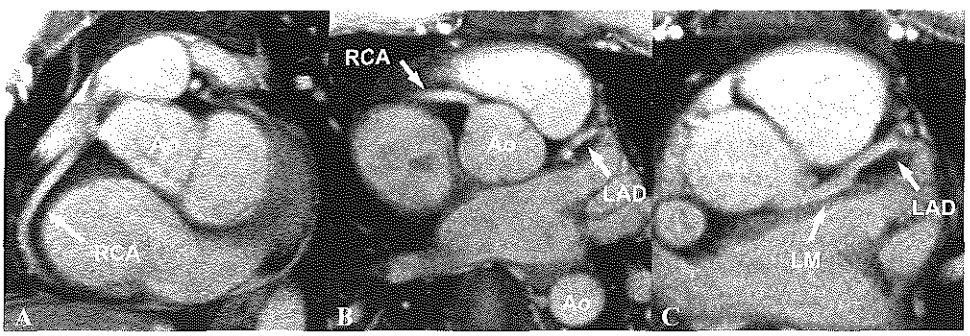

Figure 10A-C. *Cardiac triggered, breath-hold 2D segmented GRE MRCA in a healthy volunteer.* ***(A)*** *Orientation along the right coronary artery (RCA).* ***(B)*** *Orientation through the aortic root.* ***(C)*** *Orientation along LM and LAD. Every slice was collected in 22 heartbeats with a time resolution of 150 ms per shot (TR/TE = 13.7/6.7 ms, 11 lines/shot, 3 mm, 240 × 512 matrix, FOV = 285.*

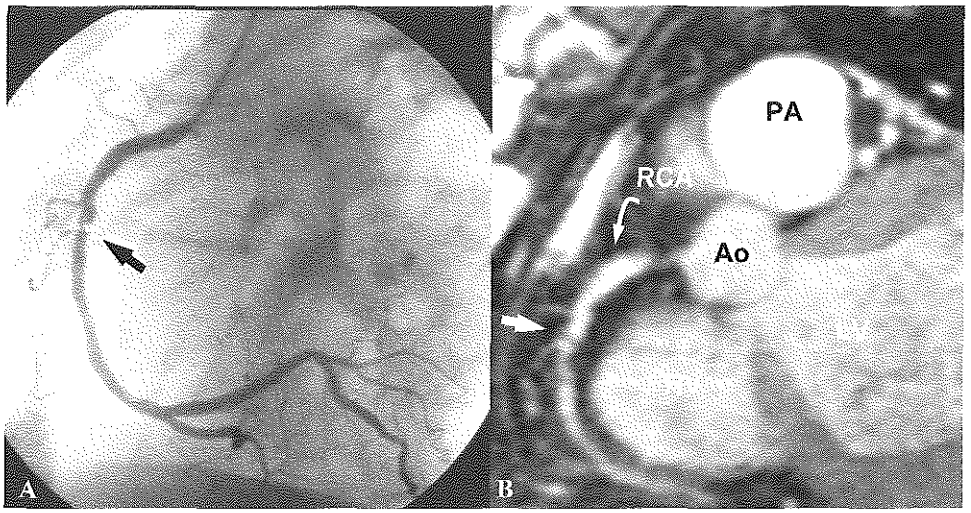

Figure 11A, B. *Patient with stenosis in the mid-segment of the right coronary artery.* ***(A)*** *Conventional coronary angiogram.* ***(B)*** *Breathhold 2D segmented GRE (turbo FLASH) image. Signal attenuation is reminiscent of the stenosis visualized in CA (arrows). Improved spatial resolution and thinner slices are necessary to evaluate the high-grade stenosis. Fourteen heartbeats were used to scan a 154 × 256 matrix, slice thickness of 3 mm, 1.25 × 1.00 mm² inplane resolution (other sequence parameters as in Figure 10). Ao aorta; RCA right coronary artery; RV right ventricle; LV left ventricle; PA pulmonary artery (figures reprinted from Wielopolski PA, et al. (1998) Coronary arteries. Eur Radiol 8: 873-885)*

(Figures. 10, 11).[6] A stack of images oriented parallel to each coronary vessel ensured coverage in case of vessel tortuosity. Scans were performed interactively with breath-hold instructions to the patient and images reviewed in situ (cine display) to appreciate the entire course of a particular coronary vessel. Decisions were made and additional images acquired perpendicular to the vessel path in possible problematic regions (signal inhomogeneities) to better detect vessel narrowing. Perpendicular images take full advantage of inflow effects, helping to obtain higher flow signal and better resolution to visualize any possible narrowing along the way. Manning et al. presented initial encouraging results in 1993 on a young group of adult volunteers.[38] Subsequently, the first clinical study was performed on 39 patients including 74% of the patients with moderate to severe coronary artery stenoses (> 50% diameter stenosis on CA).[39] In a blinded analysis the overall sensitivity and specificity was 90 and 92%, respectively. A larger study population showed again similar results;[40] however, trials performed by Duerinckx et al.,[41] Pennell et al.,[42] Post et al.,[43] Yoshino et al.[44] point out the large variability in the results obtained (see Table 1). Breathhold 2D segmented spiral scans[7] can also be included in this first-generation MRCA group. Clinical results were not reported in parallel and are at an experimental stage and not widely available for clinical use. Segmented 2D spiral scans are becoming popular with dedicated cardiac scanners, producing good-quality data results that rival those obtained with segmented 2D GRE techniques.[28]

Second-generation MRCA: improved coverage and SNR with free-breathing 2D and 3D techniques

Multi-slice 2D and 3D GRE MRCA acquisitions have been conceived under multiple scenarios to obtain extended coverage, contiguous slices, and isotropic resolution. The basic idea behind this MRCA generation is

to eliminate operator dependence on scan setup, permit image review after the examination is completed, and to produce better SNR MRCA. Given that volume data is collected, post-processing techniques can be applied, such as volume rendering (VR), maximum intensity projection (MIP), or multiplanar reformations (MPR), and show the entire course of a particular coronary segment or a display of the entire coronary tree over the heart. The 3D nature of the data sets can eliminate the overlap of unwanted structures by tissue segmentation during interpretation.

To facilitate patient comfort several free-breathing schemes were evaluated. These comprise (a) averaging multiple acquisitions,[16,17] (b) prospectively respiratory synchronized data collection,[18] and (c) retrospectively ordered respiratory gated data,[19,20] the latter two using navigator echoes (signal from a penlike excitation) to either monitor or correct the displacement of the liver diaphragm or the heart itself during the acquisition.

The method of averaging multiple acquisitions without respiratory synchronization count among the first 3D MRCA techniques used, employed by Paschal et al.[16] and Li et al.[17] with the idea to enhance the SNR of body coil acquisitions while pseudogating the data collection to overcome respiratory ghosting. Because averaging does not provide images at a particular diaphragm posi-

Table 1. Sensitivity and specificity of clinical trials with a patient population > 20 using all three generations of MRCA techniques as compared with conventional angiography (vessels with > 50% angiographic stenosis). Results are expressed in percent. n.a. not available

Reference	No. of subjects	No. of lesions[a]	Sensitivity (%)	Specificity (%)
First-generation MRCA (2D)				
Manning et al.[38]	39	52	90	92
Manning et al.[40]	72	81	90	n.a.
Duerinckx [41]	20	27	63 (0±75 %)[c]	n.a.
Pennell[42]	39	55	85[d]	n.a.
Post[43]	35	35	63 (A)[b]	89 (A)[c]
			40 (B)[c]	97 (B)[c]
Yoshino et al.[44]	36	31	83 (LAD)	98 (LAD)
			100 (RCA)	100 (RCA)
Second-generation MRCA (3D) (retrospective navigator approach)				
Post et al.[45]	20	21	38	95
Müller[46]	30	54	83	94
Kessler et al.[97]	73	43	65	n.a.
Sandstede et al.[111]	30	37	81	89
Huber et al.[47]	20	53	73	50
Van Geuns[48]	29	26	50	91
Second-generation MRCA (3D) (prospective navigator approach)				
Lethimonnier[50]	20	17	65	93
Third-generation MRCA (3D)				
Van Geuns et al.[57]	34	31	68	97
Regenfus et al.[61]	30	31	77	94

a With significant disease
b No. of vessels instead of lesions
c Variable sensitivities depending on detection threshold used to interpret images: A possible stenosis; B certain stenosis
d Study interpretation not fully blinded
e Using projection images for evaluation

tion, significant blurring was reported. To decouple and reduce maximally respiratory motion effects on the acquisition Hofman et al.[19] appended the diaphragmatic position provided by a navigator echo to the acquired data (Figure 12). The navigator echo has been produced using either a spin-echo pen-like excitation generated over the dome of the diaphragm using the intersection of a slice excited by a 90° RF pulse (sagittal) and another slice using a 180° RF pulse (sagittal to coronal orientation) or a single 2D RF excitation (defining a cylinder). Analysis of the navigator data (position histogram) was then performed to sort the data retrospectively within a predetermined reconstruction gating window (e. g., ± 1, ± 3, or ± 5 mm) that reflected a similar diaphragm position for the entire composite data set (Figure 13a). In general, the reconstructed data sets reflect an end-expiration scan in subjects with typical respiratory patterns. To ensure data sampling over the entire respiratory cycle multiple acquisitions were performed for each portion of k-space scanned per heartbeat (a constant oversampling factor of 5 or 6). Scan time is set by the number of cardiac cycles necessary to acquire one single 2D or 3D data set times the oversampling factor. The efficiency of the acquisition is defined by the number of lines accepted within the reconstruction gating range over the number of heartbeats required to complete the oversampled data set. With this approach, Li et al. reported 3D MRCA measurement in which coronary artery lengths visualized on healthy subjects were considerably longer than what was possible with comparable breath-hold 2D MRCA scans.[20] Clinical results in patients with CA are summarized in Table 1. Post et al. studied 20 patients with coronary artery disease, identifying 96% of the proximal coronary arteries, but encountered a low sensitivity of 38% and a speci-

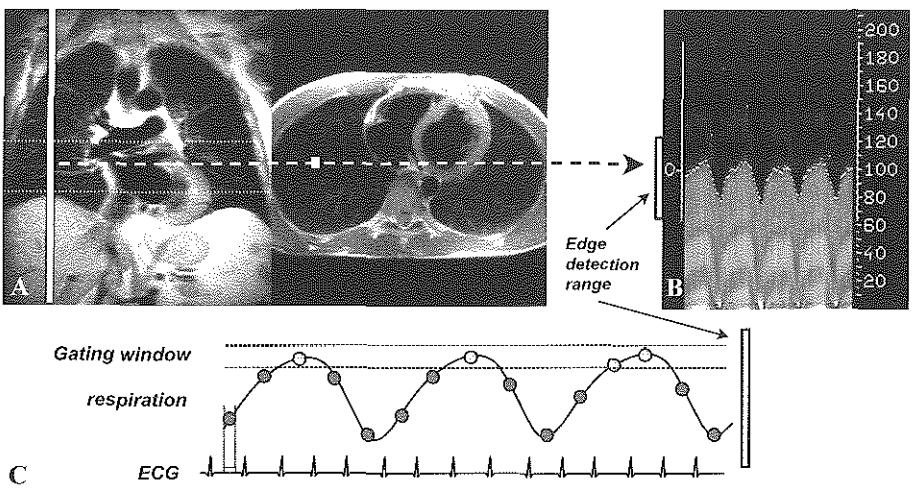

Figure 12A-C. *Collection of diaphragmatic excursion using a navigator signal. The navigator signal is generated from a spin echo using a typical SE readout with a rhomboidal cross section after the intersection of a sagittal slice defined by 90° RF pulse with an oblique slice generated by a 180° RF pulse.* ***(A)*** *Coronal scout image.* ***(B)*** *Transverse scout image.* ***(C)*** *Resulting diaphragmatic motion collected over 30 s with sampling occurring with the navigator echo collected every 240 ms. A respiratory excursion window is assigned where edge detection processing is defined over the region (to save processing time). The navigator data is attached to each data collection event in the cardiac period. The navigator data can be used retrospectively to sort the data or prospectively to make decisions in real-time on data acceptance with a predefined gating acceptance window (e. g., ± 1, ± 3, or ± 5 mm). Selected data lines lying within the desired gating window are depicted with brighter circles*

ficity of 95% for stenosis detection.[45] Müller et al. presented data on 35 patients with unpredicted success, reaching a higher sensitivity of 83% and a specificity of 94%.[46] Huber et al.[47] reported on 20 patients a sensitivity and a specificity of 73 and 50%, respectively. Van Geuns et al.[48] found a sensitivity of 50% and a sensitivity of 91% in 29 patients. Many more studies have been performed since then because of the availability of this particular MRCA protocol in many systems worldwide and reports have been generated locally and internationally with their findings. High sensitivity has been achieved once studies with sub-optimal image quality are removed from the evaluation. With successful data collection coronary stenosis can clearly be seen (Figure 14). Image quality is still problematic even in cooperative individuals, as revealed in a study by Stehling et al.[49] on young healthy volunteers.

The prospective navigator-gated acquisition tracks the diaphragmatic position with a navigator over the diaphragm (or close to the target coronary, e. g., the wall of the left ventricle for the left coronary system) similarly as in the retrospective approach. However, real-time decisions are made to accept the incoming data during mid-late diastole when sampling is performed within the desired gating window rather than oversampling to encompass the entire respiratory waveform, as previously mentioned. The approach is considered to be similar to gating the acquisition with respiratory monitoring belts used for abdominal imaging (introduced a decade ago). Two-dimensional MRCA scans using prospective navigator gating with comparable quality to breath-

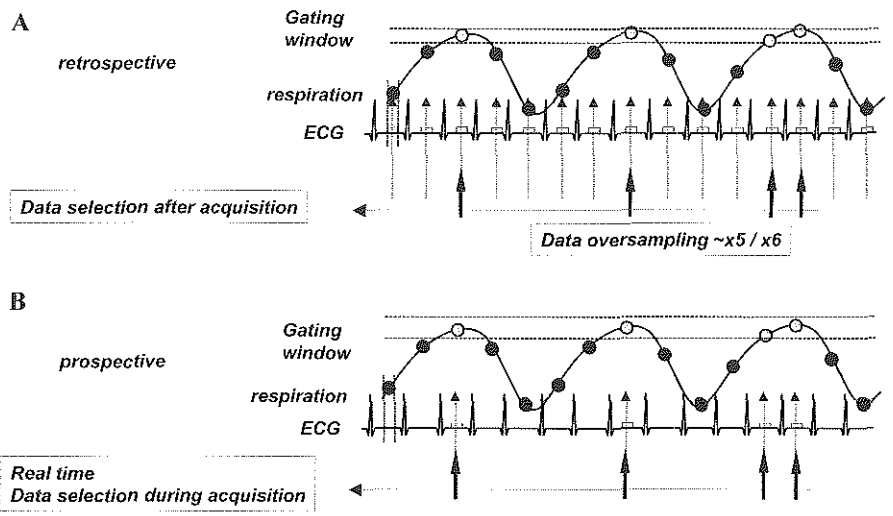

Figure 13A, B. *Retrospective and prospective navigator MRCA data collection and processing schemes.* ***(A)*** *In retrospective navigator MRCA multiple cardiac triggered data sets are collected (oversampling by five to six time) to make sure that valid data exist during the entire respiratory period that match the criteria for data selection during reconstruction within a defined small acceptance window (e. g., ± 1, ± 3, or ± 5 mm).* ***(B)*** *In prospective navigator MRCA only those lines of data synchronized with the ECG that were collected within a predefined gating acceptance window are used for the reconstruction. Gating acceptance window in prospective navigator scanning can be variable to increase scanning efficiency (e. g., ± 1 mm at the center and ± 5 mm towards the edges of k-space). Retrospective navigator data collection requires enough computer memory to hold the multiple data sets (e. g., six times more for an oversampling factor of 6); nevertheless, the acquisition time is fixed to the number of heartbeats required to collect the complete set. Selected data lines are depicted with brighter circles in both cases.*

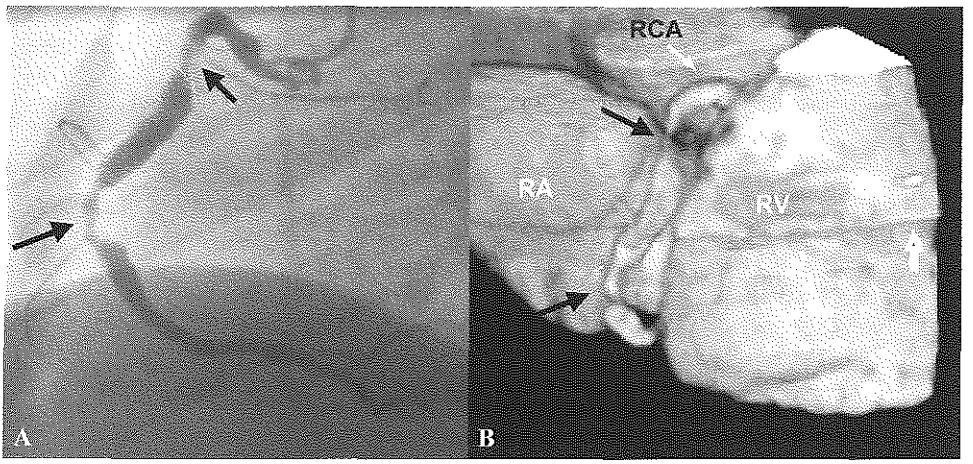

Figure14A, B. *Retrospective navigator 3D MRCA scan.* ***(A)*** *Conventional coronary angiogram.* ***(B)*** *Volume rendering of the RCA. Straight arrows indicate two stenoses located in the proximal and mid-RCA segments. Two slabs were collected with 24 2-mm-thick slices with a FOV of 280 l8 320 mm 2 and a matrix of 128 l2 256, TR/TE = 7.4/2.7 ms, time resolution of 150 ms, and data collection time of approximately 25 min. The black arrow in b demonstrates a boundary artefact that identifies the extent of each slab scanned. RCA right coronary artery; RA right atrium; RV right ventricle (with permission from ref. 48)*

holding were demonstrated by Oshinski et al.[21] Scanning time is dependent on the gating window specified (smaller windows produce sharper results but scan time may increase substantially). An additional improvement that ameliorates efficiency has been evaluated by 're-registering' the volume scanned based on the position indicated by the navigator. Using this idea, Danias et al.[31] demonstrated equivalent data to breathhold 2D acquisitions with a 33% improvement in scanning efficiency (using a 3-mm window) when compared with navigator gating without position correction. Reported clinical studies using this technique do not abound and soon reports are to be expected. A recent study by Lethimonnier et al. on 20 patients revealed a sensitivity and

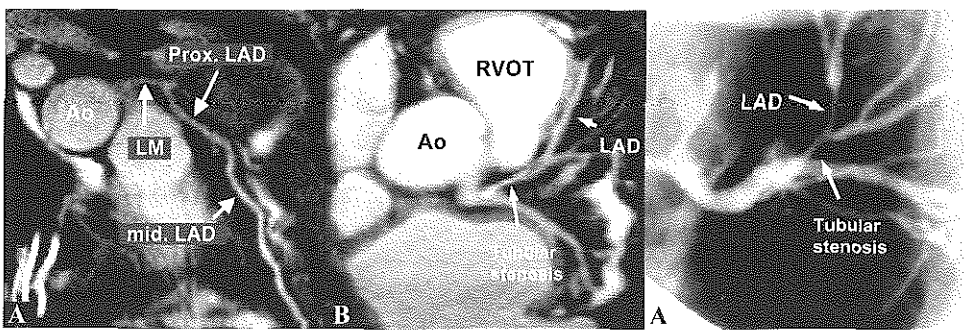

Figure 15A-C. *Examples of prospective navigator 3D MRCA.* ***(A)*** *Curved multiplanar reformation along the LAD of a 42-year-old patient with chest pain but without coronary artery stenoses.* ***(B)*** *Patient with a tubular stenosis of the LAD coronary artery corresponds nicely with CA* ***(C)****. AT2 prepared sequence was used with TEeff = 50 ms, 8 lines/shot with TR/TE = 7.4/2.5 ms (60-ms time resolution), 10 slices of 3 mm (interpolated to 20) scanned with a FOVof 305 l0 360 mm 2 and a matrix of 304 l0 512. RCA right coronary artery; LM left main; LAD left anterior descending; Ao aorta; RVOT right ventricular outflow track. (Courtesy of W. Manning, Beth Israel Deaconess Medical Center, Boston, Mass.)*

specificity of 65 and 93%, respectively.[50] Additionally, a small study reported by Stuber et al.[25] illustrates excellent image quality in healthy volunteers and good correlation with CA in 7 patients with coronary artery disease. Other schemes are available to increase scanning efficiency even further. Jhooti et al.[51] have proposed the use of centrically ordered acquisitions in which the central portion of k-space is collected with a small respiratory gating window (e. g., ± 1 mm) while the data for the outer portions of k-space are scanned with increasingly coarser gating windows (e. g., ±1 ± 3, ± 5, and ± 7 mm). This group claims that image quality is not harmed significantly with such procedure while scanning efficiency can be increased to 50%. They also affirm that consistently better image quality is obtained when compared with the retrospective navigator setup described above. The same group in a report by Yang et al.[52] investigated a 3D focused imaging approach using a volume-selective RF excitation (e. g., exciting a small cube volume of tissue inside the thorax containing only a coronary segment). The group refers to this technique as 3D zonal EPI MRCA, making it possible to concentrate on imaging only the coronary artery while achieving good image quality even with an extra 30% reduction in imaging time. The data quality with retrospective navigator MRCA approaches has been random even in healthy volunteer studies, as noted previously.[49] This has been shown experimentally by Jhooti et al.[51] investigating several schemes to compensate prospective navigator data collection while analyzing the possible pitfalls of the retrospective navigator approach. The group concluded that image quality was in direct relation to the goodness of the acquired data during the central portion of k-space. This investigation bears similarities to previous work on respiratory compensation schemes to reduce ghosting artefacts and increase scanning efficiency for freebreathing abdominal imaging such as reordered phase encoding (ROPE) and other schemes.[53] The addition here is the free choice of the gating acceptance window over different portions of k-space, thus controlling (predefining) the blurring function over the coronary vessels. A direct improvement of the retrospective navigator approach can be envisioned based on the same approach by making the constant oversampling factor used until a variable one is presented according to the region of k-space scanned. This requires further study and it is likely to increase imaging time substantially. The incorporation of segmented EPI readouts in retrospective and prospective navigator MRCA is likely to shorten scan time while maintaining good SNR and increased spatial resolution.[54,55] Another interesting free-breathing approach that is claimed to be robust was introduced recently by Hardy et al.[56] striving for high-resolution coronary images using adaptive averaging. The method is based on cross correlation of real-time acquired frames and selective averaging of those frames that contain a coronary segment in the selected imaging plane and at the proper location.

Third-generation MRCA: breath-hold volumetric MRCA with multislice 2D and 3D techniques

The trend in third-generation MRCA techniques is to acquire a volume data set in a single breath-hold. Breath-hold length, resolution, and coverage are balanced to obtain in several attempts a complete study of the coronary arteries. Although breath-hold volumetric techniques have been attempted previously with limited resolution,[3] higher resolution and speed is possible with advanced gradient hardware. This was first investigated by Wielopolski et al.,[10] using a breath-hold 3D segmented EPI approach. More recently, the addition of partial Fourier processing has shortened scanning times making it pos-

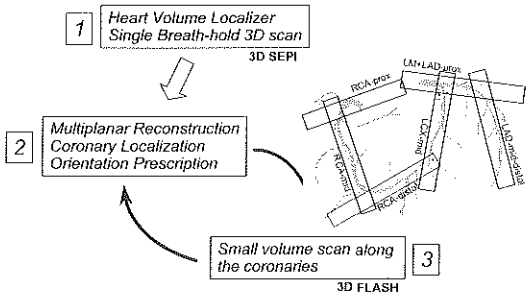

Figure 16. *One possible setup for fast coronary assessment using breath-hold 3D MRCA scans. (1) Using improved gradient hardware a volume localizer can be collected (e. g., using segmented 3D EPI scans) which provides enough spatial resolution in all directions to localize all plane orientations for coronary segments of interest (after multiplanar reformation) for targeted 3D MRCA scans (2, 3). Breath-hold targeted scans can be set from the multiplanar reformation platform directly to acquire each coronary segment (interactive mode) or all orientations are pre-recorded first prior to scanning all coronary segments at once (sequential mode)*

sible to cover the entire heart in one single breath-hold.[26] Because the 3D information is readily available after one breath-hold, MPR can be used to obtain optimal plane orientations that contain the coronary arteries and apply these for higher-resolution 2D and 3D scans that target specifically each coronary segment. This logic has been followed (dubbed VCATS for volume coronary arteriography with targeted scans) for the evaluation of a breath-hold 3D GRE sequence incorporating partial Fourier scanning to provide contiguous slices and immediate operator feedback (Figure 16). Short examination times are therefore possible, taking as few as seven breath-holds to screen the entire coronary tree with comparable imaging times and image quality to single-slice breath-hold 2D MRCA (Figures 17, 18). Despite the limited resolution that is possible in a short breath-hold with a limited number of heartbeats, signal non-uniformities and

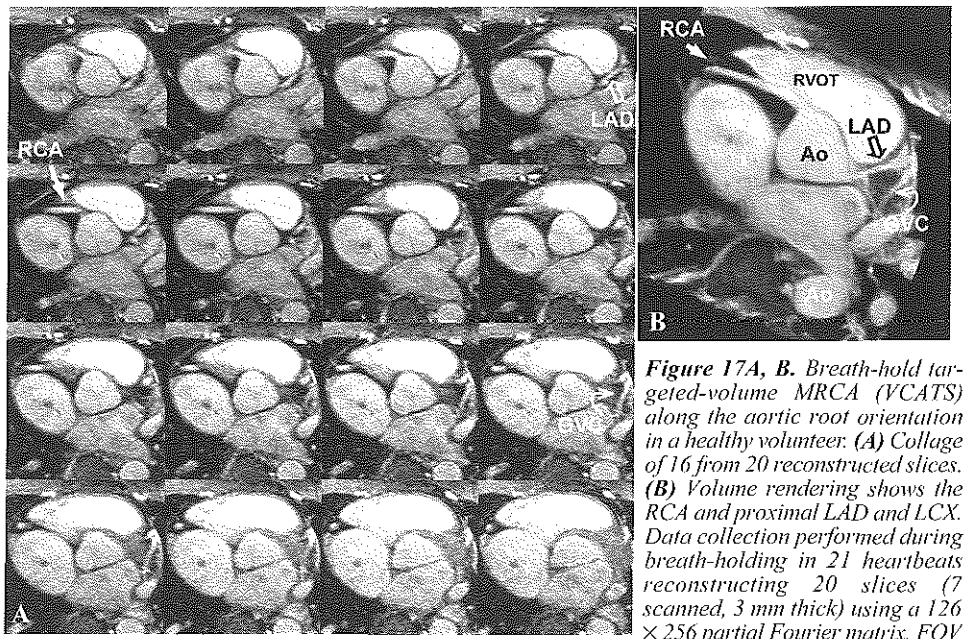

Figure 17A, B. *Breath-hold targeted-volume MRCA (VCATS) along the aortic root orientation in a healthy volunteer.* ***(A)*** *Collage of 16 from 20 reconstructed slices.* ***(B)*** *Volume rendering shows the RCA and proximal LAD and LCX. Data collection performed during breath-holding in 21 heartbeats reconstructing 20 slices (7 scanned, 3 mm thick) using a 126 × 256 partial Fourier matrix, FOV = 220 × 290 mm², 21 lines/shot with TR/TE = 4.8/2.0 ms (100-ms time resolution). Magnetization transfer contrast (MTC) is applied prior to data collection on every heartbeat. Compare to breath-hold single-slice 2D MRCA of Figures 7 b and 10b. Ao aorta; RCA right coronary artery; LM left main; LAD left anterior descending;GVC great cardiac vein*

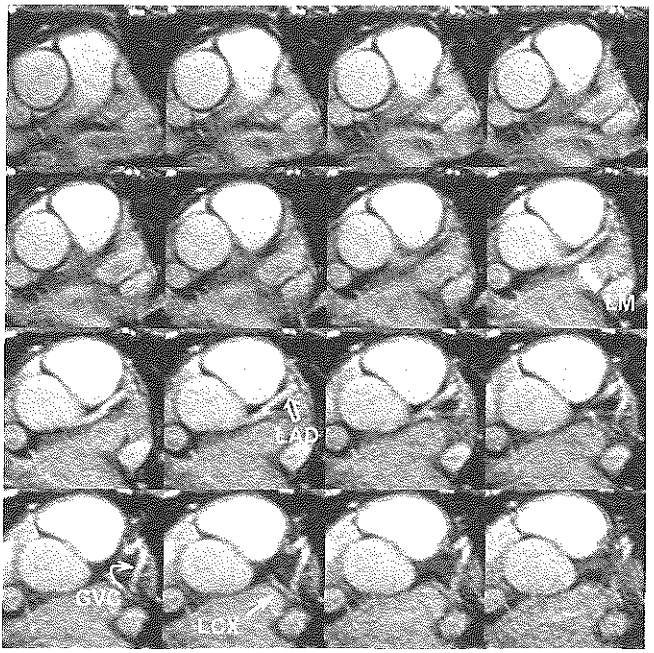

Figure 18. *Transverse targeted-volume MRCA (VCATS) at the level of the left main (LM), clearly depicting LM, left anterior descending (LAD), and left circumflex (LCX) coronary arteries. Compare with breath-hold 2D MRCA of Figs. 7 c and 10c. Imaging parameters as in Figure 17; GVC great cardiac vein.*

stenosis greater than 50% can be visualized easily when breath-hold is adequate during the acquisition (Figures 19, 20). Initial clinical results reported by Van Geuns et al.[57] on 34 patients with 31 coronary lesions (> 50% stenosis) found sensitivity and specificity values of 68% and 97%, respectively. Other approaches consider volumetric imaging using breath-hold multislice 2D segmented GRE[58] as well as spiral[28] and segmented EPI.[27] Ultrashort TR 3D contrast-enhanced MRCA with increased volume coverage has been increasingly evaluated to counteract the poor SNR of high-bandwidth acquisitions

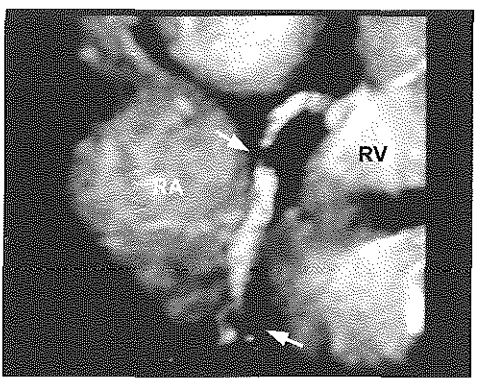

Figure 19. *Volume rendering of a VCATS tangential to the mid-RCA segment collected on the same coronary patient as shown in Figure 14. The example shows clearly the two stenotic segments (arrows). Imaging parameters as in Figure 17. RA right atrium; RV right ventricle.*

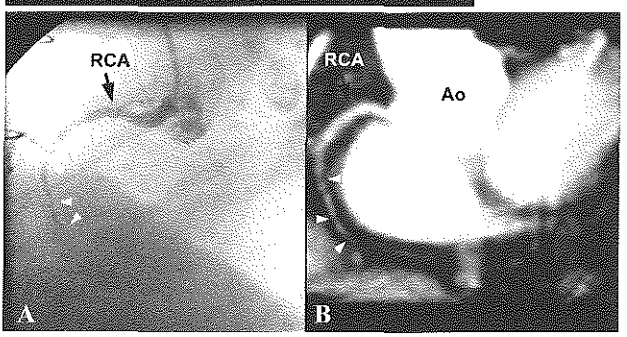

Figure 20. ***(A)*** *Conventional coronary angiogram in a patient demonstrating diffuse coronary artery disease along the RCA.* ***(B)*** *Volume rendered image of VCATS collected along the RCA demonstrates signal variations corresponding closely to those seen in CA. Arrowheads demarcate equivalent locations in both. Imaging parameters as in Figure 17. RCA right coronary artery. Ao aorta.*

with a dynamic injection of short T1 contrast agent[59-61] has produced relevant clinical results on 30 patients with a sensitivity of 77% and a specificity of 94%. With the ability to use fluoroscopic triggering, rather than using a bolus test prior to scanning, should increase the consistency of the results using contrast-enhanced MRCA and produce optimal contrast, as shown recently by Li et al.[62] To help patients to maintain a better breath-hold or to elongate the breath-hold period, the administration of oxygen during the preparation phase is helpful to ensure a successful study.[63]

ADDITIONAL APPLICATIONS OF MRCA

Coronary artery anomalies

Anomalous origins of coronary arteries appear in approximately 1.2% of patients referred for CA.[64] In the majority of cases it is benign in nature, but may be the cause of sudden death.[65,66] Detection of these anomalies can be performed with any MRCA technique available, as it has been proven that MRCA is highly effective for this indication and can be regarded as a definite tool for the diagnosis.[67] Additionally, it can be advantageous over CA in cases with inconclusive results.[68] Two blinded studies using MRCA involving 35 patients have identified the anomalous coronary artery and its course in 97% of cases.[67,68]

Assessment of coronary artery bypass graft patency

Coronary artery bypass grafts have lesser mobility with cardiac and respiratory motion and also have a larger lumen (5-10 mm) when compared with native coronary arteries. This has made it possible even for conventional SE and GRE techniques to show some success in their evaluation.[69-73] Obstacles to CABG imaging are set mainly by local image artefacts (geometric distortion and signal loss) associated with nearby metallic homeostatic clips, sternal wires, and graft markers. This has been particularly problematic for imaging internal mammary artery bypass grafts, which is the reason that they have been visualized only in a limited number of patients. With SE techniques, a patent or occluded graft is diagnosed after observing signal loss or prevalence of the

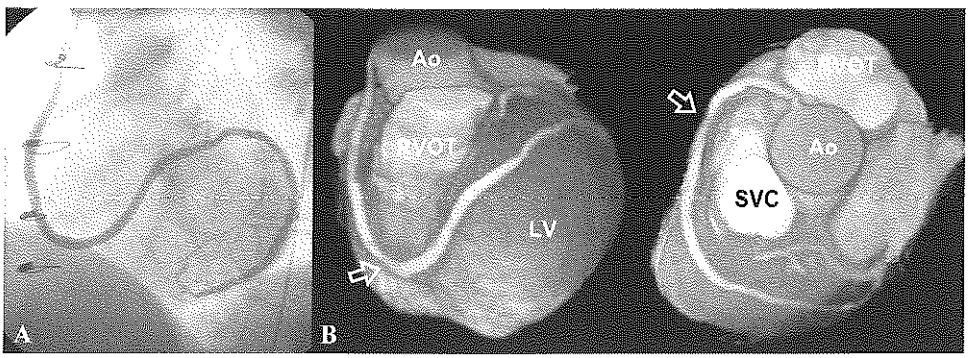

Figure 21. *(A) Another CA view of the same venous jump coronary bypass graft as demonstrated in Figure 8.* ***(B)*** *Two volume-rendered views of the retrospective navigator 3D MRCAscan demonstrate the entire course of the coronary artery bypass grafts (CABG) from the aorta crossing over the right ventricular outflow track (RVOT) towards the left anterior descending artery. The two arrows indicate the location close to the sternal wires that create some artefactual lumen thinning. Two 64-mm slabs were collected with 64 2-mm thick slices per slab (32 scanned) with a FOV of 280 × 320 mm² and a matrix of 128 × 256, TR/TE = 4.8/2.3 ms, time resolution of 154 ms, and data collection time of approximately 28 min. Magnetization transfer contrast preparation and administration of an intravascular-like/liver contrast agent (Endorem, Guerbet, Paris, France) were included to increase contrast between myocardium and blood. Note the signal attenuation from the surface coil towards the end of the graft. Ao aorta; LV left ventricle; SVC superior vena cava.*

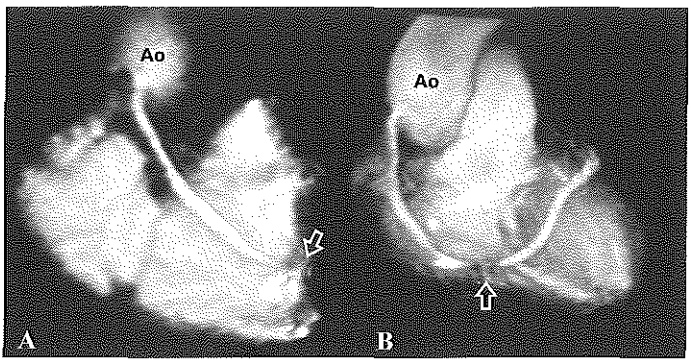

Figure 22A, B. *Two VCATS examples using two planes to depict a large portion of the venous jump CABG on the same patient as in Figure 21. Note that a similar stenosis arises from the proximity of the sternal wires (arrows), more accentuated in this case due to the slightly larger voxel acquired and a partial Fourier reconstruction. Scanning parameters as in Figure 17. Ao aorta*

graft lumen. In an early investigation by White et al.,[74] a sensitivity and a specificity of 86% and 59%, respectively, were reported. However, remnant signal in cases of stenosis from slow-flowing blood could lead to false negatives. With increasing experience and the incorporation of cine GRE techniques, many investigators obtained improved sensitivity and specificity for bypass patency but did not look into the presence of stenosis (see Table 2).[75,76] Using retrospective navigator 3D MRCA, Kessler et al. reported the results on 7 patients with CABGs within a large study on coronary artery stenosis detection, correctly classifying 4 occluded and 13 of 15 patent grafts (Figure 21).[77] Breath-hold acquisitions are becoming more popular because of increased examination speed and patient comfort. Using breath-hold contrastenhanced 3D GRE imaging, Vrachliotis et al.[78] and Wintersperger[79] also demonstrated the high sensitivity and specificity of the contrast-enhanced approach. However, the length of the acquisition window per cardiac cycle (300±500 ms) introduces blurring of those CABG segments close to the heart impairing diagnosis of stenosis. Some CABG stud-

Table 2. Sensitivity, specificity, and accuracy of various techniques in the assessment of coronary artery bypass graft patency as compared with conventional coronary angiography. CE 3DGRE refers to contrast-enhanced 3D GRE scanning during dynamic bolus contrast injection. HASTE half-Fourier acquired single-shot turbo spin echo

Reference	Technique	No. of grafts	No. of patent grafts	Sensitivity (%)	Specificity (%)	Accuracy
2D techniques						
White et al.[69]	SE	72	50	86	59	78
Rubinstein et al.[70]	SE	47	29	90	72	83
Jenkins et al.[72]	SE	41	26	89	73	83
Frija et al.[73]	SE	52	43	98	78	94
Galjee et al.[75]	SE	98	73	98	85	96
White et al.[74]	Cine-GRE	28	14	93	86	89
Aurigemma et al.[76]	Cine-GRE	45	33	88	100	91
Galjee et al.[75]	Cine-GRE	98	73	98	88	96
Kalden et al.[81]	2D HASTE	59	44	95	93	95
3D techniques						
Vrachliotis et al.[78]	CE 3D GRE	44	29	93	97	95
Wintersperger et al.[79]	CE 3D GRE	76	60	95	81	92
Kalden et al.[81]	CE 3D GRE	59	44	93	93	93

ies have been performed that do not require the administration of contrast, as previously shown with breath-hold 2D MRCA[80] and more recently with thin slab 3D breath-hold scans (Figure 22). A report combining both breath-hold black-blood fast SE (HASTE) and contrast-enhanced 3D imaging was performed recently by Kalden et al. on 22 patients (59 grafts).[81] Black-blood HASTE provided 95% and 93% for sensitivity and specificity for detection, respectively, with similar results for contrast-enhanced 3D angiography (94%). The shorter acquisition in blackblood HASTE sequence could reveal better patent distal graft anastomoses. A relevant example of this technique is shown in Figure 8.

DISCUSSION

Coronary visualization

Presently, the coronary arteries can be routinely visualized with many MRCA techniques; however, drawbacks inherent to MRI must be considered that can significantly impair image quality and diagnosis. Typical noncontrast enhanced bright-blood MRCA suffers from the same common ailments. Fat suppression (or selective water excitation) is performed to obtain the high contrast necessary to observe the coronary arteries surrounded in most of their course by pericardial fat. Fat suppression can be cumbersome to achieve over the entire heart or the thorax because of the extensive presence of air-tissue interfaces and also from the possible presence of neighboring metallic objects such as sternal wires. The geometry of the heart and the thorax also plays a role in defining a region of good magnetic homogeneity, but this issue has yet to be addressed adequately (e. g., long vs short thorax). Most likely some coronary segments will be problematic to image and localized shimming per region of interest will be necessary to ensure homogeneous fat suppression.

Coronary arteries cannot be visualized well if SNR is poor. Low-bandwidth readouts, of the order of 100-200 Hz/pixel for 2D MRCA, are used to counteract poor SNR. Nonetheless, fat chemical shift can produce enhancement or attenuation in the coronary arteries and surroundings with poor fat signal reduction. Particular choices of TE that lead to an opposed-phase behavior for fat (producing periodic reductions in its signal, e. g., at TE = 2.38 ms, TE = 7.14 ms, for 1.5 T) can help to increase contrast and to delineate the coronary vessel. Yet, a signal cancellation at fat-vessel boundaries always occurs and low-resolution scans can introduce artefactual vessel thinning leading to a false stenosis (e. g., coronary segments of the order of one pixel may appear as black lines). Another issue is the sensitivity of a technique to provide good resolution and adequate contrast for stenosis detection. In general, 2D MRCA uses long TE. Long TE can help in the detection of high-grade stenotic regions (> 70%) by leaving a small signal void trace that can be used as an indicator to a problematic region when resolution is not adequate (large voxel sizes). Generation of signal voids at longer TEs is not precisely desired, but the additional contrast between vessel wall or plaque and vessel lumen that could be obtained for enhanced differentiation is. At short TE, plaque may be indistinguishable from vessel lumen even in cases of stenosis. A downside to the better contrast is that longer TE slows down data collection because of increasing TR. Geometric distortions and signal loss induced by poor magnetic field homogeneity created by metallic materials, such as stents, sternal wires, etc., can obscure a coronary vessel (or CABGs) completely, requiring the use of shorter TE. Therefore, the issue of TE selection is a cumbersome one, and as a result of the gradient hardware improvements that lead to faster data collection, TEs between 1.8 and 2.7 ms are selected just to obtain the opposite-phase

behavior of fat and a short TR while contrast enhancement between plaque and wall and coronary lumen is generated using the previously discussed MT preparation schemes or T1-sensitive sequences after administration of contrast agents. Black-blood MRCA techniques (Fast SE based, 2D and thin-slice 3D), as shown in Figure 7, can be considered robust when looking at all problems described herein. Only cases with slow blood flow might be considered difficult to interpret. Nevertheless, the appearance of vessel lumen signal indicates that velocities may be abnormal and attention should focus in that region.

Interpretation difficulties

Primarily, SNR limits the effective spatial resolution achieveable with 2D and 3D breath-hold MRCA. Breath-hold 2D MRCA requires considerable experience in making the correct assumptions in potentially problematic regions to recognize real from artefactual information. The localization of focal coronary stenoses can only be indirectly perceived through signal fluctuations along the vessel path created by flow dephasing arising from turbulent flow behavior. However, false stenoses may be induced during the review process in cases of tortuous coronary arteries and poor breathhold reproducibility. Blood-signal saturation could be used as an indicator to poor blood-flow refreshment or complete occlusion, but this does not play a significant role for stenosis detection (see further on the issue of dynamic imaging) unless scans are performed perpendicular to the vessel path to enhance inflow effects. Other interpretation difficulties can arise. Heart motion, beat-to-beat variations, or poor breath-hold can significantly blur vessel detail. Differentiation between arteries and veins can be difficult, especially between the LAD and LCX from the great cardiac vein in distal segments.[82] The pericardial sac can appear as a linear structure with medium to high signal intensity similar to a coronary artery. Fluid in the superior pericardial recess (running posterior to the aortic root) may show as a linear structure joining the proximal LAD, making it appear as a continuation of the vessel itself. All these difficulties have been reviewed in depth by Duerinckx et al.[83] for 2D MRCA and are equally applicable to any non-contrast-enhanced bright-blood MRCA technique.

Role of dynamic imaging

Unfortunately, non-contrast-enhanced MRCA may not be as reliable an examination as initially envisioned even with perfect fat suppression and advanced gradient and signal reception hardware. As mentioned previously, non-contrast-enhanced MRCA can be considered mainly a proton-density-weighted examination for all tissues, but the signal from chemically shift suppressed fat. The reason for having a proton-density-weighted contrast is a direct consequence of the wait interval introduced by the cardiac synchronization necessary for each segment of data collected. Therefore, the signal from stagnant blood, blood clot, or plaque can recover completely and appear as integral part of coronary artery (appearing isointense), especially when SNR and resolution are not sufficient or adequate. This creates a difficulty in interpretation because of poor tissue discrimination, as exemplified in Figs. 23 and 24 from our experience, also noted by others,[84] using thin-slab 3D MRCA scans and 2D MRCA with vessels in the plane of section. This is the reason why for 2D MRCA, stenosis could be better seen with additional 2D thin slices acquired perpendicular to the coronary artery lumen.[38,39] The use of magnetization-prepared contrast in the form of MTC or T2 preparation can be helpful in such instances to produce the necessary differentiation, but this has yet to be shown. To tackle this differentiation prob-

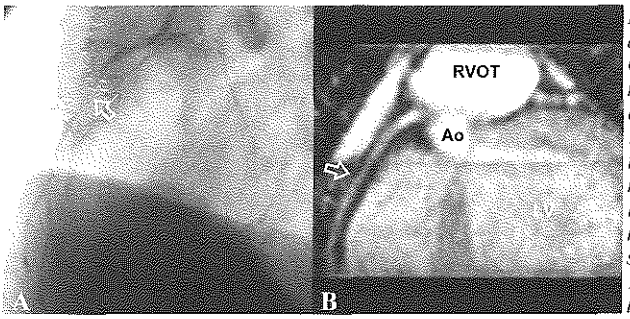

Figure 23A, B. *Patient presenting a complete occlusion of the RCA on CA* ***(A)*** *appears as normal after multiplanar reconstruction analysis of a retrospective navigator 3D MRCA scan* ***(B).*** *Arrow in a points to a severe narrowing of the RCA, not seen clearly in B despite good image quality but with a slight but noticeable decrease in signal intensity. Scan parameters as in Figure 14. Ao Aorta; RVOTright ventricular outflow track; LV left ventricle.*

lem, enhancement of a coronary segment could be monitored more closely using some form of dynamic information, similar to what can be seen in CA. One way to achieve this is by using the intrinsic contrast possible by blood motion itself through blood-tagging MRCA techniques such as reported by Edelman et al.[85] and Wang et al.[86] These techniques can tag selectively blood at the aortic root to observe blood moving into the coronary arteries after an appropriate delay between tag and imaging is selected. Subtraction is performed from an untagged blood image, collected interleaved with the tagged one. This removes interfering fat and myocardium to produce an image of only tagged blood flowing into the coronary arteries. Tagging and inflow delay selection require some experience to visualize a large portion of the coronary arteries and image quality can vary substantially depending on the range of blood flow velocities present and the fraction of tagged blood that flows into the coronary arteries. Dynamic imaging during the injection of a contrast agent using a short TR/TE T1-weighted 2D or smallslab 3D GRE or segmented EPI scan could provide a more adequate answer to the problem by providing better SNR and speed. By observing dynamically the enhancement of the vessels of interest, those vessels that are poorly enhanced or show noticeable discontinuities in their enhancement pattern are indicative of problems. The enhancement process is better observed after subtraction of a pre-contrast frame. One of several reports has investigated the role of a 2D projective-subtraction method.[87]

FUTURE DIRECTIONS

Dedicated MR cardiac scanners

The majority of MRI manufacturers of high-field systems now offer dedicated cardiac scanners with strong imaging gradients (> 30 mT/m) and fast rise times (> 150 mT/m per millisecond) optimized for a smaller effective imaging field of view to

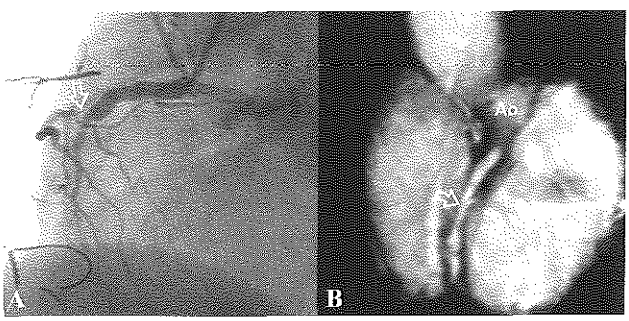

Figure 24A, B. *Another example of severe disease of the RCA comparing CA* ***(A)*** *with a volume-rendered image of a breath-hold VCATS collected tangential to the midRCA segment* ***(B).*** *While CA demonstrates an abnormal course with multiple stenotic regions after the first right ventricular branch (arrow), VCATS illustrates a vessel with abnormal signal indicating the presence of disease but with misleading lumen size. This may be consequent to remnant signal from plaque and coronary vessel wall in a scan which is mostly proton-density weighted. Scan parameters as in Figure 17. Ao aorta.*

provide speed with a higher peripheral nerve stimulation threshold. The ever-increasing addition of an arsenal of measurement tools may soon prove to encompass all that was always envisioned for an integral evaluation of the heart and the coronary arteries. These tools include real-time capabilities with interactive platforms for measurement setup (including 3D steering devices) and evaluation.[88-91] The implementation of parallel imaging strategies that dramatically shorten image acquisition times per cardiac frame may also become available on all these systems.[92] This would make it possible to evaluate the heart function and perhaps the coronary arteries with exquisite temporal resolution (not requiring ECG triggering) and spatial resolution that rivals that of ultrasound both in flexibility and image quality. This may bypass some of ultrasound's measurement disadvantages such as finding a good acoustic window, ultrasound beam attenuation, and obstacles as with chest wall interference and intervening pulmonary parenchyma.[93]

Yet some issues must be addressed before dedicated scanners enter routine clinical practice for MRCA. Breath-hold or free-breathing MRCA (or a combination of both) is still under debate to solve in a reliable and time-efficient fashion the majority of coronary cases. At this moment improvements in slice-position correction methods and special encoding schemes in free-breathing MRCA using prospective navigator gating seem sufficiently robust to adjust to every type of respiratory motion pattern and permit adequate resolution for stenosis evaluation. Research in many institutions and innumerable modifications to current MRCA techniques have marked a pace in the past 2 years to search for that reasonable balance between available and future improvements. Another important point is to provide the appropriate SNR-scanning time relationship to achieve the target resolution for stenosis quantification in short imaging times. The SNR is still a problem for high-resolution imaging at 1.5 T with phased-array coil technology. The recent introduction of 3-T whole-body systems may mark an important step for MRCA in conjunction with the commercial introduction of intravascular contrast agents. Because of SNR restrictions, scanners may not require the faster imaging gradients now available but just an 'intelligent' setup that optimizes scanning possibilities with currently available technology.

Processing power is still a major concern in current scanners, e. g., scans may take much longer to reconstruct than the actual data collection time (e.g., breathhold scans of approximately 20 s taking a minute to process before review). It is clear, however, that real-time interactive MRI will set the new pace for enhanced system platforms with better processing speed, flexibility for dynamic display, volume rendering, and data evaluation. Nevertheless, we feel that soon enough cardiac MR systems will take shape to satisfy cardiologists and provide an easy setup and the acquisition flexibility that is current in ultrasound examinations.

Intravascular contrast agents

The dramatic T1 shortening possible in blood with dynamic injections of gadolinium chelates (< 50 ms) in combination with ultrafast GRE techniques has yielded high-quality breath-hold MRA. However, providing a specific concentration to obtain consistent T1 shortening in blood is difficult because it depends on many parameters (e. g., physiology and injection settings). Furthermore, for MRCA, a single breath-hold and injection may prove inadequate for complete coverage of the coronary tree. Examination success is also measured by patient cooperation. Gadolinium (Gd) chelates and ultrasmall superparamagnetic iron particles (USPIO) as intravascular contrast agents are being tested with long blood half-lives (~ 1-2 h) with

hopes of providing the long-awaited essential boost for MRCA.[94-97] This includes agents such as Angiomark (MS-325, Gd-based, Epix Medical, Massachusetts, USA) and Clariscan (NC100150, Nycomed-Amersham, Oslo, Norway). However, it is difficult to draw conclusions about the present utility of these intravascular contrast agents which will soon enter the market if used for MRCA studies alone. Undoubtedly, the success of any intravascular contrast agents will happen once the barriers of contrast and SNR are achieved specifically for T1-weighted MRCA sequences with considerable suppression of the fat signal. This will only occur whenever the T1 relaxation in blood comes close to 50 ms or less and preferably using a 3D imaging sequence.

The choice of contrast agent used, Gd-based or USPIO, should not matter for the application. Both types can reduce the effective T1 of blood to values < 100 ms; however, Gd-based agents are presumably more advantageous than USPIO contrast agents because they maintain a longer T2* in blood with similar T1 shortening, thus reducing the constraints over how short TE must be before signal from blood decays (a special consideration for EPI scans). Contrast agents, such as dysprosium or superparamagnetic iron oxide particles (SPIO),[98] can also be effective to shorten T2* even further and can be used for blood signal suppression in coronary arteries for black-blood imaging. It must only be taken into account that myocardial perfusion imaging may be a routine part of a coronary examination, and first-pass injection of a bolus of the contrast agent chosen should be possible.

In summary, the success of a contrast agent will be strongly coupled to the MRCA technique chosen. We must consider three working regimes of vascular signal in bright-blood MRCA. Most of the scans usually performed for MRCA are proton-density weighted with the exclusion of the chemical shift fat-suppression pulse and any form of magnetization preparation (MTC, T2 prep). When inflow is present, blood signal for each data collection is completely recovered in the region of interest. In the case that no inflow is present, blood can recover substantially according to the time between the last RF pulse executed on the previous heartbeat and the first on the subsequent heartbeat. For proton-density-weighted 3D MRCA scans with large-volume coverage, it is only necessary to achieve uniform chemical shift fat suppression over the entire heart, and that blood, recovers completely before acquisition occurs on every heartbeat. To speed up the magnetization recovery of blood the administration of already approved contrast agents, such as Endorem (Guerbet, Paris, France; Feridex, Advanced Magnetics, Massachu-

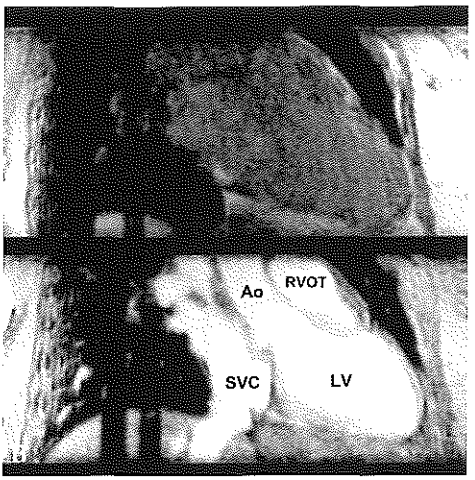

Figure 25A, B. *With large volume scanning significant blood saturation occurs even with proton-density weighted contrast 3D MRCA scans with data collection on every heartbeat. A retrospective navigator MRCA was acquired covering the entire heart* ***(A)*** *prior to and* ***(B)*** *after administration of a liver contrast agent (Endorem, Guerbet, Paris, France), a large superparamagnetic ironoxide particle (SPIO) contrast agent remaining approximately 10-20 % intravascular. The addition of Endorem makes signal from blood uniform in all blood-filled compartments and permits structure differentiation. Ao aorta; RVOT right ventricular outflow track; SVC superior vena cava; LV left ventricle.*

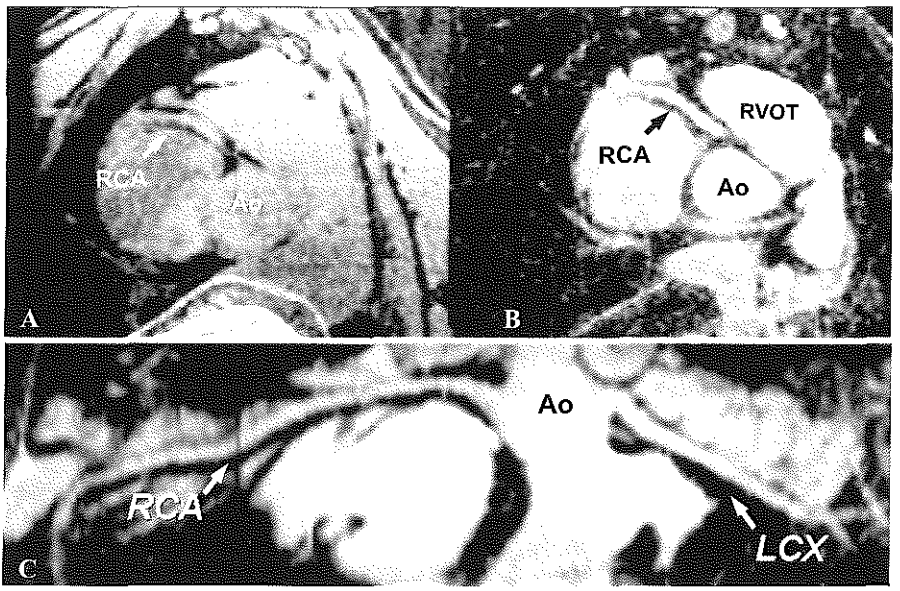

Figure 26. A, B *The effect of an intravascular contrast agent Gadomer-17 (Schering, Berlin, Germany) in improving visualization of coronary arteries in a pig. The left and right images were acquired before and after administration of Gadomer-17 (dose: 0.05 mmol/kg), respectively. A retrospective navigator 3D MRCA scan was used with a spatial resolution of 1 x 1 x 2 mm³. The SNR at the RCA was increased by a factor > 2 after contrast administration using an inversion pulse prior to signal acquisition to null the myocardium.* ***(C)*** *Curved multiplanar reconstruction of the contrast-enhanced data set, showing good delineation of both RCA and LCX. Ao aorta; RCA right coronary artery; LCX left circumflex; RVOT right ventricular outflow track. (Images courtesy of Dr Debiao Li, Northwestern University, Chicago, USA).*

setts) or Gd-DTPA, can ensure a uniform signal recovery for blood in all vascular compartments (Figure 25). For Endorem, the SPIO accumulates for 80-90% in the liver and spleen,[99] whereas a 10-20% fraction remains intravascular with a mild T1 relaxation during steady state (T1 relaxivity ~ 400-600 ms) and a long half-life.[100] Such agent is not necessary for 2D or thin-slab 3D MRCA. The last regime is that of T1-weighted scanning, to which all comments stated at the beginning of this section apply in this case (Figure 26).

These three regimes have been well described and analyzed by Johansson et al., simulating achievable contrasts and SNRs possible for different T1 characteristics of blood.[101] We encourage the reader to explore this reference as it is of major importance in the understanding of the effect of contrast agents for MRCA.

Cardiac triggering

Many cardiac examinations are hampered by suboptimal and inconsistent ECG triggering. Cardiac lead placement can be cumbersome in some cases and a good ECG trace is not guaranteed once the patient is moved into the magnet bore. Therefore, the setting process can be time-consuming if reposition is necessary and can take a considerable part of the cardiac examination time. Furthermore, with faster gradient switching ECG is frequently perturbed by voltages induced between the electrodes and on the cable-carrying signals between the electrodes and the ECG monitoring unit.

This may cause possible mistriggering, threatening to produce bad-quality images especially in first-pass contrast-enhanced 3D studies using increased high-amplitude gradient activity. The perturbation is also sequence and orientation dependent. One

solution provided by some manufacturers is an ECG system in which certain derivation can be selected at will that produces the best ECG tracing. Nevertheless, this does not guarantee complete elimination of the interference created by the gradient switching and newly developed optical ECG devices have started to appear on the market.[102] These devices amplify the ECG signal close to the reception electrodes and send the analog signal via fiber optics to the patient-monitoring unit. These devices have proven robust even with EPI acquisitions[103] and will be available with future cardiac-dedicated MRI units. Another solution proposed by Vasanawala et al.[104] uses a more exotic approach mapping the velocity profile in the aorta using a velocity-sensitive navigator echo and producing a trigger signal in real-time upon a predefined criterion in an interactive platform. A reproducibility study and quality assessment in comparison with the more conventional ECG triggering approach has proven consistent and has been judged to produce better overall image quality. The use of pulse monitoring can also be used to obtain better image quality in cases of mistriggering with standard ECG reception and processing.

Imaging of the coronary artery wall

A major challenge for MRI of the coronary arteries is to image the coronary artery wall. Coronary artery stenosis can arise from a stable atherosclerotic plaque which contains mainly fibrous tissue and calcium or a vulnerable plaque containing a large lipid core covered by a thin fibrous cap. This cannot be differentiated by CA and the vulnerable plaques are the ones that are important to detect as they are the reason that myocardial infarction occurs after the fibrous cup ruptures and a subsequent intravascular thrombus develops and blocks the coronary artery. The MRI and MRA techniques can contribute greatly by providing a more realistic picture of the problem and an answer to tissue characterization.[105] Unfortunately, SNR presently is not sufficient to visualize the coronary wall at high resolution in free-breathing examinations and less so for breath-hold acquisitions.

Attempts to produce coronary artery wall images have been presented by McConnell et al.[9] and Meyer et al.[28] using black-blood techniques. New developments in invasive MRI using intravascular catheter MR probes may overcome the SNR barrier now imposed to vessel imaging away from externally placed coils and provide some definitive answers to study more closely atherosclerosis.[106,107]

Parallel image-encoding techniques: fast techniques made ultrafast

Faster imaging is always possible by increasing the speed at which data is encoded. This is generally done by increasing readout bandwidth (stronger gradients) and minimizing gradient switching times to achieve shorter TRs (faster rise times). Nevertheless, the conventional sequential spin-warp phase-encoding process of one raw data line per readout event still proves to be the time-consuming process for extended coverage and resolution for MRCA scans. An additional speed-up factor can be achieved for any type of imaging sequence that uses spin-warp encoding (more recently studied for other k-space trajectories e. g, spirals) when multiple RF coils are used for signal reception. In principle, the idea is straightforward when bearing in mind that a coil has a limited reception region according to its specific coil sensitivity and can be precisely localized in space. It is this signal localization that can be used as an additional calculation variable to accelerate data acquisition. The concept to use the inherent spatial location of a coil in an array to reduce acquisition time has been proposed previously; however, a more elegant and recent redefinition of the concept

has appeared under the acronyms SMASH (simultaneous acquisition of spatial harmonics) imaging.[108] The spatial localization of the coil reception pattern can be made inherent to the data collected, making it possible to parallelize the conventional phase-encoding process when the phase-encoding direction is chosen, e. g., along the long axis of the coil array. SENSE (sensitivity encoding), another way to accelerate acquisition using the same principle, uses a more general formulation to solve the problem that does not the require that coils be located along the phase-encoding direction as in SMASH.[109]

The acquisition speed improvements offered by these parallel imaging techniques can be used in several ways, including constant resolution with shorter breathhold times or improved resolution, otherwise with presently used scanning times.[110]

CONCLUSION

Magnetic resonance coronary angiography has come a long way since the start of MR cardiac applications, reinforced by the fact that excellent images of the coronary arteries can be acquired. However, at this stage, no MRCA technique has yet fully proven reliable for coronary stenosis detection to be available for routine clinical work-up in the near future. The role of contrast agents for SNR and contrast enhancement is clear for contrast-enhanced MR angiography but does not yet provide the definite answer to reliability and reproducibility for MRCA. The introduction of dedicated MR cardiac scanners with high gradients and short rise times in conjunction with intravascular contrast agents with ultrashort T1 (of the order of 25 ms or less) may dictate the definite fate of MRCA in the coming years. Nevertheless, most MRCA techniques are still invaluable in clinical practice for a non-invasive, general view of the coronary system. The techniques can map the course of anomalous coronary arteries and question the patency of coronary artery bypass grafts and has proven to be a valid screening tool in young patients with unexplained arrhythmias or syncope during exercise. At present, second-generation MRCAtechniques are still under scrutiny but with a clear tendency to favor prospective navigator rather than retrospective navigator MRCA. Third-generation MRCA techniques are making their way to trials with stronger and fast imaging gradients, and may soon appear in trials linked with intravascular contrast agents. We conclude that it is still the practical goal of any MRCA technique to be reliable enough to provide a 'true' isotropic resolution with 1 mm^3 voxels for any coronary segment of interest. With adequate contrast, this resolution should make it possible to visualize hemodynamically significant stenoses.

Internet links to cardiac-related sites

Scientific communication is becoming increasingly popular using the World Wide Web (WWW) as a means to stay informed on the happenings around the MR cardiac community. Some institutions have made their internal websites public to illustrate ongoing research in the field of MRCA and related topics. Many locations exist with scattered data that can be accessed using key words such as, e. g., 'coronary MR angiography' or 'cardiac MRI' in the input of the many available web search engines. The URL that we found that is of special interest on the current image quality achievable with MRCA and other cardiac-related studies is http://www.bidmc.harvard.edu/cmr/cmr-network.html This URL provides links to other sites of interest. We encourage the use of the Internet to show current examples comparing CA with MRCA, successful and unsuccessful to help increase awareness on the problems and possible solutions that may be of interest to solve for the more technically oriented MR cardiac community.

REFERENCES

1. Haase A, Matthaei D, Bartkowski E, Duhmke E, Leibfritz D (1989) Inversion recovery snapshot FLASH MR imaging. J Comput Assist Tomogr 13: 1036-1040
2. Matthaei D, Haase A, Henrich D, Duhmke E (1990) Cardiac and vascular imaging with an MRsnapshot technique. Radiology 177: 527-532
3. Henrich D, Haase A, Matthaei D (1990) 3D-snapshot flash NMR imaging of the human heart. Magn Reson Imaging 8: 377-379
4. Edelman RR, Wallner B, Singer A, Atkinson DJ, Saini S (1990) Segmented turboFLASH: method for breath-hold MR imaging of the liver with flexible contrast. Radiology 177: 515-521
5. Atkinson DJ, Edelman RR (1991) Cineangiography of the heart in a single breath hold with a segmented turboFLASH sequence. Radiology 178: 357-360
6. Edelman RR, Manning WJ, Burnstein D, Paulin S (1991) Coronary arteries: breath-hold MR angiography. Radiology 181: 641-643
7. Meyer CH, Hu B, Nishimura DG, Macovski A (1992) Fast spiral coronary artery imaging. Magn Reson Med 28: 202-213
8. Simonetti OP, Finn JP, White RD, Laub G, Henry DA (1996) 'Black blood' T2-weighted inversion-recovery MR imaging of the heart. Radiology 199: 49-57
9. McConnell MV, Goldfarb JW, Manning WJ, Edelman RR (1997) High-resolution black-blood coronary MR imaging using navigator gating [Abstract]. In: Book of Abstracts of the 5th Meeting of the International Society of Magnetic Resonance in Medicine (ISMRM) 2: 797
10. Wielopolski PA, Manning WJ, Edelman RR (1995) Breathhold volumetric imaging of the heart using magnetization prepared 3D segmented echo planar imaging. J Magn Reson Imaging 4: 403-409
11. Jakob PM, Hillenbrand C, Sandstede J, Kenn W, Pabst T, Hahn D, Haase A (1999) MR-Cat scan: cardiac imaging with a new hybrid approach [Abstract]. In: Book of Abstracts of the 7th Meeting of the International Society of Magnetic Resonance in Medicine (ISMRM) 2: 1306
12. Paulin S, Schulthess GK von, Fossel E, Krayenbuenhl HP (1987) MR imaging of the aortic root and proximal coronary arteries. AJR 148: 665-670
13. Stehling MK, Holzknecht NG, Laub G, Bohm D, Smekal A von, Reiser M (1996) Single-shot T1- and T2-weighted magnetic resonance imaging of the heart with black blood: preliminary experience. MAGMA 4: 231-240
14. Edelman RR, Chien D, Kim D (1991) Fast selective black blood MR imaging. Radiology 181: 655-660
15. Ducrinckx AJ (1999) Coronary MR angiography. Radiol Clin North Am 37: 273-318
16. Paschal CB, Haacke EM, Adler LP (1993) Three-dimensional MR imaging of the coronary arteries: preliminary clinical experience. J Magn Reson Imaging 3: 491-500
17. Li D, Paschal CB, Haacke EM, Adler LP (1993) Coronary arteries: three-dimensional MR imaging with fat saturation and magnetization transfer contrast. Radiology 187: 401-406
18. McConnell MV, Khasgiwala VC, Savord BJ, Chen MH, Chuang ML, Edelman RR, Manning WJ (1997) Comparison of respiratory suppression methods and navigator locations for MR coronary angiography. AJR 168: 1369-1375
19. Hofman MBM, Paschal CB, Li D, Haacke EM, Van Rossum AC, Sprenger M (1995) MRI of coronary arteries, 2D breathhold versus 3D respiratory-gated acquisition. J Comput Assist Tomogr 19: 56-62
20. Li D, Kaushikkar S, Haacke EM, Woodard PK, Dhawale P, Kroeker RM, Laub G, Kuginuki Y, Gutierrez FR (1996) Three-dimensional imaging of coronary arteries with retrospective respiratory gating. Radiology 201: 857-863
21. Oshinski JN, Hofland L, Mukundan S Jr, Dixon WT, Parks WJ, Pettigrew RI (1996) Two-dimensional coronary MR angiography without breath holding. Radiology 201: 737-743
22. Wang Y, Rossman PJ, Grimm RC, Riederer SJ, Ehman RL (1996) Navigator-echo-based real-time respiratory gating and triggering for reduction of respiration effects in three-dimensional coronary MR angiography.

Radiology 198: 55-60
23. Thedens DR, Irarrazaval P, Sachs TS, Meyer CH, Nishimura DG (1999) Fast magnetic resonance coronary angiography with a three-dimensional stack of spirals trajectory. Magn Reson Med 41: 1170-1179
24. Irarrazabal P, Nishimura DG (1995) Fast three-dimensional magnetic resonance imaging. Magn Reson Med 33: 656-662
25. Stuber M, Botnar R, Danias PG, Sodickson DK, Kissinger KV, van Cauteren M, Becker J de, Manning WJ (1999) Double-oblique-breathing high resolution three-dimensional coronary magnetic resonance angiography. J Am Coll Cardiol 34: 524-531
26. Wielopolski PA, van Geuns RJ, de Feyter PJ, Oudkerk M (1998) Breath-hold coronary MR angiography with volume targeted imaging. Radiology 209: 209-219
27. Slavin GS, Riederer SJ, Ehman RL (1998) Two-dimensional multishot echo-planar coronary MR angiography. Magn Reson Med 40: 883-889
28. Meyer CH, Hu BS, Yang PC, McConnell MV, Kerr AB, Brittain JH, Pauly JM, Macovski A, Nishimura D (1999) Spiral cardiac imaging with high-performance gradients [Abstract]. In: Book of Abstracts of the 7th Meeting of the International Society of Magnetic Resonance in Medicine (ISMRM) 1: 389
29. Wang Y, Christy PS, Korosec FR, Alley MT, Grist TM, Polzin JA, Mistretta CA (1995) Coronary MRI with a respiratory feedback monitor: the 2D imaging case. Magn Reson Med 33: 116-121
30. McConnell MV, Khasgiwala VC, Savord BJ, Chen MH, Chuang ML, Edelman RR, Manning WJ (1997) Prospective adaptive navigator correction for breath-hold MR coronary angiography. Magn Reson Med 37: 148-152
31. Danias PG, McConnell MV, Khasgiwala VC, Chuang ML, Edelman RR, Manning WJ (1997) Prospective navigator correction of image position for coronary MRangiography. Radiology 203: 733-736
32. Keegan J, Gatehouse PD, Taylor AM, Yang GZ, Jhooti P, Firmin DN (1999) Coronary artery imaging in a 0.5-Tesla scanner: implementation of real-time, navigator echo-controlled segmented k-space FLASH and interleaved-spiral sequences. Magn Reson Med 41: 392-399
33. Wang Y, Grimm RC, Rossman PJ, Debbins JP, Riederer SJ, Ehman RL (1995) 3D coronary MR angiography in multiple breath-holds using a respiratory feedback monitor. Magn Reson Med 34: 11-16
34. Taylor AM, Keegan J, Jhooti P, Gatehouse PD, Firmin DN, Pennell DJ (1999) Differences between normal subjects and patients with coronary artery disease for three different MR coronary angiography respiratory suppression techniques. J Magn Reson Imaging 9: 786-793
35. Brittain JH, Hu BS, Wright GA, Meyer CH, Macovski A, Nishimura DG (1995) Coronary angiography with magnetization-prepared T2 contrast. Magn Reson Med 33: 689-696
36. Botnar RM, Stuber M, Danias PG, Kissinger KV, Manning WJ (1999) Improved coronary artery definition with T2-weighted, free-breathing, three-dimensional coronary MRA. Circulation 22: 3139-3148
37. Brittain JH, Olcott EW, Szuba A, Gold GE, Wright GA, Irarrazaval P, Nishimura DG (1997) Three-dimensional flow-in-dependent peripheral angiography. Magn Reson Med 38: 343-354
38. Manning WJ, Li W, Boyle NG, Edelman RR (1993) Fat-suppressed breath-hold magnetic resonance coronary angiography. Circulation 87: 94-104
39. Manning WJ, Li W, Edelman RR (1993) A preliminary report comparing magnetic resonance coronary angiography with conventional angiography. N Engl J Med 328: 828-832
40. Manning WJ, Li W, Wielopolski P, Gaa J, Kannam JP, Edelman RR (1994) Magnetic resonance coronary angiography: comparison with contrast angiography [Abstract]. In: Book of Abstracts of the 2nd Meeting of the Society of Magnetic Resonance (SMR)1: 368
41. Duerinckx AJ, Urman MK (1994) Two-dimensional coronary MR angiography: analysis of initial clinical results. Radiology 193: 731-738
42. Pennell DJ, Keegan J, Firmin DN, Gatehouse PD, Underwood SR, Longmore DB (1993) Magnetic resonance imaging of coronary

arteries: technique and preliminary results. Br Heart J 70: 315-326
43. Post JC, Rossum AC van, Hofman MBM, De Cock CC, Valk J, Visser CA (1997) Clinical utility of two-dimensional breath-hold MR angiography in detecting coronary artery disease. Eur Heart J 18: 426-433
44. Yoshino H, Nitatori T, Kachi E, Yano K, Taniuchi M, Hachiya J, Ishikawa K (1997) Directed proximal magnetic resonance coronary angiography compared with conventional contrast coronary angiography. Am J Cardiol 80: 514-518
45. Post JC, van Rossum AC, Hofman MB, Valk J, Visser CA (1996) Three-dimensional respiratory-gated MR angiography of coronary arteries: comparison with conventional coronary angiography. AJR 166: 1399-1404
46 Müller MF, Fleisch M, Kroeker R, Chatterjee T, Meier B, Vock P (1997) Proximal coronary stenosis: three-dimensional MRI with fat saturation and navigator echo. J Magn Reson Imaging 7: 644-651
47. Huber A, Nikolaou K, Gonschior P, Knez A, Stehling M, Reiser M (1999) Navigator echo-based respiratory gating for three-dimensional MR coronary angiography: results from healthy volunteers and patients with proximal coronary artery stenoses. AJR 173: 95-101
48. Van Geuns RJM, de Bruin HG, Rensing BJWM, Wielopolski PA, Hulshoff MD, van Ooijen PMA, Oudkerk M, de Feyter PJ (1999) MRI of the coronary arteries: clinical results from three-dimensional evaluation of a respiratory gated technique. Heart 82: 515-519
49. Stehling MK, Balci C, Reiser M (1997) Navigator echo coronary MRA: controversial results [Abstract]. In: Book of Abstracts of the 5th Meeting of the International Society of Magnetic Resonance in Medicine (ISMRM) 2: 911
50. Lethimonnier F, Furber A, Morel O, Geslin P, Hoste PL, Tadei A, Jallet P, Caron-Poitreau C, Le Jeune JJ (1999) 3D MR coronary artery imaging with prospective real-time respiratory navigator: comparison with conventional coronary angiography [Abstract]. In: Book of Abstracts of the 7th Meeting of the International Society of Magnetic Resonance in Medicine 51. Jhooti P, Keegan J, Gatehouse PD, Collins S, Rowe A, Taylor AM, Firmin DN (1999) 3D coronary artery imaging with phase reordering for improved scan efficiency. Magn Reson Med 41: 555-562
52. Yang GZ, Burger P, Gatehouse PD, Firmin DN(1999) Locally focused 3D coronary imaging using volume-selective RF excitation. Magn Reson Med 41: 171-178
53. Haacke EM, Patrick JL (1986) Reducing motion artifacts in two-dimensional Fourier transform imaging. Magn Reson Imaging 4: 359-376
54. Beek GM, Li D, Haacke EM, Noll TG, Kreitner KF, Voigtländer T, Schreiber WG, Thelen M (1999) Three-dimensional MR coronary angiography with a segmented echo-planar sequence and retrospective respiratory gating [Abstract]. In: Book of Abstracts of the 7th Meeting of the International Society of Magnetic Resonance in Medicine (ISMRM) 2: 1255
55. Botnar R, Stuber M, Kissinger KV, Danias PG, Manning WJ (1999) Free-breathing 3D coronary MRA with a fast TFE-EPI acquisition technique. In: Book of Abstracts of the 7th Meeting of the International Society of Magnetic Resonance in Medicine (ISMRM) 1: 233
56. Hardy CJ, McKinnon GC, Saranathan M (1999) High-resolution coronary artery imaging by adaptive averaging [Abstract]. In: Book of Abstracts of the 7th Meeting of the International Society of Magnetic Resonance in Medicine (ISMRM) 1: 231
57. van Geuns RJM, Wielopolski PA, de Bruin HG, van Ooijen PMA, Oudkerk M, de Feyter PJ (1998) VCATS: Volume coronary angiography using targeted scans, a new strategy in MR coronary angiography. Circulation 98:I-856
58. Wielopolski PA, Scharf JG, Edelman RR (1994) Multislice coronary angiography within a single breath-hold. J Magn Reson Imaging 4(P):80
59. Kessler W, Laub G, Achenbach S, Ropers D, Moshage W, Daniel WG (1999) Coronary arteries: MR angiography with fast contrast-enhanced three-dimensional breath-hold imaging: initial experience. Radiology 210: 566-572
60. Li D, Zheng J, Bae KT, Woodard PK,

Haacke EM (1998) Contrast-enhanced magnetic resonance imaging of the coronary arteries. A review. Invest Radiol 33: 578-586
61. Regenfus M, Ropers D, Achenbach S, Kessler W, Moshage W, Laub G, Daniel WG(1999) Gadolinium-enhanced 3D breath-hold magnetic resonance angiography for detection of coronary artery stenosis in oblique projection angiograms. In: Book of Abstracts of the 7th Meeting of the International Society of Magnetic Resonance in Medicine (ISMRM) 2: 1262
62. Li D, Munger T, Zheng J, Kroeker R, Kim RJ, Simonetti OP, Haacke EM, Finn JP (1999) 3D breath-hold, firs-pass contrast-enhanced coronary artery imaging using MR fluoroscopic triggering, partial k-space acquisition, and inversion recovery. In: Book of Abstracts of the 7th Meeting of the International Society of Magnetic Resonance in Medicine (ISMRM) 2: 1260
63. Danias PG, Stuber M, Botnar RM, Kissinger KV, Chuang ML, Manning WJ (1998) Navigator assessment of breath-hold duration: impact of supplemental oxygen and hyperventilation. AJR 171: 395-397
64. Kimbiris D, Iskandrian AS, Segal BL, Bemis CE (1978) Anomalous aortic origin of coronary arteries. Circulation 58: 606-615
65. Chaitman BR, Lesperance J, Saltiel J, Bourassa MG (1976) Clinical angiographic, and hemodynamic findings in patients with anomalous origin of the coronary arteries. Circulation 53: 122-131
66. Levin DC, Fellows KE, Abrams HL (1978) Hemodynamically significant primary anomalies of the coronary arteries: angiographic aspects. Circulation 58: 25-34
67. McConnell MV, Ganz P, Selwyn AP, Li W, Edelman RR, Manning WJ (1995) Identification of anomalous coronary arteries and their anatomic course by magnetic resonance coronary angiography. Circulation 92: 3158-3162
68. Vliegen HW, Doornbos J, de Roos A, Jukema JW, Bekedam MA, van der Wall EE (1997) Value of fast gradient echo magnetic resonance angiography as an adjunct to coronary arteriography in detecting and confirming the course of clinically significant coronary artery anomalies. Am J Cardiol 79: 773-776
69 White RD, Caputo GR, Mark AS, Modin GW, Higgins CB (1987) Coronary artery bypass graft patency: non-invasive evaluation with MR imaging. Radiology 164: 681-686
70. Rubinstein RI, Askenase AD, Thickman D, Deldman MS, Agarwal JB, Helfant RH (1987) Magnetic resonance imaging to evaluate patency of aortocoronary bypass grafts. Circulation 76: 786-791
71. Gomes AS, Lois JF, Drinkwater DC, Corday SR (1987) Coronary artery bypass grafts: visualization with MR imaging. Radiology 162: 175-179
72. Jenkins JPR, Love HG, Foster CJ, Isherwood I, Rowlands DJ (1988) Detection of coronary artery bypass patency as assessed by magnetic resonance imaging. Br J Radiol 61: 2-4
73. Frija G, Schouman-Claeys E, Lacombe P, Bismuth V, Olivier JP (1989) A study of coronary artery bypass graft patecy using MR imaging. J Comput Assist Tomogr 13: 225-232
74. White RD, Pflugfelder PW, Lipton MJ, Higgins CB (1988) Coronary artery bypass grafts: evaluation of patency with cine MR imaging. AJR 150: 1271-1274
75. Galjee MA, van Rossum AC, Doesburg T, van Eenige MJ, Visser CA (1996) Value of magnetic resonance imaging in assessing patency and function of coronary artery bypass grafts. An angiographically controlled study. Circulation 93: 660-666
76. Aurigemma GP, Reichek N, Axel L, Schiebler M, Harris C, Kressel HY (1989) Noninvasive determination of coronary artery bypass graft patency by cine magnetic resonance imaging. Circulation 80: 1595-1602
77. Kessler W, Achenbach S, Moshage W, Zink D, Kroeker R, Nitz W, Laub G, Bachmann K (1997) Usefulness of respiratory gated magnetic resonance coronary angiography in assessing narrowings ^{3} 50% in diameter in native coronary arteries and in aortocoronary bypass conduits. Am J Cardiol 15: 989-993
78. Vrachliotis TG, Bis KG, Aliabadi D, Shetty AN, Safian R, Simonetti O (1997) Contrast-enhanced breath-hold MR angiography for evaluating patency of coronary artery bypass grafts. AJR 168: 1073-1080
79. Wintersperger BJ, Engelmann MG, Smekal

A von, Knez A, Penzkofer HV, Hofling B, Laub G, Reiser MF (1998) Patency of coronary bypass grafts: assessment with breath-hold contrast-enhanced MR angiography: value of a non-electrocardiographically triggered technique. Radiology 208: 345-51
80. van Rossum AC, Galjee MA, Post JC, Visser CA (1997) A practical approach to MRI of coronary artery bypass graft patency and flow. Int J Cardiac Imaging 13: 199-204
81. Kalden P, Kreitner KF, Wittlinger T, Voigtlander T, Krummenauer F, Kestel J, Thelen MAJR (1999) Assessment of coronary artery bypass grafts: value of different breath-hold MR imaging techniques. AJR 172: 1359-1364
82. van Geuns RJ, Wielopolski PA, Rensing BJ, van Ooijen PM, Oudkerk M, de Feyter PJ (1999) Magnetic resonance imaging of the coronary arteries: anatomy of the coronary arteries and veins in three-dimensional imaging. Coronary Artery Dis 10: 261-267
83. Duerinckx AJ, Atkinson DP, Mintorovitvh J, Simonetti OP, Vrman MK (1996) Two-dimensional coronary MRA: limitations and artifacts. Eur Radiol 6: 312-325
84. Woodard PK, Li D, Haacke EM, Dhawale PJ, Kaushikkar S, Barzilai B, Braverman AC, Ludbrook PA, Weiss AN, Brown JJ, Mirowitz SA, Pilgram TK, Gutierrez FR (1998) Detection of coronary stenosis on source and projection images using three-dimensional MR angiography with retrospective respiratory gating: preliminary experience. AJR 170: 883-888
85. Edelman RR, Siewert B, Adamis M, Gaa J, Laub G, Wielopolski P (1994) Signal targeting with alternating radiofrequency (STAR) sequences: application to MR angiography. Magn Reson Med 31: 233-238
86. Wang SJ, Hu BS, Macovski A, Nishimura DG (1991) Coronary angiography using fast selective inversion recovery. Magn Reson Med 18: 417-42
87. Hennig J, Scheffler K, Laubenberger J, Strecker R (1997) Time-resolved projection angiography after bolus injection of contrast agent. Magn Reson Med 37: 341-345
88. Hardy CJ, Darrow RD, Pauly JM, Kerr AB, Dumoulin CL, Hu BS, Martin KM (1998) Interactive coronary MRI. Magn Reson Med 40: 105-111
89. Weber OM, Eggers H, Spiegel MA, Scheidegger MB, Boernert P, Boesiger P (1999) Interactive real-time MRI for the examination of left ventricular function [Abstract]. In: Book of Abstracts of the 7th Meeting of the International Society of Magnetic Resonance in Medicine (ISMRM) 2: 1299
90. Ridgway JP, Kassner A, Beacock DJ, Sivananthan UM (1999) Fast left ventricular volume measurement using a multipleslice 'real-time' acquisition: a pilot study [Abstract]. In: Book of Abstracts of the 7th Meeting of the International Society of Magnetic Resonance in Medicine (ISMRM) 1: 388
91. Bundy JM, Laub G, Kim R, Finn JP, Simonetti OP (1999) Real-time data acquisition for LV function [Abstract]. In: Book of Abstracts of the 7th Meeting of the International Society of Magnetic Resonance in Medicine (ISMRM) 1: 386
92. Sodickson DK, Stuber M, Botnar RM, Kissinger KV, Manning WJ (1999) SMASH real-time cardiac MR imaging at echocardiographic frame rates [Abstract]. In: Book of Abstracts of the 7th Meeting of the International Society of Magnetic Resonance in Medicine (ISMRM) 1: 387
93. Yang PC, Kerr AB, Liu AC, Liang DH, Hardy C, Meyer CH, Macovski A, Pauly JM, Hu BS (1998) New real-time interactive cardiac magnetic resonance imaging system complements echocardiography. J Am Coll Cardiol 32: 2049-2056
94. Grist TM, Korosec FR, Peters DC, Witte S, Walovitch RC, Dolan RP, Bridson WE, Yucel EK, Mistretta CA (1998) Steady-state and dynamic MR angiography with MS-325: initial experience in humans. Radiology 207: 539-544
95. Hofman MBM, Adzmli K, Brown J, Fisher S, Adams MD, Wickline SA, Lorenz CH (1997) Kinetics of a novel blood pool agent (MP-2269) with persistent high relaxivity for MR angiography [Abstract]. In: Book of Abstracts of the 5th Meeting of the International Society of Magnetic Resonance in Medicine (ISMRM) 1: 206
96. Alley MT, Napel S, Amano Y, Paik DS, Shifrin RY, Shimakawa A, Pelc NJ, Herfkens RJ (1999) Fast 3D cardiac cine MR imag-

ing. J Magn Reson Imaging 9: 751-755
97. Rohl L, Ostergaard L, Simonsen CZ, Vestergaard-Poulsen P, Sorensen L, Bjornerud A, Saebo KB, Gyldensted C (1999) NC100150-enhanced 3D-SPGR MR angiography of the common carotid artery in a pig vascular stenosis model. Quantification of stenosis and dose optimization. Acta Radiol 40:282-290
98. Duerk JL, Hurst GC (1994) Use of superparamagnetic contrast media to suppress signal from flowing spins: preliminary experience. J Magn Reson Imaging 4: 413-417
99. Weissleder R, Stark DD, Engelstad BL, Bacon BR, Compton CC, White DL, Jacobs P, Lewis J (1989) Superparamagnetic iron oxide: pharmacokinetics and toxicity. AJR 152: 167-173
100. Hamm B, Staks T, Taupitz M, Maibauer R, Speidel A, Huppertz A, Frenzel T, Lawaczeck R, Wolf KJ, Lange L (1994) Contrast-enhanced MRimaging of liver and spleen: first experience in humans with a new superparamagnetic iron oxide. J Magn Reson Imaging 4: 659-668
101. Johansson LO, Fischer SE, Lorenz CH (1999) Benefit of T1 reduction for magnetic resonance coronary angiography: a numerical simulation and phantom study. J Magn Reson Imaging 9: 552-556
102. Felblinger J, Lehmann C, Boesch C (1994) Electrocardiogram acquisition during MR examinations for patient monitoring and sequence triggering. Magn Reson Med 32: 523-529
103. Felblinger J, Debatin JF, Boesch C, Gruetter R, McKinnon GC (1995) Synchronization device for electrocardiographygated echo-planar imaging. Radiology 197: 311-313
104. Vasanawala SS, Sachs TS, Brittain JH, Meyer CH, Nishimura DG (1999) Prospective MR signal-based cardiac triggering. Magn Reson Med 42: 82-86
105. Zimmermann-Paul GG, Quick HH, Vogt P, Schulthess GK von, Kling D, Debatin JF (1999) High-resolution intravascular magnetic resonance imaging: monitoring of plaque formation in heritable hyperlipidemic rabbits. Circulation 99: 1054-1061
106. Quick HH, Ladd ME, Zimmermann-Paul GG, Erhart P, Hofmann E, Schulthess GK von, Debatin JF (1999) Single-loop coil concepts for intravascular magnetic resonance imaging. Magn Reson Med 41: 751-758
107. Rivas PA, McConnell MV, Nayak K, Scott G, Meyer C, Pauly JM, Nishimura DG, Macovski A, Hu BS (1999) Real-time intravascular magnetic resonance receiver probe: In vivo observations in the rabbit aorta [Abstract]. In: Book of Abstracts of the 7th Meeting of the International Society of Magnetic Resonance in Medicine (ISMRM) 1: 82
108. Sodickson DK, Griswold MA, Jakob PM (1999) Smash imaging. Magn Reson Imaging Clin North Am 7: 237-254, vii-viii
109. Weiger M, Pruessmann KP, Gösele R, Leussler C, Röschmann P, Boesiger P (1999) Specific coil design for SENSE: a six-element cardiac array [Abstract]. In: Book of Abstracts of the 7th Meeting of the International Society of Magnetic Resonance in Medicine (ISMRM) 1: 162
110. Griswold MA, Jakob PM, Chen Q, Goldfarb JW, Manning WJ, Edelman RR, Sodickson DK (1999) Resolution enhancement in single-shot imaging using simultaneous acquisition of spatial harmonics. Magn Reson Med 41: 1236-1245
111. Sandstede JJ, Pabst T, Beer M, Geis N, Kenn W, Neubauer S, Hahn D (1999) Three-dimensional MR coronary angiography using the navigator technique compared with conventional coronary angiography. AJR 172: 135-139

Chapter 4

Magnetic Resonance Imaging of the Coronary Arteries: Imaging Planes and Resulting Anatomy in Two-dimensional Imaging

R.J.M. van Geuns, P.A. Wielopolski, H.G. de Bruin,

B.J.W.M. Rensing, P.M.A. van Ooijen, M. Hulshoff,

M. Oudkerk, P.J. de Feyter.

Published in Coronary Artery Disease 1999;10(7):525-31.

ABSTRACT

Magnetic-resonance imaging techniques use different imaging planes than does conventional coronary angiography to acquire longer segments of a coronary artery in a single tomographic slice. At first sight, these planes appear rather puzzling, because the coronary arteries are displayed in unfamiliar orientations. In this article we will review the existing methodology for obtaining the orientations for the proximal coronary arteries and describe the associated anatomical landmarks that can be seen. Additional orientations for the middle portion of the circumflex and distal right coronary artery are introduced. These orientations are used both in various acquisition techniques and for evaluation of three-dimensional data when using multiplanar reformatation.

INTRODUCTION

Conventional selective coronary angiography is a very effective imaging technique for displaying important clinical information concerning the state of the coronary arteries. By selective injection of contrast agents into the coronary arteries, signals from other blood-containing structures, such as the heart chambers and coronary veins, are eliminated. Standard orientations are generally obtained and cardiologists are well used to the corresponding anatomy for these orientations. Magnetic-resonance coronary angiography uses different imaging planes that appear rather puzzling at first sight because the coronary arteries are displayed in unfamiliar orientations. In this article we will review and complement the methodology on how the orientations for all major coronary-artery segments may be obtained and discuss the anatomical landmarks that can be seen.

IMAGE ACQUISITION AND EVALUATION CONCEPTS

Early magnetic-resonance coronary angiography was performed by using two-dimensional techniques to study the coronary arteries.[1-3] To visualize longer coronary segments, particular image planes were proposed and multiple parallel slices were acquired in order to have extended coverage of the tortuous vessels.

More recently, three-dimensional magnetic-resonance imaging techniques that are more suited to the evaluation of the complex three-dimensional coronary anatomy have been introduced.[4-6] Three-dimensional datasets are advantageous in that the imaging planes acquired with two-dimensional techniques can be reproduced using multi-planar reformations (MPR) after data have been acquired. Likewise, projection images may also be reconstructed using maximum-intensity projections[7,8] or volume rendering[9,10] in order to view the coronary arteries in the same orientations and extents as are obtained in conventional angiography. Nonetheless, use of maximum-intensity projections and, in some instances, volume rendering can not avoid the overprojection of the cardiac chambers (if their signal is not removed) and the myocardium to show only the coronary arteries without any interference. Therefore, MPR is at present used for evaluating the coronaries and the procedure used to select the imaging planes is directly applicable to magnetic-resonance coronary imaging with two-dimensional techniques or three-dimensional targeted-volume techniques.[11]

TRANSVERSE OR AXIAL PLANES

Transverse planes are always the starting point for acquiring or reconstructing angulated planes. In these planes already a large part of the coronary tree can clearly be identified. Depending on the cross-sectional level of the planes obtained, the proximal or more

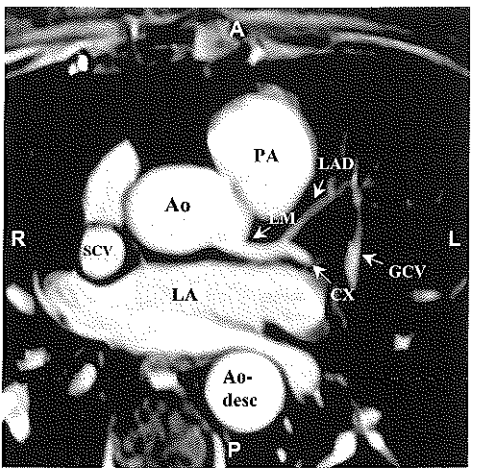

Figure 1. *Transverse slice through the aortic root. The left main coronary artery (LM) can clearly be seen, the proximal left anterior descending artery (LAD) turns around the pulmonary artery (PA) anteriorly. The circumflex coronary artery (CX) turns into the left atrioventricular groove together with the great cardiac vein (GCV). Ao, aorta; SCV, superior caval vein; LA, left atrium; A, anterior thoracic wall; P, posterior; L, left; R, right. This image was acquired with a breath-holding three-dimensional gradient echo sequence with an in-plane resolution of 1.9 × 1.25 mm and a slice thickness of 1.5 mm.*[11]

distal parts of the coronary arteries can be seen.

Left main and left anterior descending coronary arteries

In a transversal plane through the aortic root, the aorta and the pulmonary artery can easily be recognized (Figure 1). At this level the left main coronary artery originates from the left coronary cusp of the aorta. From the bifurcation of the left main coronary artery the left anterior descending (LAD) coronary artery turns around the pulmonary artery to the anterior wall of the left ventricle, while the circumflex coronary artery turns into the left atrioventricular groove. The great cardiac vein (GCV) runs parallel to the LAD coronary artery (in many cases on the left-hand side of the LAD coronary artery) and turns around to the circumflex coronary artery to eventually become the coronary sinus.

Proximal right coronary artery

Approximately 1 cm below the origin of the left main coronary artery the proximal right coronary artery originates anteriorly from the right coronary cusp and follows a course through the right atrioventricular groove between the right ventricular outflow track and the right atrium (Figure 2). At the same axial level the LAD and circumflex coronary arteries and GCV are transected on the epicardium of the left ventricle.

Distal right coronary artery and posterior descending artery

At the level of the acute margin of the left ventricle the right coronary artery (RCA) turns to the crux and can be seen entirely in transverse planes (Figure 3). The origin of the posterior descending artery (PDA) can also appear running along the inferior interventricular groove. The middle cardiac vein, which also follows a course through the

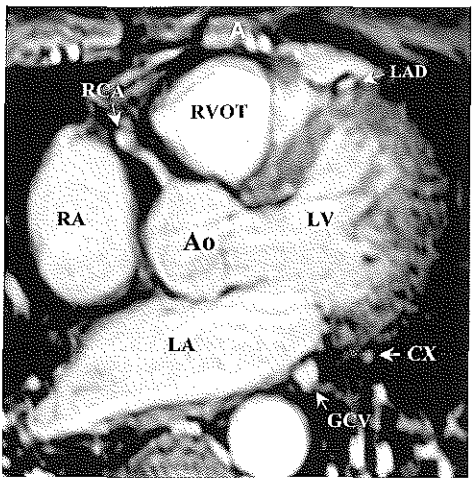

Figure 2. *Transverse slice just above the aortic valve, showing the proximal right coronary artery (RCA) and the more distal left anterior descending coronary artery (LAD), circumflex coronary artery (CX), and great cardiac vein (GCV). Ao, aorta; LV, left ventricle; RA, right atrium; LA, left atrium; RVOT, right ventricular outflow track; A, anterior thoracic wall. This image was acquired with a breath-holding three-dimensional gradient echo sequence with an in-plane resolution of 1.9 × 1.25 mm and a slice thickness of 1.5 mm.*[11]

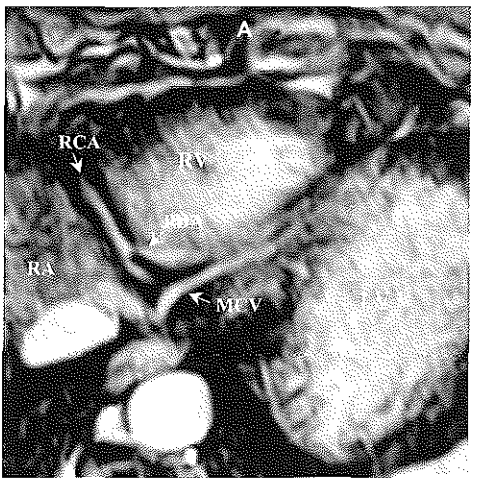

Figure 3. *Transverse slice through the inferior walls of the left ventricle (LV) and right ventricle (RV). Here the right coronary artery (RCA) runs in the right atrioventricular groove to the crux whence the posterior descending artery (PDA) originates. The middle cardiac vein (MCV) enters the coronary sinus close to the right atrium (RA). A, anterior thoracic wall. This image was acquired with a breath-holding three-dimensional gradient echo sequence with an in-plane resolution of 1.9 × 1.25 mm and a slice thickness of 1.5 mm.*[11]

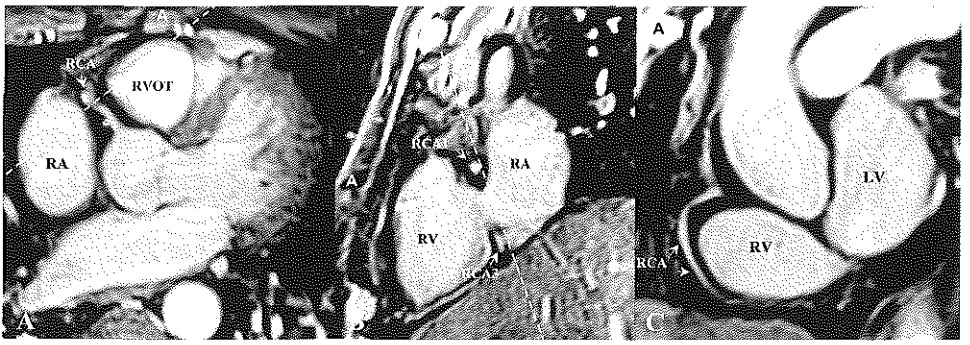

*Figure 4. Localization of the right coronary artery (RCA). **(A)** Starting from a transverse plane through the proximal RCA, a slice through the right ventricle outflow track (RVOT) and right atrium (RA) is selected (dashed line). **(B)** Image along the dashed line in (A) showing the proximal RCA (RCA1) and distal RCA (RCA3) in the atrioventricular groove. From this plane the optimal angulation for the middle of RCA is selected (dashed line). **(C)** Image along the middle segment of the RCA. RV, right ventricle; LV, left ventricle; A, anterior thoracic wall. This image was acquired with a breath-holding three-dimensional gradient echo sequence with an in-plane resolution of 1.9 × 1.25 mm and a slice thickness of 1.5 mm.*[11]

interventricular groove, is often visible. The middle cardiac vein drains into the coronary sinus, just before the coronary sinus drains into the right atrium.

DOUBLE OBLIQUE (ANGULATED) PLANES

The middle part of the RCA

The middle part of the RCA is reviewed in an angulated view. To obtain the correct angulation, a combined approach derived from Manning et al.[12] and Duerinckx[13] can be used. In this method one starts by taking a transverse plane through the proximal right coronary artery (Figure 4a). Then a second plane running through the RCA, right ventricle, and right atrium is selected, showing the proximal and distal RCA in the atrioventricular groove (Figure 4b). An image plane along the atrioventricular groove is then selected. The resulting image exhibits

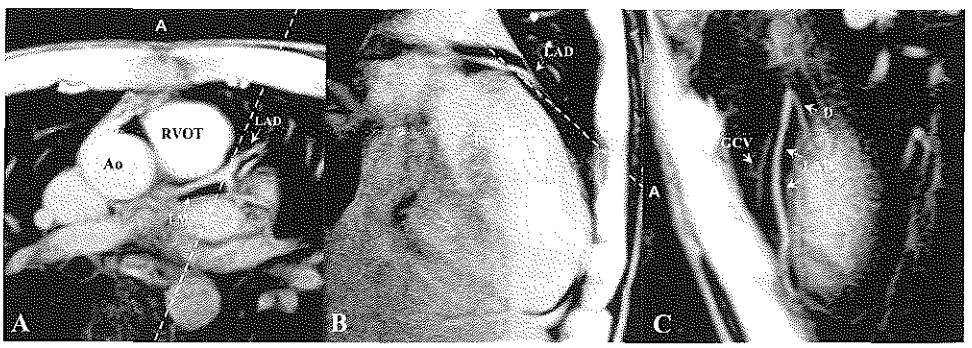

*Figure 5. Localization of the distal left anterior descending artery (LAD). **(A)** Starting from a transverse plane through the middle of LAD, a plane along the interventricular groove is selected (dashed line). **(B)** Image along the interventricular groove. The LAD runs over the interventricular septum and an optimal orientation tangential to the anterior wall of the left ventricle (LV) can be selected (dashed line). **(C)** Resulting image tangential to the LV showing the great cardiac vein (GCV), LAD, and a short part of a diagonal branch (D). RVOT, right ventricular outflow track; Ao, aorta; LM, left main coronary artery; A, anterior thoracic wall. This image was acquired with a breath-holding three-dimensional gradient echo sequence with an in-plane resolution of 1.9 × 1.25 mm and a slice thickness of 1.5 mm.*[11]

the middle part of the RCA and can also show the proximal part of the RCA (Figure 4c). This plane is similar to the left anterior oblique view of the RCA in conventional angiography. The PDA can not be perceived because its course is in another plane and will not be visible in this orientation. Multiple parallel slices are needed in order to make sure that the entire middle part of the RCA is visualized.

The middle and distal parts of the LAD coronary artery

Various orientations may be envisioned to visualize the middle and distal portions of the LAD coronary artery. An easy way is to start with a transverse plane showing the proximal and middle parts (Figure 5a). Then a plane along the LAD coronary artery (Figure 5b) is obtained. In this orientation it is difficult to distinguish between the GCV and the LAD coronary artery and therefore this view is not adequate. Instead, this projection can be used to place another plane tangentially to the anterior wall of the left ventricle.[14] Here the mid-distal LAD coronary artery is clearly visualized and can often be distinguished from the vein (Figure 5c).

The circumflex coronary artery

The circumflex coronary artery is most difficult to visualize. This is because of its complex course in several planes, making it extremely difficult to obtain one overall plane containing the circumflex coronary artery. Another problem is that the circumflex coronary artery is often (in 60% of cases)[15] crossed by the GCV or coronary sinus, which obscures the underlying circumflex coronary artery. In addition, the marginal branches run in another imaging plane than the proximal part of the circumflex. The proximal part can often be seen in transverse slices (Figure 6a). The middle part of the circumflex coronary artery can be visualized in an angulated plane through the atrioventricular groove (Figure 6b). A plane tangential to atrioventricular groove or lateral wall will occasionally contain marginal branches (Figure 6c).

The PDA

The PDA can not be seen in transverse planes through the distal RCA (Figure 7a). An image plane perpendicular to the atrioventricular groove, and along the septum, will show the direction of the interventric-

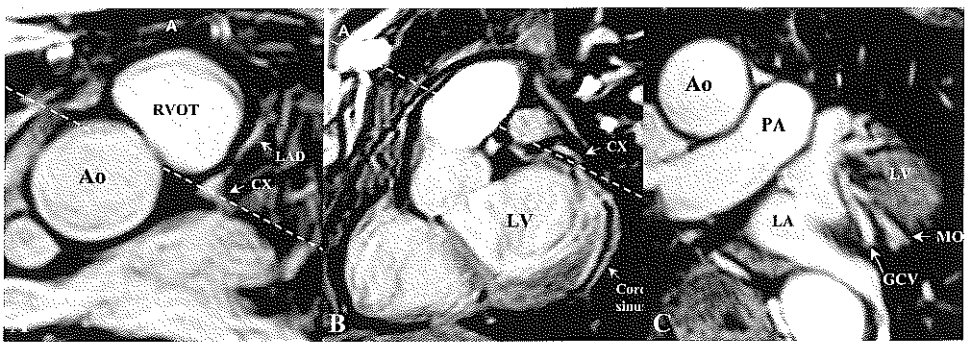

Figure 6. *Localization of the middle segment of the circumflex coronary artery (CX).* ***(A)*** *In the transverse plane a short part of the CX is seen. A plane through the left atrioventricular groove is selected (dashed line).* ***(B)*** *Resulting image through the left atrioventricular groove. From this a plane tangential to the lateral wall of the left ventricle (LV) is selected (dashed line).* ***(C)*** *Obtuse marginal branch (MO) of CX in plane along the coronary sinus. Ao, aorta; RVOT, right ventricular outflow track; LAD, left anterior descending coronary artery; PA, pulmonary artery; LA, left atrium; A, anterior thoracic wall. This image was acquired with a breath-holding three-dimensional gradient echo sequence with an in-plane resolution of 1.9 × 1.25 mm and a slice thickness of 1.5 mm.*[11]

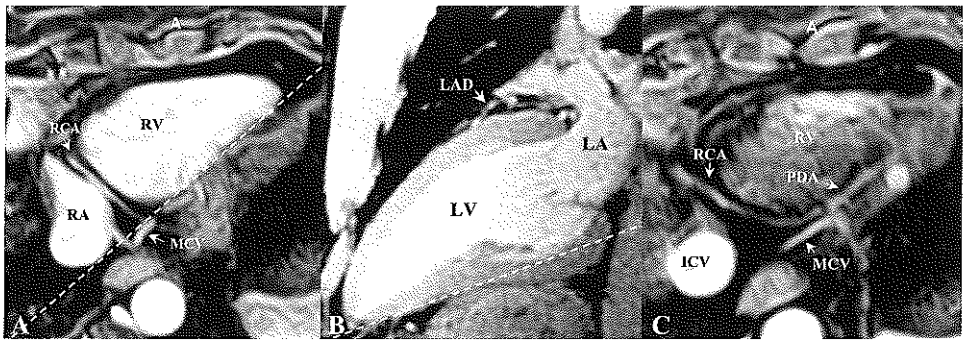

Figure 7. *Localization of the posterior descending coronary artery (PDA).* ***(A)*** *Transverse plane at the level of the distal portion of the right coronary artery (RCA). A plane along the interventricular groove is selected (dashed line).* ***(B)*** *Slice through the left ventricle (LV) along the interventricular septum, showing the left anterior descending coronary artery (LAD) and the direction of the PDA. A slice tangential to the inferior wall will show the PDA in plane* ***(C)****. MCV, middle cardiac vein; ICV, inferior caval vein; RA, right atrium; RV, right ventricle; A, anterior thoracic wall. This image was acquired with a breath-holding three-dimensional gradient echo sequence with an in-plane resolution of 1.9 × 1.25 mm and a slice thickness of 1.5 mm.*[11]

ular groove (Figure 7b). Selection of a plane tangential to the posterior walls of the ventricles and the interventricular groove can show both the distal segment of the RCA and a long part of the PDA (Figure 7c). Also the middle cardiac vein, running parallel to the PDA, is visible and can be distinguished from the PDA by virtue of its drainage into the coronary sinus (see also Figure 3).

DISCUSSION

The anatomically related imaging planes described here for the left main coronary artery and the proximal LAD coronary artery, circumflex coronary artery and RCA until the crux that are used to visualize the coronary arteries with breath-holding two-dimensional acquisition techniques have been described by several authors.[2,13] For two-dimensional acquisition strategies, the angulations are planned on previously acquired two-dimensional slices. In this article additional imaging planes for the PDA and the middle part of the circumflex coronary artery have been described. The usefulness of these orientations has been shown in a study involving 10 healthy volunteers and 25 patients known to have coronary disease.[11] The same imaging planes can be used in the evaluation of three-dimensional datasets by reconstructing multiple parallel slices in order to follow a tortuous coronary artery.[5,16,17] Post et al.[18] also showed the advantages of user-defined imaging planes over standard planes that were comparable to those used in conventional coronary angiography. A new application of the methodology to define the optimal imaging plane for the various coronary arteries was introduced by Wielopolski et al.[11] The group used MPR of a single breath-holding volume-localizer scan for fast planning of targeted volume scans long the coronary arteries. In this strategy the anatomical landmarks reviewed in this article were sufficient for obtaining the desired orientations even when the coronary arteries were not completely visible on the volume-localizer scan. In another acquisition strategy using magnetic-resonance-fluoroscopic setup[19] the user must have knowledge of the anatomical landmarks described here, in order to simplify the localization procedure.

CONCLUSION

To visualize the left main coronary artery, proximal LAD coronary artery, circumflex coronary artery, and RCA, transverse or axial

planes through the aortic root are sufficient. The distal RCA can be located in more caudal transverse slices. To visualize the mid-distal LAD coronary artery, circumflex coronary artery, RCA and PDA, angulated (oblique) slices are necessary. With the method described in this article these angulations can be obtained rapidly from planes containing the atrioventricular or interventricular grooves. The method can be applied in two-dimensional imaging strategies, in three-dimensional targeted imaging, and for the evaluation of results obtained with three-dimensional techniques covering the entire coronary tree.

REFERENCES

1 Manning WJ, Li W, Edelman RR. A preliminary report comparing magnetic resonance coronary angiography with conventional angiography. N Engl J Med 1993; 328: 828-832.

2 Pennell DJ, Keegan J, Firmin DN, Gatehouse PD, Underwood SR, Longmore DB. Magnetic resonance imaging of coronary arteries: technique and preliminary results. Br Heart J 1993; 70: 315-326.

3 Duerinckx AJ, Urman MK. Two-dimensional coronary MR angiography: analysis of initial clinical results. Radiology 1994; 193: 731-738.

4 Wielopolski PA, Manning WJ, Edelman RR. Single breath-hold volumetric imaging of the heart using magnetization-prepared 3-dimensional segmented echo planar imaging. J Magn Reson Imaging 1995; 5: 403-409.

5 Post JC, van Rossum AC, Hofman MB, Valk J, Visser CA. Three-dimensional respiratory-gated MR angiography of coronary arteries: comparison with conventional coronary angiography. Am J Roentgenol 1996; 166: 1399-1404.

6 Li D, Kaushikkar S, Haacke EM, Woodard PK, Dhawale PJ, Kroeker RM, et al. Coronary arteries: three-dimensional MR imaging with retrospective respiratory gating. Radiology 1996; 201: 857-863.

7 Murakami T, Kashiwagi T, Nakamura H, Tsuda K, Azuma M, Tomoda K, et al. Display of MR angiograms: maximum intensity projection versus three-dimensional rendering. Eur J Radiol 1993; 17: 95-100.

8 Napel S, Rubin GD, Jeffrey RB Jr. STS-MIP: a new reconstruction technique for CT of the chest. J Comput Assist Tomogr 1993; 17: 832-838.

9 Drebin R, Carpentier L, Hanrahan P. Volume rendering. Comput Graphics 1988; 22: 65-74.

10 Ney D, Fishman E, Magid D. Volumetric rendering of computed tomography data: principles and techniques. Comput Graphics Applications 1990; 10: 24-32.

11 Wielopolski P, van Geuns R, deFeyter P, Oudkerk M. VCATS, magnetic resonance coronary angiography with breath-hold volume targeted scans. Radiology 1998; (in press).

12 Manning WJ, Li W, Boyle NG, Edelman RR. Fat-suppressed breath-hold magnetic resonance coronary angiography. Circulation 1993; 87: 94-104.

13 Duerinckx AJ. MR angiography of the coronary arteries. Topogr Magn Reson Imaging 1995; 7: 267-285.

14 Sakuma H, Caputo GR, Steffens JC, M OS, Bourne MW, Shimakawa A, et al. Breath-hold MR cine angiography of coronary arteries in healthy volunteers: value of multiangle oblique imaging planes. Am J Roentgenol 1994; 163: 533-537.

15 von Ludinghausen M. Clinical anatomy of cardiac veins, Vv. cardiacae. Surg Radiol Anat 1987; 9: 159-168.

16 Muller MF, Fleisch M, Kroeker R, Chatterjee T, Meier B, Vock P. Proximal coronary artery stenosis: three-dimensional MRI with fat saturation and navigator echo. J Magn Reson Imaging 1997; 7: 644-651.

17 Kessler W, Achenbach S, Moshage W, Zink D, Kroeker R, Nitz W, et al. Usefulness of respiratory gated magnetic resonance coronary angiography in assessing narrowings > or = 50% in diameter in native coronary arteries and in aortocoronary bypass conduits. Am J Cardiol 1997; 80: 989-993.

18 Post JC, van Rossum AC, Hofman MB, Valk J, Visser CA. Protocol for two-dimensional magnetic resonance coronary angiography studied in three-dimensional magnetic resonance data sets. Am Heart J 1995; 130: 167-173.

19 Kerr AB, Pauly JM, Hu BS, Li KC, Hardy CJ, Meyer CH, et al. Real-time interactive MRI on a conventional scanner Magn Reson Med 1997; 38: 355-367

Chapter 5

Magnetic Resonance Imaging of the Coronary Arteries: Anatomy of the Coronary Arteries and Veins in Three-dimensional Imaging

R.J.M. van Geuns, P.A. Wielopolski, B.J.W.M. Rensing,

P.M.A. van Ooijen, M. Oudkerk, P.J. de Feyter

Published in Coronary Artery Disease 1999;10:261-267

ABSTRACT

Magnetic resonance imaging of coronary arteries will visualize, besides the arteries, the myocardium, blood in the cavities and cardiac veins. This will hamper the application of projectional visualization techniques such as those used in conventional coronary angiography. Volume rendering, a different visualization technique, can be used to create a three-dimensional impression of a magnetic resonance data set on a two-dimensional surface. In this article, we will review the volume-rendering technique and anatomy of the coronary arteries and veins in the obtained images. Also we will discuss the relation between arteries and veins and the possible sites of confusion.

INTRODUCTION

Coronary angiography is a very effective imaging technique for displaying the coronary anatomy. With selective injection of a contrast agent, blood in the chambers and coronary veins does not interfere with the visualization of the coronary arteries. In addition, myocardium and other soft tissues are hardly seen because of their low absorption of X-rays. Coronary angiograms use projections performed in various orientations so that the cardiologist can perceive the three-dimensional anatomy of the coronary arteries. This is quite different for imaging techniques such as magnetic resonance imaging (MRI). In MRI the myocardium and blood in the cavities and coronary veins are present and projectional techniques are of limited use. Overlap of structures that obscure coronary imaging can be avoided by multiplanar reconstruction using thin slices in any desired orientation. However, in that case much of the three-dimensional information is not used. In this article, we will give an introduction to evaluation of three-dimensional MRI data sets[1,2] with a volume-rendering technique that creates a three-dimensional impression on a two-dimensional surface.[3] These images look much like the gross anatomy of the heart. In this article we will review the processing technique used and the anatomy in relation to the course of the coronary arteries.

IMAGE SEGMENTATION

Cross-sectional images from MRI also include non-cardiac structures such as thoracic wall and spine. In three-dimensional visualization these structures will obstruct the visualization of the coronary arteries. However, several computer-segmentation techniques are available that allow removal of undesired structures, so that only structures of interest, in our case the coronary arteries, can be further analysed (Figure 1).[4] So far, these techniques are extremely time-consuming because, although they are computerized, they require intensive interaction with an investigator, so that it takes about 45 min to perform segmentation of 60 slices.

THREE-DIMENSIONAL REPRESENTATION USING VOLUME RENDERING

Several means of processing to evaluate a three-dimensional data set in a two-dimensional display are available.[5] Volume rendering is often used nowadays. In volume rendering, all the image pixels of a three-

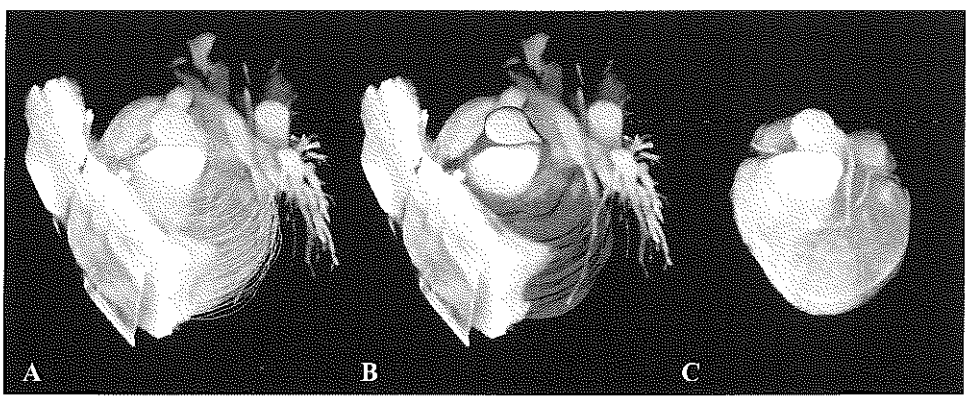

Figure 1. *Image segmentation has to be performed before volume rendering can take place. The magnetic resonance images are obtained with a respiratory-gated three-dimensional gradient echo technique. Resolution 1.9 mm x 1.25 mm × 2 mm.* ***(A)*** *On all slices of a data set contours are drawn to select the desired structures.* ***(B)*** *From these contours a subvolume is created automatically.* ***(C)*** *The structures that are not selected are removed, so that the coronary arteries can be analysed without obstruction.*

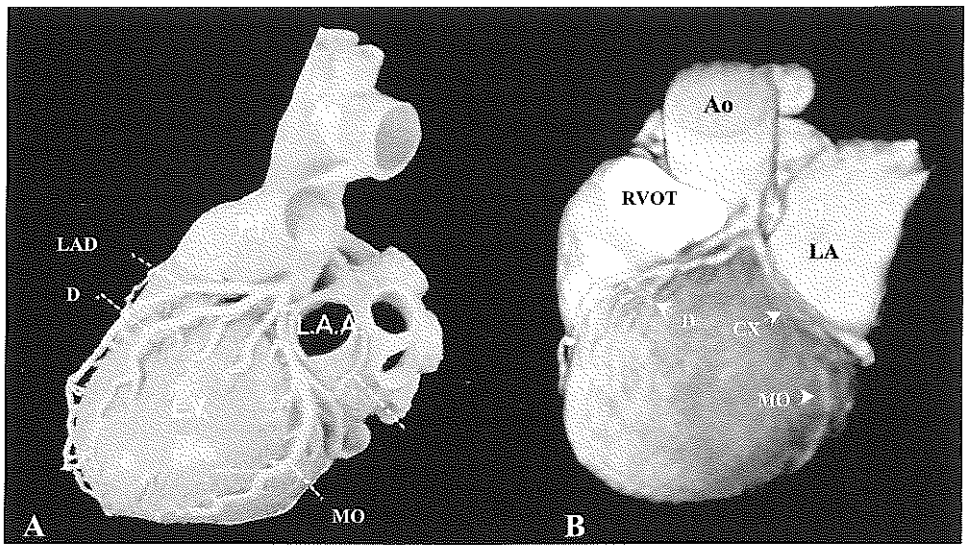

Figure 2. (A) *Anatomical view of the left coronary artery (reproduced with permission from McAlpine.[17] The auricle of the left atrium (L.A.A.) overlapping the circumflex coronary artery is removed. The left main (LM) artery divides beneath the L.A.A. in the left anterior descending (LAD) and circumflex (CX) coronary arteries. From the LAD artery diagonal branches (D) arise. The margo obtusus (MO) arises from the CX artery.* ***(B)*** *A comparable non-invasive coronary angiogram with respiratory-gated three-dimensional magnetic resonance imaging. Technique same as in Figure 1. Ao, aorta; PT, pulmonary trunk; LA, left atrium, after removal of the auricle; LV, left ventricle; RVOT, right ventricular outflow track.*

dimensional data set are used to create a two-dimensional image. A certain opacity is assigned to every pixel, on the basis of its value in the data set. A projection method will transverse all the pixels from back to front and display them on the screen.[6,7] This technique allows one to visualize the three-dimensional data set from various angles so that anatomic details can be displayed from an optimal direction. A drawback of volume rendering was the prohibitively long computation time; however, with current hardware, interactive

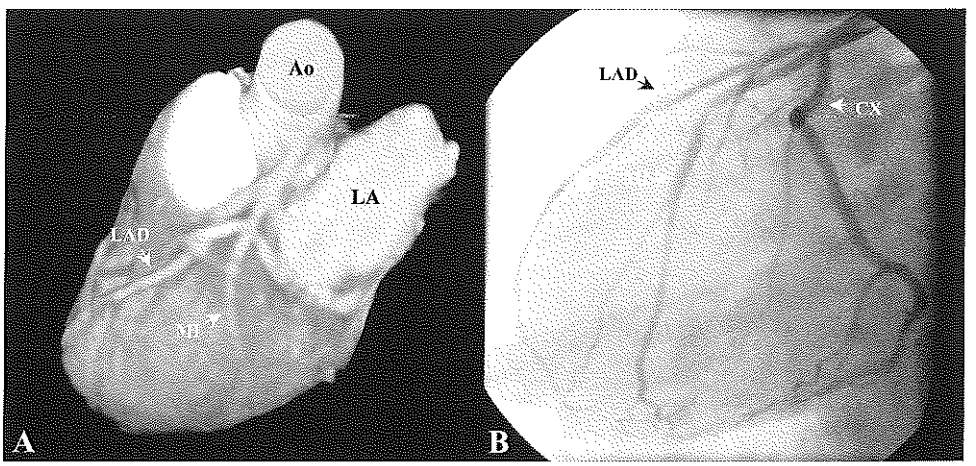

Figure 3. (A) *Magnetic resonance imaging, trifurcation of the left main artery into left anterior descending (LAD), circumflex (CX) and intermediate (MI) arteries. Technique same as in Figure 1.* ***(B)*** *A conventional coronary angiogram of the same patient. Ao, aorta; LA, left atrium.*

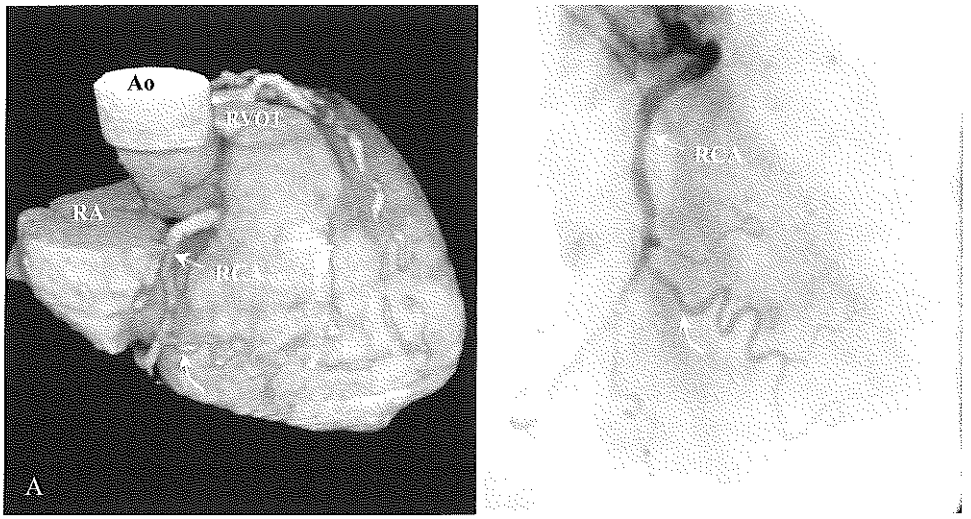

Figure 4. *(A) Magnetic resonance imaging, right anterior view. Right coronary artery (RCA) in right atrioventricular groove between the right atrium (RA) and right ventricular outflow track (RVOT). Right ventricular branch, curved arrow. Technique same as in Figure 1.* ***(B)*** *A conventional coronary angiogram of the same patient. Ao, Aorta.*

three-dimensional volume rendering can be performed at an acceptable speed.[8]

CORONARY ARTERY ANATOMY

The left main coronary artery arises from the left posterior aortic sinus. Its length is variable, but usually 1-2 cm.[9] In a small proportion of cases the left main coronary artery is very short and bifurcates almost immediately. In 0.41% of the cases the left main

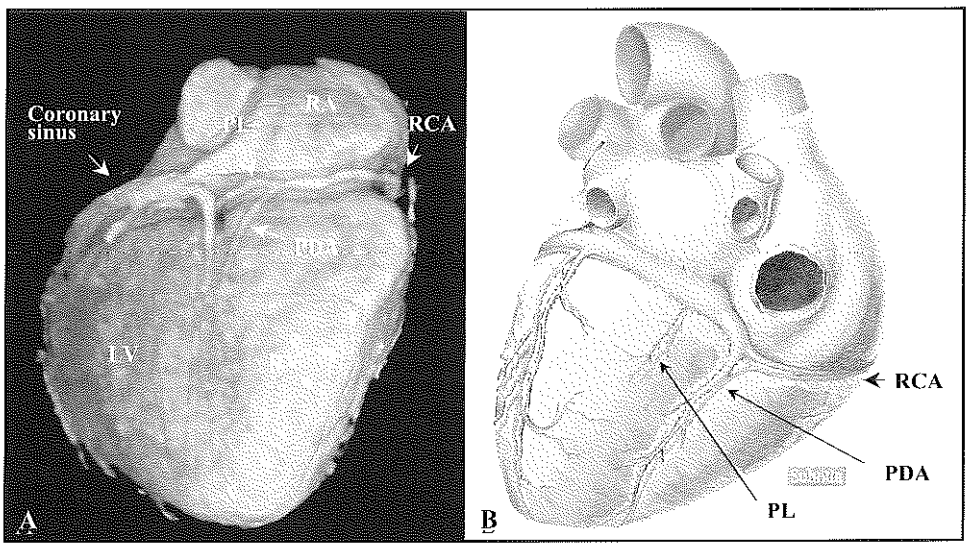

Figure 5. *Distal right coronary artery (RCA), diaphragmatic view.* ***(A)*** *Magnetic resonance imaging. At the crux the RCA divides into the postero-descending artery (PDA) and postero-lateral (PL) branch over the inferior wall of the left ventricle (LV). Technique same as in Figure 1. RV, right ventricle; RA, right atrium.* ***(B)*** *Anatomical view. (Reproduced with permission from the Medical Illustration Library, Williams & Wilkins, Baltimore.)*

coronary is not developed and there are two orifices in the left coronary sinus.[10] In two thirds of the subjects the main left coronary artery divides, beneath the left atrial appendix, into the left anterior descending (LAD) and the circumflex arteries (Figure 2).[11] The LAD artery passes to the left of the pulmonary trunk and turns forwards to run downwards in the anterior interventricular groove. The LAD artery provides two main groups of branches. First, the septal branches which supply the anterior two thirds of the septum and second the diagonal branches, which lie on the lateral aspect of the left ventricle. The circumflex artery turns backwards shortly beyond its origin to run downwards in the left arterioventricular groove. It too, gives rise to a variable number of branches, which lie on the lateral aspect of the left ventricle (the marginal branches). In the atrioventricular groove the circumflex artery is often covered by the auricle of the left atrium, which obstructs visualization and therefore has to be removed from the data set. In

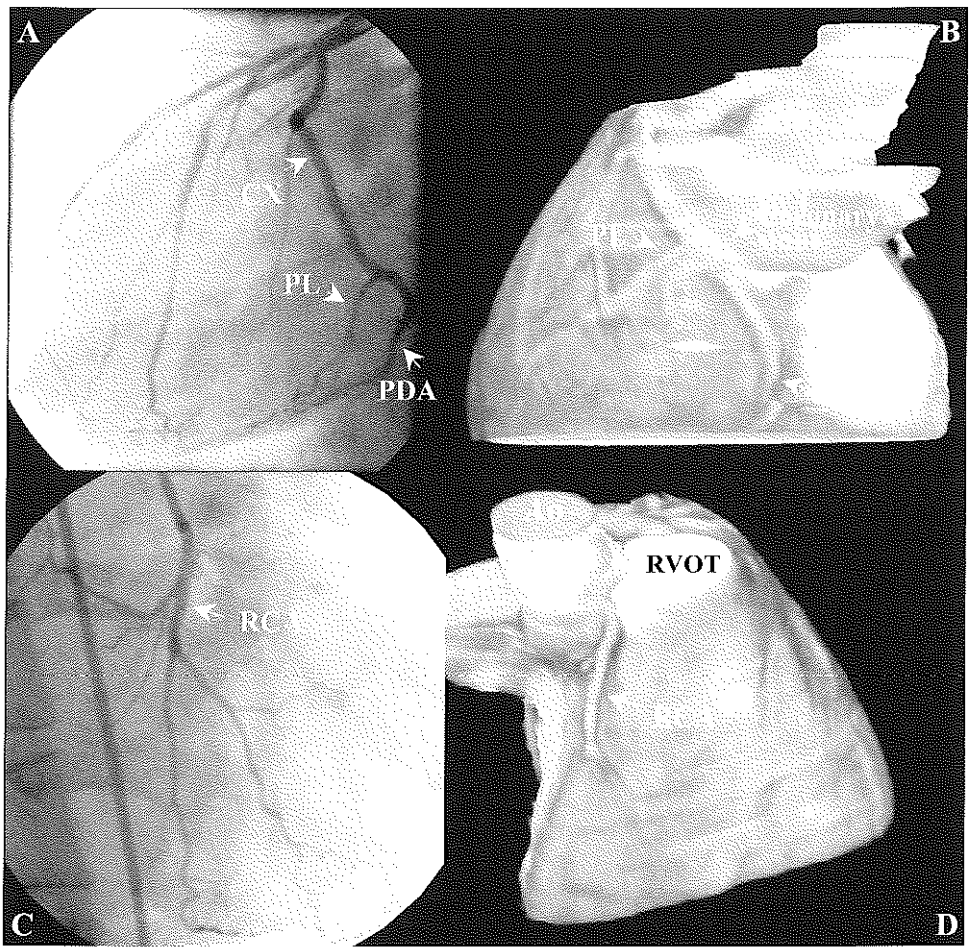

Figure 6. *Left coronary artery dominance. Posterior descending artery (PDA) and postero-lateral (PL) branch originate from the circumflex (CX) coronary artery. In* ***(A)*** *and* ***(C)*** *the images are obtained by conventional coronary angiography.* ***(B)*** *Magnetic resonance imaging, left posterior view. Coronary sinus covers CX artery.* ***(D)*** *Magnetic resonance imaging, right anterior view. In left coronary artery dominance there is only a small right coronary artery (RCA). Technique same as in Figure 1. Ao, Aorta; RVOT, right ventricular outflow track.*

one-third of the subjects the left main coronary artery trifurcates into the aforementioned branches and an intermediate artery, which follows a course between the circumflex and LAD arteries over the antero-lateral wall of the left ventricle (Figure 3).[11] The right coronary artery (RCA) arises from the anterior aortic sinus, passes forwards and then downwards in the right atrioventricular groove (Figure 4) and continues around the margin of the heart towards the crux, a point below where the atrioventricular groove and the posterior interventricular groove meet. In the majority (80%) of individuals the RCA continues forwards from the crux along the posterior interventricular groove to become the posterior descending artery (PDA), running to the apex of the heart (Figure 5). This is by convention called RCA dominance.[12] Septal branches supplying the posterior third of the septum arise from the PDA. The postero-lateral branch supplying the postero-inferior aspect of the left ventricle also arises from the RCA close to the crux. Left coronary dominance exists when the PDA arises from the circumflex artery (Figure 6).

CORONARY VENOUS ANATOMY

There are two major systems of epicardial cardiac veins: tributaries of the coronary sinus and anterior cardiac veins (Figure 7). In principle the veins run parallel to the arteries. The great cardiac vein (GCV), receiving blood from the anterior two thirds of the septum, runs parallel to the LAD artery in the anterior interventricular groove. At the origin of the LAD artery the GCV turns into the left atrioventricular groove, running parallel to the circumflex artery, where it drains into the coronary sinus. The anatomical transition of the GCV into the coronary sinus is at the site of entrance of the oblique vein of the left atrium.[13] The coronary sinus continues parallel to the circumflex artery and drains into the right atrium. The ostium of the coronary sinus in the right atrium is most frequently covered by a thick valve (the valve of the coronary sinus or Thebesian valve).[13]

The middle cardiac vein (MCV), receiving blood from the posterior third of the septum, runs parallel to the PDA and enters the coronary sinus in 87% of the cases.[14] In only 36% of the cases is there a small cardiac vein,

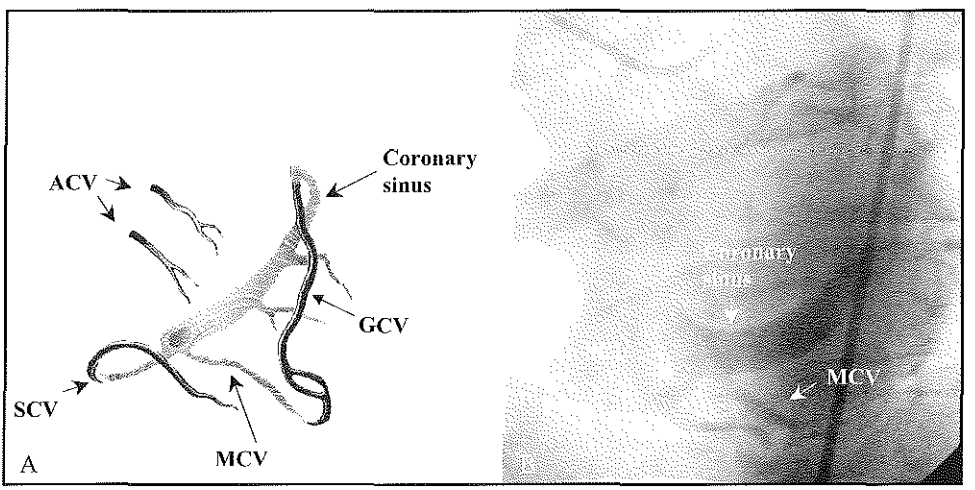

Figure 7. *Coronary veins.* ***(A)*** *Anatomical view. Two cardiac venous systems: anterior veins (ACV) and tributaries of the coronary sinus [great cardiac vein (GCV), middle cardiac vein (MCV) and small cardiac vein (SCV)].* ***(B)*** *Conventional coronary angiography, venous phase.*

draining the blood of the right ventricle into the coronary sinus.[14]
The other epicardial venous system, that of the anterior veins, drains the blood from the right ventricular wall into the right atrium via atrial sinuses.[15] Sometimes this so-called 'sinus coronarius atrii dextri' is quite large[14] and can be confused with the RCA in MRI.

RELATION BETWEEN ARTERIES AND VEINS

LCA and GCV

The GCV is the longest venous vessel of the heart. The vein originates at the anterior interventricular groove, near the apex of the heart, and it empties into the coronary sinus. In the lower and the middle parts of the interventricular groove the GCV runs most often to the right of its related artery.[16] The GCV crosses over the LAD artery and all of it branches in 49% of the cases (Figure 8). On reaching the atrioventricular groove the GCV crosses the LAD and circumflex arteries forming the base of the triangle of Brocq and Mouchet.[16] The distance from the GCV of the left main coronary artery is variable (0-7 mm)[16] and sometimes the GCV touches the left main coronary artery and turns with a very sharp angle to the left atrioventricular groove, crossing under the branches of the left main coronary artery (Figure 9). The circumflex artery is covered by the GCV in 60% of the cases so that the underlying anatomy of circumflex artery is obscured or inadequately visualized.

RCA and coronary sinus

At the crux of the heart the RCA is, with very rare exceptions, inferior to the coronary sinus. The middle cardiac vein crosses over the postero-lateral branch of the RCA and stays left of the PDA when running in the posterior interventricular groove (Figure 10). In cases of left circumflex artery dominance, veins draining blood from the inferior wall of the left ventricle cross over the artery before entering the coronary sinus.

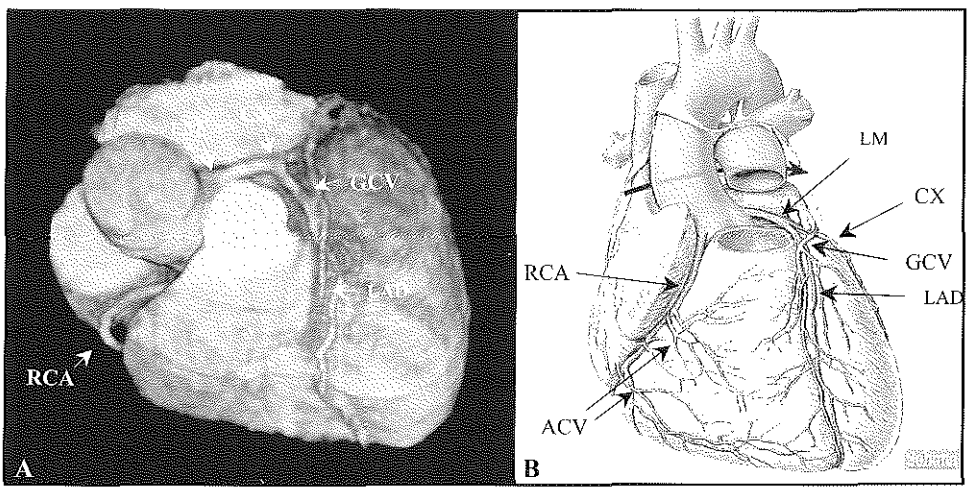

Figure 8. *The great cardiac vein (GCV) turns from the anterior interventricular groove into the atrioventricular groove, crossing all the branches of the left coronary artery and forming the triangle of Brocq and Mouchet together with the left anterior descending (LAD) and circumflex (CX) coronary arteries.* ***(A)*** *Magnetic resonance imaging, the view at the CX artery is obstructed by the GCV. Technique same as in Figure 1.* ***(B)*** *Comparative anatomical view (reproduced with permission from the Medical Illustration Library, Williams & Wilkins, Baltimore). LM, left main artery; RCA, right coronary artery; ACV, anterior cardiac veins.*

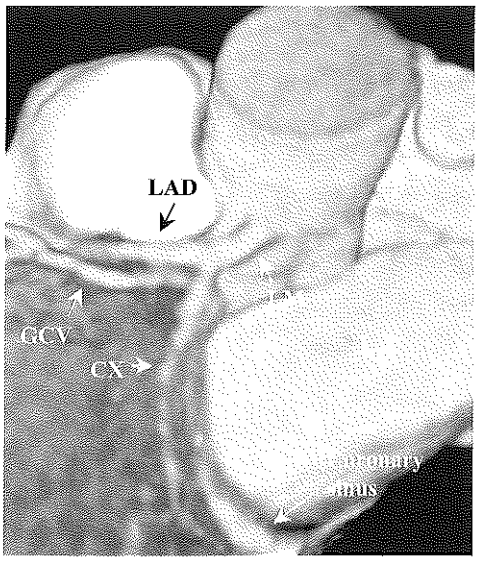

Figure 9. *Great cardiac vein (GCV) crossing under the circumflex coronary artery (CX) with no impairment of one's view of the artery. LAD, left anterior descending artery; LM, left main artery. Technique same as in Figure 1.*

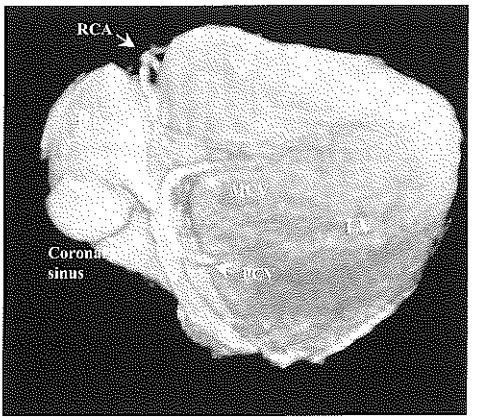

Figure 10. *Right coronary artery (RCA) in the inferior atrioventricular groove partly covered by the middle cardiac vein (MCV) and the coronary sinus. PCV, posterior cardiac vein; RA, right atrium; LV, left ventricle. Technique same as in Figure 1.*

CONCLUSION

Three-dimensional data sets from non-invasive three-dimensional coronary imaging techniques such as MRI are displayed with a volume-rendering technique. This provides images of the coronary arteries and veins much like their real anatomy,[17] which are not always familiar to the practicing cardiologist. Knowledge of the course of the epicardial coronary arteries and veins is required for accurate analysis.

REFERENCES

1 Li D, Kaushikkar S, Haacke EM, Woodard PK, Dhawale PJ, Kroeker RM, et al. Coronary arteries: three-dimensional MR imaging with retrospective respiratory gating. Radiology 1996; 201:857-863.

2 Post JC, van Rossum AC, Hofman MB, Valk J, Visser CA. Three-dimensional respiratory-gated MR angiography of coronary arteries: comparison with conventional coronary angiography. Am J Roentgenol 1996; 166:1399-1404.

3 Achenbach S, Kessler W, Moshage WE, Ropers D, Zink D, Kroeker R, et al. Visualization of the coronary arteries in three-dimensional reconstructions using respiratory gated magnetic resonance imaging. Coronary Artery Dis 1997; 8:441-448.

4 van Ooijen P, de Feyter P, Oudkerk M. An introduction to three-dimensional cardiac imaging, rendering and processing. Cardiologie 1997; 4:312-319.

5 Fishman EK, Magid D, Ney DR, Chaney EL, Pizer SM, Rosenman JG, et al. Three-dimensional imaging. Radiology 1991; 181:321-337.

6 Drebin R, Carpentier L, Hanrahan P. Volume rendering. Comput Graphics 1988; 22:65-74.

7 Ney D, Fishman E, Magid D. Volumetric rendering of computed tomography data: principles and techniques. Comput Graphics Appl 1990; 10:24-32.

8 Johnson PT, Heath DG, Kuszyk BS, Fishman EK. CT angiography: thoracic vascular imaging with interactive volume rendering technique. J Comput Assist Tomogr 1997; 21:110-114.

9 James T. Anatomy of the coronary arteries in health and disease. Circulation 1965; 32:1020-1033.

10 Yamanaka O, Hobbs R. Coronary artery anomalies in 126,595 patients undergoing coronary angiography. Cathet Cardiovasc Diagn 1990; 21:28-40.

11 Levin DC, Harrington DP, Bettmann MA, Garnic JD, Davidoff A, Lois J. Anatomic

variations of the coronary arteries supplying the anterolateral aspect of the left ventricle: possible explanation for the 'unexplained' anterior aneurysms. Invest Radiol 1982; 17:458-462.

12 Braunwald E. Heart disease. A textbook of cardiovascular medicine. Fourth edition. Philadelphia: W.D. Saunders Company; 1992.

13 Maric I, Bobinac D, Ostojic L, Petkovic M, Dujmovic M. Tributaries of the human and canine coronary sinus. Acta Anat (Basel) 1996; 156:61-69.

14 von Ludinghausen M. Clinical anatomy of cardiac veins. Vv. cardiacae. Surg Radiol Anat 1987; 9:159-168.

15 Pina JA. Morphological study on the human anterior cardiac veins, venae cordis anteriores. Acta Anat (Basel) 1975; 92:145-159.

16 Pejkovic B, Bogdanovic D. The great cardiac vein. Surg Radiol Anat 1992; 14:23-28.

17 McAlpine. Heart and coronary arteries. Berlin: Springer-Verlag; 1975.

Chapter 6

Magnetic Resonance Imaging of the Coronary Arteries: Clinical Results from Three Dimensional Evaluation of a Respiratory Gated Technique

R.J.M. van Geuns, H.G. de Bruin, B.J.W.M. Rensing,

P.A. Wielopolski, M.D. Hulshoff, P.M.A. van Ooijen,

M. Oudkerk, P.J. de Feyter.

Published in Heart 1999;82:515–519

ABSTRACT

Background:
Magnetic resonance coronary angiography is challenging because of the motion of the vessels during cardiac contraction and respiration. Additional challenges are the small calibre of the arteries and their complex three dimensional course. Respiratory gating, turbo-flash acquisition, and volume rendering techniques may meet the necessary requirements for appropriate visualisation.

Objective:
To determine the diagnostic accuracy of respiratory gated magnetic resonance imaging (MRI) for the detection of significant coronary artery stenoses evaluated with three dimensional postprocessing software.

Methods:
Thirty-two patients referred for elective coronary angiography were studied with a retrospective respiratory gated three dimensional gradient echo MRI technique. Resolution was $1.9 \times 1.25 \times 2$ mm. After manual segmentation three dimensional evaluation was performed with a volume rendering technique.

Results:
Overall 74% (range 50% to 90%) of the proximal and mid coronary artery segments were visualised with an image quality suitable for further analysis. Sensitivity and specificity for the detection of significant stenoses were 50% and 91%, respectively.

Conclusions:
Volume rendering of respiratory gated MRI techniques allows adequate visualisation of the coronary arteries in patients with a regular breathing pattern. Significant lesions in the major coronary artery branches can be identified with a moderate sensitivity and a high specificity.

INTRODUCTION

Magnetic resonance imaging (MRI) is a truly non-invasive technique which is not associated with radiation and is nowadays available for clinical use. MRI of the coronary arteries is, however, a challenging task owing to motion of the vessels during cardiac contraction and respiration, the complexity of the anatomy in three dimensions, the small calibre of the vessels, and the fact that the vessels are embedded in fat which produces a competing signal.

Coronary artery motion during cardiac contraction is successfully minimised by ECG triggering, with data collection over 100 to 150 ms during mid to late diastole. Reduction of respiratory motion is achieved with breath holding or with respiratory gated techniques. The complex course of the coronary anatomy can be evaluated with two dimensional (2D) or preferably three dimensional (3D) acquisition techniques.

MRI of the coronary arteries (MRCA) was first performed in 1993 with a single slice breathhold technique (2D-MRCA).[1-3] Although initial results seemed encouraging, the use of 2D-MRCA is limited by its complex setup for image orientation and its dependency on consistent breath holding.[4,5] The use of a respiratory gated technique (navigator) for MRCA[6,7] was introduced later as another possibility to reduce respiratory blur. Without restrictions in imaging time imposed by the patient's breathhold limits, longer imaging sequences can be used. This allows the complex coronary artery anatomy to be studied with a three dimensional technique (3D-MRCA).

Evaluation of a 3D-MRCA dataset can be performed with multiplanar reformatting techniques,[8,9] producing slices in any desired plane through the volume. However, this technique is limited because it does not use all the information present in a three dimensional dataset. This can be overcome by using the volume rendering technique[10] present in special three dimensional viewing software, which uses all the information in a three dimensional dataset.

In this study we determined the diagnostic accuracy of respiratory gated 3D-MRCA for the detection of coronary artery stenoses evaluated with a volume rendering technique.

METHODS

Patients

The study population consisted of 32 patients (20 men, 12 women; age 32 to 73 years) who were referred for elective coronary angiography. Exclusion criteria were previous coronary bypass operation, intracoronary stent implantation, artificial pacemaker, intracranial clips, claustrophobia, and non-sinus rhythm. The protocol was approved by our hospital committee on medical ethics and clinical investigation.

Magnetic resonance imaging

Subjects were studied in a supine position, with a four channel quadrature body phased array coil placed over the thorax, in a 1.5 T whole body magnetic resonance imaging system (Vision; Siemens, Erlangen, Germany). Coronary artery imaging was performed using a standard Siemens three dimensional gradient echo sequence with retrospective respiratory gated technique described by Li et al. A chemical shift fat suppression pulse was used to suppress the signal from the epicardial fat sur-rounding the coronary arteries. In our setup we used three slabs of 32 mm thickness with a 25% overlap; section thickness was 2 mm. The matrix size was 128×256 with a rectangular field of view of 240×320 mm, resulting in an inplane resolution of 1.9×1.25 mm. The time of repetition (TR) was 7.4 ms, the time of echo (TE) was 2.7 ms, and the flip angle varied from 20° to 90°. The acquisition window (128 ms) was set for mid to

late diastole. Each slab was acquired in eight to 12 minutes, depending on the heart rate. Retrospective respiratory gating was performed by a navigator echo created with two excitation bands placed to intersect at the dome of the right hemidiaphragm (Figure 1). Together, these two bands measure the diaphragmatic position before data acquisition. The most common position of the diaphragm is determined and chosen as the gating centre. Commonly this is end expiration. Each line of data was acquired five times to ensure complete sampling of the respiratory excursion. Data within a range of ± 1 mm from the gating centre are used for image reconstruction. If no acquisitions of a certain data line are within the acceptance range, the acquisition obtained at the diaphragm displacements closest to the gating centre are used at image reconstruction. The total examination time for MRI of each subject, including positioning of the patient, scout imaging, and setting up the navigator, was approximately one hour.

CONVENTIONAL CORONARY ANGIOGRAPHY

All subjects underwent standard selective coronary artery angiography within one month of the magnetic resonance examination. Angiography was performed using the Judkins technique.[11] The selective angiograms were jointly interpreted by two experienced cardiologists not familiar with the MRI results. The coronary tree was divided into proximal and mid segments according to AHA guidelines.[12] These segments were graded as either no significant disease (< 50% diameter stenosis) or significant disease (> 50% diameter stenosis). In case of disagreement a final decision was made by a third cardiologist.

INTERPRETATION OF MAGNETIC RESONANCE CORONARY ANGIOGRAMS

The magnetic resonance datasets were transferred to a stand alone workstation (MagicView; Siemens, Erlangen, Germany). By manual segmentation, the chest wall, lung vessels, and overlapping parts of the left and right auricle were removed from the dataset. Manual segmentation required 20 to 30 minutes for 60 slices. After image segmentation the datasets were transferred to a dedicated graphic workstation (Indigo2; Silicon Graphics, Mountain View, California, USA) for three dimensional evaluation with a volume rendering technique[13-15] using commercially available software (VoxelView; Vital Images Inc, Minneapolis, Minnesota, USA). In the volume rendering technique, all image pixels are integrated to project a three dimensional data-set as a single image. For this a certain opacity is assigned to each pixel, based on its value in the dataset. A pro-

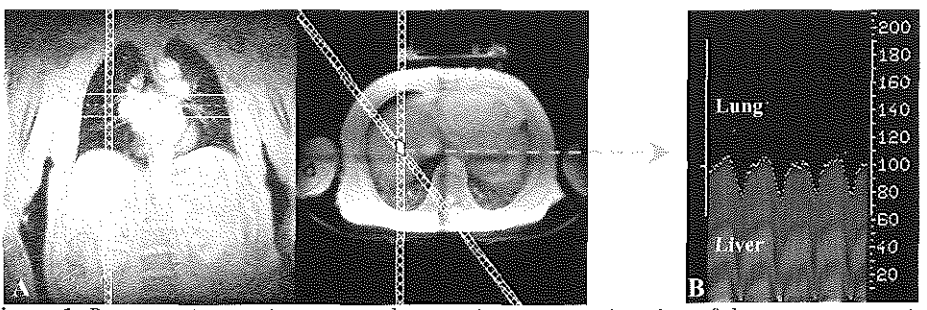

Figure 1. *Retrospective respiratory gated magnetic resonance imaging of the coronary arteries.* ***(A)*** *Respiratory motion is determined by two excitation bands that intersected at the dome of the right hemidiaphragm.* ***(B)*** *Respiration pattern during 30 seconds. The diaphragm position is determined for each acquisition window. Retrospectively only data from end expiration are selected for image reconstruction.*

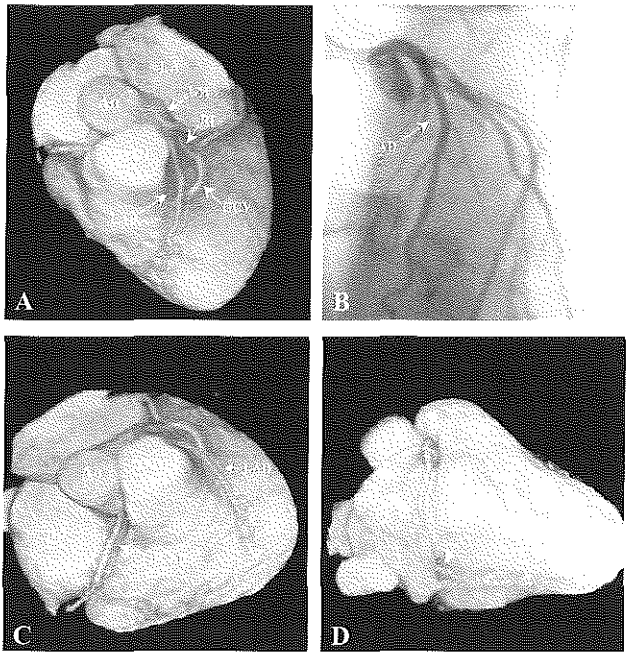

Figure 2. *Volume rendering of a patient without significant stenoses.* ***(A)*** *Cranial view of the left anterior descending coronary artery (LAD). The great cardiac vein (GCV) overlaps intermediate branches (RI), which hampers evaluation of this segment.* ***(B)*** *Corresponding conventional selective coronary angiogram.* ***(C)*** *Rotation to right cranial view for proximal right coronary artery (RCAp) between right ventricular outflow tract (RVOT) and right atrium (RA). The right auricle is manually removed from the data.* ***(D)*** *Rotation to right caudal view for distal right coronary artery (RCAd) and origin of posterior descending artery (PDA). Ao, aorta; LA, left atrium.*

jection method will pass through all the pixels from back to front and calculates a value to display on the screen. The opacity for certain structures will improve the three dimensional impression of the image. The datasets can be rotated in every direction for optimal visualisation of the major coronary artery branches (Figure 2). The three dimensional reconstructions together with the original axial slices were reviewed independently by a radiologist and a cardiologist. The left main coronary artery, proximal and mid right coronary artery, left anterior descending coronary artery, and circumflex artery were graded as assessable, non-assessable, or outside the acquired volume. The assessable segments were graded as either no significant or significant disease. In case of disagreement a third investigator made a final decision.

Statistics

A selective coronary angiogram served as the gold standard for determining the diagnostic value of the non-invasive coronary angiogram. The diagnostic accuracy of magnetic resonance coronary angiography for detecting significant stenoses in a segment is expressed as sensitivity, specificity, and positive and negative predictive value. The diagnostic value for the presence of significant coronary artery disease was also calculated on a per patient basis.

RESULTS

Of the 32 studies, three were not completed owing to ECG triggering problems, technical failure, or unknown claustrophobia. The mean interval between the exami-

Table 1 Assessability of different coronary artery segments by magnetic resonance coronary angiography

	MRI
RCA-proximal part	93%
RCA-middle part	76%
LM	97%
LAD-proximal part	90%
LAD-middle part	76%
LCx-proximal part	76%
LCx-middle part	28%

LAD, left anterior descending coronary artery; LCx, leftcircumflex coronary artery; LM, left main coronary artery; RCA, right coronary artery.

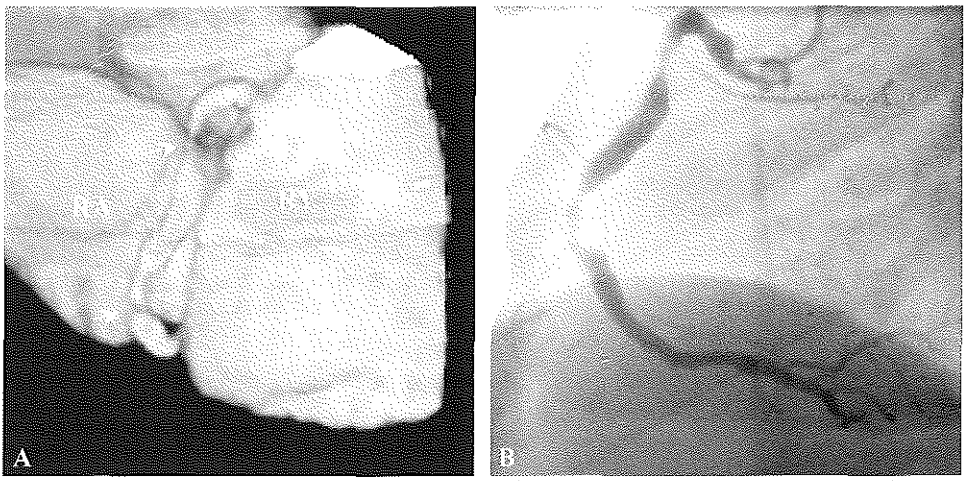

Figure 3. *(A) Magnetic resonance imaging. Detailed view on the right coronary artery in the atrioventricular groove between the right ventricle (RV) and atrium (RA). The arrows indicate stenoses in the proximal and mid segment.* ***(B)*** *Corresponding conventional coronary angiogram.*

nations was 15 days. Overall 151 (74%) of the 203 coronary artery segments were assessable by MRCA, ranging from 97% for the left main coronary artery to 28% for the mid-circumflex coronary artery (table 1). In these segments 26 significant lesions were present (left main and left anterior descending, 11; right coronary, 11; circumflex, 4). An example of two consecutive stenoses in the right coronary artery is shown in Figure 3; an example of a stenosis in the left anterior descending coronary artery is shown in Figure 4. The sensitivity and specificity for the detection of a stenosis in a segment were 50% and 91%, respectively. The diagnostic accuracy for the individual vessels is summarised in table 2. The sensitivity for selection of patients with any significant disease was 76%, with a specificity of 73%.

DISCUSSION

In this study we used a standard technique available on a modern magnetic resonance scanner. The use of a single navigator signal from the diaphragm increases the image quality of MRCA.[16] The results reported by other investigators using this technique for the detection of coronary artery stenosis differ widely, ranging from inadequate to reasonably accurate.[8,17,18] Here we showed high specificity but only moderate sensitivity, owing to insufficient image quality. The major reason for poor image quality is residual respiratory blur originating from irregular respiration patterns,[19] with data acquisition outside the desired gating window.[18,20] In general only 25-30% of the data are acquired within the gating window. False negative MRCA interpretations are caused

Table 2. Diagnostic accuracy for the detection of significant coronary artery stenosis by magnetic resonance coronary angiography

	Total	LM + LAD	LCX	RCA	Patient
Sensitivity	50%	55%	50%	45%	76%
Specificity	91%	92%	95%	87%	73%
PPV	54%	55%	67%	50%	81%
NPV	90%	92%	91%	85%	67%

LAD, left anterior descending coronary artery; LCX, left circumflex coronary artery; LM, left main coronary artery; NPV, negative predictive value; PPV, positive predictive value; RCA, right coronary artery.

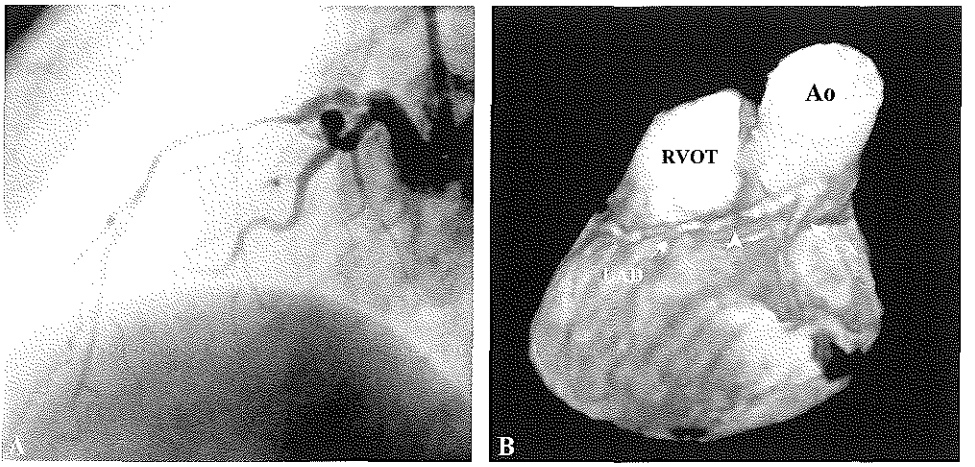

Figure 4. *Example of a significant stenosis (arrow head) in the left anterior descending coronary artery (LAD).* ***(A)*** *Conventional coronary angiogram.* ***(B)*** *Magnetic resonance imaging. Ao, aorta; LM, left main; LV, left ventricle; RVOT, right ventricular outflow tract.*

by retrograde flow distal to complete occlusions and volume averaging of vessels with adjacent structures,[21] or by the inability to distinguish coronary arteries from veins.[5] False positive interpretations arise from the low contrast between the coronary arteries and their surrounding tissue, motion artefacts,[20] or errors during manual segmentation. A negative test result from a test with a sensitivity of only 50% unfortunately does not rule out the undetected presence of significant coronary artery disease. This will limit the use of this technique as a clinical screening method. This may be even more problematic in a group of patients with a lower prevalence of disease, compared with our patients who were referred for elective coronary angiography.

Improvement in image quality of respiratory gated MRCA will reduce false interpretations. This can be achieved by correlating image position with respiratory motion.[22] The acquisition volume is shifted caudally over a certain distance during inspiration so that the percentage of data within the gating window increases. The shifted distance is different for each coronary artery and has to be determined for every patient individually. So far clinical applicability has not been reported. Alternatively MRCA can be performed with new breath holding techniques, such as volume coronary angiography using targeted scans (VCATS), that acquire targeted volumes along the coronary arteries.[23] Respiratory blur is minimised, and acquisition time is reduced to less than 30 minutes. The use of bolus injections of contrast agents, given over a 20 second period, has dramatically improved magnetic resonance angiography of peripheral arteries.[24,25] Gadolinium-DTPA, the contrast agent most often used, diffuses rapidly extravascularly and it is therefore not possible to maintain a high intracoronary concentration during 30 to 40 minutes after intravenous injection. Intravascular magnetic resonance contrast agents may be an alternative. Both respiratory gated and breath hold techniques are expected to benefit from intravascular contrast agents.[26,27] The resulting increase of contrast to noise ratio will improve visualisation of the coronary arteries and allow the use of high resolution techniques. Unfortunately intravascular contrast agents are presently in a preclinical phase and registration may still take several years.

Volume rendering as a technique for evaluation of three dimensional datasets on a two

dimensional surface has proved valuable in magnetic resonance and computed tomographic angiography of both central and peripheral arteries.[28,29] Recently the same technique has been introduced in the evaluation of electron beam tomography.[30] Its main advantage is the nearly anatomical images produced, with the possibility of viewing the data from different angles to obtain optimal orientation for individual coronary arteries. The high computational power necessary for this technique has limited its use hitherto but with the present commercially available hardware and software volume rendering can now be performed with reasonable speed.

CONCLUSIONS

Respiratory gated MRCA is a technique with an uncomplicated setup that can be performed in a clinical setting. At this stage of development image quality is sufficient in only 70% of patients. In patients with a regular breathing pattern significant lesions in the major coronary artery branches can be identified with moderate sensitivity and high specificity. Volume rendering of respiratory MRCA creates highly interpretable images, but improvements in the magnetic resonance technique are necessary before it becomes a clinically reliable tool.

REFERENCES

1 Manning WJ, Li W, Boyle NG, et al. Fat-suppressed breath-hold magnetic resonance coronary angiography. Circulation 1993;87:94-104.

2 Pennell DJ, Keegan J, Firmin DN, et al. Magnetic resonance imaging of coronary arteries: technique and preliminary results. Br Heart J 1993;70:315-26.

3 Duerinckx AJ, Urman MK. Two-dimensional coronary MR angiography: analysis of initial clinical results. Radiology 1994;193:731-8.

4 van Rossum AC, Post JC, Visser CA. Coronary imaging using MRI. Herz 1996;21:97-105.

5 Duerinckx AJ, Atkinson DP, Mintorovitch J, et al. Two-dimensional coronary MRA: limitations and artifacts. Eur Radiol 1996;6:312-25.

6 Hofman MB, Paschal CB, Li D, et al. MRI of coronary arteries: 2D breath-hold vs 3D respiratory-gated acquisition. J Comput Assist Tomogr 1995;19:56-62.

7 Li D, Kaushikkar S, Haacke EM, et al. Coronary arteries: three-dimensional MR imaging with retrospective respiratory gating. Radiology 1996;201:857-63.

8 Kessler W, Achenbach S, Moshage W, et al. Usefulness of respiratory gated magnetic resonance coronary angiography in assessing narrowings > or = 50% in diameter in native coronary arteries and in aortocoronary bypass conduits. Am J Cardiol 1997;80:989-93.

9 Post JC, van Rossum AC, Hofman MB, et al. Protocol for two-dimensional magnetic resonance coronary angiography studied in three-dimensional magnetic resonance data sets. Am Heart J 1995;130:167-73.

10 Drebin R, Carpentier L, Hanrahan P. Volume rendering. Comput Graphics 1988;22:65-74.

11 Judkins MP. Selective coronary arteriography. I. A percu ta-neous transfemoral technic. Radiology 1967;89:815-24.

12 Austen WG, Edwards JE, Frye RL, et al. A reporting system on patients evaluated for coronary artery disease. Report of the Ad Hoc Committee for Grading of Coronary Artery Disease, Council on Cardiovascular Surgery, American Heart Association. Circulation 1975;51(suppl):5-40.

13 Ney D, Fishman E, Magid D. Volumetric rendering of computed tomography data: principles and techniques. Comput Graphics Applic 1990;10:24-32.

14 Johnson PT, Heath DG, Kuszyk BS, et al. CT angiography with volume rendering: advantages and applications in splanchnic vascular imaging. Radiology 1996;200:564-8.

15 Fishman EK, Magid D, Ney DR, et al. Three-dimensional imaging. Radiology 1991;181:321-37.

16 Wang Y, Rossman PJ, Grimm RC, et al. Navigator-echo-based real-time respiratory gating and triggering for reduction of respiration effects in three-dimensional coronary

MR angiography. Radiology 1996;198:55-60.
17 Post JC, van Rossum AC, Hofman MB, et al. Three-dimensional respiratory-gated MR angiography of coronary arteries: comparison with conventional coronary angiography. Am J Roentgenol 1996;166:1399-404.
18 Muller MF, Fleisch M, Kroeker R, et al. Proximal coronary artery stenosis: three-dimensional MRI with fat saturation and navigator echo. J Magn Reson Imaging 1997;7:644-51.
19 Taylor AM, Jhooti P, Wiesmann F, et al. MR navigator-echo monitoring of temporal changes in diaphragm position: implications for MR coronary angiography. J Magn Reson Imaging 1997;7:629-36.
20 Achenbach S, Kessler W, Moshage WE, et al. Visualization of the coronary arteries in three-dimensional reconstructions using respiratory gated magnetic resonance imaging. Coron Artery Dis 1997;8:441-8.
21 Woodard PK, Li D, Haacke EM, et al. Detection of coron-ary stenoses on source and projection images using three-dimensional MR angiography with retrospective res-piratory gating: preliminary experience. Am J Roentgenol 1998;170:883-8.
22 Danias PG, McConnell MV, Khasgiwala VC, et al. Prospec-tive navigator correction of image position for coronary MR angiography. Radiology 1997;203:733-6.
23 Wielopolski P, vanGeuns R, deFeyter P, et al. Breath-hold coronary MR angiography with volume targeted imaging. Radiology 1998;209:209-19.
24 Leung DA, McKinnon GC, Davis CP, et al. Breath-hold, contrast-enhanced, three-dimensional MR angiography. Radiology 1996;200:569-71.
25 Prince MR, Narasimham DL, Stanley JC, et al. Breath-hold gadolinium-enhanced MR angiography of the abdominal aorta and its major branches. Radiology 1995;197:785-92.
26 Lauffer RB, Parmelee DJ, Dunham SU, et al. MS-325: albumin-targeted contrast agent for MR angiography. Radiology 1998;207:529-38.
27 Li D, Zheng J, Weinmann H, et al. Comparison of intravascular and extravascular contrast agents in coronary artery imaging [abstract]. Proceedings of the sixth meeting of the International Society for Magnetic Resonance in Medicine. Sydney, 1998.
28 Johnson PT, Heath DG, Kuszyk BS, et al. CT angiography: thoracic vascular imaging with interactive volume render-ing technique. J Comput Assist Tomogr 1997;21:110-14.
29 Kuszyk BS, Heath DG, Ney DR, et al. CT angiography with volume rendering: imaging findings. Am J Roentgenol 1995; 165:445-8.
30 Rensing BJ, Bongaerts A, van Geuns RJ, et al. Intravenous coronary angiography by electron beam computed tomography: a clinical evaluation. Circulation 1998;98:2509-12.

Chapter 7

Breath-hold Coronary MR Angiography with Volume Targeted Imaging

P.A. Wielopolski, R.J.M. van Geuns, P.J. de Feyter, M. Oudkerk.

Published in Radiology 1998;209:209-219

ABSTRACT

Purpose:
To illustrate a new concept for fast coronary artery screening with breath-hold volume targeted magnetic resonance (MR) imaging.

Materials and Methods:
Ten volunteers and 25 patients were imaged at a field strength of 1.5 T with an MR system with phased-array-coil reception and capable of echo-planar imaging. End-expiration breath-hold volume localization of the entire heart was performed with three-dimensional (3D) multishot segmented echo-planar imaging in 16-22 heartbeats. Interaction with a multiplanar reformation platform provided the optimal double-oblique volumes necessary to target seven coronary segments. Each segment was evaluated with 24-mm-thick volumes and breath holds at end expiration and magnetization transfer-enhanced 3D turbo fast low-angle shot imaging in 21 heartbeats. An intravascular contrast agent was used on eight patients to improve the blood-myocardium contrast for the heart volume localizer acquisitions.

Results:
The entire coronary tree was consistently covered in fewer than 13 breath holds. The scheme was successful in all volunteers and 22 patients who could achieve adequate breath hold. With end-expiration acquisitions, the prescribed 24-mm-thick volumes were reproducible for all coronary segments in all cooperative subjects.

Conclusion:
Despite its status as the indisputable standard of reference for the detection of coronary artery disease, conventional coronary angiography remains costly and highly invasive, with associated risks of major complications, including stroke and death. Breath-hold volume targeted acquisitions permit rapid localization and coverage of the entire coronary tree with adequate resolution for evaluating the coronary arteries.

INTRODUCTION

Direct visualization of the coronary arteries has been attempted with contrast material-enhanced two-dimensional (2D) echocardiography.[1] Drawbacks still remain in that only the proximal coronary segments may be occasionally observed and considerable chest wall interference and intervening pulmonary parenchyma may hinder visualization. Trans-esophageal 2D echocardiography has been explored with encouraging initial results for the detection of left main coronary artery stenoses.[2] Nonetheless, relative invasiveness of the technique, the low frequency of left main coronary stenosis, and the inability of the technique to reveal distal portions of the coronary tree limit its clinical utility.

Breath-hold contrast-enhanced electron-beam computed tomography has proven successful for imaging the proximal portion of the coronary tree.[3,4] Although completely noninvasive, it exposes the patient to ionizing radiation and requires the use of iodinated contrast material, which occasionally causes severe allergic reactions. With excellent soft-tissue contrast and double-oblique tomographic section capability, magnetic resonance (MR) imaging appears to be a promising imaging technique in this regard. Both cardiac anatomy[5,6] and physiology[7,8,9] can be assessed in a single comprehensive session. However, the sensitivity of MR imaging to motion has always posed a major challenge for imaging the beating heart. Blurring and ghosting induced by respiratory motion are among the many problems that have hampered reliable MR image quality in cardiac examinations, especially for screening the small coronary arteries.

In the past few years, faster cardiac MR imaging techniques have been introduced that provide considerable time savings, flexibility, and motion artifact reduction without a significant compromise in image quality. With the introduction of the turbo fast low-angle shot (Turbo-FLASH; Siemens, Erlangen, Germany) sequence,[10] several sections could be encoded in a single breath hold with subsecond (300-700 ms) acquisition windows using magnetization preparation pulses and short repetition times (TRs). Nevertheless, to keep blurring within acceptable limits, the number of k-space lines collected had to be reduced to produce shorter acquisition windows (<150 ms). Enhanced temporal and spatial resolution was then obtained with the segmented TurboFLASH technique, which distributed the acquisition over multiple cardiac cycles.[11] This approach was initially investigated for screening of the coronary arteries, with encouraging results,[12] and has remained the MR imaging reference standard for the evaluation of more recent coronary MR angiography techniques.[13]

State-of-the-art gradient hardware has become widely available in new commercial MR units, providing stronger imaging gradients (>20 mT/m) and enhanced rise times (slew rates >80 mT/m/msec). Additionally, phased-array coil technology can deliver a higher signal-to-noise ratio (SNR) over a wide field of view (FOVs). These together have made it practical to reduce TR for TurboFLASH readouts, effectively increasing the number of k-space lines collected per unit time and thereby providing faster acquisitions, higher spatial resolution, and more reliability for breath-hold cardiac examinations. High-performance gradient systems have also made it possible to perform three-dimensional (3D) volumetric imaging of the heart with segmented echo-planar techniques.

Single-breath-hold volumetric imaging of the heart with isotropic resolution has been introduced recently.[14,15] The inspection of such volume data sets by means of multiplanar reformation (MPR) can yield information on the optimal-double oblique volume orientation for further investigation of the entire

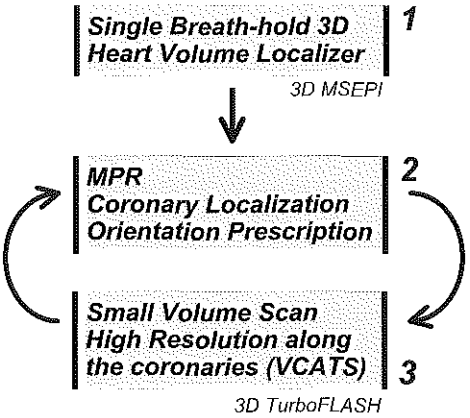

Figure 1. Acquisition steps. The first step involves the acquisition of a scout volumetric data set during endexpiration using 3D multi-shot segmented echo-planar imaging (MSEPI). The volume data are subsequently evaluated within a MPR platform to interactively compute the optimal orientation for imaging of the coronary arteries with an end-expiration breath-hold 3D segmented TurboFLASH sequence (VCATS). MPR evaluation and imaging with the 3D segmented TurboFLASH sequence is performed interactively until all necessary orientations covering all major coronary segments are interrogated.

coronary anatomy with smaller targeted volumes. In the present study, we explore this possibility and take advantage of the high-performance gradient hardware available for obtaining the highest in-plane resolution and volume coverage possible within a comfortable breath hold. We lable this approach volume coronary angiography using targeted scans (VCATS), with the primary goal to cover the coronary anatomy in a few breath holds and to avoid the section misregistration problems during review that are present with breath-hold single-section 2D single-slice coronary MR angiography.[16-19]

MATERIALS AND METHODS

Subjects

Ten healthy young adult volunteers (eight men, two women; age range, 22-47 years; mean, 30.6 years) were initially evaluated to tune the measurement protocol. In addition, 25 patients with known coronary artery disease (20 men, five women; age range, 43-73 years; mean, 57.7 years) were included to study the proposed methodology in a clinical setting. Only 13 patients underwent conventional coronary angiography within 1 month that would be suitable for comparison. In eight patients, superparamagnetic iron oxide particles (AMI 25; Laboratoire Guerbet, Aulnay-sous-bois, France) were administered to study the possible contrast enhancement between blood and myocardium. A suspension containing 89.6 mg of iron (11,2 mg/ml iron) diluted in 100 ml of isotonic glucose solution was infused intravenously through a filter in 30 minutes. Imaging was performed within 1 hour of contrast material administration. The protocol was approved by the Hospital Committee on Clinical Investigation, and informed consent was obtained from all participants.

Acquisition procedures

Coronary screening is performed with two 3D MR pulse sequences with two clearly defined objectives: localization and targeting. A volume localizer sequence is used to image the entire heart volume to provide the necessary input data for targeted imaging of the coronaries (VCATS). The diagram of Figure 1 illustrates the logic followed during each imaging session.

The procedure for the localization and evaluation of all coronary segments is summarized in the following steps:

1. A single end-expiration breath-hold 3D localizer sequence is used to cover the entire heart.
2. The heart volume localizer data are loaded into the MPR platform and evaluated with focus on one coronary segment at a time.
3. The optimal double-oblique plane and slab position containing the coronary segment of interest is recorded.
4. Slab position and double-oblique plane orientation are used for the end-expiration

Table. Coronary Segments Routine Evaluated Volume

No.*	Coronary segment evaluated
1	Plane along left main artery, proximal LCX, and proximal LAD (transverse)
2	Plane of proximal RCA (transverse)
3	Plane along distal RCA and PDA (oblique)
4	Plane through aortic root and proximal RCA and leftmain (oblique)
5	Plane along LCX (oblique)
6	Plane along distal LAD (oblique)
7	Plane along middle portion of RCA (oblique)

Note.-LAD = Left anterior descending artery, LCX = Left circumflex artery, RCA = Right coronary artery, PDA = Posterior descending artery.

**The coronary segments were acquired in the same order as indicated by the volume number.*

breath-hold VCATS.

5. The process is repeated (steps 2-4) until all coronary segments are evaluated.

Coronary segments evaluated

The coronary segments that were studied during all evaluations are summarized in the Table. Additional planes could be included, with use of orthogonal orientations to the standard defined views-for example, a plane containing the RCA along the atrioventricular groove and tangential to the heart wall, or the distal portion of the LCX, tangential to the posterolateral wall of the heart.

Coronary plane selection for VCATS

When using an axial heart volume localizer sequence, the transverse sections reconstructed already identify the levels at which the proximal RCA, left main, LCX, LAD and, occasionally the distal portion of the RCA should be interrogated with VCATS. To obtain the slab position and plane orientation information containing the coronary segments of interest, MPRs are performed on the heart volume localizer data in the same order as illustrated in the table. The logic behind the MPR platform described is based on that of the package delivered as part of the Siemens Magnetom imager (Numaris 3 software level). A short description of this MPR platform follows.

The MPR platform in double-oblique mode uses three displays (output quadrants or Qs). Quadrants Q1 and Q2 are used for double-

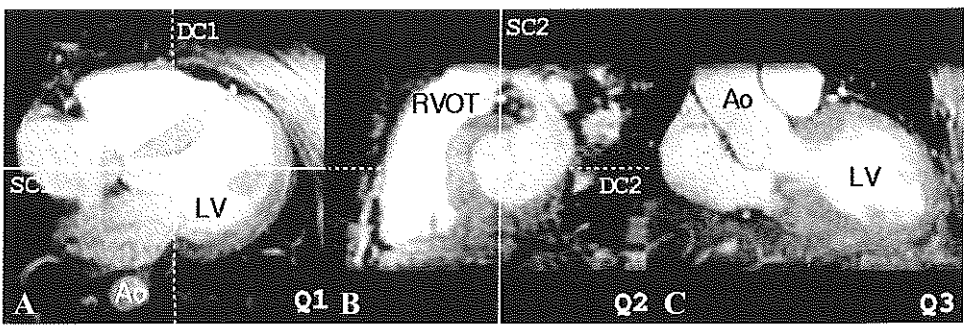

Figure 2. *Heart volume localizer images as seen on the MPR platform. The images show* ***(A)*** *transverse,* ***(B)*** *sagittal, and* ***(C)*** *coronal reformations on display quadrants Q1, Q2, and Q3, respectively. The solid and dashed cursor lines in Q1 and Q2 are used to control the orientation and position of the image in Q3. Dashed cursor DC1 produces the imaging plane of Q2. Solid cursors SC1 and SC2 determine the tilt seen in Q3. Cursors SC1 and DC1 are coupled to each other as they rotate and translate. Cursors SC2 has complete freedom of movement, and dashed cursor DC2 moves only from top to bottom to change the section position in Q1. The data was acquired in 16 heartbeats by using a 64h × 256 matrix (where h denotes partial Fourier encoding), FOV of 170 × 340 mm, and 90 1.25 mm-thick sections. An intravascular contrast agent was administered to enhance the myocardium-blood contrast-to-noise ratio. Ao = aorta, LV = left ventricle, RVOT = right ventricular outflow track.*

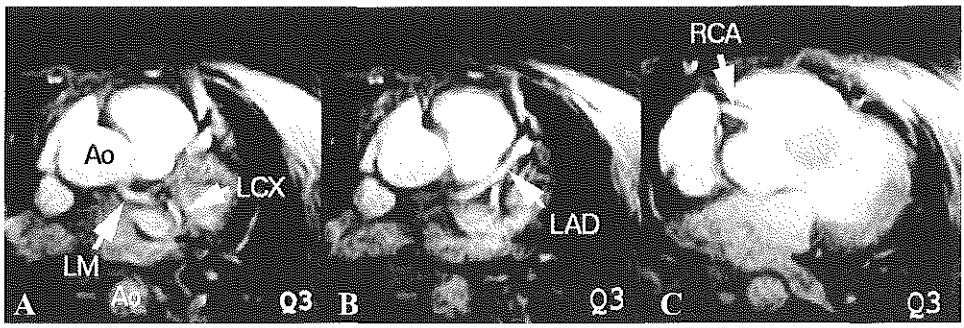

Figure 3. *Locations of interest in the transverse sections of the volume localizer acquisition are the* ***(A)*** *left main (LM) and LCX (Ao = aorta),* ***(B)*** *LAD, and* ***(C)*** *RCA. Q3 = display quadrant 3.*

oblique localization. Quadrant Q3 displays the resulting image from which plane orientation and slab shift are recorded for VCATS. Plane manipulation cursors in Q1 and Q2 permit the double-oblique tilt of Q3. Figure 2 depicts the starting point of the MPR evaluation, showing the extent of the heart volume covered. Both solid cursors available in Q1 and Q2 (SC1 and SC2, respectively) tilt the reconstructed plane in Q3. A plane along the dashed cursor in Q1 (DC1) appears in Q2. The dashed cursor in Q2 (DC2) controls the section position of the image displayed in Q1. The resultant image plane in Q3 is perpendicular to those defined by cursors SC1 and SC2.

Positioning of the cursors in Q1 and Q2 is described for each coronary segment. It is assumed that for all segments, an axial section is always displayed in Q1.

Volumes 1 and 2: Plane for left main, proximal LAD, proximal LCX and proximal RCA.

A transverse orientation can be chosen directly in the measurement platform for VCATS. The appropriate slab position is determined from transverse reformations using the MPR platform in an orthogonal mode. The following positions are recorded by shifting any available cursor along the cranialcaudal direction (on a coronal or a sagittal reformation):

1. Level of the left main artery (for imaging the left main artery, proximal LAD and proximal LCX) (Figures 3A,B).
2. Level of the proximal RCA (Figure 3C).

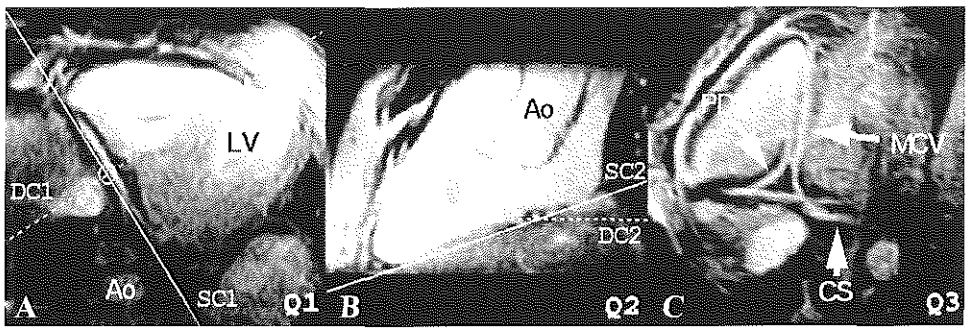

Figure 4. *Position and plane determination for the distal RCA and PDA.* ***(A)*** *In display quadrant Q1, solid cursor SC1 is placed along the atrioventricular groove, while dashed cursor DC1 is halfway between the middle portion of the RCA and the bifurcation to the PDA. LV = left ventricle.* ***(B)*** *In Q2, solid cursor SC2 is placed along the liver-heart interface. DC2 = Dashed Cursor 2.* ***(C)*** *The resultant image in Q3 shows the PDA, surrounded by the confluence of the coronary sinus (CS) and the middle cardiac vein (MCV). Ao = descending aorta.*

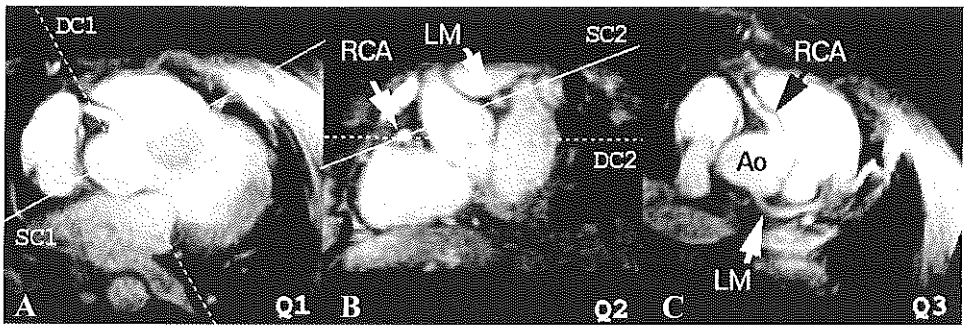

Figure 5. *Position and plane determination for the aortic root, proximal RCA and left main artery (LM).* ***(A)*** *After a plane containing the proximal RCA is selected in display quadrant Q1, dashed cursor DC1 is positioned along the atrioventricular groove, with solid cursor SC1 crossing the center of the aortic root.* ***(B)*** *In Q2, solid cursor SC2 connects the RCA and left main artery. DC2 = Dashed Cursor 2.* ***(C)*** *The resultant image in Q3 shows the aortic root plane. Ao = aorta.*

Volume 3: Plane for the distal RCA and the PDA.

The distal RCA and the PDA can be seen on transverse-plane images whenever the RCA turns to the inferior wall of the ventricles. However, only short segments may be visualized, depending on the patient's thoracic geometry. Shorter thoracic cavities most frequently present both the distal RCA and PDA in transverse sections. Subjects with longer thoracic cavities necessitate a plane tilt towards the cranialcaudal direction.

With use of cursor DC2, an image showing the distal RCA is selected in Q1. Cursor SC1 can than be placed parallel to the distal RCA (Figure 4A). In Q2, a parasagittal reconstruction appears, demonstrating the interface between the liver and wall of the right ventricle (Figure 4B). By shifting DC1, the RCA can be identified as it runs along the atrioventricular groove, tangential to the heart wall, and later along the heart-liver interface. Cursor SC2 is than placed along the liver-heart interface to produce an image in Q3 that is tangential to the bottom of the heart, showing the PDA and the coronary sinus and drainage of the middle, posterior, and small cardiac veins (Figure 4C).

Volume 4: Plane for the aortic root and proximal RCA and left main artery.

With use of cursor DC2 to obtain a suitable transverse plane in Q1 (showing the aortic root and start of descent of the RCA), DC1 is placed parallel to the atrioventricular groove, while SC1 transverses through the

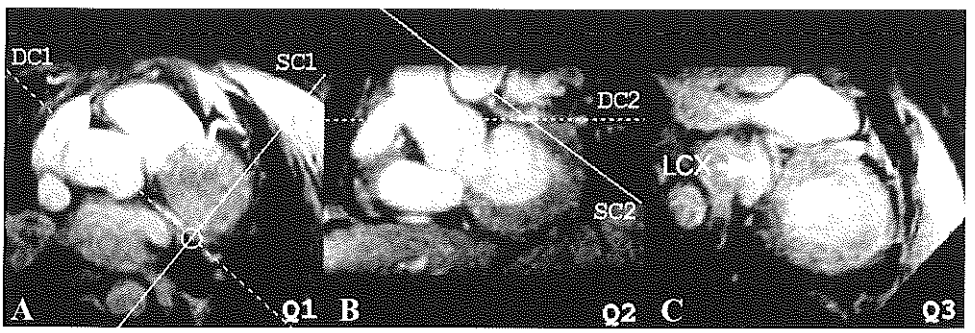

Figure 6. *Position and plane determination for the LCX.* ***(A)*** *On an image in display quadrant Q1showing part of the LCX, dashed cursor DC1 is placed along the length of the LCX. SC1 = solid cursor 1.* ***(B)*** *In Q2 solid cursor SC2 is positioned along the LCX to illustrate a larger portion of the artery. DC2 = dashed cursor 2.* ***(C)*** *In the resultant image in Q3, the larger portion of the LCX is shown inplane.*

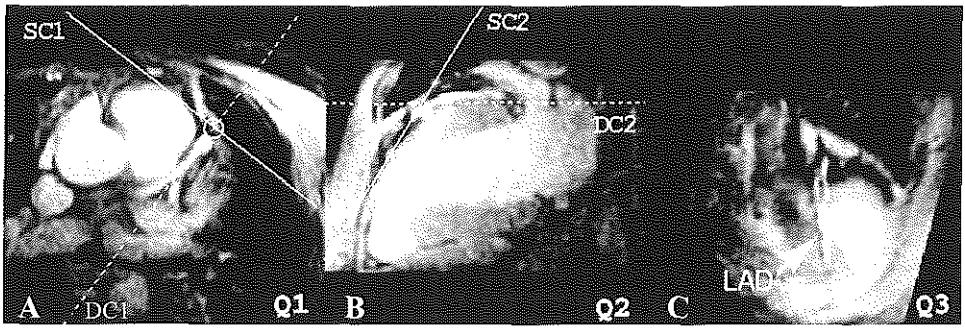

Figure 7. *Position and plane determination for the distal LAD.* ***(A)*** *In display quadrant Q1, dashed cursor DC1 is placed along the proximal LAD and solid cursor SC1 close to the anterior wall.* ***(B)*** *In Q2, this produces an image with the LAD along the anterior wall of the heart. Solid cursor SC2 is then placed along the heart-anterior thorax interface. DC2 = dashed cursor 2.* ***(C)*** *On the resultant image in Q3, the distal portion of the LAD can be identified.*

aortic root (Figure 5A). By shifting (and rotating) DC1, the image in Q2 demonstrates the origin and course of both the RCA and left main artery (Figure 5B). Cursor SC2 is used to connect both vessels to obtain the desired plane in Q3 (Figure 5C).

Volume 5: Plane for the proximal and distal LCX

The proximal LCX can be readily observed on transverse sections. However, a longer view may be reconstructed that can show the LCX from its bifurcation from the left main artery. By selecting a transverse reformation in Q1 in which the LCX is seen (Figure 6A), cursor DC1 can be placed along its length to demonstrate a parasagittal section in Q2 (Figure 6B). By shifting DC1, the LCX will be better appreciated, and cursor SC2 is placed along the LCX to obtained the desired view in Q3 (Figure 6C).

To evaluate a more distal portion of the LCX, cursor DC1 may be shifted to show in Q2 the LCX running along the posterolateral wall of the heart. Cursor SC2 can then be placed along this portion of the LCX.

Volume 6: Plane for middle and distal portions of the LAD

The orientations for viewing the mid- and distal portions of the LAD were reviewed by Sakuma et al.[20]

By using a thick volume, both the middle and distal portions of the LAD may be viewed

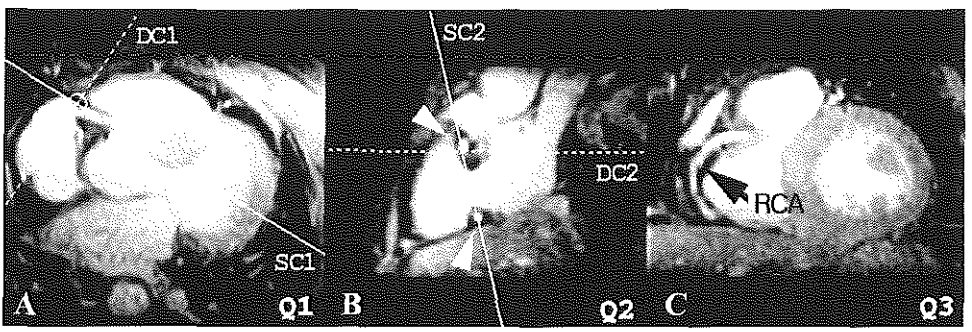

Figure 8. *Position and plane determination for the middle portion of the RCA.* ***(A)*** *In display quadrant Q1, solid cursor SC1 is directed along the proximal RCA and dashed cursor DC1 along the edge of the heart.* ***(B)*** *in Q2, this produces a perpendicular view of the RCA (tangential view of the atrioventricular groove), Solid cursor SC2 is then placed along the groove intercepting both proximal and distal RCA (arrowheads). DC2 = dashed cursor 2.* ***(C)*** *The resultant image in Q3 shows the middle portion of the RCA.*

with one single orientation and position with VCATS. With the use of DC2 to locate the level of the proximal LAD in Q1, cursor DC1 can be positioned along the vessel (Figure 7A) to provide a parasagittal section in Q2, with the LAD advancing towards the anterior wall of the heart (Figure 7B). Cursor SC2 is used to find the average tilt between the middle and distal LAD, taking into account the volume scanned in VCATS. Figure 7C shows the reformation of the distal LAD.

Volume 7: Plane for the middle portion of the RCA.

The double-pblique plane is determined as proposed by other investigators.[16,21] Cursor DC2 is used to view the proximal RCA in Q1. Cursor DC1 is positioned perpendicular to the RCA and close to the edge of the heart, perpendicular to the RCA, as illustrated in Figure 8A. This produces an image in Q2 (Figure 8B) showing the atrioventricular groove, with the RCA entering and leaving the plane of section (proximal and distal RCA, respectively). By placing cursor SC2 along the atrioventricular groove and intercepting the RCA in the two points observed, Q3 will demonstrate a long view of the middle portion of the RCA (Figure 8C).

Imaging

Imaging was performed with the 1.5-T Siemens Magnetom Vision platform. The whole-body coil was used for signal excitation. All subjects were positioned supine with a four-channel quadrature body phased-array coil placed over the thorax for signal reception. Sequences were designed to use the maximum gradient strength available, 25 mT/m, and gradient rise times of 300 msec (83 T/m/s) in resonant mode for the heart volume localizer sequence and 600 msec (42 T/m/s) in nonresonant mode for VCATS. The acquisition modules used for the measurement protocol are described below.

2D localizer sequence and assessment of overall fat suppression

A selective water-excitation three-plane scout sequence (5 seconds) permits rapid anatomic positioning and assessment of magnetic field homogeneity over the entire thorax. The standard shim setting of the systems for a body acquisition was used. The imaging protocol continued only if fat suppression was uniform over the liver, arms, and anterior and posterior thoracic walls while the signal intensity of blood in the cardiac chambers remained high. Otherwise, the shim channels were adjusted manually or automatically using the manufacturer's shimming platform (MAP-shim; Siemens)[22] until the scout scan showed the desired results.

Heart volume localizer sequence

A 3D multishot segmented echo-planar imaging sequence was chosen. A 150-msec data collection window was assigned per cardiac cycle to encode 56 sections shared over two cardiac cycles. An echo-planar readout with four echoes per radio-frequency excitation was used, with an echo spacing of 1 msec and signal sampling performed with a nonlinear analog-to-digital-converter trigger raster during the entire echo-planar readout. This trigger raster could sample k-space uniformly using only 256 sampled points per echo during the varying gradient waveform (trapezoidal gradient readout with 300-msec sinusoidal ramps and a 400-msec flat top and equivalent readout bandwidth of 1,280 Hz per pixel. The echoes were mapped along the in-plane phase encoding direction using an interleaved k-space trajectory[23,24] with partial Fourier encoding and reconstruction. An effective echo time (TE_{eff}) (echo time of the first echo of the echo-planar train) of 1.4 msec was chosen, providing a readout packet with TR msec

/TE_{eff} msec of 5.55/1.4. Imaging time was set to 16-24 heartbeats by using a minimum FOV of 160 × 320 mm with a 64h-96h × 256 matrix. An incremental flip angle series was used to optimize SNR (linear increment, 16°-25°). In general, 90 sections were reconstructed by using a volume of 120 mm. Data acquisition was performed during middle-to-late diastole with a breath hold at end-expiration.

Magnetization transfer contrast (MTC) preparation was included (500-msec application period) before application of a single chemical shift fat suppression pulse to increase contrast between the blood pool and myocardium. The MTC irradiation consisted of a train of 25 radio-frequency pulses of 7.680-msec duration, Gaussian profile, 250-Hz bandwidth, 1.5-kHz offset frequency, and 6-mT amplitude applied with an interpulse spacing of 20 msec. A 9.728-msec Hamming-filtered sync pulse with a bandwidth of 200 Hz was used for fat suppression.

VCATS

A double-oblique 3D segmented TurboFLASH sequence (5.3/2.3) was selected to target each coronary segment. The readout module acquired 21 lines per segment with partial Fourier encoding with an acquisition window of 110 msec per cardiac cylce. The volume targeted was set to a thickness of 24 mm. The sequence was tailored to permit a minimum FOV of 230 mm for a 256 × 256 matrix acquired with a readout bandwidth of 390 Hz per pixel. MTC radio-frequency pulses were applied prior to a single chemical shift fat suppression pulse with the same irradiation time and characteristics as in the heart volume localizer sequence. Seven section-select phase-encoding steps encoded the volume, and the number of reconstructed sections was freely selectable to ease the review process (default of 16 1.5-mm-thick reconstructed sections). The selection-select profile was optimized to deliver a sharply defined volume with minimal aliasing and SNR loss at the edge sections. An incremental flip angle series was used to optimize SNR (linear increment, 14°-34°). The measurement time was 21 heartbeats for a 126h × 256 acquisition matrix. An FOV of 320 mm was selected, with a rectangular FOV ratio of 3:4. The trigger delay matched that of the volumetric heart localizer sequence, and the data was acquired during end expiration. To reduce reconstruction time, only the anterior elements from the four-channel phased-array coil were used to image volumes 6 and 7.

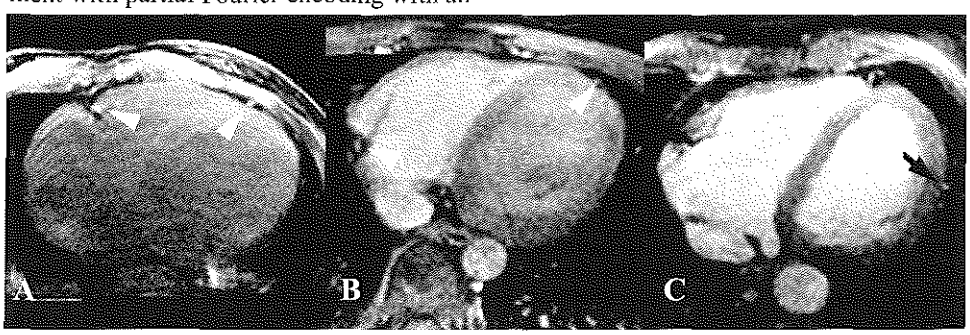

Figure 9. *Determination of the effectiveness of the application of MTC and intravascular contrast agents on the heart volume localizer images (three different subjects). These transverse sections were reconstructed with a 5-mm thickness.* ***(A).*** *On image obtained without MTC or intravascular contrast, blood remains saturated (myocardium has slightly higher signal intensity).* ***(B)*** *MTC without contrast agents provides slight but positive contrast between blood and myocardium. Arrowheads in A and B point at the RCA and LAD, which are clearly visible when surrounded by suppressed fat.* ***(C)*** *MTC with contrast agent provides better depiction of vascular structures (arrow) over the myocardium.*

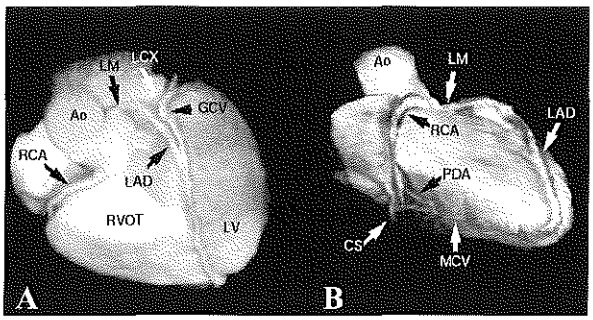

Figure 10. *(A) Cranialcaudal and* ***(B)*** *lateral views of the coronary arteries after volume rendering of the heart volume localizer data, used for MPR, as shown in Figures 2-8. The data was acquired in 16 heartbeats. The patient received intravascular contrast agent to enhance contrast between blood and myocardium. Ao = aorta, CS = coronary sinus, GCV = great cardiac vein, LV = left ventricle, MCV = middle cardiac vein, RVOT = right ventricular outflow track.*

Ghosting and aliasing artifact reduction

Two saturation bands were used to reduce ghosting or aliasing or both. A single oblique saturation band was placed over the anterior chest wall and maintained for all volume orientations. For volume 7 (middle portion of the RCA), a second saturation band covered the left thoracic cage and arm to avoid aliasing.

Data evaluation

With 3D multishot echo-planar volume localizer imaging, the heart could be segmented from surrounding structures and volume rendered to display the coronaries over the heart from any desired view. Heart segmentation was performed on a MagicView viewing station (Siemens). The segmented data was then transferred to an Indigo2 workstation (Silicon Graphics, Mountain View, Calif), and volume rendering was performed with VoxelView (Vital Images, Minneapolis, Minn).

Comparison between conventional coronary angiography and VCATS was performed only when major stenoses were detected on the former. The VCATS data was reviewed with the dynamic display option of the MR system, showing the reconstructed sections in a cine. The VCATS data could also be segmented to eliminate unwanted structures and volume rendered to show the entire coronary segment.

RESULTS

Good quality data were obtained in all volunteers and in 22 patients who were able to endure a 21-second breath-hold acquisition. Figure 9 illustrates the effect that the addition of the intravascular contrast agent has on the contrast-to-noise for blood and myocardium. Figure 9A illustrates a transverse section close to the heart apex from a 3D multishot segmented echo-planar acquisition without MTC and contrast agent. Figure 9B illustrates a case in which only MTC was applied, while Figure 9C demonstrates the contrast enhancement possible with both MTC and the intravascular contrast agent. It can be noted that even without the contrast agent, the coronary arteries can be visualized in Figure 9A and 9B because the vessels are surrounded by fat (vessels indicated by arrowheads). However, the higher contrast-to-noise ratio possible with the intravascular contrast agent enhances the image postprocessing if the heart volume localizer is volume rendered to produce a 3D display. The data from the heart volume localizer illustrated in Figures 2-8, also acquired with the intrasvascular contrast agent, were used to demonstrate this possibility, resulting in two volume-rendered views (cranialcaudal and lateral) of the heart (Figure 10). The VCATS results from this patient are demonstrated for comparison with the localization procedure described in the Materials and Methods section.

Five example VCATS are depicted in Figures 11 and 12. Figure 11A-11D displays selected views from four VCATS acquired in the region of the proximal RCA and left

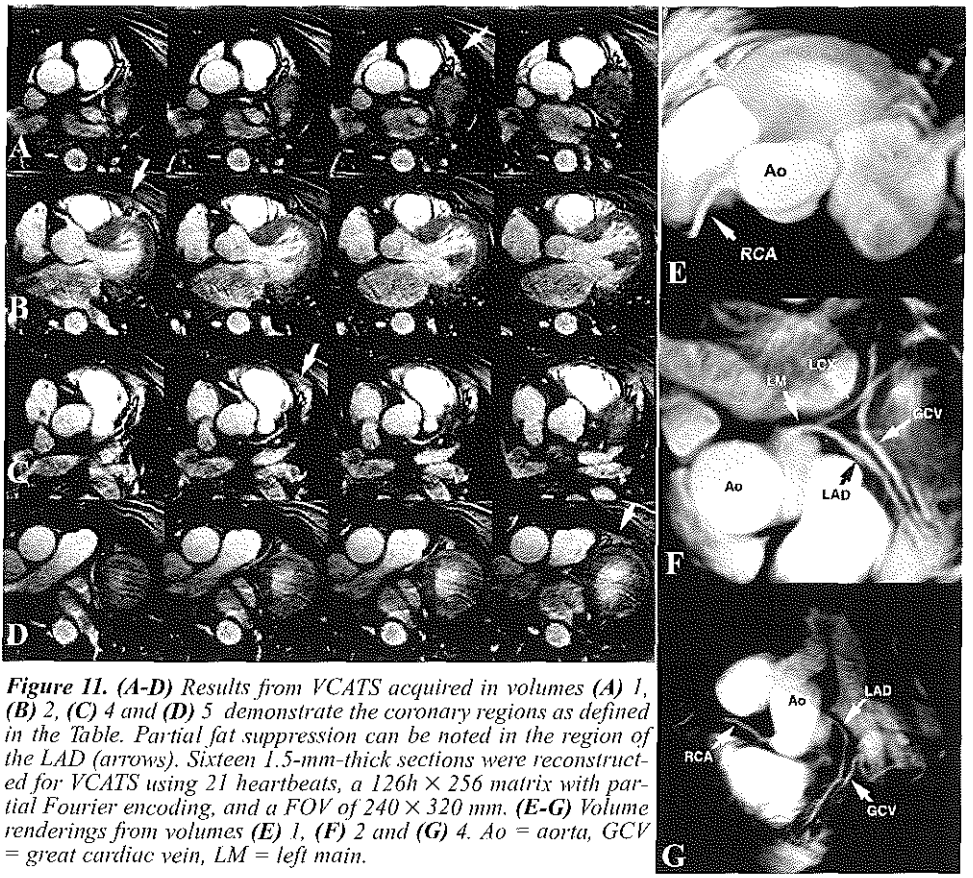

Figure 11. *(A-D) Results from VCATS acquired in volumes* ***(A)*** *1,* ***(B)*** *2,* ***(C)*** *4 and* ***(D)*** *5 demonstrate the coronary regions as defined in the Table. Partial fat suppression can be noted in the region of the LAD (arrows). Sixteen 1.5-mm-thick sections were reconstructed for VCATS using 21 heartbeats, a 126h × 256 matrix with partial Fourier encoding, and a FOV of 240 × 320 mm.* ***(E-G)*** *Volume renderings from volumes* ***(E)*** *1,* ***(F)*** *2 and* ***(G)*** *4. Ao = aorta, GCV = great cardiac vein, LM = left main.*

main artery (volumes 1-3, 5, respectively). Volume 5 (Figure 11D, VCATS along the LCX) shows a slight ghost of the anterior chest wall over the left ventricle. This ghost arose because of an inadequate breath hold. With a 126h × 256 in-plane matrix, three ghosts will appear if inconsistent breath holding and provide direct feedback for the operator to repeat the acquisition. The VCATS from target volumes 1, 2 and 4 were volume rendered and are depicted in Figures 11E-G, respectively. Nine sections from volume 3 (distal RCA and PDA) and the corresponding rendered volume are demonstrated in Figure 12. Homogeneous fat suppression was not always present over the entire volume, as

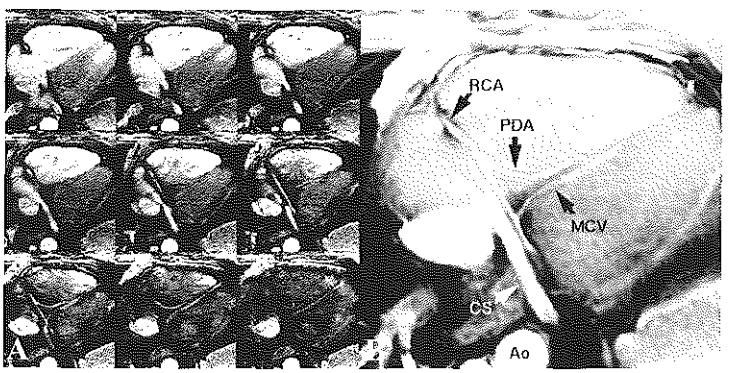

Figure 12. *Targeting of the distal RCA and PDA.* ***(A)*** *The center nine sections (from 16 reconstructed for VCATS) are displayed.* ***(B)*** *Volume rendering integrates the entire course of the distal RCA. Acquisition parameters as in Figure 11. Ao = aorta, CS = coronary sinus, MCV = middle cardiac vein.*

seen in Figures 11 and 12. This was a problem in the region of the middle and distal LAD in most subjects. In these cases, the cancellation effect from the opposed-phase behavior of fat helped to delineate the boundary between the distal LAD branch and surrounding fat. The vessel lumen will always be somewhat reduced, especially when the vessel is small relative to the voxel size used. A volume localizer image was reconstructed for a patient with a severe stenosis in the LAD (shown on the conventional coronary angiogram in Figure 13A). Figure 13B illustrates the that a large lesion can be detected of on the volume localizer image after volume rendering. Figure 13C depicts the volume-rendered data from VCATS (volume 1), clearly demonstrating the stenotic LAD.

DISCUSSION

Breath-hold 2D coronary MR angiography targets the coronary arteries interactively using an acquisition positioning platform and the results from several localizer acquisitions during previous breath holds. Once the double-oblique plane and section position are identified, several breath holds follow during which neighboring locations are imaged to account for vessels with a tortuous path. Although the localization procedure has been standardized for certain segments, this does not include situations in which coronary arteries have an abnormal course, such as in congenital anomalies[25,26] or heart rotation after infarction or heart transplantation.[27] Rapid localization of coronary bypass grafts can be even more cumbersome.

The motivation for 3D coronary MR angiography (with free breathing and averaging and retrospective and prospective navigator approaches) was to the need for providing an easy setup that covered the entire heart and eliminated the burden of requiring a highly skilled operator performing the examination. The availability of 3D processing tools permits appropriate data management and evaluation after data collection is completed. Regardless of the method of choice, however, high-resolution, isotropic-voxel 3D coronary MR angiography remains a lengthy examination despite the advances made in gradient and signal reception hardware and sophisticated measurement controls. This is where our approach differs from a 3D evaluation of the coronary tree. We believe that VCATS along the main course of the coronaries can provide the necessary resolution to quantify stenosis and remains the fastest imaging approach.

Coronary localization with the heart volume

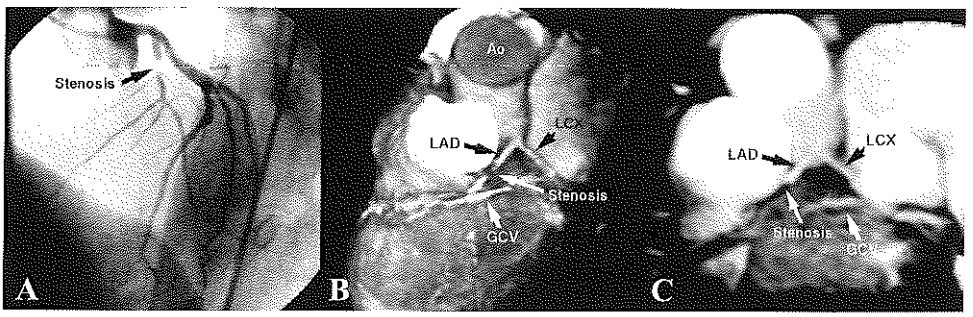

Figure 13. *Images obtained in a patient with LAD stenosis.* ***(A)*** *Conventional coronary angiography demonstrates the severity of the lesion. (B) The large stenosis can be detected on the volume rendered images obtained from the heart volume localizer data. Ao = aorta.* ***(C)*** *Volume rendering from the sections acquired with VCATS provides a clear depiction of the stenosis. The subject did not receive the intravascular contrast agent. Data for the localizer images were acquired in 22 heartbeats, with an 88h × 256 matrix with partial Fourier encoding, an FOV of 160 × 320 mm, and 120 reconstructed sections (1.16 mm thick). GCV = great cardiac vein.*

localizer sequence, based on standard landmarks in the heart, is easy for a trained operator. The same procedure that has been followed with 2D breath-hold imaging can be performed interactively during data collected without the necessity of instructing the patient to perform numerous breath holds, which are necessary only for VCATS. The volume that VCATS focuses on can be readily seen on the MPR platform, and the coverage necessary can be adjusted accordingly, provided that breath-hold position at end expiration is consistent. In our experience, seven volumes can target the entire coronary tree and all required orientations can be determined. An approach that is comparable to our setup but with use of a real-time MR fluoroscopic imaging system[28] has been proposed. The MR fluoroscopy system can position planes interactively over the beating heart and transfer position and plane orientation information automatically for a high-resolution 2D breath-hold acquisition. The following points touch on the potential advantages and drawbacks of the method and generalize some aspects that are applicable to 2D and 3D coronary MR angiography implementations that uses proton-density-weighted segmented TurboFLASH readouts.

Resolution of the heart volume localizer sequence

Even in the case of a low-resolution heart volume localizer sequence (on imaging systems with weaker and slower gradients), it is possible to determine the coronary planes without a good depiction of the coronary arteries themselves, on the basis of known landmarks in the heart (as described in the Materials and Methods section). Improved resolution is necessary only for the localization of certain coronary segments with smaller lumens, such as the distal LCX. Operators can be trained in the procedures on higher-resolution heart volume data sets (eg, acquired with 3D navigator approaches) to improve confidence in localization.

Coronary visualization

Fat suppression is of utmost importance for coronary MR angiography techniques that use a proton-density-weighted approach to unequivocally observe the coronary vessels, which are generally surrounded by pericardial fat. Nonetheless, most techniques have relied on the choice of an opposed-phase echo time for detection of the dark boundary arising between coronaries and fat in cases with poor fat suppression. The volume localizer sequence has a unique advantage in that it can provide immediate volumetric information on the quality of the fat suppression over the heart. In regions such as the distal LAD, fat suppression has been routinely difficult, and this could be detected immediately after the initial evaluation of the volume acquisition on the MPR platform. As a result, shim settings could be readjusted to deliver a more homogenous field over the entire heart. In five of our patients, shim settings were changed based on this basis. With the flexibility for rapid localization described, shimming may be customized per region evaluated to ensure the best results. This has been attempted, but it requires a rather cumbersome time-consuming protocol. Future enhancements of this technique will include automatic localized shimming. The use of a spectral spatial radio frequency excitation (eg, binomial series 1-1, 1-3-1 and so on, where _ means a 180° phase shift in the precession of fat protons) is clearly superior than frequency-selective chemical shift fat suppression schemes.[29] Good water-only selectivity is time-consuming if applied to each radio frequency excitation in a TurboFLASH imaging scheme, lengthening TR. With a longer TR, resolution would have to be sacrificed to maintain the acquisition window per cardiac cycle of less than 150 msec. Spectral spatial excitations have been only realistic for coronary MR angiog-

raphy techniques that use spiral imaging readouts, in which a single excitation is generally used per cardiac cycle or cardiac phase in cine acquisition.

Likewise, suboptimal fat suppression can induce some ghosting artifacts on the 3D multishot segmented echo-planar volume localizer acquisition due to high-signal-intensity fat close to the reception coils. Ghosting intensified as more echoes per excitation were collected (due to amplitude modulation from T2* decay and the in-phase, opposed-phase behavior in the echo train).

Stronger main magnetic field and improved gradient hardware

At 1.5T, the use of more compact gradient waveforms to speed the acquisition may not be realized, as most techniques have relied on an echo time with an opposed fat-water behavior to circumvent poor fat suppression while still showing the course of a coronary artery. It is foreseen that coronary MR angiography at higher field strengths (> 1.5T) will benefit not only from higher SNR but also from the addition of stronger and faster local imaging gradients tailored for imaging the heart. Also, at higher field strengths, the out-of-phase fat-water condition would occur at shorter echo times, and with these, there is less sensitivity to phase errors due to flow effects. Furthermore, stronger gradients could increase the overall resolution of 3D multishot segmented echo-planar imaging and permit breath-hold studies with contrast administration at true 1-mm^3 voxel sizes.

Blood-myocardial contrast with magnetization preparations and vessel selectivity

MTC irradiation was applied for both the heart volume localizer sequence and VCATS to improve the blood-myocardium contrast. This enhancement mechanism was proposed previously for 3D coronary MR angiography acquisitions.[30] The application of MTC to the 3D coronary MR angiography acquisition helped in recognizing coronary segments surrounded mostly by myocardium. Addition of the intravascular contrast agent helped improve contrast further and made it possible to produce cleaner volume renderings of the coronary artery tree without major post-processing (Figure 10). The MTC irradiation used enhanced the blood-myocardial contrast by approximately 75%, with a 16% reduction in the signal intensity from the blood pool.

Blood-myocardium contrast could be more pronounced using a T2 preparation scheme with a long TE_{eff} This scheme has been applied previously for 2D[31] and 3D[13,32] imaging in the heart. By choosing a TE_{eff} on the order of 100 msec, suppression of venous signal is possible as a result of the shorter T2 in the presence of lower oxygenation levels.[33] This helps distinguish the LAD and LCX, which run parallel to the great cardiac vein.

Stenosis visualization

Only significant stenoses (larger than the voxel size) have been observed on the heart volume localizer images (Figure 13). It is believed that even with the maximum resolution attainable ($1.25 \times 1.25 \times 1.25$ mm voxels in 32 heartbeats), identification of slight stenosis may still be problematic and that the technique cannot be relied on for routine diagnosis despite the good visualization of all coronary segments.

The spatial resolution possible with breath-hold MR angiogprahy techniques cannot yet match that offered by contrast coronary arteriography. SNR is the greatest limiting factor. The VCATS implementation can acquire a true section thickness of 2 mm and an in-plane resolution of 1.5×0.75 mm in 21 heartbeats. At this resolution, noise prevails. Other breath-hold techniques face the same SNR problem if resolution is not an issue.

At present, the only possibility for high in-plane resolution with adequate SNR is the implementation of a low-readout-bandwidth free-breathing technique that can precisely compensate for cardiac and respiratory motion.

Uniform resolution using a constant breath-hold approach

Patients can have substantially different cardiac periods. To maximize the amount of data collected, four acquisition settings were envisioned initially for the volume localizer and VCATS, with data collection windows of 95, 125, 150, and 180 msec, respectively. With this in mind, the spatial resolution encoded for a specific breath-hold period could be the same for all cardiac rates by using the maximum number of k-space lines that met this design criterion. This approach was abandoned because it involved an operator decision, and a single collection window of 150 msec was adopted for 3D multishot segmented echo-planarimaging and 110 msec for VCATS were adopted to simplify the imaging protocol. Perhaps a more sophisticated pulse-measurement control could make the choice automatically on the basis of the subject's cardiac rate, so that it would appear transparent to the user.

Lumen definition and assessment of breath-hold quality

Two approaches involve encoding k-space. In the present implementation, the section-select phase-encoding steps are collected first (inner loop), with only several k-space along the in-plane phase encoding direction. This k-space filling scheme leads to ghosting similar to what has been observed with 2D coronary MR angiography with poor breath holds. The second option is to change the order in which the phase encodings are performed, that is, to collect the in-plane phase encoding steps first (inner loop) following each section-select-phase encoding step. The first scheme requires a consistent breathhold throughout the acquisition; the breath-hold quality can then be clearly identified and the acquisition repeated if necessary. If ghosting occurs, it will be discrete (three ghosts appear with a 126h × 256 matrix) and can interfere with the visualization of a particular coronary segment. With the second acquisition order, cleaner images may be obtained even without adequate breath holds. The scheme compares with that used in partially gated acquisitions or respiratory ordered phase encoding.[34] However, blurring along both phase-encoding directions and may be difficult to recognize and can easily hide a stenosis. In this lattercase, a navigator echo positioned over the diaphragm could indicate to operator the quality of the breath hold for appropriate feedback.

In our experience, an imaging time of 21 heartbeats is well tolerated. In acquisitions in which the patient could not achieve adequate breath hold, data could be acquired again (or the number of phase-encoding steps could be reduced-eg, 14 heartbeats for a 84h × 256 matrix). Breath-hold acquisitions eliminate vessel blurring due to respiratory motion and can produce more realistic vessel lumens compared with some implementations of free-breathing coronary MR acquisitions (eg, retrospective respiratory-gated 3D navigator coronary MR angiography).

Partial Fourier imaging

Partial Fourier encoding was performed to halve the acquisition time and obtain reasonable coverage and in-plane spatial resolution in a single breath hold. However, partial Fourier acquisitions can produce signal intensity changes and distortion in the image, especially in gradient echo acquisitions. Two potential problems were noted but were seldom observed during this study. A local smear over a coronary could appear when the vessel was surrounded by unsup-

pressed fat. This artifact arises from a poor phase estimate in voxels containing similar water and fat contributions. A streamline effect was noted in vessels oriented obliquely and was attributed to flow-induced phase errors affecting the phase estimate, especially in acquisitions in which no flow compensation is used, as in the present study. This was apparent only near the origin of the RCA in two subjects. The acquisition window occurs during middle-to-late diastole, with peak flow velocities in the coronary arteries. By reducing the echo time, faster imaging gradients may prove useful to decreasing the prevalence of such artifacts.

Contrast agents

In the present study, the parameters used for VCATS were tailored for acquisitions that did not require the administration of an intravascular contrast agent. VCATS uses a proton-density approach that benefits marginally from the presence of contrast agents, especially when targeting a small volume in which blood refreshment most likely occurs with every heartbeat.

With large volumes, such as those used for the heart volume localizer sequence, the slight T1 shortening in blood with the intravascular contrast agent provided greater magnetization recovery in blood between heartbeats. This was enough to maintain a stable contrast-to-noise ratio for cardiac muscle and blood in any compartment, independent of flow patterns and volume scanned (Figure 2-9). The T1 shortening was not quantified, as it may vary with the remaining level of superparamagnetic iron oxide particles in blood after liver uptake (T1 ~ 450-700 msec); thus, the enhancement remains somewhat cardiac rate dependent. Although the use of this contrast agent for cardiac imaging is not optimal, it is advantageous because it helps to improve SNR and contrast-to-noise ratio in volumetric data acquisitions and is readily available on the market.

Future directions

A drawback of the current implementation is the lack of a truly interactive single platform that can integrate both the MPR and the measurement control. Currently, the oblique-plane selection parameters computed by MPR are fed manually to the measurement platform for every volume targeted. This slows planning and acquisition. Automation of this process would greatly enhance the evaluation and this will be a goal for future improvement.

Breath-hold VCATS is a promising alternative for coronary screening, if image resolution can be improved by keeping SNR at levels adequate for providing the necessary diagnostic confidence. This may be possible in the near future with the introduction of contrast agents that produce short T1s (< 50 ms) in blood and provide the necessary SNR enhancement. Contrast agents can also provide fat signal reduction by with a T1-weighted approach that could eliminate the field homogeneity dependent chemical shift fat suppression.

CONCLUSIONS

In this present study, we have described an alternative methodology, VCATS, for fast 3D localization and targeted imaging of the coronary arteries. This protocol, as implemented on our imager, permits rapid imaging of the coronary anatomy in several breath holds, with patient examination times of less than 30 minutes. Furthermore, it provides interactive positioning for optimal coronary viewing, fast feedback, and a nearly operator-independent evaluation.

REFERENCES

1 Weyman AE, Feigenbaum H, Dillon JC, Jhonston KW, Eggelton RC. Noninvasive visualization of the left main coronary artery by cross-sectional echocardiography. Circulation 1976; 54: 169-174.

2 Yoshida K, Yoshikawa J, Hozumi T, et al. Detection of left main coronary artery

stenosis by transesophageal color Doppler and two-dimensional echocardiography. Circulation 1990; 81; 1271-1276.
3 Schmermund A, Baumgart D, Gorge G, Seibel R, Gronemeyer D, Erbel R. Non-invasive visualization of coronary arteries with and without calcification by electron beam computed tomography. Herz 1996; 21(2):118-126.
4 Detrano RC. Coronary artery scanning using electron beam computed tomography. Am J Card Imaging 1996; 10(2):97-100.
5 Crooks LE, Barker B, Chang H, et al. Magnetic resonance imaging strategies for heart studies. Radiology 1984; 153(2): 459-465.
6 Stark D, Higgins CB, and Lanzer P. Magnetic resonance imaging of the pericardium: normal and pathologic findings, Radiology 1984; 150(2): 469-474.
7 Fisher MR, von Schulthess GK, Higgins CB. Multiphase cardiac magnetic resonance imaging: normal regional left ventricular wall thickening. AJR 1985; 145(1):27-30.
8 Pettigrew RI. Dynamic cardiac MR imaging techniques and applications. Radiol Clin North Am 1989; 27:1183.
9 Higgins CB, Holt W, Pflugfelder P, et al. Functional evaluation of the heart with magnetic resonance imaging. Magn Reson Med 1988; 6:121-139.
10 Haase A, Matthaei D, Bartkowski E, Duhmke E, Leibfritz D. Inversion recovery snapshot FLASH MR imaging. J Comp Assist Tomogr 1989; 13:1036-1040.
11 Edelman RR, Wallner HP, Singer A, et al. Segmented turboFLASH: Method for breath-hold MR imaging of the liver with flexible contrast. Radiology 1990; 177:515-521.
12 Edelman RR, Manning WJ, Burstein D, Paulin S. Breath-hold MR angiography of human coronary arteries. Radiology 1991; 181:641-643.
13 Wielopolski PA, Manning WJ, Edelman RR. Breath-hold Volumetric Imaging of the Heart using Magnetization Prepared 3D Segmented Echo Planar Imaging. J. Magn. Reson. Imaging 1995; 4:403-409.
14 Wielopolski P, Feyter P de, Jaegere P de, Bruin H de, Oudkerk M. Single Breathhold Three-dimensional MR Coronary Arteriography. Society of Magnetic Resonance 1996, (abstract) p451.
15 Wielopolski PA, Feyter P de, Bruin H de, Bongaerts AHH, Oudkerk M. Screening with breath-hold 3D MR coronary arteriography. European Society of Radiology 1997, 1124 (abstract), p224.
16 Manning WJ, Li W, Boyle NG, Edelman RR. Fat-suppressed breath-hold magnetic resonance coronary angiography. Circulation 1993; 87(1):94-104.
17 Manning WJ, Li W, Edelman RR. A preliminary report comparing magnetic resonance coronary angiography with conventional angiography. N Engl J Med 1993; 328(12):828-832.
18 Pennell DJ, Bogren HG, Keegan J, Firmin DN, Underwood SR. Assessment of coronary artery stenosis by magnetic resonance imaging. Heart 1996; 75(2):127-133.
19 Duerinckx AJ, Urman MK. Two-dimensional coronary MR angiography: analysis of initial clinical results. Radiology 1994;193(3):731-738.
20 Sakuma H, Caputo GR, Steffens JC, et al. Breath-hold MR cine angiography of coronary arteries in healthy volunteers: Value of multiangle oblique imaging planes. AJR 1994; 163:533-537.
21 Duerinckx AJ. MR angiography of the coronary arteries. Top Magn Reson Imaging 1995; 7(4):267-285.
22 Manabe A. Multi-angle projection shim (MAPshim): in vivo shim adjustment up to 2nd order with 0.2 second sequence time. Society of magnetic resonance 1994, (abstract) p765.
23 McKinnon GC. Ultrafast interleaved gradient-echo-planar imaging on a standard scanner. Magn Reson Med 1993; 30:609-616.
24 Butts K. Riederer SJ, Ehman RL, Thompson RM, Jack CR. Interleaved echo planar imaging on a standard MRI scanner. Magn Reson Med 1994; 31(1)67-72.
25 McConnell MV, Ganz P, Selwyn AP, Li W, Edelman RR, Manning WJ. Identification of anomalous coronary arteries and their anatomic course by magnetic resonance coronary angiography. Circulation 1995; 92(11):3158-3162.
26 Post JC, van Rossum AC, Bronzwaer JG, de Cock CC, Hofman MB, Valk J, Visser CA.

Magnetic resonance angiography of anomalous coronary arteries. A new gold standard for delineating the proximal course? Circulation 1995; 92(11):3163-3171.

27 Davis SF., Kannam JP, Wielopolski P, Edelman RR, Anderson TJ, Manning WJ. Magnetic resonance coronary angiography in heart transplant recipients. J Heart Lung Transplant 1996; 15(6):580-586.

28 Kerr AB, Pauly JM, Hu BS, et al. Real-time interactive MRI on a conventional scanner. Magn Reson Med 1997; 38:355-367.

29 Thomasson DM, Purdy DE, Moore JR, Finn JP. Phase-modulation binomial spatial-spectral pulse design for spin-echo applications. Society of Magnetic Resonance 1995, (abstract) p561.

30 Li D, Paschal CB, Haacke EM, Adler LP. Coronary arteries: three-dimensional MR imaging with fat saturation and magnetization transfer contrast. Radiology 1993;187(2):401-406.

31 Brittain JH, Hu BS, Wright GA, Meyer CH, Macovski A, Nishimura DG. Coronary angiography with magnetization-prepared T2 contrast. Magn Reson Med 1995; 33:689-696.

32 Irarrazabal P, Sachs TS, Meyer C, Brittain J, Nishimura DG. Fast volumetric imaging of the heart. Society of magnetic resonance 1995, (abstract) p1393.

33 Wright GA, Hu BS, Macovski A. Estimating oxygen saturation of blood in vivo with MR imaging at 1.5T. J. Magn Reson. Imaging 1991; 1:275-283.

34 Haacke EM, Patrick JL. Reducing motion artifacts in two-dimensional Fourier transform imaging. Magn Reson Imaging 1986; 4(4):359-376.

Chapter 8

VCATS: Volume Coronary Angiography Using Targeted Scans:

A new strategy in MR Coronary angiography.

R.J.M. van Geuns, P.A. Wielopolski, A.J. Wardeh, H.G de Bruin,

M. Oudkerk, P.J. de Feyter.

Int J Card Imaging, accepted

ABSTRACT

The aim of this study was to explore the clinical possibilities of a new strategy for magnetic resonance imaging of the coronary arteries. 13 patients were studied by Volume Coronary Angiography using Targeted Scans (VCATS) to visualize the major coronary arteries in a series of breathholds. The proximal coronary arteries were clearly seen in 92% and the mid segments in 50 to 70% of the patients. VCATS was able to visualize a total vessel length of the LM (mean: 9.4 ± 3.4 mm), of the LAD 69 ± 20 mm, of the RCA 90 ± 33 mm and of the CX 41 ± 18 mm. There was a reasonable correlation between the VCATS and conventional coronary angiography for vessel diameter ($r = 0.71$), with a slight overestimation of 0.7 mm by VCATS. There were 9 significant stenoses present of which 6 were correctly detected, three were missed and 1 false positive was present.
VCATS is fast strategy for visualizing the major coronary artery branches and has the potential to detect significant stenoses in these branches.

INTRODUCTION

Magnetic resonance angiography of the coronary arteries (MRCA) has been attempted with two-dimensional (2D)[1,2,3] and three-dimensional (3D) techniques [4] either using breath-hold or free breathing acquisitions. To date, most experience has been gathered using a 2D breath-hold segmented gradient echo technique. With this technique, several breath-holds are necessary to scan each coronary segment and this can introduce artifacts when breath-holding is inconsistent, especially with tortuous coronaries.[5] Respiratory gating allows longer acquisition times, which permits the usage of 3D MR-sequences which are better suited to study the complex coronary artery anatomy.[6,7] However the clinical application of this technique is limited by the long acquisition time and residual image blur. A new strategy using targeted volumes along the coronary arteries combining the advantages of 2D-breathhold and 3D coverage may overcome these problems. In this study we will explore the clinical potential of this new strategy which we refer to as Volume Coronary Angiography using Targeted Scans (VCATS).

METHODS

Patients

The study population consisted of 13 patients (9 men, mean age 60 years) who were referred for elective coronary angiography. Exclusion criteria were previous coronary bypass operation, intracoronary stent implantation, artificial pacemakers, intracranial clips, atrial fibrillation, severe claustrophobia, and severe lung disease restricting breathholding capabilities to less then 30 seconds. The protocol was approved by our hospital committee of medical ethics and clinical investigation.

MR angiography

The 13 patients were examined with the new VCATS protocol.[8] The patients were studied in a supine position, with a 4-channel quadrature body phased array coil placed over the thorax, in a 1.5T whole body MR imaging system (Vision; Siemens, Erlangen, Germany). Within the protocol each coronary segment was covered with a 24 mm thick volume containing sixteen 1.5 mm slices. The targeted volume was acquired in 21 heartbeats with a double oblique 3D segmented gradient echo sequence (TR/TE=5.3/2.3 ms) with a partial Fourier matrix of 126 × 256. Resolution was 1.9 × 1.25 × 1.5 mm. Seven breath-hold volumes were used to cover the Left Main (LM), Left Anterior Descending (LAD), Circumflex (CX) and Right Coronary Artery (RCA)(Table 1). To determine the imaging planes for each coronary segment, multiplanar reformations (MPR) were performed on a volume collected in a single breath-hold acquired with a multi-shot echo planar imaging (EPI) sequence prior to VCATS. Total examination time was 30 minutes.

Table 1. Coronary Segments Routine Evaluated Volume

No.*	Coronary segment evaluated
1	Plane along left main artery, proximal LCX, and proximal LAD (transverse)
2	Plane of proximal RCA (transverse)
3	Plane along distal RCA and PDA (oblique)
4	Plane through aortic root and proximal RCA and leftmain (oblique)
5	Plane along LCX (oblique)
6	Plane along distal LAD (oblique)
7	Plane along middle portion of RCA (oblique)

Note.-LAD = Left anterior descending artery, LCX = Left circumflex artery, RCA = Right coronary artery, PDA = Posterior descending artery.
*The coronary segments were acquired in the same order as indicated by the volume number.

MR image analysis

The vessel length of non-occluded arteries visualized was measured with an on screen cursor available in the standard MR evaluation package. Vessel diameter was measured from a spatial profile curve over the proximal coronary arteries. The vessel edge was determined at 50% of the peak intensity of the intravascular lumen.

For the detection of coronary artery stenoses the 16 source images were analyzed in a dynamic loop, independently by a cardiologist and radiologist who were unaware of the cardiac catheterization results. In case of non-agreement consensus was achieved in a joined session with a third blinded investigator. Of the left coronary artery the left main (LM), proximal and mid left anterior descending (LAD) and circumflex (CX) were evaluated. Of the right coronary artery (RCA) the proximal, mid and distal (until the crux) segments were included in this study. These segments were graded as assessable or non-assessable dependent on image quality resulting from signal-to-noise ratio, image blur and presence of breathholding artifacts. The assessable segments were graded as having either no significant or significant disease.

Table 2. Visualization of different coronary artery segments

Segment	No visualized
RCA prox	12 (92%)
RCA mid	7 (54%)
RCA dist	7 (54%)
RDP	4 (31%)
LM	12 (92%)
LAD prox	12 (92%)
LAD mid	11 (85%)
LAD dist	8 (62%)
CX prox	10 (77%)
CX mid	7 (54%)

Conventional coronary angiography

Conventional selective contrast-enhanced coronary angiography (CAG) was performed using the Judkins technique.[9] The mean vessel diameter was measured off-line by an experienced observer using quantitative coronary angiography in a commercial package (CAAS II, Pie Medical, Maastricht, The Netherlands). For the detection of coronary artery stenoses two cardiologists graded the same coronary segments as in MRCA as being either normal or having minimal disease (<50%) versus significant disease (>50%).

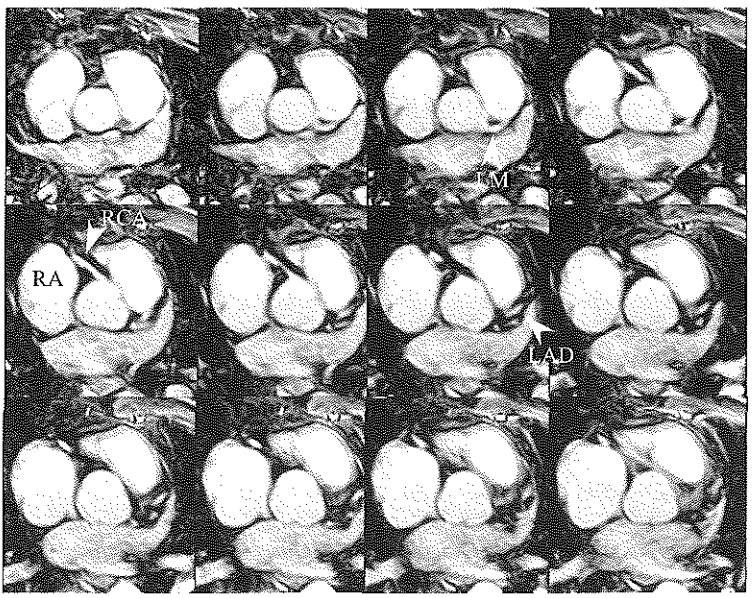

Figure 1. *Example of 12 slices from a volume of 16 slices in a single breathhold targeted for the aortic root. RCA =Right coronary artery, Ao = Aorta, LM = Left main, RA = Right atrium, LAD = Left anterior descending artery.*

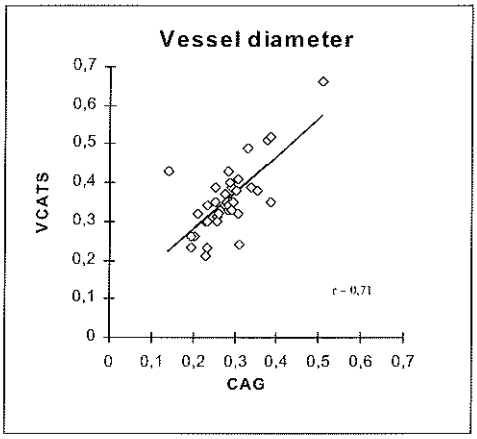

Figure 2. Correlation in vessel diameter between VCATS and conventional angiography (CAG)

Statistical analysis

All values are expressed as mean ± SD. The correlation of the two measurements was performed by least-squares linear regression. The agreement between vessel diameter on MRCA and CAG was tested with the method of Bland and Altman.[10]

RESULTS

The proximal coronary arteries were clearly seen in 92% of the patients. The results for the individual segments are listed in Table 2. The LM was always visualized over it's full length (mean: 9.4 ± 3.4mm), the LAD over 69 mm ± 20 mm and the RCA over 90 mm ± 33 mm. The CX was only visualized over 41 mm ± 18 mm. Figure 1 illustrates an example of 12 slices from VCATS performed on the LM and proximal-LAD. There was a reasonable correlation between the mean vessel diameter in MRCA and CAG (r = 0.71)(figure 2). The diameter on MRI (3.6 ± 0.7 mm) was significant (p = <0.01) larger compared to CAG (2.9 ± 0.7 mm) (figure 3).

Of the 104 proximal segments 79 were suitable for blind comparison with the conventional coronary angiogram. In these 79 segments 9 significant stenoses were present of which MR correctly detected 6. Three stenoses were missed (3 false negatives) and 1 stenosis was overestimated (1 false positive). Figure 4 illustrates a stenoses in the mid segment of the RCA. Inconsistent breath-hold, poor fat suppression or poor signal-to-noise ratio hampered visualization of distal segments.

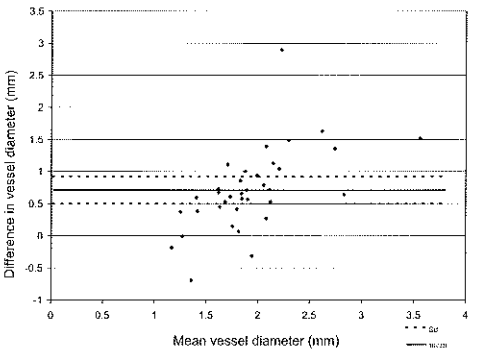

Figure 3. Bland-Altman analysis with significant (p<0.01) overestimation (0.6mm) of the vessel diameter in MRCA.

DISCUSSION

The visualized length of the major coronary artery branches is comparable with the results from other studies using breathhold techniques.[11-13] Measurements of the visualized vessel length may be used to compare different techniques, but the outcome should be viewed with caution because results may be influenced by differences in anatomy, tortuous vessels and interobserver variation originating from continuous measurements of a single vessel from one image to anoth-

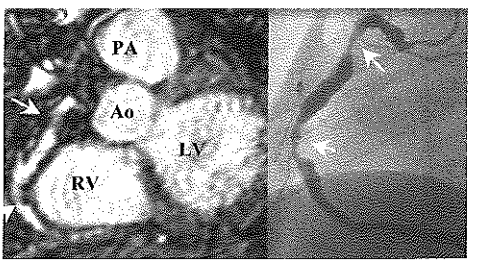

Figure 4. Example of two stenosis in the right coronary artery (arrow heads). Left: MRCA with VCATS, Right: Conventional coronary angiography. Ao = Aorta, PA = Pulmonary artery. LV = Left ventricle, RV = Right ventricle

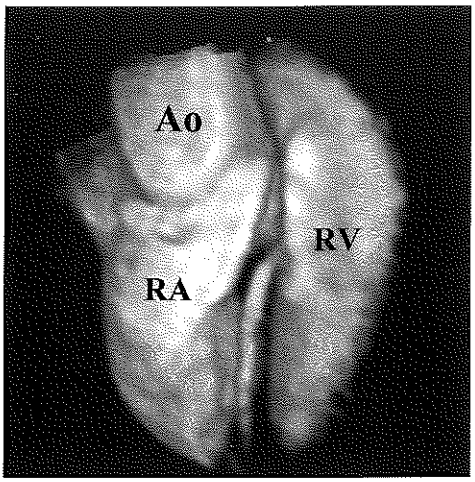

Figure 5. *3D postprocessing by volume rendering of a targeted acquisition for the right coronary artery visible between the right atrium (RA) and right ventricle (RV). Ao = Aorta*

er with different orientations. Furthermore vessel length does not express the ability to detect coronary artery stenoses. The 3D respiratory gated techniques were able to visualize slightly longer parts of the LAD and CX, but due to more residual image blur and longer acquisition time this technique has not evolved as a practical tool for the detection of coronary artery stenoses.[7,14] This technique may be improved by using a prospective gating algorithm rather than a retrospective gating algorithm.[15,16]

There was a reasonable correlation between the vessel diameter in MRCA and CAG. The slight over estimation of MRCA over CAG may result from residual blur during cardiac motion or involuntary respiratory motion. The difference in vessel diameter may also be a result from the different algorithm used in QCA for vessel contour detection, the minimum cost algorithms, which differs principally from the simple algorithm used in this study. In a study on 2D-breathhold MRCA the diameter taken at 50% of the peak also over estimated vessel diameter,[17] whereas the diameter at 65% of the peak intensity corresponded best with QCA.

Advantages

In the VCATS protocol the optimal orientations for the targeted volume are obtained by MPR of a single breathhold volume localizer scan. This simplifies the setup procedure compared to 2D-breathhold techniques so that with some experience a MR technologist is able to find the orientations (much alike a technologist performing standard echocardiography studies). Another advantage of the targeted volume acquisition is a reduction in the number of breathholds (7-10) compared to a complete study with 2D techniques (30-40). Also VCATS may lead to less false positive results which originate from inconsistent breathholding in 2D breathhold techniques.[5] Finally three-dimensional post-processing by Volume Rendering may improve evaluation of MRCA studies (figure 5). However the large amount of observer interaction which is presently necessary for image segmentation using volume rendering restricts it is clinical use.

Limitations

In this study despite the rather crude resolution (1.9 × 1.25 × 1.5 mm) permitted to identify significant coronary artery stenoses, obviously the resolution needs to be improved for more reliable evaluation of the detected stenoses. With the present technique a resolution 1.5 × 0.75 × 1 mm can be achieved, however the signal-to-noise ratio is rather low. Perhaps the introduction of intravascular contrast agents will provide the necessary boost in signal-to-noise ratio necessary.

The low rate of visibility of the CX remains a immense problem due to its complex course and close anatomical relation to the great cardiac vein and coronary sinus. Improved resolution will reduce this problem. In addition, better differentation could be achieved by reducing the signal from venous blood by incorparating a T2 preparation prior to data collection.[18,19]

CONCLUSION

We evaluated VCATS as a new protocol for MRCA. The technique simplifies the setup procedure and allows frequent visualization of the major coronary artery branches. There is a reasonable correlation between vessel diameter in VCATS and CAG. VCATS has the potential to detect clinical relevant coronary stenoses. The effectiveness of this protocol has yet to be shown in a larger blinded study.

REFERENCES

1. Manning WJ, Li W, Edelman RR. A preliminary report comparing magnetic resonance coronary angiography with conventional angiography. N Engl J Med 1993;328(12):828-32.
2. Pennell DJ, Bogren HG, Keegan J, Firmin DN, Underwood SR. Assessment of coronary artery stenosis by magnetic resonance imaging. Heart 1996;75(2):127-33.
3. Post JC, van Rossum AC, Hofman MB, de Cock CC, Valk J, Visser CA. Clinical utility of two-dimensional magnetic resonance angiography in detecting coronary artery disease. Eur Heart J 1997;18(3):426-33.
4. Li D, Paschal CB, Haacke EM, Adler LP. Coronary arteries: three-dimensional MR imaging with fat saturation and magnetization transfer contrast. Radiology 1993;187(2):401-6.
5. Duerinckx AJ, Atkinson DP, Mintorovitch J, Simonetti OP, Vrman MK. Two-dimensional coronary MRA: limitations and artifacts. Eur Radiol 1996;6(3):312-25.
6. Li D, Kaushikkar S, Haacke EM, et al. Coronary arteries: three-dimensional MR imaging with retrospective respiratory gating. Radiology 1996;201(3):857-63.
7. Post JC, van Rossum AC, Hofman MB, Valk J, Visser CA. Three-dimensional respiratory-gated MR angiography of coronary arteries: comparison with conventional coronary angiography. AJR Am J Roentgenol 1996;166(6):1399-404.
8. Wielopolski P, vanGeuns R, deFeyter P, Oudkerk M. Breath-hold Coronary MR Angiography with Volume Targeted Imaging. Radiology 1998;209:209-219.
9. Judkins MP. Selective coronary arteriography. I. A percutaneous transfemoral technique. Radiology 1967;89(5):815-24.
10. Bland J, Altman D. Statistical methods for assessing agreement between two methods of clinical measurement. Lancet 1986;1:307-310.
11. Manning WJ, Li W, Boyle NG, Edelman RR. Fat-suppressed breath-hold magnetic resonance coronary angiography. Circulation 1993;87(1):94-104.
12. Pennell DJ, Keegan J, Firmin DN, Gatehouse PD, Underwood SR, Longmore DB. Magnetic resonance imaging of coronary arteries: technique and preliminary results. Br Heart J 1993;70(4):315-26.
13. Duerinckx AJ, Urman MK. Two-dimensional coronary MR angiography: analysis of initial clinical results. Radiology 1994;193(3):731-8.
14. Achenbach S, Kessler W, Moshage WE, et al. Visualization of the coronary arteries in three-dimensional reconstructions using respiratory gated magnetic resonance imaging. Coron Artery Dis 1997;8(7):441-8.
15. Stuber M, Botnar RM, Danias PG, Kissinger KV, Manning WJ. Submillimeter three-dimensional coronary MR angiography with real-time navigator correction: comparison of navigator locations. Radiology 1999;212(2):579-87.
16. Stuber M, Botnar RM, Danias PG, et al. Double-oblique free-breathing high resolution three-dimensional coronary magnetic resonance angiography. J Am Coll Cardiol 1999;34(2):524-31.
17. Shimamoto R, Suzuki J, Nishikawa J, et al. Measuring the diameter of coronary arteries on MR angiograms using spatial profile curves. AJR Am J Roentgenol 1998;170(4):889-93.
18. Brittain J, Hu B, Wright G, Meyer C, Macovski A, Nishimura D. Coronary angiography with magnetization-prepared T2 contrast. Magn Reson Med 1995;33(5):689-96.
19. Botnar RM, Stuber M, Danias PG, Kissinger KV, Manning WJ. Improved coronary artery definition with T2-weighted, free-breathing, three-dimensional coronary MRA. Circulation 1999;99(24):3139-48.

Chapter 9

Quantitative Analysis of Coronary Artery Lumen Defenition for Breath-hold and Free-breathing Retrospective Respiratory Gated Magnetic Resonance Coronary Angiography

R.J.M. van Geuns, P.A. Wielopolski, A.J Wardeh,

H.G. de Bruin, P.J. de Feyter, M. Oudkerk.

Submitted

ABSTRACT

It is still disputed that superior border definition in magnetic resonance coronary angiography (MRCA) is provided by breath-hold or respiratory gated MRCA. The purpose of our study is to compare quantitatively coronary artery diameter and vessel boundary sharpness of respiratory gated MRCA (NAV-MRCA) and breath-hold MRCA (BH-MRCA) techniques. For this twenty-six patients were studied with both BH-MRCA and NAV-MRCA. BH-MRCA was performed with Volume Coronary Angiography using Targeted Scans (VCATS) along the major coronary segments, which uses a double oblique 3D segmented turboFLASH sequence (TR/TE=5.3/2.3ms). NAV-MRCA was performed with a 3D segmented turboFLASH sequence (TR/TE=7.4/2.7ms) and retrospective respiratory gating by using a navigator signal from the right hemidiaphragm. In the MRCA studies vessel diameter and boundary sharpness were measured in the proximal coronary arteries. Quantitative conventional selective coronary angiography (CAG) was used as the gold standard to assess vessel diameter. Both NAV-MRCA and BH-MRCA significantly overestimated vessel diameter compared to CAG (NAV-MRCA: 3.93 ± 1.05 mm, BH-MRCA: 3.56 ± 0.74, CAG: 2.97 ± 0.68, $p<0.01$). The overestimation in NAV-MRCA was significantly more compared to BH-MRCA ($p<0.01$). Boundary sharpness was significantly better in BH-MRCA compared to NAV-MRCA (BH-MRCA: 4.44 ± 0.93, NAV-MRCA: 3.98 ± 0.89, $p<0.01$). In conclusion, our study demonstrates the preference of BH-MRCA over NAV-MRCA for obtaining more consistent images quality, because sharper and more realistic vessel diameter of the coronary arteries are obtained compared to NAV-MRCA.

INTRODUCTION

Magnetic resonance coronary angiography (MRCA) is a non-invasive imaging technique of the coronary artery anatomy. However, the degradation in image quality of coronary MRCA due to respiratory and cardiac motion poses a big challenge to reliably image the coronaries with minimal blurring and ghosting artifacts. The respiratory motion problem can be addressed with either breath-hold or respiratory synchronized free-breathing techniques.

Breath-hold acquisitions produce reliable coronary images if the patient can withstand breath-hold times of approximately 20 sec.[1-4] Four free-breathing methods are alternatives for breath-hold imaging: averaging multiple acquisitions,[5] respiratory gating using respiratory bellows,[6] retrospective respiratory navigator gated acquisition and reconstruction (NAV-MRCA)[7,8] and prospective real-time navigator respiratory data collection.[9-11] Recently, a breath-hold small volume acquisition, targeted for the coronary arteries (VCATS, Volume Coronary Angiography with Targeted Scans) has been introduced which provides extended coverage, contiguous slices and isotropic resolution.[12]

In the development of new MRCA sequences the choice between breath-hold imaging and free breathing imaging remains unresolved. Comparison of image quality has been performed only qualitatively using visual assessment by different observers. In this study we compared image blur and vessel diameter of breath-hold and retrospective respiratory gated 3D-MRCA using quantitative measurements for vessel sharpness and diameter using conventional coronary angiography as a standard for the coronary vessel diameter.

MATERIALS AND METHODS

Patients

The study population consisted of 26 patients (19 men, 8 women, mean age 57.7 years) who underwent a conventional coronary angiography. To accurately assess vessel diameter only patients without angiographic atherosclerotic disease visible in the proximal coronary arteries (Segments 1, 6 or 11 according to the AHA-guidelines) where included in this study. Exclusion criteria were: previous coronary bypass operation, intracoronary stent implantation, artificial pacemakers, intracranial clips, atrial fibrillation, severe claustrophobia, and severe lung disease restricting breath-holding capabilities to less then 30 seconds. The protocol was approved by our hospital committee of medical ethics and clinical investigation and written informed consent was obtained before the examination.

Scanning

The study was performed on a 1.5T Magnetom Vision scanner (Siemens Medical Systems, Erlangen, Germany) using the body coil for RF excitation and a 4-channel quadrature body phased array coil placed over the chest. Scanning proceeded after a selective water excitation 3-plane scout (5 sec) provided rapid anatomical positioning and assessment of the magnetic field homogeneity over the entire thorax. Shim settings were altered if homogeneous fat suppression was not possible with the systems standard shim setting for a body acquisition. The protocol consisted of 2 parts: the respiratory gated MRCA and the breath-hold MRCA technique.

Respiratory gated 3D MRCA (NAV-MRCA)

Free breathing MRCA was performed using a standard Siemens 3D gradient echo sequence with the retrospective respiratory gated technique described by Li et al.[7] A chemical shift fat suppression pulse was used to suppress the signal from the epicardial fat surrounding the coronary arteries. In this study we used two 25% overlapping trans-

verse slabs of 32 mm thickness, with 16 section of 2 mm covering the proximal left and right coronary arteries. The matrix size was 128 × 256 with a rectangular field of view of 240 × 320 mm, resulting in an inplane resolution of 1.9 × 1.25 mm. The TR was 7.35 ms, the TE was 2.68 ms with a linear incremental flip angle series from 20° to 90°. The acquisition window (128 ms) was set for mid to late diastole. Using an oversampling factor of 4 each slab was acquired in 8-12 minutes depending on the heart rate.

Retrospective respiratory gating was performed by a navigator echo created with two excitation bands intersecting at the dome of the right hemidiaphragm, to measure the diaphragmatic position before data acquisition. Each line of data was acquired five times to ensure complete sampling of the respiratory excursion. Data within a range of ± 1 mm from the gating center were used for image reconstruction. If none of the acquisitions of a certain data-line were within the acceptance range, the acquisition obtained at diaphragm displacements closest to the gating center were used for image reconstruction. The total examination time for NAV-MRCA was around 20 minutes.

Breath-hold 3D MRCA (BH-MRCA)

The VCATS protocol is performed with two 3D MR pulse sequences with two different objectives: localization and targeted imaging. For the localizer a breath-hold 3D multishot segmented echo-planar imaging (TR/TE= 5.55/1.4 ms) sequence covering the whole volume of the heart is used. Within this volume the optimal imaging planes along the coronary arteries are defined. Targeted breath-hold volumes were then acquired during 21 heartbeats with a double oblique 3D segmented gradient echo sequence (TR/TE=5.3/2.3 ms, flip angle = 14°-34°, linear increment) with a matrix of 126 × 256 partial Fourier. The images were reconstructed using 118 k-lines resulting in a resolution of 2.0 × 1.25 × 1.5 mm. The acquisition window (110 ms) was set for mid to late diastole. Magnetization transfer contrast (MTC) preparation and a single chemical shift fat suppression pulse were applied before the actual acquisition window. Three volumes were used: a transverse volume covering the left main (LM) and proximal left anterior descending (LAD) coronary artery, a second transverse volume for the proximal left circumflex (LCX) coronary artery and a double oblique volume through the right atrioventricular groove to cover the right coronary artery (RCA). All acquisitions were performed with breath-holding during expiration. The total examination time, including the localizer sequence, determination and acquisition of the targeted volumes was 10-15 minutes.

MR image analysis

To compare the two MRCA techniques the vessel diameter and boundary sharpness of the proximal coronary arteries were measured by a physicist and a cardiologist and the average and interobserver variability of both measurements are reported. A spatial profile curve was constructed at approxi-

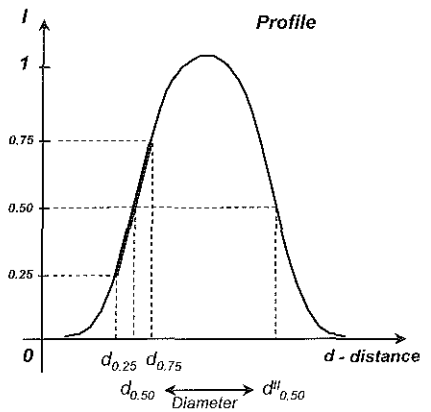

Figure 1. *Measurement of vessel diameter and image blur on MRCA. The vessel edge is determined at 50% of the maximun intensity (I) of the profile across the vessel. For image blur the boundary sharpness was calculated from the slope from 25% to 75% of maximum vessel intensity.*

mately 1 cm of the origin of the proximal coronary arteries where the vessel was for a longer section within the imaging plane. The exact distance to the origin was measured to ensure the same location was used in all the measurements of one patient. The following points were identified: 25% ($d_{0.25}$), 50% ($d_{0.50}$) and 75% ($d_{0.75}$) of the peak intensity of the intravascular lumen on the upstroke side and 50% ($d^{II}_{0.50}$) on the downslope side (figure 1). The vessel diameter was defined as the distance between $d_{0.50}$ and $d^{II}_{0.50}$ (Diameter = $d^{II}_{0.50}$ - $d_{0.50}$). The relative diameter was the diameter from MRCA divided by the diameter from CAG. To assess image blur the boundary sharpness was calculated from the slope from ($d_{0.25}$) to ($d_{0.75}$) by: $0.5/(d_{0.75} - d_{0.25})$.
The proximal LAD and LCX were measured in transverse images. The proximal RCA was measured in cranial-caudal direction for BH-MRCA and in multiplanar reconstruction (MPR) images for NAV-MRCA (figure 2).

Conventional coronary angiography

Conventional selective contrast-enhanced coronary angiography (CAG) was performed using the Judkins technique.[13] Off-line analysis of at least two orthogonal planes was performed by an experienced observer using quantitative coronary angiography (CAAS II, Pie-medical, Maastricht, The Netherlands). Calibration was based on dimensions of the catheters not filled with contrast medium. In this system the centerline of the vessel is first indicated by the observer with centerline points and subsequently the program recomputes the centerline. The vessel edges are determined by computing the first and second derivative functions of the brightness profile along scanlines perpendicular to the centerline. Final contour detection of a segment is defined by the application of a minimal cost

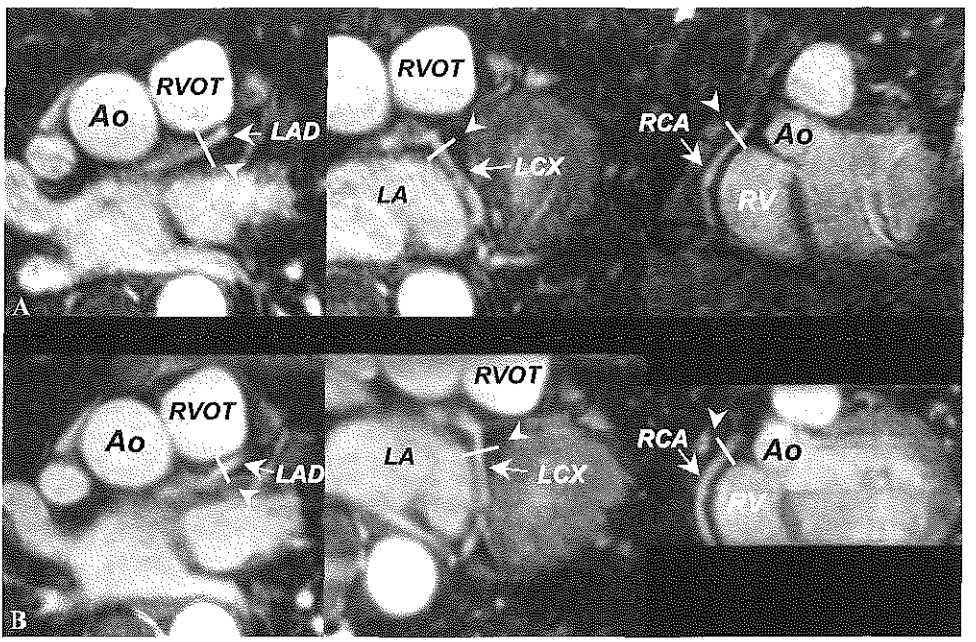

Figure 2. *Locations (arrow heads) for vessel diameter and image blur measurements in the right coronary artery (RCA), left anterior descending coronary artery (LAD) and left circumflex coronary artery (LCX). In patients with a regular breathing pattern no major differences in vessel sharpness are visible between BH-MRCA* ***(A)*** *and NAV-MRCA* ***(B)****. Ao = Aorta, RVOT = Right ventricular outflow tract, LM = Left main, RV = Right ventricle.*

algorithm which takes into account all the intensity and derivative information along the coronary segment. The vessel diameter was obtained by an interpolation method along the coronary segment evaluated.[14,15]

Statistical analysis

All values are expressed as mean ± standard deviation. The interobserver variability of the vessel diameter and slope in MRCA was calculated as the averaged difference between the two measurements and the 95% confidence intervals (coefficient of repeatability = 2 × SD).[16] The paired Student t-test was used to determine significance of the difference between two paired measurements, an unpaired Student t-test was used for unpaired measurements.

RESULTS

In 2 of the 26 patients the LCX could not be visualized with MRCA due to the small vessel size and low signal-to-noise ratio as a consequence of the distance to the surface coils. During conventional coronary angiography two RCA's were not visualized, one originating from the left coronary cusp, the other was not properly engaged due to an aneurysm of the ascending aorta. In one patient the RCA was not filmed at all. Thus 73 segments (LAD: 26, LCX: 24, RCA: 23) were available for evaluation. The mean acquisition time for a single volume by BH-MRCA and NAV-MRCA was 22 seconds and 11 minutes respectively. The mean total acquisition time for BH-MRCA was 14 minutes including the setup of the localizer scan and the determination of the optimal imag-

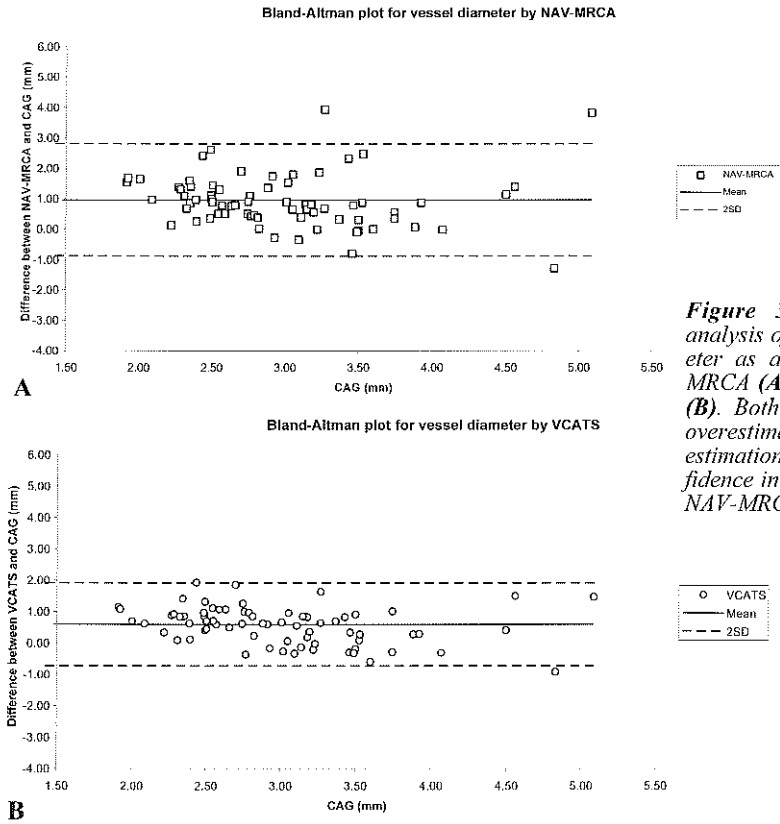

Figure 3. *Bland-Altman analysis of the vessel diameter as assessed by NAV-MRCA* ***(A)*** *and BH-MRCA.* ***(B)****. Both graphs show an overestimation and a larger confidence interval is noted for NAV-MRCA.*

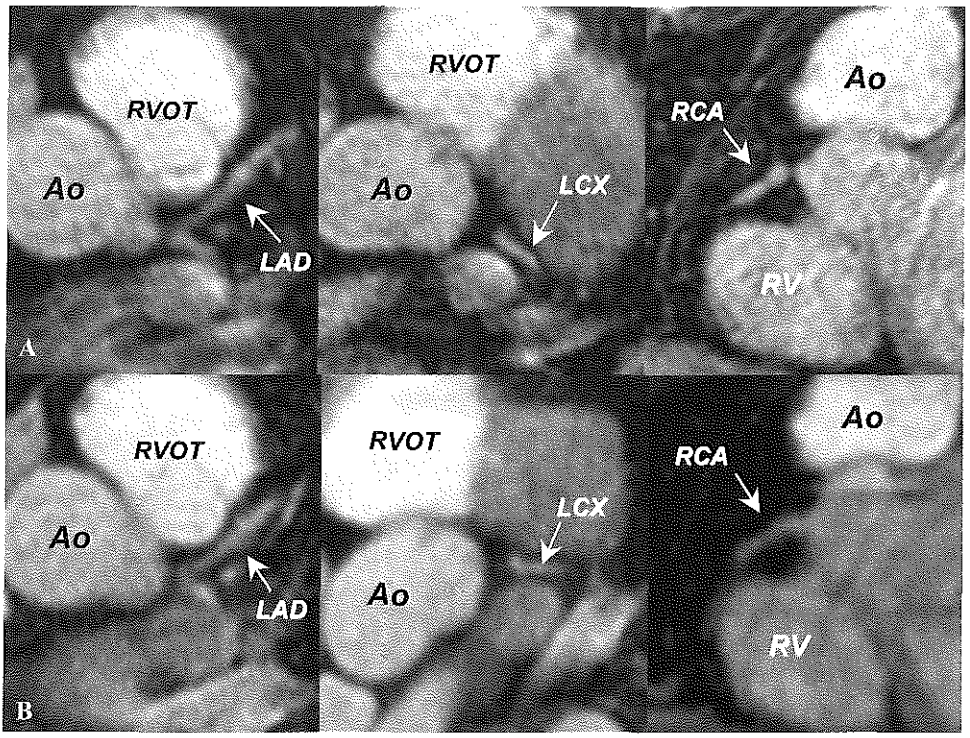

Figure 4. *Comparison between BH-MRCA* ***(A)*** *and NAV-MRCA* ***(B)*** *in a patient with an irregular breathing pattern with decreased vessel sharpness in NAV-MRCA as assessed with quantitative measurements. Ao = Aorta, RVOT = Right ventricular outflow tract, RV = Right ventricle, LA = Left atrium, LM = Left main, LAD = Left anterior descending artery, RCA = Right coronary artery, LCX = Left circumflex coronary artery.*

ing plane for the RCA. The mean acquisition time for the two NAV-MRCA slabs was 25 minutes including setup time.

The mean vessel diameter of all vessels in NAV-MRCA was 3.93 ± 1.05 mm, in BH-MRCA 3.56 ± 0.74 mm and in CAG 2.97 ± 0.68 mm. The interobserver variability for vessel diameter measurements was 0.18 ± 0.90 mm (coefficient of repeatability = 1.80 mm) for NAV-MRCA and 0.11 ± 0.66 mm (coefficient of repeatability = 1.33 mm) for BH-MRCA. Data of the individual vessels are listed in Table 1. Both NAV-MRCA and BH-MRCA significantly overestimated ves-

Table 1. Vessel diameter

	NAV-MRCA		BH-MRCA		CAG
	(mm)	(%)	(mm)	(%)	(mm)
RCA	4.42 ± 1.35*	144 ± 46‡	3.86 ± 0.96†	128 ± 44‡	3.16 ± 0.84
LAD	3.83 ± 0.91*	133 ± 32	3.53 ± 0.62†	122 ± 23	2.94 ± 0.55
LCX	3.55 ± 0.56*	131 ± 34	3.31 ± 0.48†	121 ± 26	2.83 ± 0.62
Overall	3.93± 1.05*	136 ± 38	3.56 ± 0.74†	124 ± 32	2.97 ± 0.68

NAV-MRCA = Retrospective respiratory gated magnetic resonance coronary angiography, BH-MRCA = Breath-hold volume coronary angiography using targeted scans, CAG = Conventional coronary angiography, RCA = Right coronary artery, LAD = Left anterior descending coronary artery, LCX = Left circumflex coronary artery

** $p < 0.01$ compared to CAG and BH-MRCA, † $p < 0.01$ compared to CAG, ‡ $p > 0.05$ compared to LAD and LCX.*

Table 2. Vessel boundary sharpness. Larger values denote increased sharpness.

	NAV-MRCA	BH-MRCA
RCA	3.58 ± 0.88*†	4.18 ± 0.91
LAD	4.04 ± 0.69*	4.49 ± 0.96
LCX	4.32 ± 0.94	4.65 ± 0.88
Overall	3.98 ± 0.89*	4.44 ± 0.93

NAV-MRCA = Retrospective respiratory gated magnetic resonance coronary angiography, BH-MRCA = Breath-hold volume coronary angiography using targeted scans, RCA = Right coronary artery, LAD = Left anterior descending coronary artery, LCX = Left circumflex coronary artery
** p < 0.05 compared to BH-MRCA, † p <0.05 compared to LAD + LCX.*

sel diameter compared to CAG (NAV-MRCA: +0.96 ± 0.92 mm, BH-MRCA: +0.59 ± 0.66 mm, p<0.01, figure 3). Vessel diameter was larger with a wider confidence interval in NAV-MRCA compared to BH-MRCA (p<0.01). The relative vessel diameter of the RCA was larger compared to the LAD and CX diameters, although this was not statistically significant (p=0.23).

The difference in vessel sharpness between NAV-MRCA and BH-MRCA is illustrated in figures 4 and 5. The vessel boundaries where sharper in BH-MRCA compared to NAV-MRCA (BH-MRCA: 4.44, NAV-MRCA: 3.98, p<0.01). The interobserver variability for vessel boundary sharpness was 0.08 ± 1.08 (coefficient of repeatability = 1.26) for NAV-MRCA and 0.10 ± 1.08 (coefficient of repeatability = 2.16) for BH-MRCA. The boundaries of the RCA with the MRCA-NAV sequence were significantly (p=0.01) less sharp compared to the LAD and LCX, but with the BH-MRCA sequence this difference was not significant (Table 2). In a separate analysis of transverse images only, where the LAD and LCX run in-plane, the vessel diameter in MRCA-NAV was still significant larger compared to BH-MRCA (NAV-MRCA: 3.71 ± 0.61 mm, BH-MRCA:

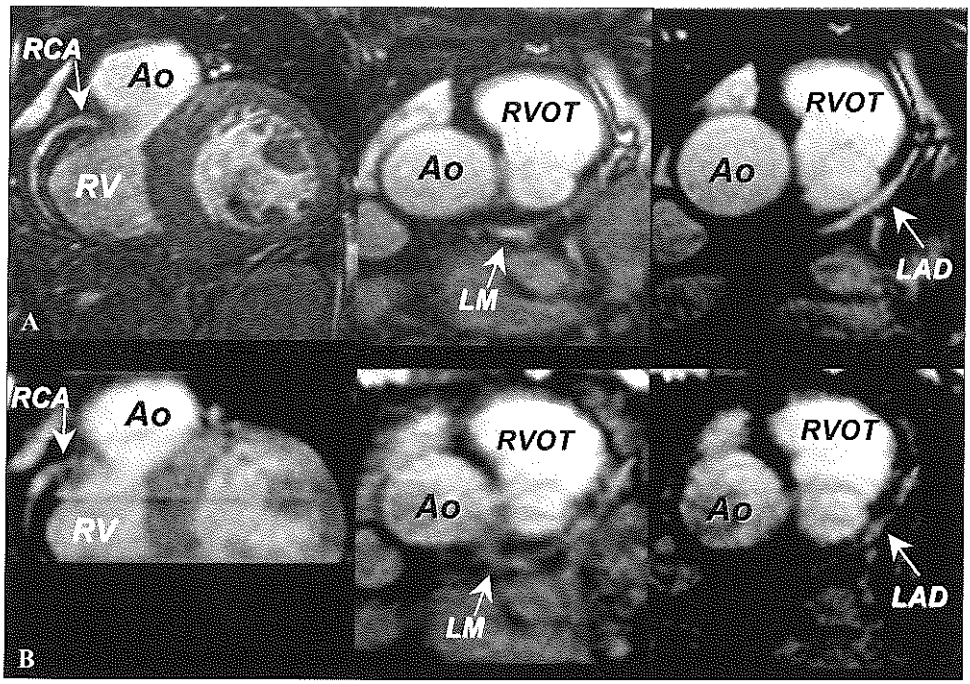

Figure 5. *Comparison between BH-MRCA **(A)** and NAV-MRCA **(B)**. Even without quantitative measurements the difference in image quality is clearly demonstrated. LA = Left atrium, LM = Left main, LAD = Left anterior descending artery, RCA = Right coronary artery, LM = Left main coronary artery.*

3.43 ± 0.30 mm, p<0.01). The vessel boundary in these images were significantly sharper in BH-MRCA compared to MRCA-NAV (BH-MRCA: 4.56, NAV-MRCA: 4.14, p<0.01).

DISCUSSION

In this study image quality of two different MRCA techniques was quantified by measuring the vessel diameter and the boundary sharpness. The vessel diameters were compared with conventional coronary angiography which served as the gold standard. Measurements in two different projections of the CAG were used to approximate the true coronary lumen. MRCA-NAV significantly overestimated vessel diameter and yielded less sharp defined vessel boundaries than breath-hold imaging. This may be explained by the inappropriate retrospective gating algorithm in which only 30 to 40% of the k-lines are acquired within a 2 mm gating window, whereas the remaining k-lines are selected at a diaphragm displacement which is closest to the gating center and thus may result in blurred images. Prospective respiratory gating may improve image quality for free breathing MRCA.[9-11,17] In clinical practice prospective respiratory gating may be of limited value due to the unpredictable and often long scanning time and the slow feedback makes it difficult to judge and if necessary to correct image quality.

The significant difference in vessel boundary sharpness and the overestimation of the RCA diameter in cranial-caudal direction may be explained by the motion of the vessel with respiration which is larger in cranial-caudal direction then the anterior-posterior motion of the LAD and LCX.[18] The difference of the RCA diameter measurements between the two techniques is probably increased by the difference in the resolution of both techniques. The images on the RCA with BH-MRCA are obtained with maximum resolution in cranial-caudal direction (1.25 mm), while the NAV-MRCA used MPR with resolution of 2 mm in the cranial-caudal direction. The effect of respiratory motion on the diameter and boundary sharpness of the RCA should ideally be compared with BH-MRCA using double oblique imaging for both techniques. To minimize the effect of resolution on the results we performed a separate analysis for transverse images where the inplane resolution is the same. These analysis confirmed our conclusions that BH-MRCA provides sharper images with a more realistic vessel diameter then NAV-MRCA.

The slight overestimation of BH-MRCA over CAG may result from residual blur during cardiac motion or involuntary respiratory motion. Other 2D-MRCA sequences also showed an overestimation of 0.2 ± 0.5 mm of vessel diameter by MR.[1,19] It remains to be determined at which level of peak-intensity one determines the coronary boundary. The diameter taken at 50% of the peak intensity seems to overestimated vessel diameter, whereas for breath-hold 2D-MRCA the diameter at 65% of the peak intensity corresponded best with CAG.[20] We demonstrated that vessel diameter in MRCA is dependent on the technique used, and in our opinion the vessel size overestimation in breath-hold 2D-MRCA is also due to residual image blur from motion during the acquisition of 100 ms and 25 second breath-hold.

Some limitations were present in this study. MTC preparation which suppress the signal from the myocardium may also suppress signal from the vessel wall.[21,22] This was only applied in the BH-MRCA sequence, where it was present in the original VCATS design[12] while it was not applied in NAV-MRCA[7] therefore this may have selectively improved the VCATS measurements.

The vessel diameters have been related to quantitative CAG, which served as the standard of reference. The quantitative CAG algorithm has shown to be quite accurate

with a precision of 0.18 mm, although a tendency to underestimate large diameter (> 3 mm) was present[14] which are the vessel sizes measured in this study.

CONCLUSION

Breath-hold MRCA with VCATS results in a more realistic vessel diameter with better definition of the vessel boundaries than retrospective respiratory gated MRCA. VCATS is recommended as the most optimal MRCA sequence in patients who are able to suspend their breath for 20 seconds. The navigator techniques should be used in patients who have difficulty in withholding their breath for a sufficient long period.

REFERENCES

1. Manning WJ, Li W, Boyle NG, et al. Fat-suppressed breath-hold magnetic resonance coronary angiography. Circulation. 1993;87:94-104.
2. Manning WJ, Li W, Edelman RR. A preliminary report comparing magnetic resonance coronary angiography with conventional angiography. N Engl J Med. 1993;328:828-32.
3. Pennell DJ, Bogren HG, Keegan J, et al. Assessment of coronary artery stenosis by magnetic resonance imaging. Heart. 1996;75:127-33.
4. Duerinckx AJ, Urman MK. Two-dimensional coronary MR angiography: analysis of initial clinical results. Radiology. 1994;193:731-8.
5. Paschal CB, Haacke EM, Adler LP. Three-dimensional MR imaging of the coronary arteries: preliminary clinical experience. J Magn Reson Imaging. 1993;3:491-500.
6. McConnell MV, Khasgiwala VC, Savord BJ, et al. Comparison of respiratory suppression methods and navigator locations for MR coronary angiography. AJR Am J Roentgenol. 1997;168:1369-75.
7. Li D, Kaushikkar S, Haacke EM, et al. Coronary arteries: three-dimensional MR imaging with retrospective respiratory gating. Radiology. 1996;201:857-63.
8. Hofman MB, Paschal CB, Li D, et al. MRI of coronary arteries: 2D breath-hold vs 3D respiratory-gated acquisition. J Comput Assist Tomogr. 1995;19:56-62.
9. Oshinski JN, Hofland L, Mukundan S, Jr., et al. Two-dimensional coronary MR angiography without breath holding. Radiology. 1996;201:737-43.
10. Wang Y, Rossman PJ, Grimm RC, et al. Navigator-echo-based real-time respiratory gating and triggering for reduction of respiration effects in three-dimensional coronary MR angiography. Radiology. 1996;198:55-60.
11. Stuber M, Botnar RM, Danias PG, et al. Submillimeter three-dimensional coronary MR angiography with real-time navigator correction: comparison of navigator locations. Radiology. 1999;212:579-87.
12. Wielopolski P, vanGeuns R, deFeyter P, et al. Breath-hold Coronary MR Angiography with Volume Targeted Imaging. Radiology. 1998;209:209-219.
13. Judkins MP. Selective coronary arteriography. I. A percutaneous transfemoral technic. Radiology. 1967;89:815-24.
14. Haase J, Escaned J, van Swijndregt EM, et al. Experimental validation of geometric and densitometric coronary measurements on the new generation Cardiovascular Angiography Analysis System (CAAS II). Cathet Cardiovasc Diagn. 1993;30:104-14.
15. Di Mario C, Hermans WR, Rensing BJ, et al. Calibration using angiographic catheters as scaling devices--importance of filming the catheters not filled with contrast medium [letter; comment]. Am J Cardiol. 1992;69:1377-8.
16. Bland J, Altman D. Statistical methods for assessing agreement between two methods of clinical measurement. Lancet. 1986;1:307-310.
17. Jhooti P, Keegan J, Gatehouse PD, et al. 3D coronary artery imaging with phase reordering for improved scan efficiency. Magn Reson Med. 1999;41:555-62.
18. Wang Y, Riederer SJ, Ehman RL. Respiratory motion of the heart: kinematics and the implications for the spatial resolution in coronary imaging. Magn Reson Med. 1995;33:713-9.
19. Pennell DJ, Keegan J, Firmin DN, et al.

Magnetic resonance imaging of coronary arteries: technique and preliminary results. Br Heart J. 1993;70:315-26.
20. Shimamoto R, Suzuki J, Nishikawa J, et al. Measuring the diameter of coronary arteries on MR angiograms using spatial profile curves. AJR Am J Roentgenol. 1998;170:889-93.
21. Meyer CH, Hu BS, Yang PC, et al. Spiral cardiac imaging with High-Performance Gradients (abstr). In: Proceedings of the Seventh Meeting of the International Society for Magnetic Resonance in Medicine. Philadelphia; 1999.
22. Botnar RM, Stuber M, Danias PG, et al. Improved coronary artery definition with T2-weighted, free-breathing, three-dimensional coronary MRA. Circulation. 1999;99:3139-48.

Chapter 10

MR Coronary Angiography with Breath-hold Targeted Volumes: Preliminary Clinical Results

R.J.M. van Geuns, P.A. Wielopolski, H.G. de Bruin,

B.J.W.M. Rensing, M. Hulshoff, P.M.A. van Ooijen,

P.J. de Feyter, M Oudkerk.

Published in Radiology 2000; 217:270–277

ABSTRACT

Purpose:

To assess the clinical value of a magnetic resonance (MR) coronary angiography strategy involving a small targeted volume to image one coronary segment in a single breath hold for the detection of greater than 50% stenosis.

Materials and Methods:

Thirty-eight patients referred for elective coronary angiography were included. The coronary arteries were localized during single-breath-hold, three-dimensional imaging of the entire heart. MR coronary angiography was then performed along the major coronary branches with a double-oblique, three-dimensional, gradient-echo sequence. Conventional coronary angiography was the reference-standard method.

Results:

Adequate visualization was achieved with MR coronary angiography in 85%-91% of the proximal coronary arterial branches and in 38%-76% of the middle and distal branches. Overall, 187 (69%) of 272 segments were suitable for comparison between conventional and MR coronary angiography. The diagnostic accuracy of MR coronary angiography for the detection of hemodynamically significant stenoses was 92%; sensitivity, 68%; and specificity, 97%. The sensitivity in individual segments was 50%-77%, whereas the specificity was 94%-100%.

Conclusion:

Adequate visualization of the major coronary arterial branches was possible in the majority of patients. The observed accuracy of MR coronary angiography for detection of hemodynamically significant coronary arterial stenosis is promising, but it needs to be higher before this modality can be used reliably in a clinical setting.

INTRODUCTION

Magnetic resonance (MR) coronary angiography has undergone numerous developments during the past decade. Alternative techniques account for multiple two- and three-dimensional (3D) protocols with breath-hold and free-breathing approaches, or a combination of both.[1-4] The clinical data reported[5-9] have been hampered mainly by technical problems that include blurring, long imaging times, inadequate coronary arterial coverage, and misregistration.[10,11] We previously described a methodology to address some of these problems by using a breath-hold, targeted-volume imaging approach—that is, volume coronary angiography with targeted volumes (VCATS)—to image particular coronary arterial segments with reasonable resolution and thus identify hemodynamically significant stenoses.[12] With targeted-volume imaging, data are acquired with optimal orientations along the coronary arterial branches of interest obtained from a single-breath-hold, low-resolution sequence for the entire volume of the heart. The purpose of this study was to assess the ability of VCATS to enable visualization of the major coronary arteries and the accuracy of this technique in the detection of stenosis, with conventional coronary angiography used as the standard of reference.

MATERIALS AND METHODS

Patients

The study population consisted of 38 patients (11 women, 27 men; age range, 43-72 years) who were referred for coronary angiography. Two cardiac research slots per week were available at our MR imaging site. Patients scheduled for elective coronary angiography were approached to participate in the MR coronary angiography study. The first two patients who agreed were scheduled to fill the available research slots. Exclusion criteria were previous coronary bypass surgery, intracoronary stent implantation, artificial pacemakers, intracranial clips, atrial fibrillation, severe claustrophobia, and severe lung disease that restricted breath-holding capability to less than 30 seconds. The study protocol was approved by our hospital committee on medical ethics and clinical investigation. Written informed consent was obtained from all patients prior to the MR imaging examinations.

MR Imaging

The studies were performed with a 1.5-T whole-body MR imaging system (Magnetom Vision; Siemens, Erlangen, Germany). Patients were placed in a supine position, and a four-channel quadrature phased-array body coil was placed over the thorax. Electrocardiographic electrodes were always set over the anterior part of the thorax and readjusted, if necessary, to obtain reasonable amplitude and clean signal trace in the monitoring unit after the patient was placed inside the magnet bore. After patient positioning, the magnetic field homogeneity over the thorax and heart was assessed to obtain uniform fat suppression in sequences that involved chemical shift fat suppression. This assessment was performed by comparing two three-plane, single-shot spin-echo train imaging (HASTE; Siemens) localizer sequences with and without a chemical shift fat suppression pulse applied. When the reduction of fat signal intensity was deemed inadequate, the shim currents were manipulated and the single-shot spin-echo train imaging localizer sequence with chemical shift fat suppression was repeated until satisfactory results were obtained.

To start the coronary localization procedure, a 3D single-breath-hold, multishot, segmented, echo-planar sequence was used to image the entire heart, with a 120-mm section obtained at end expiration. The data were subjected to multiplanar evaluation to determine the optimal imaging planes for the

major coronary arterial branches (Table 1, Figure 1). This localization process has been described in detail previously.[12] Seven orientations were obtained with multiplanar reformation before imaging with the breath-hold VCATS protocol proceeded.

Targeted-volume coronary angiography was performed with a 3D, double-oblique, segmented, gradient-echo—that is, turbo fast low-angle shot (TurboFLASH; Siemens)—sequence (5.3/2.3 [repetition time msec/echo time msec], incremental flip angle, 21 lines per segment, 110-msec acquisition window). A 24-mm-thick section (seven encoded partitions, 16 reconstructed by zero filling) was used with a 126 × 256 matrix and partial Fourier reconstruction. The imaging time was 21 heartbeats, and the imaging window coincided with middle-to-late diastole. The field of view was maintained constant at 240 × 320 mm2, providing a resolution of 1.9 × 1.25 × 1.5 mm^3. Magnetization transfer irradiation for myocardium-blood contrast-to-noise ratio enhancement (irradiation duration, 500 msec) and a single chemical shift fat suppression pulse were applied before data collection for each cardiac window. The orientation prescriptions were manually registered into the measurement platform for each targeted MR coronary angiogram. Breath holding was performed at end expiration to achieve position and plane reproducibility with respect to the multiplanar reformation data generated by using the volume localizer.

Table 1. Routine Targeted Volumes Acquired and Coronary Segments Covered

No.*	Coronary segment evaluated
1	Plane along LM, proximal LCX, and proximal LAD (transverse)
2	Plane of proximal RCA (transverse)
3	Plane along distal RCA and PDA (oblique)
4	Plane through aortic root and proximal RCA and leftmain (oblique)
5	Plane along LCX (oblique)
6	Plane along distal LAD (oblique)
7	Plane along middle portion of RCA (oblique)

Note.-LM = Left main coronary artery, LAD = Left anterior descending artery, LCX = Left circumflex artery, RCA = Right coronary artery, PDA = Posterior descending artery.

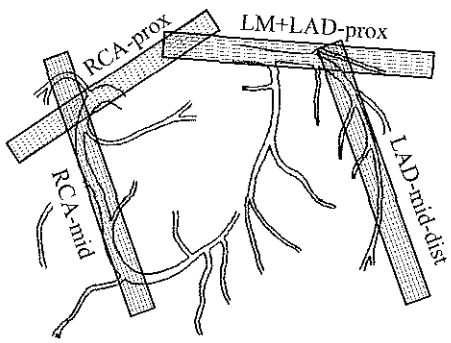

Figure 1. *Drawing illustrates breath-hold 3D imaging of the coronary arteries with VCATS protocol. Different volumes are targeted for a detailed examination of selected coronary arterial segments. The major coronary segments can be imaged during seven breath holds. Four examples of possible angulations (rectangles) are illustrated. LAD = left anterior descending coronary artery, LM = left main coronary artery, RCA = right coronary artery.*

The breath-hold quality was assessed on every attempt by observing the ghost artifacts of the anterior thoracic wall over the heart. In case ghost artifacts appeared, repeated imaging of a particular volume was allowed. If severe ghost artifacts were present and the patient could not hold his or her breath adequately within four attempts, he or she was regarded as nonsuitable for the imaging procedure and thus excluded from the study.

To improve coronary arterial depiction on the volume localizer image, superparamagnetic iron oxide particles (AMI-25 [Endorem]; Laboratoire Guerbet, Roissy, France) were administered as a suspension containing 89.6 mg of iron (11.2 mg/mL) diluted in 100 mL of isotonic glucose solution. The solution was administered in a slow drop infusion for 30 minutes.

Conventional Coronary Angiography

All subjects underwent selective coronary arterial angiography by means of the Judkins technique[13] within 1 month before or after the MR examination. Two experienced cardiologists (B.J.W.M.R., P.J.d.F.) jointly interpreted the angiograms. The coronary tree was divided into proximal, middle, and distal segments according to American Heart Association guidelines.[14] Under these guidelines, the left main coronary artery has a single segment. The proximal segment of the left anterior descending artery extends from the bifurcation to the first septal branch. The middle segment of the left anterior descending artery extends from the first to the third septal artery, whereas the distal segment extends from the third septal artery to the apex. The left circumflex coronary artery is divided into three segments by the first and second marginal branches. The proximal segment extends from the bifurcation to the first marginal branch, the middle segment extends from the first to the second marginal branch, and the distal segment extends from the second marginal branch to the posterior lateral branch. The proximal right coronary artery extends from the origin to the first large acute marginal branch, the middle segment extends from the first to the third acute marginal branch, and the distal segment extends from the third acute marginal branch to the posterior descending branch. These segments were visually graded as either having no hemodynamically significant disease—that is, less than 50% diameter stenosis—or having hemodynamically significant disease—that is, greater than 50% diameter stenosis. In cases of disagreement, a third cardiologist made the final decision.

MR Image Interpretation

From each targeted volume, 16 source images in a dynamic loop (Movie 1, *http://radiology.rsnaljnls.org/cgi/content/full/217/1/270/DC1*) were analyzed independently by a cardiologist (R.J.M.v.G.) and a radiologist (H.G.d.B.), who were unaware of the cardiac catheterization results. In cases of disagreement, consensus was achieved in a joint session with a third investigator (M.O.). Of all the coronary segments defined in the American Heart Association guidelines, only eight segments—those of the left main artery; proximal and middle left anterior descending arteries; proximal and middle left circumflex coronary arteries; and proximal, middle, and distal right coronary arteries—were included in this study. This selection resulted in the evaluation of 272 segments in 34 complete patient studies. These segments were regarded as assessable if overlapping structures (ie, veins, pericardium, and unsuppressed fat), image blurring, and/or ghost artifacts could be distinguished from the vessel itself. The segments included in more than one volume were finally evaluated in the volume with the best image quality. The assessable segments were graded as either not having hemodynamically significant diameter stenosis (<50%) or having hemodynamically significant stenosis (>50%).

To investigate the possibilities of integrating the coronary arterial path within a targeted volume into a single image, data sets were reconstructed by using a volume-rendering program (voxelview; Vital Images, Minneapolis, Minn) that was run on a dedicated graphic workstation (Indigo2; Silicon Graphics, Mountain View, Calif). Segmentation was required to eliminate unwanted structures and view the coronary segment from any viewing angle and thus better assess the presence of any detected stenoses at the initial review. Volume-rendered data were not evaluated for their additional diagnostic value, but rather this technique was used strictly as an exploratory tool to conjecture about the possible likeness of volume-rendered images to the corresponding coronary angiograms.

Statistical Analyses

Conventional coronary angiography served as the standard of reference for determining the diagnostic value of MR coronary angiography. The diagnostic value for the detection of hemodynamically significant (>50% diameter) stenosis in a segment was expressed in sensitivity, specificity, positive predictive, negative predictive, and diagnostic accuracy values.

RESULTS

The mean interval (± SD) between cine-mode angiography and MR coronary angiography was 10 days ± 7. In four of the 38 patients who agreed to participate in this study, the MR examination was not completed owing to hardware problems (n = 1), unexpected claustrophobia (n = 2), or inability to suspend respiration for 21 heartbeats according to the study design (n = 1). Thus, MR imaging studies were performed in the remaining 34 subjects with minor technical, operational, and patient-related problems. The mean attempted number of volumes (± SD) collected per patient was 10.0 ± 2.3. The minor technical difficulties included problems performing good electrocardiographic tracing in three (9%) patients and mistriggering from imaging gradient-induced interference in some volume orientations in 30 (8.8%) of 340 measurements. Incomplete fat suppression within the set of volumes collected per patient was always present to a certain degree, and it was prevalent in the distal portion of the left anterior descending artery. Operational problems included input errors in the volume orientation prescription in eight (2.4%) of 340 measurements. Patient-related problems were those due to an inconsistent breath-hold position with respect to the volume localizer in 17 (5.0%) of 340 measurements and incomplete acquisition of all targeted volumes in two patients (five [1.5%] of 340 measurements).

Because of the fast feedback on the data

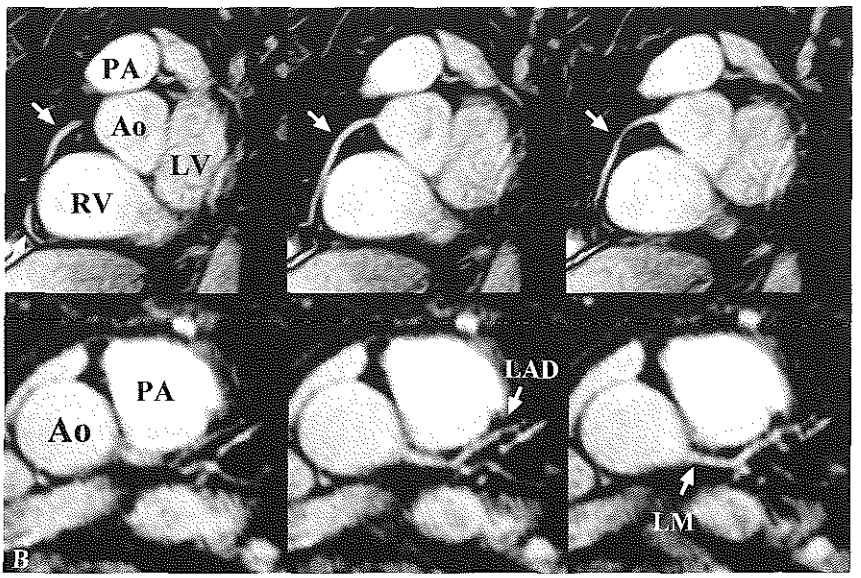

Figure 2. *In a and b, Ao = aorta, PA = pulmonary artery.* ***(A)*** *Double-oblique, 3D, breath-hold, segmented, gradient-echo MR images (TurboFLASH, 5.3/2.3, incremental flip angle, 21 lines per segment, 110-msec acquisition window, 1.9 × 1.25 × 1.5-mm resolution with interpolation by zero filling) of the middle segment of the right coronary artery in a 45-year-old man. Three consecutive sections show the continuation of a nondiseased tortuous vessel (arrows) through the volume. LV = left ventricle, RV = right ventricle.* ***(B)*** *Transverse targeted-volume images of the left main (LM) and proximal left anterior descending (LAD) arteries in a 45-year-old woman.*

acquired, corrections were directly applied to acquire the desired volume; this resulted in 100% data collection in the segments studied. The mean (± SD) breath-hold time per acquired targeted volume was 23 ± 4 seconds. The acquisition of the volume localizer image, selection of the optimal plane location and orientation of the targeted volumes with multiplanar reformation, and acquisition of the targeted-volume images were consistently completed in less than 30 minutes. Of the 272 possible coronary arterial segments in the 34 patients, 187 (69%) were deemed to be assessable by using MR coronary angiography. The range of assessability varied substantially, from 91% for the left main coronary artery to 38% for the middle left circumflex coronary artery. The resultant data on the assessability of individual segments are listed in Table 2.

Table 2. Assessability of different coronary artery segments by MR-coronary angiography.

Segment	Assessability*
RCA-prox	29 (85%)
RCA-mid	22 (65%)
RCA-dist	17 (50%)
LM	31 (91%)
LAD-prox	31 (91%)
LAD-mid	26 (79%)
LCX-prox	18 (53%)
LCX-mid	13 (38%)

**Data are numbers of patients in whom the given segment was assessable with MR coronary angiography, based on a total of 34 patients. Numbers in parentheses are percentages. LAD = left anterior descending coronary artery, LCX = left circumflex, LM = left maincoronary artery, RCA = right coronary artery.*

The conventional coronary angiograms showed hemodynamically significant stenosis in 23 patients—three-vessel disease in three patients, two-vessel disease in 10, and single-vessel disease in another 10. Overall, 41 stenoses were present in the eight major coronary arterial branches. Thirty-one of these stenoses were located in the 187 assessable segments, and 10 were in the nonassessable segments (Table 3). Two examples of targeted-volume images of nondiseased vessels are shown in Figure 2. Examples of two stenoses in the right coronary artery are shown in Figure 3. An example of stenosis of the left anterior descending artery segment

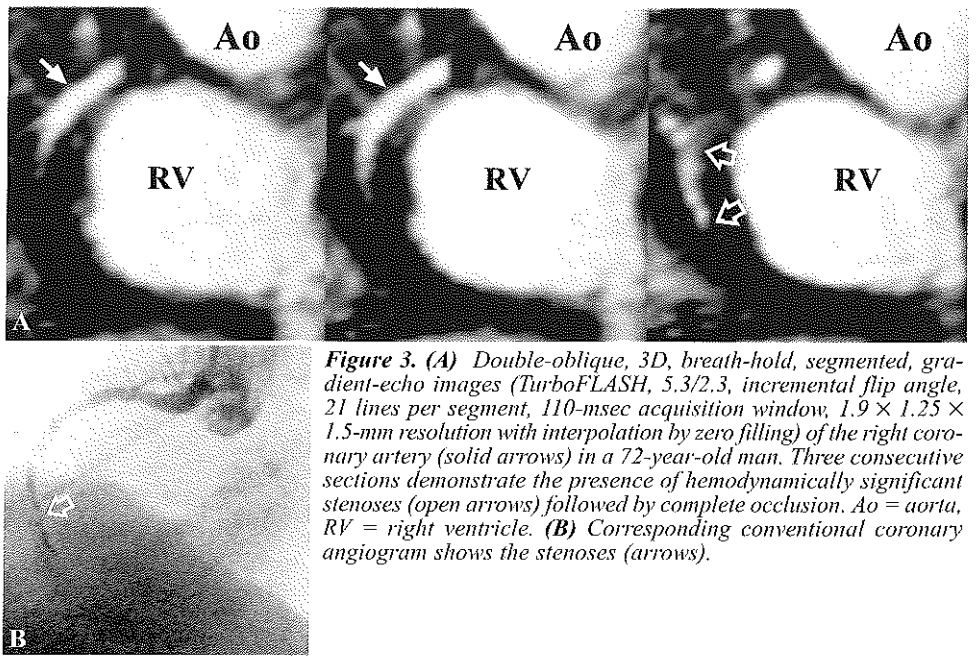

Figure 3. ***(A)*** *Double-oblique, 3D, breath-hold, segmented, gradient-echo images (TurboFLASH, 5.3/2.3, incremental flip angle, 21 lines per segment, 110-msec acquisition window, 1.9 × 1.25 × 1.5-mm resolution with interpolation by zero filling) of the right coronary artery (solid arrows) in a 72-year-old man. Three consecutive sections demonstrate the presence of hemodynamically significant stenoses (open arrows) followed by complete occlusion. Ao = aorta, RV = right ventricle.* ***(B)*** *Corresponding conventional coronary angiogram shows the stenoses (arrows).*

is shown in Figure 4.

The findings for the detection of hemodynamically significant stenosis (>50% of observable diameter) are summarized in Table 4. The sensitivity of MR coronary angiography ranged from 50% to 77%, and the specificity ranged from 94% to 100%. The overall sensitivity and specificity were 68% and 97%, respectively, with an accuracy of 92%.

Table 3. Relation between angiographic status of coronary arterial segments and assessability by MRCA.

MR Imaging	Lesion Absent at Angiography	Lesion Present at Angiography	Total
Assessable	156	31	187
Nonassessable	75	10	85
Total	231	41	272

Note.—Data are numbers of coronary arterial segments.

DISCUSSION

Despite all the technical improvements in MR imaging during the past decade, MR coronary angiography remains a challenging clinical investigation. Many techniques have been explored to date; these include two-dimensional breath-hold, single-section, gradient-echo and 3D free-breathing, respiratory-gated, gradient-echo acquisitions. These techniques have their advantages and disadvantages. Although two-dimensional breath-hold techniques are fast and provide immediate feedback to the imaging operator, image and section misregistration between several acquired sections along a coronary arterial segment of interest can lead to an inaccurate measurement of stenosis in a tortuous coronary segment. This problem has been addressed by using free-breathing MR coronary angiography (ie, retrospective and prospective gated navigator 3D imaging) techniques that enable imaging of a larger volume with a better signal-to-noise ratio (SNR) and good data consistency for diagnosis in a 3D reconstruction platform after data have been acquired (using multiplanar reformation or volume rendering). Nonetheless, free-breathing MR coronary angiography has a major drawback in terms

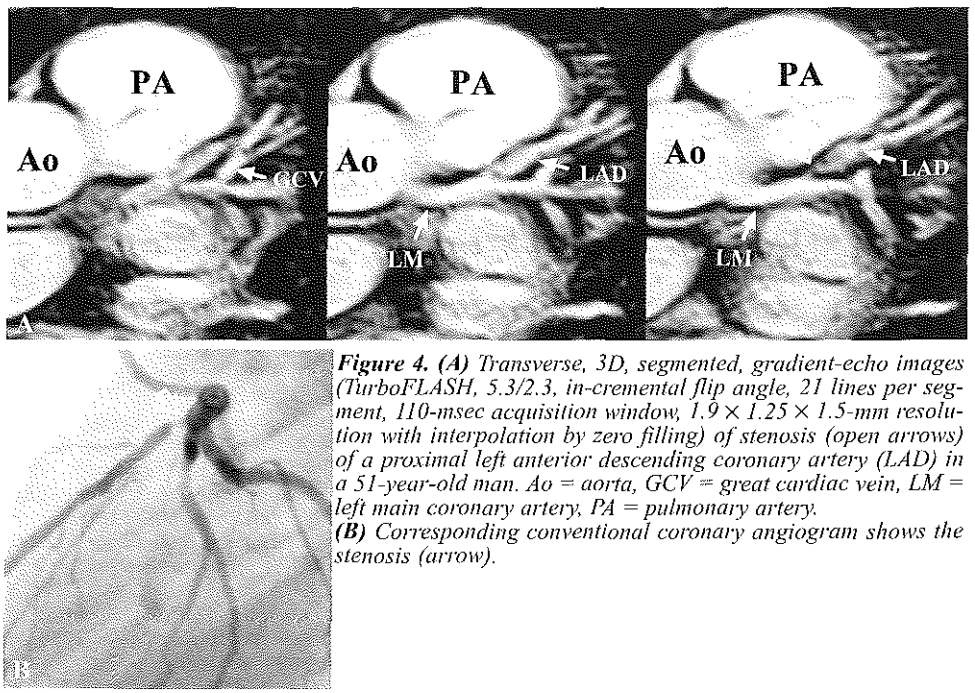

Figure 4. ***(A)*** *Transverse, 3D, segmented, gradient-echo images (TurboFLASH, 5.3/2.3, in-cremental flip angle, 21 lines per segment, 110-msec acquisition window, 1.9 × 1.25 × 1.5-mm resolution with interpolation by zero filling) of stenosis (open arrows) of a proximal left anterior descending coronary artery (LAD) in a 51-year-old man. Ao = aorta, GCV = great cardiac vein, LM = left main coronary artery, PA = pulmonary artery.*
(B) *Corresponding conventional coronary angiogram shows the stenosis (arrow).*

Table 4. Diagnostic accuracy of MR Coronary Angiography for Detection of Greater than 50% Diameter Stenosis

Segments	Visualized	# stenoses	Sens.	Spec.	PV+	PV-	Acc
LM+LAD	88 (86%)	13	77%	97%	83%	96%	94%
RCA	68 (67%)	14	64%	94%	75%	91%	88%
LCX	31 (46%)	4	50%	100%	100%	93%	94%
Overall	187 (69%)	31	68%	97%	81%	94%	92%

Note. — LAD = left anterior descending coronary artery, LCX = left circumflex coronary artery, LM = left main coronary artery, RCA = right coronary artery, NPV = negative predictive value, PPV = positive predictive value, Acc = diagnostic accuracy.
** Data are the combined numbers of segments that could be assessed at MR coronary angiography (see Table 2). Numbers in parentheses are percentages, calculated y averaging the sum of percentages for a given segment in Table 2.*

of acquisition slowness, which results in poor operator feedback in cases in which imaging must be repeated when image detail loss occurs owing to an inconsistent respiratory pattern during the acquisition. However, MR imaging operator expertise is less relevant with 3D measurements than with two-dimensional breath-hold measurements.

In this work, we evaluated our initial clinical experience with a breath-hold VCATS protocol that aims to address some of the known difficulties with MR coronary angiography described earlier. Breath-hold acquisitions reduce breathing artifacts, whereas the use of a small imaging volume yields the data consistency required to evaluate MR coronary angiographic data sets for specific coronary segments. In addition, with the 3D nature of the VCATS measurement sequence described, there is the potential to compensate for the SNR loss in faster acquisition scenarios. Nonetheless, all MR coronary angiography techniques must account for the superposition of motion of the coronary vessels during cardiac contraction, which leads to the loss of image detail, and the resolution and SNR deficiencies that are inherent to MR imaging and limit the accurate depiction of the small caliber of the coronary vessels and possible stenoses. Because images are formed from composite data collected during many heartbeats, slow or sudden alterations in the cardiac rhythm during the acquisitions can lead to additional loss of vessel detail.

Breath-hold MR coronary angiography was possible in the majority of patients in this study. Patients with known severe pulmonary disease were excluded in the selection process; this resulted in the acquisition of more reproducible data from cooperative individuals. The free-breathing MR coronary angiography technique with navigator gating may have been a suitable imaging alternative in the excluded patient population. Claustrophobia and inadequate electrocardiographic tracing—the latter of which is associated with small amplitude of the R wave and prone to interference from imaging gradient activity—were among the factors that resulted in the late exclusion of patients and reduced efficiency during imaging. These limitations may improve with the availability of short-bore dedicated cardiac MR imaging systems and optical-transmission electrocardiographic electrodes.[15,16]

We believe that in this study with the described MR coronary angiography technique, we achieved a promising level of sensitivity and specificity in the detection of hemodynamically significant coronary arterial stenosis in the symptomatic patient group that was selected. Such patients have a high preexamination likelihood of having coronary arterial stenosis. In general, it is impossible to predict the sensitivity and specificity of a diagnostic examination in patients who are less strictly selected. In addition, the

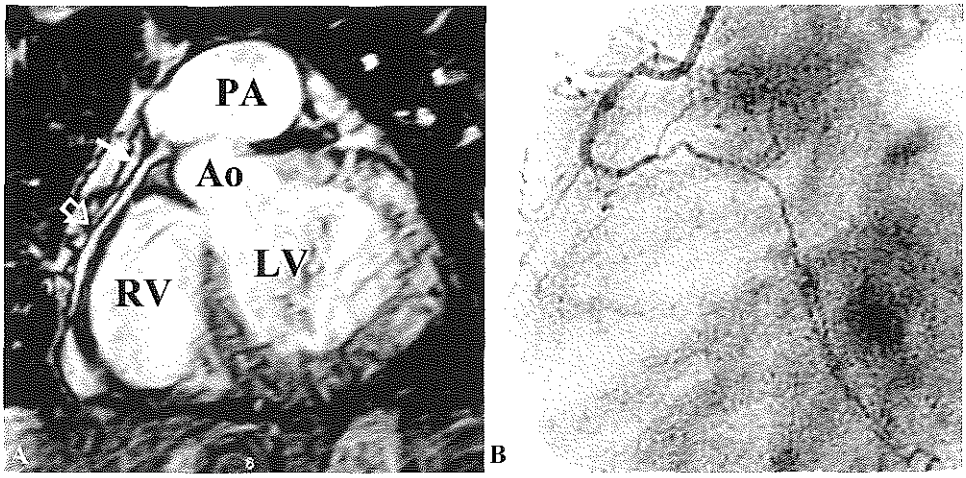

Figure 5. *False-negative findings of stenosis.* ***(A)*** *Double-oblique, 3D, breath-hold, segmented, gradient-echo image (TurboFLASH, 5.3/2.3, incremental flip angle, 21 lines per segment, 110-msec acquisition window, 1.9 × 1.25 × 1.5-mm resolution with interpolation by zero filling) of the right coronary artery in a 44-year-old woman. The clearly delineated vessel (arrows) seems to be patent for at least 5 cm. Ao = aorta, LV = left ventricle, PA = pulmonary artery, RV = right ventricle.* ***(B)*** *Corresponding conventional coronary angiogram shows the vessel in a (open and solid arrows) with an occluded middle segment (open arrow).*

results could have changed substantially with the exclusion of nonassessable segments. This was hinted at by the number of stenoses detected by using VCATS—only 21 (51%) of the 41 stenoses detected in total at conventional angiography. Additional points regarding the study setup must be clarified. The MR sequence selected for VCATS is not without limitations. First, the SNR that is considered adequate for diagnosis limits the submillimeter resolution that is possible with the described sequence (minimum true voxel size for 21 heartbeats, 1.30 × 0.95 × 2.5 mm^3). In practice, an image with lower resolution is feasible, and only vessels with a diameter larger than approximately 2 mm are suitable for evaluation. At present, with conventional coronary angiography, a resolution of 0.1 mm can be obtained and stenoses of high (>70%) and moderate (50%-70%) grades can be differentiated. Therefore, with the current resolution setting in the VCATS protocol, no specific grading of MR angiograms can be attempted.

Second, our MR coronary angiography technique and that of many others are proton density weighted in nature (due to the long magnetization recovery period between data acquisitions, the presence of inflow, and imaging with an incremented flip angle series), despite the additional application of magnetization transfer contrast irradiation to improve myocardial and perhaps plaque signal suppression. Therefore, false-negative results (Figure 5) can be expected, with a normal appearance of the coronary segment at MR coronary angiography and complete occlusion on the corresponding conventional coronary angiogram. The effects of magnetization transfer contrast irradiation on atherosclerotic plaque have been investigated by Pachot-Clouard et al.[17] This group suggests that magnetization transfer contrast irradiation-induced signal drop occurs in atherosclerotic plaque components with an effect that is more pronounced for the fibrous cap and media than for the lipid core and adventitia. Nonetheless, with the present setup, in which triggered images are used, it is difficult to define the exact contribution of magnetization transfer contrast irradiation in signal attenuation from plaque for different

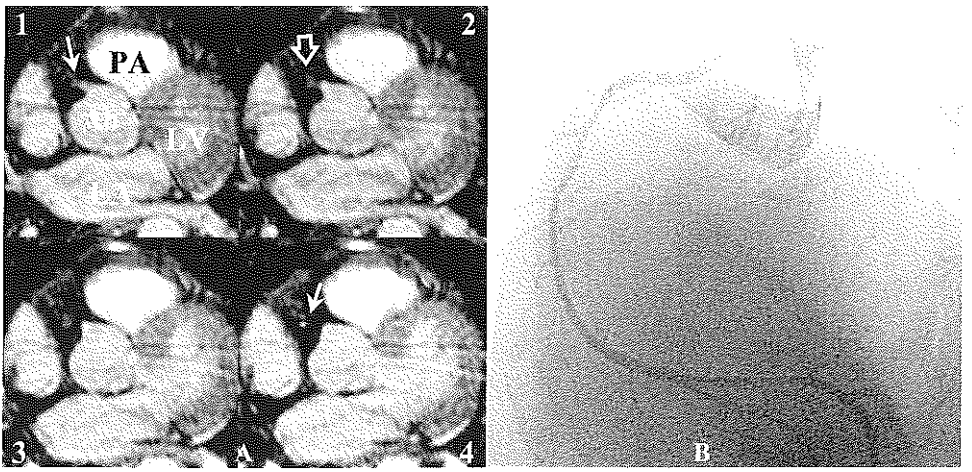

Figure 6. *False-positive findings of stenosis.* ***(A)*** *Transverse, 3D, segmented, gradient-echo images (TurboFLASH, 5.3/2.3, incremental flip angle, 21 lines per segment, 110-msec acquisition window, 1.9 × 1.25 × 1.5-mm resolution with interpolation by zero filling) through the proximal right coronary artery in a 71-year-old man. On four consecutive sections, the right coronary artery (open arrow) seems to be occluded beyond 0.5 cm of its origin (solid arrows) owing to incomplete fat suppression and partial Fourier reconstruction. Ao = aorta, LA = left atrium, LV = left ventricle, PA = pulmonary artery.* ***(B)*** *Corresponding conventional coronary angiogram shows the vessel to be patent.*

cardiac rates.

Third, it was difficult to achieve complete fat suppression in all coronary segments. Remnant nonsuppressed fat can induce particular artifacts, such as blurring, vessel shift, and thin dark lines when partial Fourier reconstruction is used. These artifacts can have a major role in the diagnosis of particular coronary segments and, if the reader is not well aware of the limitations, render a segment nonassessable, as demonstrated in a false-positive case in our study (Figure 6). The addition of the partially intravascular superparamagnetic iron oxide contrast medium produced some T1 shortening in blood; however, this may not substantially change the resultant SNR using a small targeted volume mainly obtained with proton density weighting, in which enough longitudinal magnetization recovery and inflow effects combined reduce the overall effectiveness of any contrast medium that is present in blood. The T1 shortening obtained did provide substantially better SNR results on the volume localizer images, because a larger volume of blood was saturated with every heart cycle and inflow effects of fully magnetized blood spins were not expected. The superparamagnetic iron oxide contrast medium remains approximately 10%-20% intravascular, with an approximate T1 relaxation time of 400-700 msec, which is stable for several hours after the initial infusion.

Visualization of the left circumflex coronary artery is difficult with all MR coronary angiography techniques, and the present protocol cannot completely solve this problem. One problem arises from the lower SNR caused by the relatively large distance between the left circumflex coronary artery and the surface coils placed around the chest wall. In addition, the close relation between the left circumflex coronary artery, the coronary sinus, and the auricle of the left atrium hampers evaluation of the vessel owing to the lack of resolution and insufficient SNR and contrast-to-noise ratio. Furthermore, the application of magnetization transfer contrast irradiation for an improved contrast-to-noise ratio between the myocardium and blood pools is not without consequences. Magnetization transfer contrast irradiation

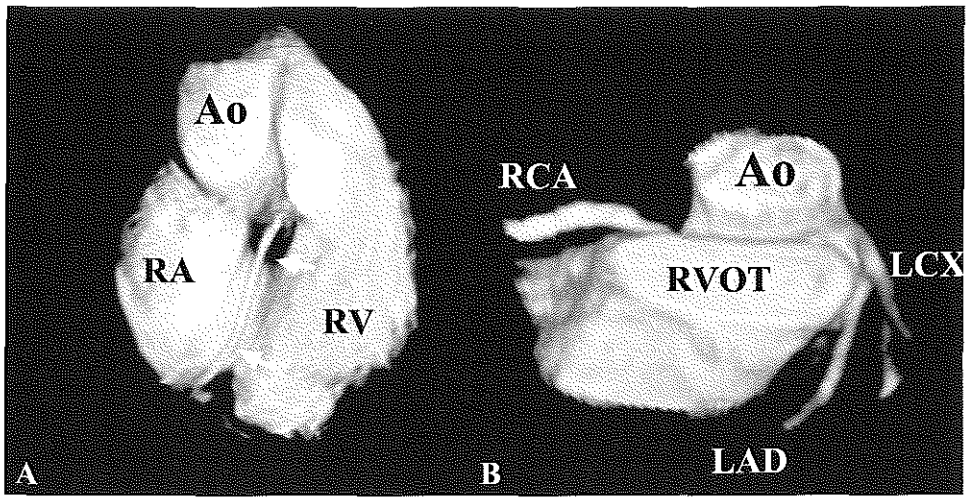

Figure 7. ***(A)*** *Right anterior, volume-rendered, double-oblique, 3D, breath-hold, segmented, gradient-echo image (TurboFLASH, 5.3/2.3, incremental flip angle, 21 lines per segment, 110-msec acquisition window, 1.9 × 1.25 × 1.5-mm resolution with interpolation by zero filling) of a targeted volume of a nondiseased right coronary artery (arrows) in a 43-year-old man. Ao = aorta, RA = right atrium, RV = right ventricle.* ***(B)*** *Anterior cranial volume-rendered image of a targeted volume of the aortic root in the same patient. Ao = aorta, LAD = left anterior descending coronary artery, LCX = left circumflex coronary artery, RCA = right coronary artery, RVOT = right ventricular outflow tract.*

increases the specific absorption ratio in the patient and reduces the SNR that may be achievable in blood without its application. The application of volume rendering techniques makes it possible to integrate the 3D course of a coronary segment on a single image. This appears to be useful for delineating the coronary anatomy, as demonstrated in Figures 7-9, and helping to identify coronary lesions from any viewing angle. Nonetheless, postprocessing adds appreciable time to the overall examination. Data transfer to a specialized workstation and the preparation of data by segmenting the unwanted structures before acquiring the final volume-rendered image can be time consuming. Manual segmentation requires 5-15 minutes for each volume; therefore, no attempt was made to render all seven volumes collected in each patient. However, the

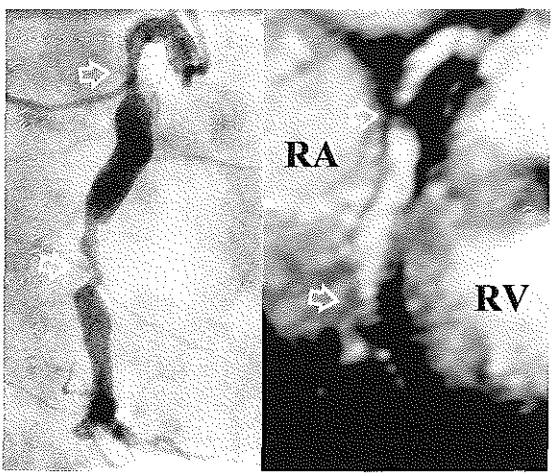

Figure 8. *Right anterior, volume-rendered, double-oblique, 3D, breath-hold, segmented, gradient-echo image (TurboFLASH, 5.3/2.3, incremental flip angle, 21 lines per segment, 110-msec acquisition window, 1.9 × 1.25 × 1.5-mm resolution with interpolation by zero filling) (right) and corresponding conventional coronary angiogram (left) of a targeted volume of a right coronary artery in a 57-year-old man show two hemodynamically significant stenoses (arrows). RA = right atrium, RV = right ventricle.*

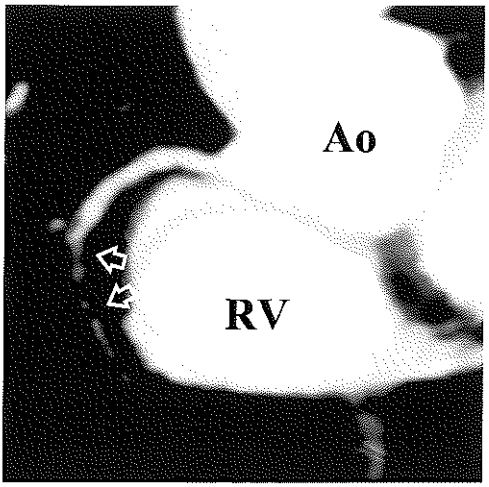

Figure 9. *Anterior volume-rendered image (1.9 × 1.25 × 1.5-mm resolution with interpolation by zero filling) of the right coronary artery in the patient in Figure 3 with hemodynamically significant stenoses (arrows) followed by complete occlusion. Ao = aorta, RV = right ventricle.*

use of improved software may substantially reduce this manipulation time to make this display utility suitable for routine use.

In total, 72 targeted volumes in 25 patients were reconstructed with volume rendering and believed to enable proper visualization of the coronary segment in question compared with conventional angiography. The settings for the voxel opacity (or transparency) were manipulated to demonstrate an appearance of features similar to that on conventional angiograms, because the effects of the signal intensity distribution observed during review of individual sections of the corresponding VCATS volume were not known a priori. Therefore, the volume-rendered data on the diseased vessels presented in Figures 8 and 9 were obtained retrospectively on the basis of findings on the conventional angiograms. This procedure was feasible in this preliminary study because the volume rendering technique is fairly new and has not been adequately assessed for MR imaging data sets, especially with signal intensity histograms and signal intensity ranges that are different in each targeted coronary volume. This is in contrast to the more routine volume rendering processing performed on CT data, in which attenuation value ranges (in HU) in tissues are predictable to well known and, in turn, provide a well-defined intensity histogram. However, MR data are heavily dependent on the reception pattern of the coil array surrounding the thorax—that is, dependent on patient size. No attempts to correct the signal intensity profile of each phased-array coil and thus homogenize the image data were made; therefore, the volume rendering settings were an operator-related choice.

In spite of many measurement difficulties, the visualization on and quality of the images in this initial evaluation were encouraging enough to warrant continued, more extensive clinical trials with the proposed VCATS methodology. The proposed protocol is practical for a clinical setup and provides the means for fast assessment of the coronary arteries with acquisition times of less than 30 minutes. We envision that further improvements in the presently used MR pulse sequence that yield better signal-to-noise and contrast-to-noise ratios and better resolution with a shorter breath-hold time will substantially help increase the sensitivity and specificity of the approach. On the basis of theoretical estimates,[18] the addition of intravascular contrast media that provide very short T1 relaxation times in blood (<40 msec) can facilitate some of the improvements[19] needed to consider the routine use of a VCATS protocol for the evaluation of coronary arteries. Furthermore, contrast media may improve the differentiation between the vessel lumen and coronary arterial wall by enabling the acquisition of only a luminogram. In conclusion, the described VCATS protocol makes it possible to localize the major coronary arterial branches in a short examination time, and the observed degree of accuracy in the detection of

hemodynamically significant stenoses within these branches is encouraging. The selected measurement sequence for VCATS needs improved SNR and spatial resolution with shorter measurement times to facilitate a more adequate scenario for coronary arterial assessment on a broader scale. We envision that further refinements in the hardware and software in MR cardiac machines and the introduction of T1-efficient intravascular contrast media will considerably augment the dependability of the proposed methodology.

REFERENCES

1. Edelman RR, Manning WJ, Burstein D, Paulin S. Coronary arteries: breath-hold MR angiography. Radiology 1991; 181:641-643.
2. Wang Y, Grimm RC, Rossman PJ, Debbins JP, Riederer SJ, Ehman RL. 3D coronary MR angiography in multiple breath-holds using a respiratory feedback monitor. Magn Reson Med 1995; 34:11-16.
3. Li D, Kaushikkar S, Haacke EM, et al. Coronary arteries: three-dimensional MR imaging with retrospective respiratory gating. Radiology 1996; 201:857-863.
4. McConnell MV, Khasgiwala VC, Savord BJ, et al. Prospective adaptive navigator correction for breath-hold MR coronary angiography. Magn Reson Med 1997; 37:148-152.
5. Manning WJ, Li W, Edelman RR. A preliminary report comparing magnetic resonance coronary angiography with conventional angiography. N Engl J Med 1993; 328:828-832.
6. Duerinckx AJ, Urman MK. Two-dimensional coronary MR angiography: analysis of initial clinical results. Radiology 1994; 193:731-738.
7. Pennell DJ, Bogren HG, Keegan J, Firmin DN, Underwood SR. Assessment of coronary artery stenosis by magnetic resonance imaging. Heart 1996; 75:127-133.
8. Post JC, van Rossum AC, Hofman MB, de Cock CC, Valk J, Visser CA. Clinical utility of two-dimensional magnetic resonance angiography in detecting coronary artery disease. Eur Heart J 1997; 18:426-433.
9. van Geuns RJM, de Bruin HG, Wielopolski PA, et al. MRI of the coronary arteries: clinical evaluation from three-dimensional evaluation of a respiratory gated technique. Heart 1999; 82:515-519.
10. Post JC, van Rossum AC, Hofman MB, Valk J, Visser CA. Three-dimensional respiratory-gated MR angiography of coronary arteries: comparison with conventional coronary angiography. AJR Am J Roentgenol 1996; 166:1399-1404.
11. Duerinckx AJ, Atkinson DP, Mintorovitch J, Simonetti OP, Vrman MK. Two-dimensional coronary MRA: limitations and artifacts. Eur Radiol 1996; 6:312-325.
12. Wielopolski P, van Geuns R, de Feyter P, Oudkerk M. Breath-hold coronary MR angiography with volume targeted imaging. Radiology 1998; 209:209-219.
13. Judkins MP. Selective coronary arteriography. I. A percutaneous transfemoral technique. Radiology 1967; 89:815-824.
14. Austen WG, Edwards JE, Frye RL, et al. A reporting system on patients evaluated for coronary artery disease: report of the Ad Hoc Committee for Grading of Coronary Artery Disease, Council on Cardiovascular Surgery, American Heart Association. Circulation 1975; 51(suppl):5-40.
15. Felblinger J, Lehmann C, Boesch C. Electrocardiogram acquisition during MR examinations for patient monitoring and sequence triggering. Magn Reson Med 1994; 32:523-529.
16. Felblinger J, Debatin JF, Boesch C, Gruetter R, McKinnon GC. Synchronization device for electrocardiography gated echo-planar imaging. Radiology 1995; 197:311-313.
17. Pachot-Clouard M, Vaufrey F, Darrasse L, Toussainti JF. Magnetization transfer characteristics in atherosclerotic plaque components assessed by adapted binomial preparation pulses. MAGMA 1998; 7:9-15.
18. Johansson LO, Fischer SE, Lorenz CH. Benefit of T1 reduction for magnetic resonance coronary angiography: a numerical simulation and phantom study. J Magn Reson Imaging 1999; 9:552-556.
19. Lauffer RB, Parmelee DJ, Dunham SU, et al. MS-325: albumin-targeted contrast agent for MR angiography. Radiology 1998; 207:529-538.

Chapter 11

Magnetic Resonance Angiography of Single and Sequential Venous Bypass Grafts:

Assessment of Patency over the Entire Length of the Graft

R.J.M. van Geuns, P.A. Wielopolski, H.G. de Bruin,B.J.W.M. Rensing,

P.M.A. van Ooijen, M. Oudkerk, P.J. de Feyter.

Submitted

ABSTRACT

Background:
So far the patency of coronary artery bypass grafts by magnetic resonance imaging was assessed on cross-section images located in a proximal part of the graft. More comprehensive imaging over the entire length, particular in sequential grafts, is desirable. A recently introduced breath-hold magnetic resonance technique using targeted volume scans (VCATS) allows rapid imaging of longer segments of coronary arteries and bypass grafts. The aim of this study was to assess the diagnostic value of VCATS to assess the patency over the entire length of venous bypass grafts.

Materials and methods:
Seventeen patients with 21 venous grafts (5 single grafts, 16 sequential grafts) were studied with the VCATS protocol on a 1.5 T scanner with a phased array body coil. The grafts were first localised with a single breath-hold volume scan acquired with a multishot echo planar imaging sequence. Then, several targeted volume scans were made with a 3D breath-hold turboFlash sequence with a resolution of 1.9 × 1.25 × 1.5 mm in about 30 minutes. In sequential grafts a segment was defined as a part of the bypass graft between two successive anastomotic sites. A total of 50 segments was available for comparison with selective angiography.

Results:
All fifty graft segments could successfully be evaluated. On selective coronary angiography 30 segments were patent and 20 were occluded. The sensitivity and specificity of VCATS for the detection of patent grafts segments were 93% (28/30) and 95% (19/20) respectively with an overall accuracy of 94% (47/50). Sternal wires induced local artefacts in 10 of the proximal graft segments, but did not preclude to evaluate patency of these segments could be evaluated outside the artefact.

Conclusion:
The single breath-hold EPI localiser scan is adequate for graft localisation. VCATS showed a high sensitivity and specificity for the establishment of venous bypass graft patency over it's entire length.

INTRODUCTION

Coronary artery bypass graft surgery is used worldwide as a successful technique to revascularize coronary artery obstruction using, preferentially arterial grafts and otherwise venous bypass grafts. However the attrition rate of these grafts is substantial and requires repeated evaluation. Consequently there is a strong demand for a reliable, noninvasive procedure that can be performed repeatedly at postoperative follow-up. Magnetic resonance imaging (MRI) is a noninvasive technique that has the potential to visualize the coronary arteries and coronary artery bypass grafts. Several MRI techniques have been validated for the detection of bypass grafts patency with reported excellent sensitivity and specificity. However most of the studies have been restricted to single or the proximal segments of sequential grafts and were unable to evaluate the entire length of sequential grafts. With improved MRI scanner hardware it has been possible to reduce the imaging time for MR coronary angiography using a breath-hold targeted imaging approach (VCATS, volume coronary angiography using targeted scans.[1] In this study we investigated the diagnostic accuracy of VCATS to assess the patency of single and sequential venous coronary artery bypass grafts over their entire length.

MATERIAL AND METHODS

Patients

Seventeen patients with 21 grafts, and 52 distal anastomoses with a history of coronary artery bypass grafts surgery were studied shortly after standard selective coronary (bypass) angiography. The mean age was 56 years (range 47 to 73), and the patients were studied an average of 7.3 years after bypass surgery. Standard selective angiography was performed to evaluate ischemic chest pain in all patients.

Exclusion criteria artificial pacemakers, intracranial clips, atrial fibrillation, severe claustrophobia, and severe lung disease restricting breath-holding capabilities to less than 30 seconds. The protocol was approved by our hospital committee on medical ethics and clinical investigation. Written informed consent was obtained prior to the MRI examination.

MRI

The studies were performed on a 1.5 whole-body MRI system (Magnetom Vision, Siemens, Erlangen, Germany). Patients were placed in a supine position with a 4-channel quadrature body phased array coil placed over the thorax. ECG electrodes were always positioned on the anterior thoracic wall. To start with the coronary localization procedure, a single breath-hold 3D multi-shot segmented EPI (3D-MSEPI) sequence was used to cover the entire heart using a 120 mm slab at end-expiration. The data were subjected to multi-planar (MPR) evaluation to determine the suspected aorta-bypass anastomosis of the coronary bypass grafts and optimal imaging planes along the course of visible grafts (Figure 1) with the help of

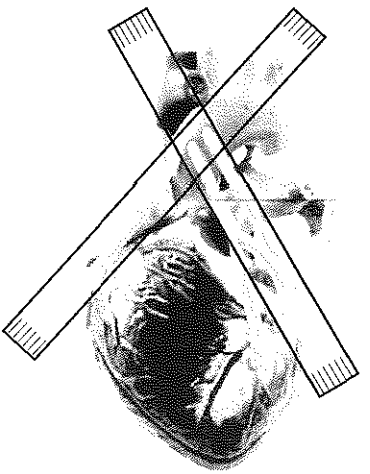

Figure 1. *Illustration of the principle of volume coronary angiography with targeted volume scans (VCATS) to study sequential venous coronary artery bypass grafts. Several targeted volumes are used to cover all the segments of a sequential graft.*

the surgical notes on the number of grafts and sites of anastomosis which were available during the investigation. After all orientations were obtained with MPR, imaging proceeded with the breath-hold VCATS protocol. Targeted bypass angiography was performed with a double oblique 3D-segmented gradient echo (GE) sequence (TurboFLASH, TR/TE=5.3/2.3 ms, incremental flip angle, 21 lines per segment, 110 msec acquisition window). A 24 mm thick slab (7 encoded partitions, 16 reconstructed by zero filling) was used with a 126×256 matrix and partial Fourier reconstruction. Scan duration was 21 heartbeats and the imaging window coincided with mid-late diastole. The field-of-view (FOV) was maintained constant at 240×320 mm^2, providing a resolution of $1.9 \times 1.25 \times 1.5$ mm^3. Magnetization transfer irradiation (MTC) for myocardium-blood contrast-to-noise ratio (CNR) enhancement (irradiation duration of 500 ms) and a single chemical shift fat suppression pulse were applied prior to data collection for each cardiac window. Breath-holding was performed at end-expiration to obtain position and plane reproducibility with respect to the MPR data generated using the volume localizer. Breath-hold quality was assessed immediately after every acquisition by observing ghosting artifacts of the anterior thoracic wall over the images. In case ghosting appeared, repeated imaging of a particular volume was allowed. If severe ghosting artifacts were present and the patient could not hold the breath adequately within 4 attempts, the patient was regarded as non-suitable for the scanning procedure and excluded from the study.

Conventional coronary angiography

All subjects underwent selective coronary artery bypass angiography using the Judkins technique[2] within 1 month of the MR examination. Two experienced cardiologists jointly interpreted the angiograms. Sequential coronary artery bypass grafts were divided into successive segments between each anastomosis site (figure 2). All segments were visually graded as either being patent or occluded. In case of disagreement a third cardiologist made a final decision.

MR interpretation

From each targeted volume the 16 source images were analyzed in a dynamic loop, independently by a cardiologist and a radiologist who were unaware of the cardiac catheterization results. In case of disagreement consensus was achieved in a joint session with a third investigator. These segments were graded as assessable if overlapping structures (veins, pericardium, and unsuppressed fat), image blur and ghosting artifacts could be distinguished from the vessel itself. Segments covered by more than one volume were finally evaluated in the volume with the best image quality. The whole sequential graft was considered occluded if the graft origin was not visualized in a set of transverse targeted volumes through the aortic root. Segments were considered patent if the graft was visualized in more than one slice of a targeted volume for the graft segment. In proximal open sequential grafts all graft segments distal to the last visualized patent segment were considered as occluded.

To investigate the possibilities to integrate the coronary path within a targeted volume into a single image, data sets were reconstructed using a volume rendering program (VoxelView, Vital Images Inc, Minneapolis, Minnesota, USA) running on a dedicated graphic workstation (Indigo2, Silicon Graphics, Mountain View, California, USA). Segmentation was required to discard overlapping to view the coronary artery bypass graft from any viewing angle.

Statistical Analysis

The conventional coronary angiogram served

Table 1. Patency of different coronary artery bypass graft segments by coronary angiography.

Segment	N	Patency
1st	21	16 (76%)
2nd	16	10 (63%)
3rd	6	2 (33%)
4th	4	1 (25%)
5th	3	1 (33%)

as the gold standard for determination of the diagnostic value of MR-coronary angiography. For the detection of graft patency in a segment sensitivity, specificity, positive and negative predictive value and diagnostic accuracy, as well as 95% confidence intervals were established to evaluate the diagnostic value.

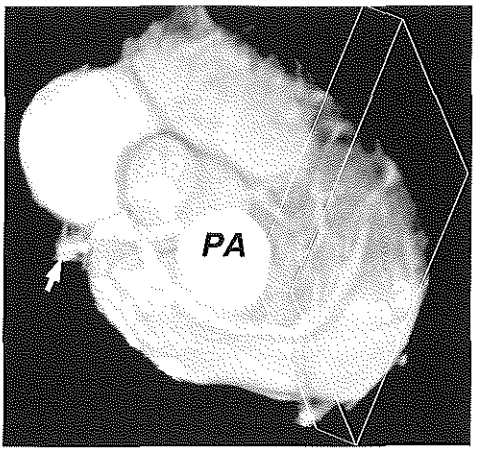

Figure 2. *Example of the volume localizer scan covering the whole volume of the heart. In this volume the exact course of the graft (curved arrows) can be determined and the optimal imaging planes for the targeted volumes can selected. Also some parts of the native coronary arteries are visualized. Ao = Aorta, PA = Pulmonary artery, RCA = right coronary artery, LAD = left anterior descending coronary artery.*

RESULTS

The mean time interval and standard deviation between cine-angiograms and magnetic resonance angiography was 10 ± 7 days. Of the 17 patients examinations one study was incomplete due to insufficient time available to use the MRI scanner. Within these patients 21 venous grafts were succesfully studied . Of the 21 grafts 5 were single grafts, and 16 were sequential grafts (ten with 2 distal anastomoses, two with 3 distal anastomoses, one with 4 distal anastomoses and three with 5 distal anastomoses) with a total of 50 segments available for analysis.

Conventional coronary angiography demonstrated graft patency for 60% (30/50) of all graft segments, which ranged from 76% for the proximal graft segments to 25% for distal grafts segments. The data on the individual segments are listed in Table 1.

The mean and standard deviation of the number of targeted volumes collected per patient with MRI was 10 ± 2.3. The mean and standard deviation of the breath-hold time per acquired targeted volume was 24 ± 5 seconds. The acquisition of the volume localizer scan, the selection of the optimal plane location and orientation of the targeted volumes with MPR and the acquisition of the targeted scans were always completed in less than 30 minutes. The volumes for the proximal graft segments contained sternal wires which induced local artifacts in 10 of the 16 patent proximal graft segments, but fortunately the size of the artifact was limited and

Table 2. Diagnostic accuracy for the detection of graft patency by MR-coronary angiography.

Segm.	Sensensitivity	Specificity	PV+	PV-	Acc
1	100%(100-100%)	100%(100-100%)	100%(100-100%)	100%(100-100%)	100%(100-100%)
2	80% (55-100%)	100%(100-100%)	100%(100-100%)	75%(45-100%)	88%(71-100%)
3-5	100%(100-100%)	89%(68-100%)	80% (45-100%)	100%(100-100%)	92%(78-107%)
Overall	93%(84-100%)	95%(85-100%)	97%(90-100%)	90%(78-100)	94%(87-100%)

PPV = positive predictive value, NPV = negative predictive value, Acc = diagnostic accuracy.

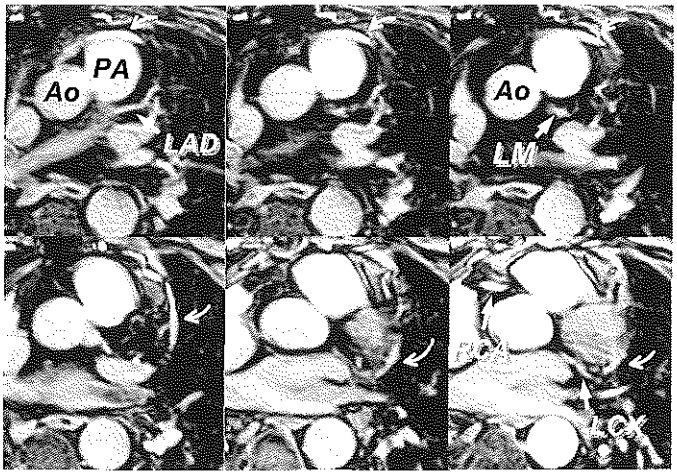

Figure 3. Original slices of a transverse targeted volume at the level of the aortic root (Ao). From the top slices at the upper left the proximal segment of a venous graft (curved arrows) can be followed anterior of the pulmonary artery (PA) to the anastomosis on a diagonal branch in the fourth slice. The second segment can be followed to an anastomosis on the branch of the left circumflex coronary artery (LCX) in caudal slice in the lower right panel.

did not preclude to assess the patency of these segments.

The volume localizer scan was adequate for graft localization in all patients (Figure 2) and the targeted volumes showed a high quality images for proximal bypass graft segments on the original slices (Figure 3). For these targeted volumes postprocessing with volume rendering was able to integrate the individual slices to a single image to visualize the entire course of the bypass graft path through the volume (Figure 4). With VCATS it was possible to visualize all of the patent distal segments of sequential bypass grafts (Figure 5).

VCATS correctly classified 28 of the 30 patent graft segments (sensitivity 93%)(Figure 5) and 19 of the 20 occluded segments (specificity 95%). An example of a sequential graft occluded after the third anastomosis is shown in Figure 6. The findings for the detection of graft patency for the different segments are summarized in table 2. Sensitivity ranged from 80% for distal graft segments to 100% for proximal graft segments and specificity from 89% to 100%.

DISCUSSION

Within the first year after coronary artery bypass graft surgery, the occlusion rate of venous coronary artery bypass grafts is 15-25%[3-5], and after 10 years 40-50% of the venous grafts are occluded.[6,7]

Non-invasive assessment of graft patency may be useful because graft occlusions may occur clinically silent and only in later stages of progression these patients become symptomatic. Regular follow-up after bypass surgery using MRI may depict graft disease before total occlusion is present. At that stage angioplasty will be more successful and may prevent progression to total occlusion. This

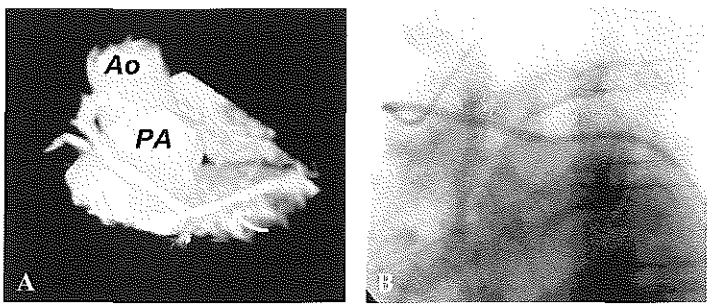

Figure 4. (A) Example of the use of volume rendering to integrate all the slices of a targeted volume (same as in figure 3) into a single images. The patency of the graft (curved arrows) is clearly demonstrated.
(B) Corresponding conventional angiogram.

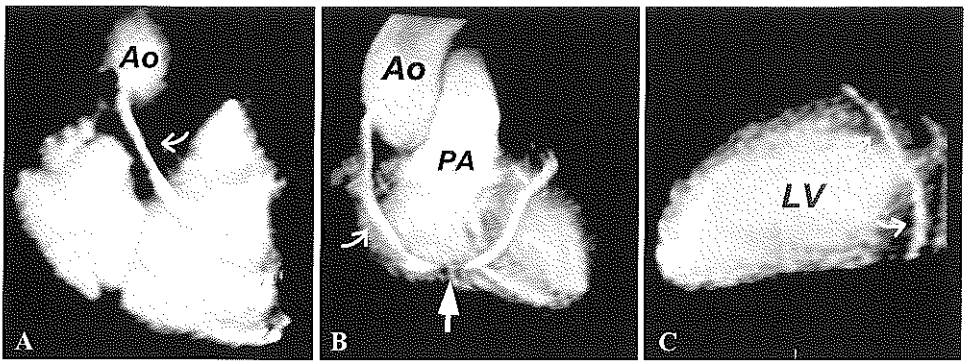

Figure 5. *(A) Volume rendered image of the slices of a targeted volume for the proximal segment of a venous graft (curved arrows) from the aorta (Ao) across the right atrio-ventricular groove and right ventricle (RV).* ***(B)*** *Second volume for the graft segment anterior of the pulmonary artery (PA) illustrating the possibility to asses graft patency despite the presence of a sternal wire related artifact (straight arrow).* ***(C)*** *Third volume targeted for the graft segment over the lateral wall of the left ventricle (LV)*

may increase graft survival and possibly reduce the number of repeat bypass operations.

Since the introduction of MRI many techniques and sequences have been developed to visualize the coronary arteries. None of these techniques has been successful to reliably detect all coronary artery stenoses. Due to the relative large size (4-6 mm in diameter) and lesser movement of coronary artery venous bypass grafts the assessment of patency is less demanding in terms of resolution and acquisition speed. The first study used a conventional Spin-echo sequence to assess bypass graft patency and achieved a sensitivity of 86% and a rather low specificity of 59%.[8] These initial results were improved with the introduction of gradient-echo imaging [9-14] but these techniques only provided cross sectional images of proximal bypass graft segments, limiting the application in clinical practice. More recently contrast-enhanced magnetic resonance angiography (MRA) has been used to study longer segments of coronary artery bypass grafts.[15,16] However, these examinations only provide information on bypass patency of the proximal segments and no information about

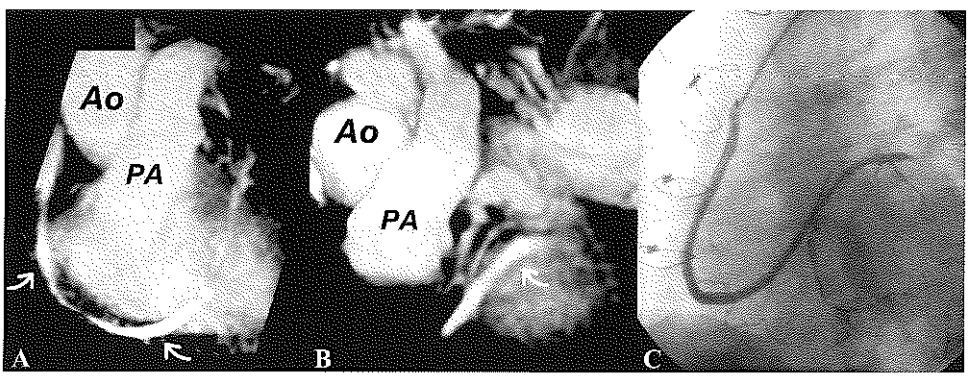

Figure 6. *(A) MRI image of a partially occluded venous graft. The proximal segment to the first anastomosis is patent (curved arrows) while the second segment is patent but with diminished image quality.* ***(B)*** *Second MRI volume targeted for the third anastomosis demonstrating the occlusion of the graft distal to the anastomosis.* ***(C)*** *Corresponding conventional coronary angiography confirming the patency of the proximal graft segments, the diseased third segment and occluded distal segments.*

graft patency distal to the first coronary artery anastomosis is obtained. The first MR evaluation of sequential bypasses over their full length was obtained with a HASTE (Half Fourier Single shot Turbospin-Echo) MRI technique.[17] The sensitivity and specificity for the detection of proximal graft occlusion were excellent (95% and 93% respectively), but sensitivity was less (83%) for distal bypass graft segments.

In our study we demonstrated the possibility to determine the patency of all segments of single and sequential venous bypass graft using VCATS. The overall sensitivity and specificity of 93% and 95% respectively, were excellent and importantly, all patent graft segments, including the most distal were visualized (sensitivity 100%).

All the above techniques, including ours, used sequences to study coronary artery bypass grafts morphology. However, MRI also allows functional imaging of vessels by using flow velocity information which is impaired by significant obstructions. Indeed MRI phase velocity imaging has been used to study flow velocities in coronary artery bypass grafts[18,19] with varying success. However the reliability of velocity measurements is hampered by the fact that coronary bypass flow in rest is variable and dependent on the size and number of revascularized coronary artery branches. This latter problem may be overcome by pharmacological stress induced measurements of the flow reserve. So far, this method has not been used frequently but preliminary data have demonstrated that impaired flow reserve is associated with myocardial ischemia in graft dependent regions.[20]

A limitation of this study is that non-occlusive obstructions were hardly present in our patient population and therefore no diagnostic accuracy could be calculated. In one patient the ability of VCATS to visualize non-occlusive obstructions was demonstrated (Figure 6). To study the diagnostic value of VCATS for the detection of bypass graft stenosis requires an increase in the spatial resolution.

Due to the extreme length of LIMA bypass grafts, the abundant present imaging artifacts related to metallic clip, and the relatively small size of these vessels we did not attempt to study arterial grafts.

CONCLUSION

The VCATS setup makes it possible to localize the course of sequential venous coronary artery bypass grafts in a short examination time and determine patency over the entire length of single and sequential venous bypass grafts with a high degree of accuracy. The selected measurement sequence for VCATS still requires improvements in SNR and spatial resolution to be able to reliable assess the presence of non-occlusive obstructions.

REFERENCES

1. Wielopolski P, vanGeuns R, deFeyter P, et al. Breath-hold Coronary MR Angiography with Volume Targeted Imaging. Radiology. 1998;209:209-219.
2. Judkins MP. Selective coronary arteriography. I. A percutaneous transfemoral technic. Radiology. 1967;89:815-24.
3. Chesebro JH, Fuster V, Elveback LR, et al. Effect of dipyridamole and aspirin on late vein-graft patency after coronary bypass operations. N Engl J Med. 1984;310:209-14.
4. van der Meer J, Hillege HL, Kootstra GJ, et al. Prevention of one-year vein-graft occlusion after aortocoronary-bypass surgery: a comparison of low-dose aspirin, low-dose aspirin plus dipyridamole, and oral anticoagulants. The CABADAS Research Group of the Interuniversity Cardiology Institute of The Netherlands. Lancet. 1993;342:257-64.
5. van der Meer J, Brutel de la Riviere A, van Gilst WH, et al. Effects of low dose aspirin (50 mg/day), low dose aspirin plus dipyridamole, and oral anticoagulant agents after internal mammary artery bypass grafting: patency and clinical outcome at 1 year. CABADAS Research Group of the

Interuniversity Cardiology Institute of The Netherlands. Prevention of Coronary Artery Bypass Graft Occlusion by Aspirin, Dipyridamole and Acenocoumarol/ Phenprocoumon Study. J Am Coll Cardiol. 1994;24:1181-8.
6. Bourassa MG, Enjalbert M, Campeau L, et al. Progression of atherosclerosis in coronary arteries and bypass grafts: ten years later. Am J Cardiol. 1984;53:102C-107C.
7. Campeau L, Enjalbert M, Lesperance J, et al. The relation of risk factors to the development of atherosclerosis in saphenous-vein bypass grafts and the progression of disease in the native circulation. A study 10 years after aortocoronary bypass surgery. N Engl J Med. 1984;311:1329-32.
8. White RD, Caputo GR, Mark AS, et al. Coronary artery bypass graft patency: noninvasive evaluation with MR imaging. Radiology. 1987;164:681-6.
9. Rubinstein RI, Askenase AD, Thickman D, et al. Magnetic resonance imaging to evaluate patency of aortocoronary bypass grafts. Circulation. 1987;76:786-91.
10. Jenkins JP, Love HG, Foster CJ, et al. Detection of coronary artery bypass graft patency as assessed by magnetic resonance imaging. Br J Radiol. 1988;61:2-4.
11. Frija G, Schouman-Claeys E, Lacombe P, et al. A study of coronary artery bypass graft patency using MR imaging. J Comput Assist Tomogr. 1989;13:226-32.
12. Galjee MA, van Rossum AC, Doesburg T, et al. Value of magnetic resonance imaging in assessing patency and function of coronary artery bypass grafts. An angiographically controlled study. Circulation. 1996;93:660-6.
13. White RD, Pflugfelder PW, Lipton MJ, et al. Coronary artery bypass grafts: evaluation of patency with cine MR imaging. AJR Am J Roentgenol. 1988;150:1271-4.
14. Aurigemma GP, Reichek N, Axel L, et al. Noninvasive determination of coronary artery bypass graft patency by cine magnetic resonance imaging. Circulation. 1989;80:1595-602.
15. Vrachliotis TG, Bis KG, Aliabadi D, et al. Contrast-enhanced breath-hold MR angiography for evaluating patency of coronary artery bypass grafts. AJR Am J Roentgenol. 1997;168:1073-80.
16. Wintersperger BJ, Engelmann MG, von Smekal A, et al. Patency of coronary bypass grafts: assessment with breath-hold contrast-enhanced MR angiography--value of a non-electrocardiographically triggered technique. Radiology. 1998;208:345-51.
17. Kalden P, Kreitner KF, Wittlinger T, et al. Assessment of coronary artery bypass grafts: value of different breath-hold MR imaging techniques. AJR Am J Roentgenol. 1999;172:1359-64.
18. Hoogendoorn LI, Pattynama PM, Buis B, et al. Noninvasive evaluation of aortocoronary bypass grafts with magnetic resonance flow mapping. Am J Cardiol. 1995;75:845-8.
19. Galjee MA, van Rossum AC, Doesburg T, et al. Quantification of coronary artery bypass graft flow by magnetic resonance phase velocity mapping. Magn Reson Imaging. 1996;14:485-93.
20. Kawada N, Sakuma H, Nomura Y. Value of breath-hold MR flow measurement in evaluating stenosis of the internal mammary artery bypass graft. (abstract). Circulation. 1999;98:I-515.

Chapter 12

Improvements in Magnetic Resonance Imaging of the Coronary Arteries with a Clinical Available Intravascular Contrast Agent

R.J.M. van Geuns, P.A. Wielopolski, H.G de Bruin,

P.J. de Feyter, M. Oudkerk.

Submitted

ABSTRACT

Purpose:
To investigate the effect on signal-to-noise ratio (SNR) and contrast-to-noise ratio (CNR) of a clinically approved MR contrast agent for liver imaging with a partial intravascular behaviour on a specific magnetic resonance coronary angiography (MRCA) technique.

Methods and materials:
Six patients (4 males, 2 females) were investigated using a intravenous administration of a suspension of 89.6 mg ferumoxide (AMI-25, Endorem; Guerbet S.A., Aulnay-sous-Bois, France) diluted in 100 ml of isotonic glucose, during 30 minutes. T_1 measurements were performed with a series of inversion recovery gradient echo images with varying inversion times. MRCA was performed with a cardiac triggered three-dimensional gradient echo sequence (TR/TE = 2.6/1.3 ms) with retrospective respiratory gating. Matrix size was 128 × 256, field of view was 240 × 320 and slab thickness of 120 mm.

Results:
T_1 relaxation time of blood was reduced from 1562 ± 130 ms to 642 ± 244 ms ($p< 0.01$), while for myocardium there was no significant change (T_1-pre: 1058 ± 30 ms, T_1-post: 1001 ± 138 ms, $p = 0.48$). Post-contrast the SNR of blood in the aortic root and the right atrium improved by 90.5% and 44.1% respectively. The blood versus myocardium CNR improved by 60.8%.

Conclusion:
SNR and CNR for volumetric MRCA can be significantly improved with a MR contrast agent approved for liver imaging which partially behaves as an intravascular contrast agent.

INTRODUCTION

Magnetic resonance coronary angiography (MRCA) has been attempted with several segmented two-dimensional (2D) and three-dimensional (3D) gradient echo techniques.[1-5] All of them depend on the inflow of blood from the left ventricular cavity or aortic root into coronary arteries and T_1 relaxation effects between successive heartbeats. Small imaging volumes (30 mm) are used to minimize blood saturation effects. If the T_1 of blood is reduced, a larger recovery of the longitudinal magnetization is possible between two heartbeats for previously excited blood spins remaining in the imaging volume and consequently larger volumes can be imaged. Gadolinium based agents used for contrast enhanced magnetic resonance angiography of the aorta and peripheral vessels are distributed initially within the intravascular compartment but diffuse rapidly throughout the extracellular (vascular plus interstitial) space. This limits their possible use in the long acquisition schemes frequently used in coronary imaging. Therefore intravascular MR contrast agents have been developed. Two categories can be recognized: Gadolinium based agents and iron oxide particles. Gadolinium compounds with a longer blood half-life time are still in pre-clinical phase. The iron oxides can be divided in: superparamagnetic iron oxides (SPIO) with a particle size between 40 to 80 nm mainly developed for liver imaging and ultrasmall super paramagnetic iron oxides with a particle size of 17-20 nm (USPIO) with a longer blood half-life targeted for MR angiography. SPIO agents (as AMI-25 and SH U 555A) efficiently accumulate for 80-90 % in liver and spleen within minutes of their administration.[6] This selective uptake by liver is used for the detection of liver metastases.[7-11] The remaining 10-20% behaves like a intravascular contrast agent with a longer blood half-life time of between 2.4 and 3.6 hours[12] and may be used for improvement of MR angiography studies.[13] Ferumoxide with dextran coating, AMI-25, is a clinically approved contrast agents that provides this partial intravascular behavior and thus could improve the visualization of the coronary arteries with magnetic resonance imaging.

MATERIALS AND METHODS.

Six patients (4 males, 2 females; 60.2 years of age, 74.0 kg) underwent MRCA after intravenous administration of AMI-25. Pre- and post-contrast studies were performed on the same day in three patients while in two the interval between both studies was 7 days. On 1 patient MRCA was only performed after the infusion of the contrast agent. Before the contrast administration the T_1 relaxivity of blood and myocardium was measured. These measurements were immediately followed by a large volume MRCA scan. After contrast administration the MRCA sequence was repeated followed by a second measurement of the T_1 relaxivity. Exclusion criteria were: previous coronary bypass operation, intracoronary stent implantation, artificial pacemakers, intracranial clips, atrial fibrillation, severe claustrophobia. The protocol was approved by our hospital committee of medical ethics and clinical investigation and informed consent was obtained before the examination.

Contrast agent and Administration

A suspension of 89.6 mg ferumoxide (AMI-25, Endorem; Guerbet S.A., Aulnay-sous-Bois, France) in 100 ml isotonic glucose was drip-infused at a dose of 10-15 umol Fe/kg body weight over 30 min with a flow rate of approximately 3 ml/min. The particle diameter (iron oxide core coated with dextran) is approximately 35 nm.[14] Relaxivity measurements yield a R_1 of 40 $mmol^{-1}sec^{-1}$ and a R2 of 160 $mmol^{-1}sec^{-1}$.[6]

Imaging technique

Subjects were studied in a supine position,

with a four channel quadrature body phased array coil placed over the thorax, in a 1.5 T whole body MR imaging system (Vision; Siemens, Erlangen, Germany).

To estimate the T_1 relaxation time of blood a series of T_1-weighted inversion recovery gradient echo (TurboFlash, IR-TF) images was acquired with and without the contrast agent. The T_1 in inversion recovery spin-echo (IR-SE) imaging can be derived from the inversion time (TI) value that maximal suppresses the signal from blood using $TI_{null} = T_1 \cdot \ln [2/(1 + e^{-TR/T_1})]$. For a sufficiently long repetition time (TR) (TR $>3 \times T_1$ of blood) the null point is $TI_{null} = \ln(2)\, T_1$ and so $T_1 = TI_{null}/\ln(2)$.[15] For IR-TF imaging the approximate behavior to IR-SE can be achieved using a small number of phase encoding lines (course matrix of 32×128), a very short TR (3.3 ms) and a very low flip angle for signal read-out (4°).

Coronary artery imaging was performed using a three dimensional gradient echo sequence with the retrospective respiratory gated technique described by Li et al.[1] This sequence has been modified to cover the whole volume of the heart in a single acquisition and take maximum advantage of the contrast agent used. With the possibilities of the gradient system of the MR scanner the TR was reduced to 2.6 ms, with a TE of 1.3 ms. Within an acquisition window of 160 ms during mid to late diastole 60 phase encoding steps were performed, these were zero-filled to obtain a section thickness of 1 mm over a 120 mm thick volume.

Furthermore magnetization transfer contrast (MTC) preparation was included (500 ms application period) before application of a single chemical shift fat suppression pulse to increase contrast between the blood pool and myocardium and surrounding fat. The MTC irradiation consisted of a train of 25 radiofrequency pulses of 7.680 ms duration, Gaussian profile, 250 Hz bandwidth, 1.5 kHz offset frequency, and 4 mT amplitude applied with an interpulse spacing of 20 ms. The flip angle varied from 20° to 90°. The matrix size was 128×256 with a rectangular field of view of 240×320 mm, resulting in an inplane resolution of 1.9×1.25 mm.

Retrospective respiratory gating was performed by a navigator echo created with two excitation bands placed to intersect at the dome of the right hemidiaphragm. Each line of data was acquired five times to ensure complete sampling of the respiratory excursion. The acquisition MRCA sequence was completed in 8-15 minutes, depending on the heart rate.

Image analysis

For each subject, blood signal measurements were performed on pre- and post-contrast images in the transverse plane on the aortic root, left ventricle, right ventricle and septal myocardium. To measure the standard deviation of noise, a ROI was placed outside the body. Using the fact that the SD of the noise is the mean intensity of the background Rayleigh noise divided by 1.25, the blood signal-to-noise ration (SNR) and the contrast-to-noise (CNR) between blood and myocardium were calculated as follows[16]

$$SNR = 1.25 \frac{\text{Blood signal intensity}}{\text{mean intensity of background}}$$

$$CNR = 1.25 \frac{\text{Signal difference between blood and myocardium}}{\text{mean intensity of background}}$$

Statistical analysis

All values are expressed as mean ± standard deviation. The paired, two-tailed Student t-test was used to determine significance of the difference between two paired measurements, an unpaired Student t-test was used for unpaired measurements.

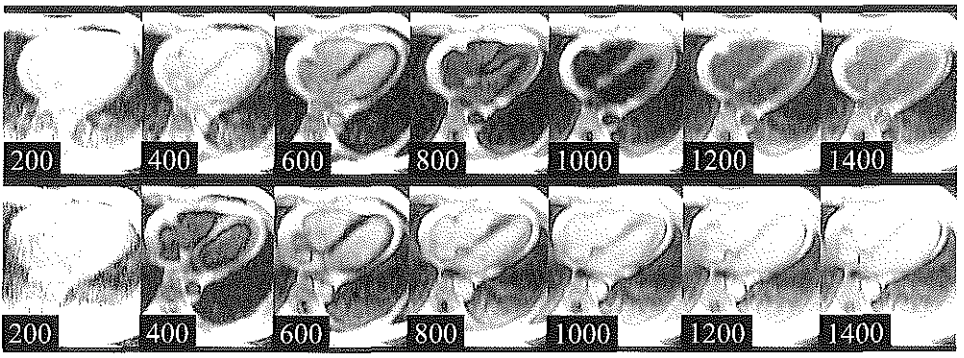

Figure 1. *Pre and post AMI-25 administration on signal intensity changes in IR-TF for different TI values. Before infusion the signal from blood is minimal at a TI of 1078 ms (upper row), while after infusion the TI for the minimal signal intensity is observed at 480 ms (lower row).*

RESULTS

The T_1 relaxation time of blood was significantly decreased from 1562 ± 130 ms to 642 ± 244 ms ($p < 0.01$). The T_1 relaxation time of myocardium did not change significantly (T_1 pre: 1058 ± 30 ms, T_1 post: 1001 ± 138 ms, $p = 0.48$). See figure 1.

The mean acquisition time for the MRCA sequence was 12 minutes and 20 seconds. The heart rate varied between 44 and 66 beats per minute. The signal intensity in the aorta showed a significant relation with the duration of the heartcycle ($r = 0.71$) with a higher signal intensity at longer RR-intervals. Due to saturation effects there was a clear reduction in signal intensity in the aorta before contrast administration compared to the LV and RA (figure 2). Post-contrast the signal intensity was equal in all heart chambers. Additionally AMI-25 drastically improved the contrast between the blood and the myocardium improving the visualization of the coronary arteries (figure 3). These benefits are again shown in a third example using three-dimensional postprocessing software (figure 4). Improvement in signal intensity was equally present in patients with a longer and shorter RR-intervals, with better CNR values on the patients with shorter RR-intervals. Figure 5 illustrates a sagittal acquisition covering the entire heart and the aorta proving the constant enhancement possible in all blood compartments after the administration of AMI-25.

With quantitative analysis AMI-25 improved the SNR in the aortic root by 90.3% ($p < 0.05$). Suffering less from saturation effects, the SNR in the right atrium only improved by 44.1% ($p > 0.05$) making it comparable to the aortic root (figure 6). The blood/myocardium CNR of the aortic root improved by 60.8%.

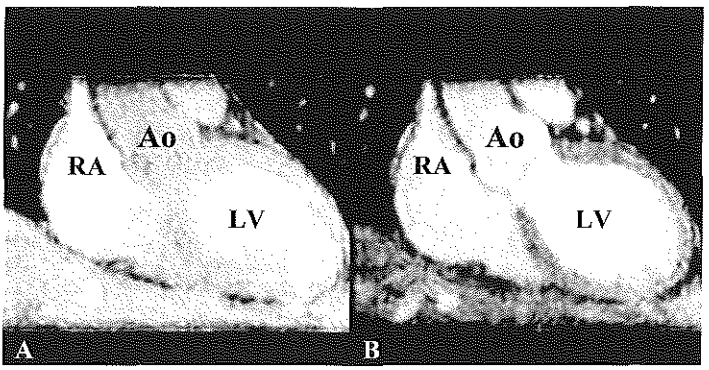

Figure 2. *Oblique coronal images through the aorta (Ao), right atrium (RA) and left ventricle (LV). **(A)** Before contrast agent administration there is a significant loss of signal intensity due to saturation effects in the aorta. **(B)** After contrast agent administration the signal intensities in the Ao, RA and LV have improved and are all equal.*

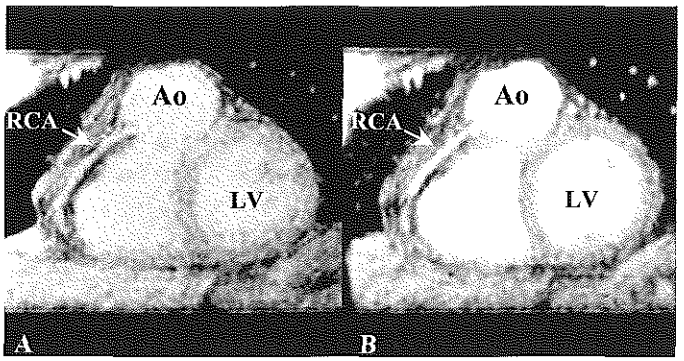

Figure 3. *Visualization of the right coronary artery before and after administration of AMI-25.* ***(A)*** *Before the contrast agent administration there is only a limited contrast between the blood and the myocardium.* ***(B)*** *After administration of the contrast medium the contrast improves and the right coronary artery (RCA) can be visualized more clearly. Ao = Aorta, LV = Left ventricle, RA = Righ atrium.*

DISCUSSION

Recently, gadolinium-based contrast enhanced MRA has dramatically improved the depiction of the great and peripheral arteries.[17-21] However, this is not the case for MRCA yet. MRA studies outside the heart do not require cardiac triggered scans and saturation effects can be dramatically reduced with the presence of a strong T_1 shortening contrast agent.[17,18] Nonetheless, standard, ECG triggered non-contrast enhanced MRCA sequences benefit from blood inflow effects between successive heartbeats making the signal amplitude of blood less dependent on the T_1 relaxivity of blood. Improvements have been envisioned only if the T_1 of blood is reduced to values less then 50ms (or shorter T_1s with the faster TRs possible in new MR gradient systems)[22] Presently several new intravascular contrast agents (e.g AMI-227, Combidex; MS-325, AngioMark; Gadomer-17 and NC 100150, Clariscan) have been developed which all have a T_1 between 50 and 100ms in clinical doses.[23-26] These agents have shown to improve coronary artery SNR and CNR.[27] In this study we demonstrated that a presently available contrast agent nearly halving the T_1 relaxation of blood for a long period of time, was able to increase SNR and CNR for MRCA. The T_1 shortening effect of AMI-25 was insufficient to make use of an inver-

Figure 4. *Example of improvement in three-dimensional postprocessing of MRCA datasets due to increase in signal intensity by the administration of AMI-25.* ***(A)*** *Pre-contrast image.* ***(B)*** *Post-contrast image. Ao = Aorta, LAD = Left anterior descending coronary artery, RCA = Right coronary artery, GCV = Great cardiac vein.*

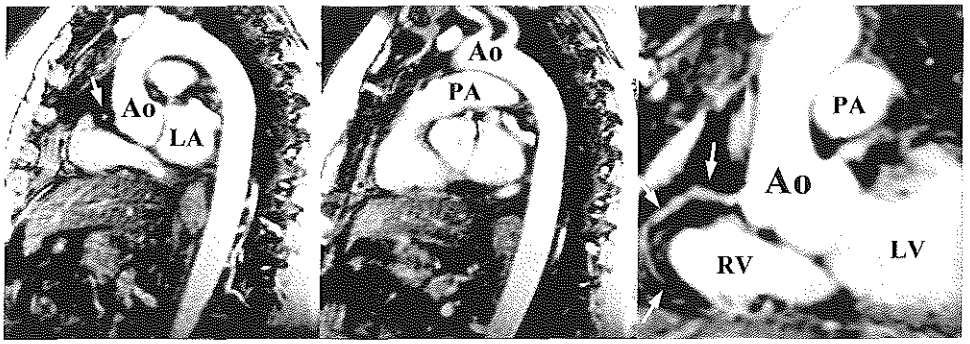

Figure 5. Sagittal acquisition covering the entire heart and thoracic aorta. In this ECG-triggered sequence the origin of the right coronary artery (straight arrow, left image) and the left main (curved arrow, middle image) can be depicted clearly. The aorta (Ao) and pulmonary artery (PA) do not suffer from saturation effects due to the presence of the contrast agent. Using small volume 3D post-processing the right coronary artery can be visualized over a longer distance (straight arrows in right image)

sion recovery prepulse prior to data collection to minimize the myocardial signal, similarly as used for other studies using extravascular (dynamic acquisition during injection) and intravascular (steady state imaging) contrast agents. We chose a MTC preparation to increase CNR between blood in the coronaries and myocardium, providing an improved delineation and assessment of the coronary arteries. MTC is known to have a small effect in the signal attenuation of blood but has a larger effect on myocardial muscle, as hown by Wolff, Balaban and Li.[28,29]

In this study, AMI-25 has been proven to remain mostly in the blood pool, direct reflection that T_1 (and SNR) of myocardium did not change significantly after the contrast agent administration. We have not observed any adverse effect either, making AMI-25 a relatively safe drug if drip-infused in glucose or saline at a dose of 10-15 umol Fe/kg body weight over 30 min with a flow rate of approximately 3 ml/min.[30-35]

Limitations

Some limitations of this study should be considered. First, dosage was not regulated completely, as it was administered independent of patient's weight. Secondly, the T_1 measurements were performed right after the infusion of AMI-25 and not repeated at the end

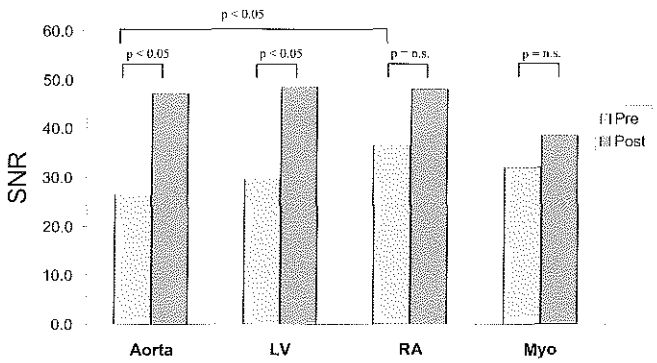

Figure 6. Improvement in signal-to-noise ratio (SNR) by the use of AMI-25. Pre-contrast the SNR in the aorta is significantly less compared to the right atrium (RA). Post-contrast the SNR in the Aorta and left ventricle (LV) improves significantly and is equal for all the heart chambers. The SNR of the myocardium (Myo) is unchanged by the use of the contrast agent.

of the volume scan to show differences in blood concentration or a stable T_1 relaxivity. Third, the heart rate pre- and post-contrast administration can change the amount of enhancement observed.

CONCLUSION

AMI-25 is presently clinically available contrast agent that partially behaves as an intravascular agent. It improves SNR and CNR in three-dimensional magnetic resonance coronary angiography.

REFERENCES

1. Li D, Kaushikkar S, Haacke EM, et al. Coronary arteries: three-dimensional MR imaging with retrospective respiratory gating. Radiology 1996;201(3):857-63.
2. Manning WJ, Li W, Boyle NG, Edelman RR. Fat-suppressed breath-hold magnetic resonance coronary angiography. Circulation 1993;87(1):94-104.
3. Pennell DJ, Bogren HG, Keegan J, Firmin DN, Underwood SR. Assessment of coronary artery stenosis by magnetic resonance imaging. Heart 1996;75(2):127-33.
4. Ducrinckx AJ, Urman MK. Two-dimensional coronary MR angiography: analysis of initial clinical results. Radiology 1994;193(3):731-8.
5. Hofman MB, Paschal CB, Li D, Haacke EM, van Rossum AC, Sprenger M. MRI of coronary arteries: 2D breath-hold vs 3D respiratory-gated acquisition. J Comput Assist Tomogr 1995;19(1):56-62.
6. Weissleder R, Stark DD, Engelstad BL, et al. Superparamagnetic iron oxide: pharmacokinetics and toxicity. AJR Am J Roentgenol 1989;152(1):167-73.
7. Oudkerk M, van den Heuvel AG, Wielopolski PA, Schmitz PI, Borel Rinkes IH, Wiggers T. Hepatic lesions: detection with ferumoxide-enhanced T_1-weighted MR imaging. Radiology 1997;203(2):449-56.
8. Clement O, Siauve N, Cuenod CA, Frija G. Liver imaging with ferumoxides (Feridex): fundamentals, controversies, and practical aspects. Top Magn Reson Imaging 1998;9(3):167-82.
9. Hahn PF, Saini S. Liver-specific MR imaging contrast agents. Radiol Clin North Am 1998;36(2):287-97.
10. Lencioni R, Donati F, Cioni D, Paolicchi A, Cicorelli A, Bartolozzi C. Detection of colorectal liver metastases: prospective comparison of unenhanced and ferumoxides-enhanced magnetic resonance imaging at 1.5 T, dual-phase spiral CT, and spiral CT during arterial portography. Magma 1998;7(2):76-87.
11. Ward J, Naik KS, Guthrie JA, Wilson D, Robinson PJ. Hepatic lesion detection: comparison of MR imaging after the administration of superparamagnetic iron oxide with dual-phase CT by using alternative-free response receiver operating characteristic analysis. Radiology 1999;210(2):459-66.
12. Hamm B, Staks T, Taupitz M, et al. Contrast-enhanced MR imaging of liver and spleen: first experience in humans with a new superparamagnetic iron oxide. J Magn Reson Imaging 1994;4(5):659-68.
13. Knollmann FD, Bock JC, Rautenberg K, Beier J, Ebert W, Felix R. Differences in predominant enhancement mechanisms of superparamagnetic iron oxide and ultrasmall superparamagnetic iron oxide for contrast-enhanced portal magnetic resonance angiography. Preliminary results of an animal study original investigation. Invest Radiol 1998;33(9):637-43.
14. Jung CW, Jacobs P. Physical and chemical properties of superparamagnetic iron oxide MR contrast agents: ferumoxides, ferumoxtran, ferumoxsil. Magn Reson Imaging 1995;13(5):661-74.
15. Stark DD, Bradley WG. Magnetic Resonance Imaging. St. Louis: Mosby-Year Book, 1992. vol 1).
16. Henkelman RM. Measurement of signal intensities in the presence of noise in MR images. Med Phys 1985;12(2):232-3.
17. Prince MR, Narasimham DL, Stanley JC, et al. Breath-hold gadolinium-enhanced MR angiography of the abdominal aorta and its major branches. Radiology 1995;197(3):785-92.
18. Prince MR, Narasimham DL, Jacoby WT, et al. Three-dimensional gadolinium-enhanced

MR angiography of the thoracic aorta. AJR Am J Roentgenol 1996;166(6):1387-97.
19. Leung DA, McKinnon GC, Davis CP, Pfammatter T, Krestin GP, Debatin JF. Breath-hold, contrast-enhanced, three-dimensional MR angiography. Radiology 1996;200(2):569-71.
20. Rofsky NM. MR angiography of the aortoiliac and femoropopliteal vessels. Magn Reson Imaging Clin N Am 1998;6(2):371-84.
21. Krinsky GA, Rofsky NM, DeCorato DR, et al. Thoracic aorta: comparison of gadolinium-enhanced three-dimensional MR angiography with conventional MR imaging. Radiology 1997;202(1):183-93.
22. Johansson LO, Fischer SE, Lorenz CH. Benefit of T_1 reduction for magnetic resonance coronary angiography: a numerical simulation and phantom study. J Magn Reson Imaging 1999;9(4):552-6.
23. Anzai Y, Prince MR, Chenevert TL, et al. MR angiography with an ultrasmall superparamagnetic iron oxide blood pool agent. J Magn Reson Imaging 1997;7(1):209-14.
24. Lauffer RB, Parmelee DJ, Dunham SU, et al. MS-325: albumin-targeted contrast agent for MR angiography. Radiology 1998;207(2):529-38.
25. Dong Q, Hurst DR, Weinmann HJ, Chenevert TL, Londy FJ, Prince MR. Magnetic resonance angiography with gadomer-17. An animal study original investigation. Invest Radiol 1998;33(9):699-708.
26. Wagenseil JE, Johansson LOM, Lorenz CH. Characterization of T_1 Relaxation and Blood-Myocardial Contrast Enhancement of NC100150 Injection in Cardiac MRI. Proceedings of the Seventh Meeting of the International Society for Magnetic Resonance in Medicine. Philadelphia, 1999:1176.
27. Stillman AE, Wilke N, Li D, Haacke M, McLachlan S. Ultrasmall superparamagnetic iron oxide to enhance MRA of the renal and coronary arteries: studies in human patients. J Comput Assist Tomogr 1996;20(1):51-5.
28. Li D, Paschal CB, Haacke EM, Adler LP. Coronary arteries: three-dimensional MR imaging with fat saturation and magnetization transfer contrast. Radiology 1993;187(2):401-6.
29. Wolff SD, Balaban RS. Magnetization transfer imaging: practical aspects and clinical applications. Radiology 1994;192(3):593-9.
30. Reimer P, Tombach B. Hepatic MRI with SPIO: detection and characterization of focal liver lesions. Eur Radiol 1998;8(7):1198-204.
31. Bellin MF, Zaim S, Auberton E, et al. Liver metastases: safety and efficacy of detection with superparamagnetic iron oxide in MR imaging [see comments]. Radiology 1994;193(3):657-63.
32. Ros PR, Freeny PC, Harms SE, et al. Hepatic MR imaging with ferumoxides: a multicenter clinical trial of the safety and efficacy in the detection of focal hepatic lesions. Radiology 1995;196(2):481-8.
33. Duda SH, Laniado M, Kopp AF, et al. Superparamagnetic iron oxide: detection of focal liver lesions at high- field-strength MR imaging. J Magn Reson Imaging 1994;4(3):309-14.
34. Winter TCd, Freeny PC, Nghiem HV, et al. MR imaging with i.v. superparamagnetic iron oxide: efficacy in the detection of focal hepatic lesions. AJR Am J Roentgenol 1993;161(6):1191-8.
35. Li D, Dolan RP, Walovitch RC, Lauffer RB. Three-dimensional MRI of coronary arteries using an intravascular contrast agent. Magn Reson Med 1998;39(6):1014-8.

Part 2

Electron Beam Computed Tomography

Chapter 13

Intravenous Coronary Angiography using Electron Beam Computed Tomography

B.J. Rensing, A.H.H. Bongaerts, R.J.M. van Geuns,

P.M.A. van Ooijen, M. Oudkerk, P.J. de Feyter.

Published in Progress in Cardiovascular Disease 1999;42(2):149-156

ABSTRACT

Intravenous coronary angiography with electron beam computed tomography (EBCT) allows for the noninvasive visualization of coronary arteries. With dedicated computer hardware and software, three-dimensional renderings of the coronary arteries, veins and other cardiac structures can be constructed from the individual transaxial tomograms. Interest in this technique is growing, and recently a number of clinical studies have been published comparing EBCT coronary angiography with conventional cine-coronary angiography. In this article, image acquisition, postprocessing techniques, and the results of recently published clinical studies are discussed. EBCT coronary angiography is a promising imaging technique of coronary arteries. Currently, it is a reasonably robust technique for the visualization and assessment of the left main and left anterior descending coronary artery. However, at the moment a relatively high proportion of the right and circumflex coronary angiograms is noninterpretable. Improvements in image acquisition and postprocessing techniques are expected to improve visualization and diagnostic accuracy of the technique.

INTRODUCTION

The small size and fast movement of human coronary arteries pose a formidable challenge for an imaging technique. For accurate visualisation, it has to combine a high spatial resolution with a high temporal resolution. Modern coronary cine-angiography with direct intracoronary contrast injection has a spatial resolution of 5 linepairs per mm and a temporal resolution of up to 50 frames/s. This allows the accurate visualization of the epicardial luminal coronary trajectory during the complete cardiac cycle and has become the undisputed reference technique for coronary imaging. These specifications come at a price, however: the procedure is costly, invasive, and carries a small risk of serious adverse events.

Recently, electron beam computed tomography (EBCT) after intravenous injection of contrast medium has emerged as an imaging technique of coronary arteries.[1-7] Using modern image processing technology, three-dimensional (3D) reconstruction of the heart and coronary arteries can be made from 40 to 60 consecutive tomograms. The individual tomograms have a resolution of 4 to 6 linepairs/cm, and the scan time for each tomogram is 100 ms. Although this falls short of the spatial and temporal resolution of conventional coronary angiography, proximal and middle parts of the coronary arteries can be visualized with this technique.

In this article image, image acquisition, image processing techniques, and clinical studies that compared EBCT coronary angiography to conventional coronary angiography will be reviewed.

METHODOLOGY

EBCT Coronary angiography

The EBCT scanner, also called ultrafast-CT or cine-CT (Siemens Evolution, Munich, Germany), is a CT scanner that allows the acquisition of high-resolution electrocardiogram (ECG)-triggered tomograms in 100ms. This is fast enough to reduce cardiac motion artefacts and to reliably visualize the fast-moving coronary arteries, especially when the acquisition window is set during diastasis. The scanner was originally designed for cardiac function studies and was later applied to quantify coronary calcifications. A detailed description of scanner specifications can be found elsewhere.[8] Scanning is performed with the patient in the supine position. To ensure optimal coronary opacification during image acquisition, the circulation time has to be determined. Therefore, 10 ml of contrast medium (iopromide 350 mg/ml) is injected through an antecubital vein at 4 ml/s. The passage of the contrast bolus through the ascending aorta is visualized by tomograms at the aortic root level. The time from contrast injection to

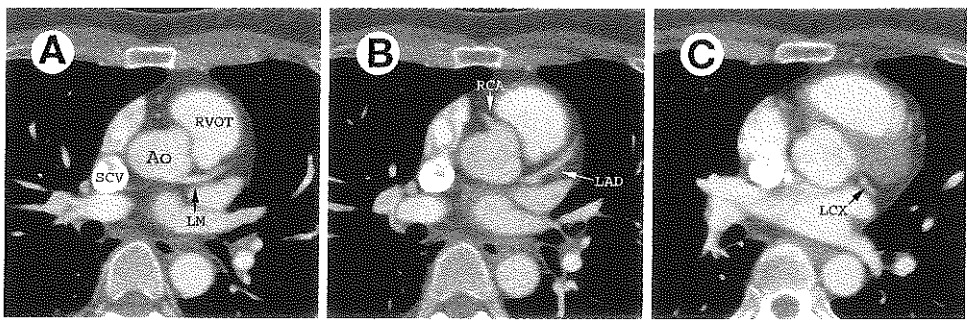

Figure 1. *Transaxial tomograms at different levels.* ***(A)*** *At the level of the ostium of the left main coronary artery.* ***(B)*** *At the level of the ostium of the right coronary artery (RCA, arrowhead) LAD, proximal left anterior descending coronary artery.* ***(C)*** *Proximal circumflex coronary artery (arrow) Ao, ascending aorta; RVOT, right ventricular outflow tract; SCV, superior caval vein.*

peak aorta density is considered the circulation time.

Next several localising scans over the aortic root are made at inspiration to determine the exact level of the left main coronary artery.

Acquisition of the 3D dataset starts with the injection 120 to 180 ml of contrast medium at 3 to 4 ml/s through an antecubital vein. During the circulation time, patients are asked to mildly hyperventilate by breathing in and out at the word of the CT technician. Just before the circulation time, the patient is asked to hold his/her breath at a comfortable inspiratory level. At the circulation time, scanning commences just proximal to the left main coronary artery after an ECG trigger at 80% of the RR interval (diastasis). Tomogram thickness is set at 1.5 or 3 mm. Table increment after each tomogram is set at 1.5 mm or 2 mm, resulting in contiguous nonoverlapping slices or slices with 1 mm overlap. A total of 40 to 60 transaxial tomograms are made during a single breathhold (Figure 1). Breath holding is necessary during data acquisition to avoid respiratory motion artefacts. Field of view size is generally set at 18 cm with a matrix size of 512 × 512 pixels, yielding a pixel size of 0.35 × 0.35 mm. To speed up image acquisition and to shorten breath-hold time, atropine 0.5 to 1 mg intravenously can be administered when heart rate is less than 60 min-1. Breath-holding time in the cited studies was between 20 and 50 seconds and is dependent on the heart rate and the number of tomograms made. Effective radiation dose is estimated to be less than 10 mSv.[9,10] This is approximately one third to one fifth of the radiation dose at diagnostic coronary angiography.[9,11]

Image Processing

For accurate assessment of the anatomy and integrity of the epicardial coronary arteries, merely evaluating the axial tomograms is inadequate. The 3D trajectory of the coronary arteries spans almost the complete set of 40 to 60 tomograms, and therefore some form of 3D reconstruction of the tomographic data is necessary to keep track of the exact course of the arteries and to accurate-

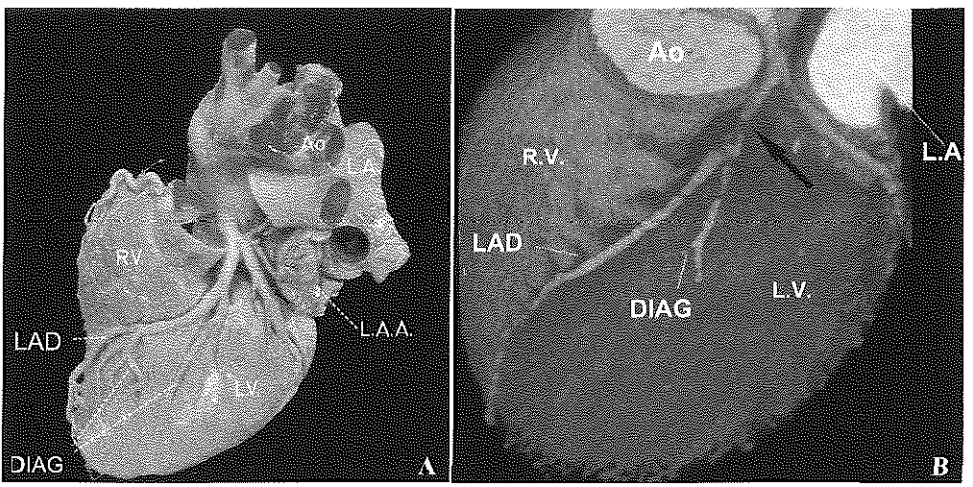

Figure 2. (A) *Pressure fixed anatomical specimen showing the left coronary artery. Reprinted with permission from McAlpine WA: Heart and Coronary Arteries. Heidelberg, Germany, Springer-Verlag, 1975 p 159, fig 1. Copyright by Springer-Verlag.* ***(B)*** *3D rendering of the left coronary artery of a patient with a severe stenosis (arrow) of the bifurcation of the proximal left anterior descending artery and diagonal artery (LAD and Diag). Ao, Aorta; LAA, left atrial appendage; LA, left atrium; RV, right ventricle; LV, left ventricle.*

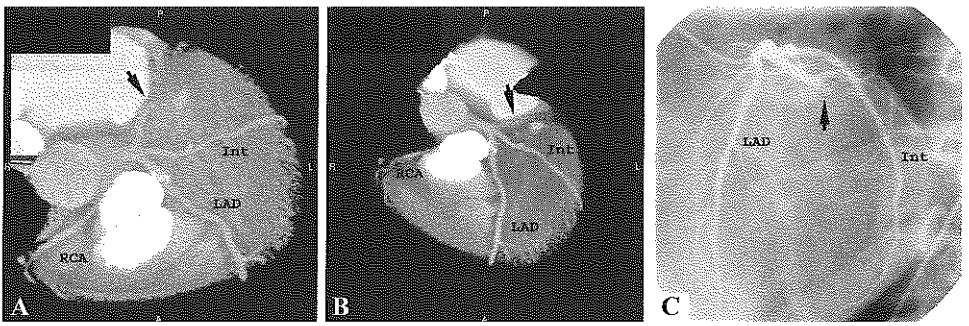

Figure 3. *Volume rendering showing an occluded circumflex artery (arrows).* ***(A)*** *View from the top.* ***(B)*** *View from a more anterior angle.* ***(C)*** *Corresponding coronary angiogram. LAD, left anterior descending artery; Int, intermediate branch.*

ly read the EBCT angiogram. Furthermore, respiration and rhythm artefacts are readily apparent with most 3D reconstruction methods. Indeed, all published studies used 3D reconstruction methods to assess the EBCT coronary angiograms. 3D reconstruction starts with transferring the two-dimensional (2D) transaxial tomograms to a computer workstation where they are stacked and interpolated to form a 3D volume using special computer software. This process creates a database representation of a 3D object. This database consists of millions of volume elements (voxels), each with its own Hounsfield unit or density value. With special rendering techniques, this database representation of the 3D object can be projected onto a viewing surface. This creates the illusion of looking at a 3D object.

Rendering Techniques

Volume rendering.

Volume rendering is a rendering technique that retains all the voxels from the original 3D dataset during each rendering. This process is computationally intensive but has the advantage that no information is discarded during the process and that several image-processing techniques are still possible.[12] For instance, each voxel can be assigned an opacity and colorvalue. Based on these values, the intensity of each voxel is calculated and used for the display of the voxel. Volume rendering allows certain parts of the 3D object to be transparent so that structures behind it are still visible. It can, by assigning the right color and opacity values to different tissues, simulate real anatomy in much the same way as pictures in an anatomic atlas (Figures 2 and 3).[13]

The development of dedicated computer hardware and software now allows volume rendering to be performed on a desktop computer workstation, whereas only a few years ago the technique was reserved for large mainframe computers. Computation time for a single rendering is now a matter of seconds, which is fast enough to allow rapid and comfortable user interaction. It is expected that volume rendering on a personal computer platform will be possible in the near future.

Image processing techniques such as segmentation and filtering have to be applied to better visualize the coronary arteries among the other contrast-enhanced and sometimes overlapping cardiac structures.[14] For instance, the thorax wall, lung vessels, and cardiac structures such as the left and right auricle have to be removed from the dataset (Figure 4) to be able to see the coronary arteries. This segmentation has to be done on the individual tomographic level. Although some automation is possible, a large part still has to be done manually. On average, an experienced technician can perform this seg-

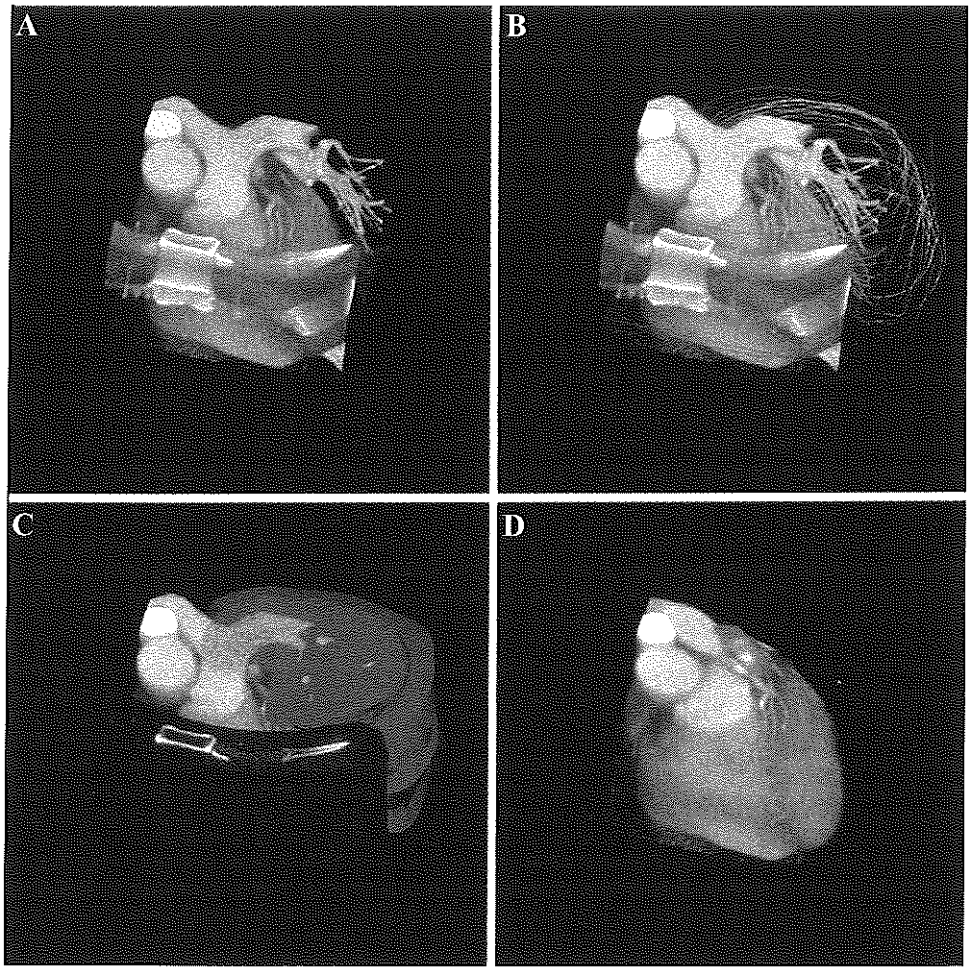

Figure 4. *Visualization of contour segmentation of the heart within the thorax.* ***(A)*** *Volume rendering of the heart and part of the chest wall and pulmonary vessels.* ***(B)*** *The circles depict the contour lines drawn on the individual axial tomograms.* ***(C)*** *The computer can be ordered to delete all image data that is outside the contours, here depicted by the grey volumes.* ***(D)*** *Final result after segmentation. The coronary arteries can now be seen without interference of the chestwall, pulmonary arteries and veins, and cardiac venous structures.*

mentation in 15 to 20 minutes. Dedicated segmentation software is under development and is expected to substantially shorten total image-processing time.

Surface rendering.

This is a rendering technique that displays only a fraction of the 3D data (Figure 5). In a first step, threshold values are set so only voxels within a prespecified density interval are retained. After this selection process a simplified approximation of the surface of the selected object is calculated by assigning polygons (eg, triangles) to this surface. As in volume rendering, segmentation steps to remove objects that obscure the outlook on the coronary arteries are also necessary with surface rendering. An advantage of the technique is that after the initial computational intensive rendering steps, further interactive viewing of the mathematically defined surface is very fast. Disadvantages

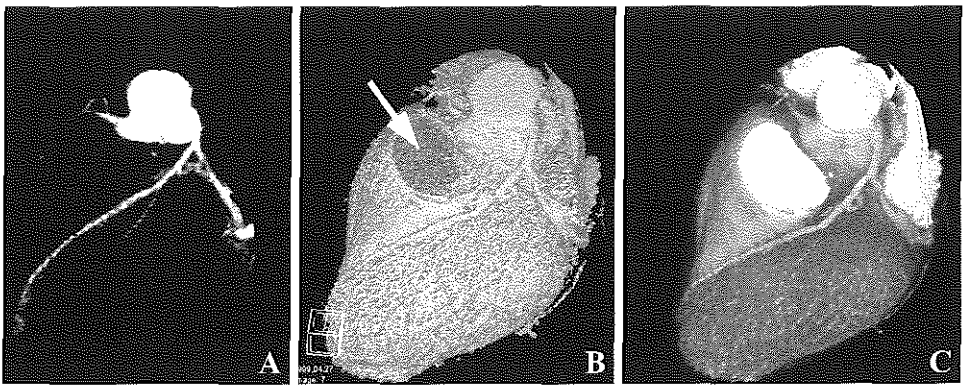

Figure 5. ***(A)*** *Maximum intensity projection of the left coronary artery. Before the coronary arteries can be visualized with this technique, denser structures in the path of the imaginary rays (see text for explanation) have to be removed first. After extensive segmentation only the aortic root and the coronary arteries are retained in the volume. The left main coronary artery cannot be discerned in this projection because of overlap with the much denser aortic root. The dotted appearance of the LAD is due to partial volume effects.* ***(B)*** *Surface rendering showing the LAD. The pulmonary artery and right ventricular outflow tract have been segmented out on the individual tomograms. On the surface rendering at this area, a hole in the surface can be seen (arrow).* ***(C)*** *Same dataset now visualized with volume rendering.*

are the loss of surface details by the polygon approximation, the inability to display internal structures, and the time-consuming optimization of the threshold settings.

Multiplanar reformatting (MPR).

For this rendering technique, coronal, saggital, transversal, or double oblique sections are made through the 3D volume to target the course of the coronary artery. A set of tomograms parallel to the double oblique slice can then be reconstructed to completely visualize and appreciate the often tortuous trajectory of the coronary arteries. A related technique is curved multiplanar reformatting. Here the operator indicates the artery on each of the original axial tomograms or on the reconstructed double oblique slices (Figure 6). The computer connects the artery segments on every tomogram or slice and projects the reconstructed course onto a 2D surface. Both techniques are simple and fast and do not need manual segmentation of structures that obscure the outlook on the coronary arteries. On the other hand, MPR is operator-dependent and requires a thorough understanding of coronary anatomy.

Maximum intensity projection (MIP).

MIP is a rendering technique in which imaginary rays are cast through the 3D dataset from any viewpoint the image-analyst chooses (Figure 5). The highest intensity voxel encountered by each ray is used to construct a 2D image of the 3D dataset. Usually these are voxels within the contrast-filled vessels. Images resemble classic angiograms. This rendering technique is fast and generally gives a good differentiation between vascular and nonvascular structures. For coronary angiography, however, this technique is not very well suited because denser noncoronary structures, such as contrast filled cavities (left ventricle, right ventricle, atria) and bony structures, have to be removed first from the dataset to ensure visualization of the coronary arteries. Furthermore, the technique is sensitive to partial volume effects and uses only 10% of the available imaging data.

EBCT ANGIOGRAPHY OF NATIVE CORONARY ARTERIES

Several studies have recently been published comparing intravenous EBCT coronary

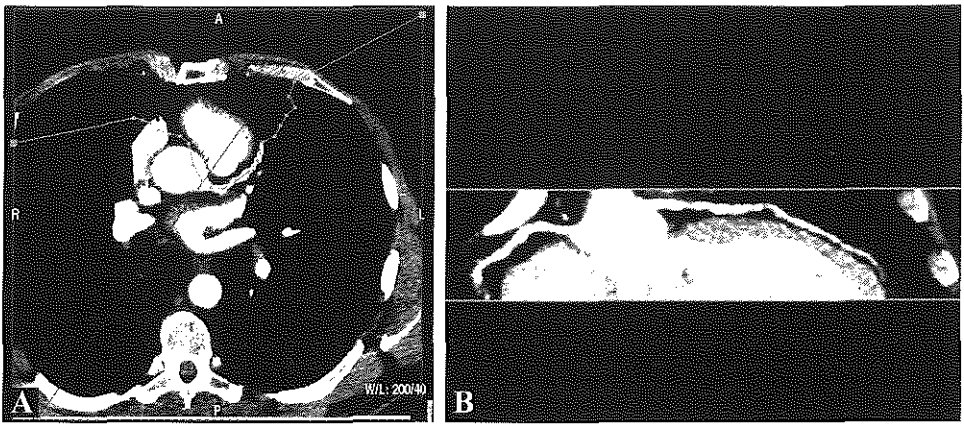

Figure 6. *Curved multiplanar reformation.* ***(A)*** *Single proximal transaxial tomogram, showing the left main coronary artery and the proximal LAD. The dotted line is the projection on this tomogram of the line connecting the right coronary artery, the aorta and the left anterior descending coronary artery through different tomographic levels.* ***(B)*** *Actual curved multiplanar reformation. The 3D course of the vessels is projected onto a 2D plane.*

angiography to conventional angiography[2-7] (Table 1). The image acquisition protocols for all these studies were basically the same as described in the methodology section. Differences were the amount of tomograms made (40 or 60) and the tomogram thickness/table increment used (either 1.5 mm thickness, 1.5 mm table increment or 3 mm thickness with 2 mm table increment) Three-dimensional image rendering techniques also differed among the studies (Table 1). All used both the original axial tomographic data and the reconstructed 3D data to assess the EBCT coronary angiograms.

Visualisation

Overall, the technique allowed interpretable visualization of the proximal and mid coronary arteries in approximately 80 to 90% of cases (Table 1). Clearly, the right coronary artery (RCA) and left circumflex coronary artery (LCX) were less often assessable than the left anterior descending (LAD). Most often this was caused by cardiac motion artifacts. The RCA and LCX are vulnerable to motion artefacts because a large part of their course is in the atrioventricular groove in close vicinity to the atria. Atrial contraction during the 100-ms image acquisition window can cause these motion artefacts. Other reported causes of nonassessability are small size of the arteries, partial overlap with other contrast-filled structures such as the coronary sinus and the atrial appendages, and poor opacification of the smaller, distal coronary arteries at the end of the contrast injection. Also, heavy, circular calcification of the coronary artery wall can obscure the coronary lumen and render the coronary segment noninterpretable. If not recognised, circular calcification can be a cause of false negative[2-4] or false positive[6] results. Achenbach[4] reported respiratory motion artefacts to be the main cause of nonassessability in his patient population. This was, however not found to be a major factor in the other studies.

Diagnostic Accuracy

Diagnostic accuracy for the detection of significant coronary artery disease was best for the left main coronary artery. Not all studies included patients with left main stenoses, but false positive test results were very rare (Table 1). Reported specificities ranged

from 96 to 100%. The 3 left main stenoses that were reported[3,5] were all correctly diagnosed by EBCT angiography (sensitivity 100%).

Diagnostic accuracy for the detection of significant stenoses in the proximal and middle LAD was uniformly found to be good. Sensitivity values ranged from 82 to 98% and specificity values ranged from 63% [6] to 98%. The high amount of false-positive test results in the LAD reported in the study by Reddy et al, was due to misinterpretation of areas with heavy calcification. They used maximum intensity projections for interpretation, and it is known that partial volume effects on MIP renderings can give the impression of a stenosis in heavily calcified parts of the coronary arteries.[6] Furthermore, it is known from EBCT calcification studies that heavily calcified sites do not necessarily coincide with a significant stenosis.[15,16] In general, diagnostic accuracy was a poorer for the RCA and LCX as compared to the LAD. The lower specificity can be attributed to the smaller size of these vessels, especially the LCX.[2-4] Further, poor contrast opacification and partial volume effects can give the impression of a stenosis in these smaller arteries and lead to a false-positive result. The lower sensitivity can be explained by the fact that a large part of the course of the RCA and LCX is perpendicular to the imaging plane.[4] Resolution in the scanning direction is lower than the in tomographic plane (tomograms are 1.5-mm thick), and these vessels are thus for a large part visualized with a lower spatial resolution. Short stenoses can thus be missed, resulting in a higher false-negative rate.

The reported numbers of false-positive tests were low, which means a high specificity and high negative predictive value. This potentially makes EBCT coronary angiography a very useful test to rule out significant coronary artery disease and thus to avoid conventional coronary angiography in a large group of patients. It is important to realize, however, that diagnostic accuracy calculations can only be based on the coronary segments that were assessable in the first place. The fact that on average only 70 to 75% of EBCT angiograms were of sufficient quality to allow assessment of the right and circumflex coronary artery makes this technique at the moment unsuited as an alternative for conventional coronary angiography.

EBCT ANGIOGRAPHY TO ASSES BYPASS GRAFT PATENCY

In the 1980s several EBCT studies have been conducted to assess coronary venous and arterial bypass graft patency [17-19] (Table 2). Three-dimensional rendering techniques were not available at that time and therefore only patency of the grafts could be deter-

Table 1. Diagnostic accuracy for detection of greater than 50% diameter stenosis by EBCT angiography in several published studies

	Patients	Rendering Technique	Arteries Interpretable	Sens/ Spec(%)	LM Int/Sens/ Spec(%)	LAD Int/Sens/ Spec(%)	LCX Int/Sens/ Spec(%)	RCA Int/Sens/ Spec(%)
Schmermund et al[2]	28	SR/MPR/MIP	88%	83/91	100/-/100	90/82/98	71/75/81	91/90/83
Rensing et al[3]	37	VR	81%	77/94	97/100/100	95/82/92	76/83/89	66/60/97
Achenbach et al[4]	125	SR	75%	92/94	84/-/99	80/98/88	66/78/88	70/93/96
Nakanishi et al[5]	37	MPR	NR	74/91	NR/100/100	NR/83/84	NR/67/96	NR/63/79
Reddy et al[6]	23	MIP	90%	88/79	100/-/96	100/93/63	95/100/67	74/67/77
Budoff et al[7]	52	MIP/SR	90%	78/91	100/-/100	92/82/90	85/67/86	79/83/79

Abbreviations: Int, Interpretable, good enough visualization to allow classification; LM, left main coronary artery; Sens, sensitivity; Spec, specificity; NR, not reported.

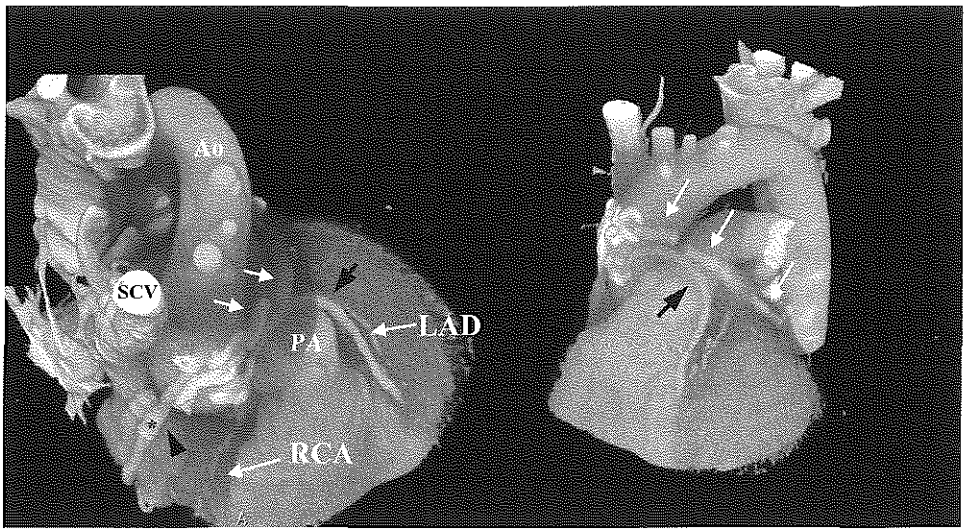

Figure 7. *Example of 3D rendering of venous bypass grafts. Shown are volume renderings from different angles. This patient has a single venous bypass graft to the LAD (black arrow), a single venous graft to the right coronary artery (arrowhead), and a single graft to the circumflex coronary artery (small white arrows). In the graft to the RCA the contours of a stent can be appreciated (asterisk). The graft to the circumflex area is totally occluded at the anastomosis with the aorta. Three stents had been implanted earlier and can still be appreciated on the 3D renderings. No contrast material is present between the stents, proving that the graft is totally occluded. Ao, ascending aorta; LAD, native left anterior descending artery; Pa, pulmonary artery; RCA, native right coronary artery; SCV, superior caval vein.*

mined by assessment of the individual transaxial tomograms. Only few arterial bypass grafts were included in these studies, but diagnostic accuracy appears to be equal for both type of conduits (Table 2). With the advent of 3D reconstruction techniques (Figure 7), a renewed interest in EBCT bypass graft visualization arose. Achenbach et al[20] and Jong-Won et al [21] used surface rendering to assess bypass graft patency (Table 2). Diagnostic accuracy was similar to that reported in the older studies using tomographic assessment. However, 3D rendering offers the possibility not only to assess patency but also to visualize haemodynamically significant stenoses in bypass grafts. This was studied by Achenbach et al. They were able to evaluate 84% of patent grafts. Sensitivity and specificity to detect a significant stenosis was 100% and 97%, respectively. The main reasons for noninterpretability were breathing artefacts and misplacement of the imaging volume, which caused part of the graft not to be visualised.

Table 2. Patency assessment of bypass grafts by EBCT

	No of venous grafts	No of arterial grafts	Analysis technique	Sens/Spec Venous graft	Sens/Spec Arterial grafts
Stanford[17]	116	11	Tomograms	94/88	88/100
Bateman[18]	39	-	Tomograms	95/86	-
Bateman[19]	68	12	Tomograms	95/97	100/100
Achenbach[20]	55	1	3D	100/100	NV
Jong-Won[21]	57	22	3D	92/91	80/82

Abbreviations: NV, not visualized; Sens, sensitivity; Spec, specificity.

Jong-Won et al found a lower diagnostic accuracy with 3D renderings for the assessment of arterial grafts as compared to venous grafts. They attribute that to the smaller size of these grafts and the fact that metal surgical clips are more abundantly used. These clips are known to cause beam hardening and stellate artefacts.

TECHNICAL IMPROVEMENTS

Technical improvements should primarily be directed towards reducing the amount of noninterpretable EBCT angiograms. Currently work is being conducted to reduce the tomogram acquisition time from 100 ms to 50 ms. In combination with better ECG triggering protocols, end-diastolic motion artefacts can probably be reduced. Recently a new detector array was introduced that is expected to improve the in-plane resolution with 30% to 10 linepairs/cm. It is expected that this will increase assessability and diagnostic accuracy in smaller vessels and improve discrimination between the coronary arteries and overlapping structures.

Breath-holding limitations and single tomogram acquisition per heartcycle limit the volume of the heart that can be visualized during 1 contrast injection. Therefore, the distal coronary arteries can not be visualized during a single contrast injection in all patients. This can be solved by a second contrast injection at the expense of an increased contrast volume. Furthermore, tomograms that are obtained during the later phase of the contrast injection suffer from a reduced contrast resolution between the contrast-enhanced myocardium and (small) coronary arteries.[7]

Ideally, the complete heart should be scanned within a few heartbeats. This would shorten breath-holding time, decrease the probability of artefacts caused by arrhythmias and reduce the total amount of contrast medium necessary for opacification. Therefore, to decrease image acquisition time, a tomographic imaging technique must be able to perform to multiple, simultaneous, parallel tomograms and thus become more of a volume scanner. Thomas et al. used the multislice mode of the EBCT scanner to obtain 8 tomograms (slice thickness 8 mm) of a thorax phantom within 224 msec.[22] The complete heart and coronary arteries could be visualized in 6 heartbeats. However, very extensive and time-consuming computations were necessary to correct for the noncoplanar orientation of the targetrings relative to the detector ring and to deconvolve the overlapping 8-mm slices into thinner slices. Although the image acquisition window is probably to long and the deconvolved slice thickness still to high to reliably depict coronary arteries in vivo, this report shows that multislice EBCT coronary angiography is possible and represents a promising alternative to single slice angiography.

A solution to the problem of circular calcification of the vessel wall (a major source of false negatives) might be visualising the coronary artery from the inside. A post processing technique called "fly through virtual angioscopy" tracks the contrast-enhanced lumen of the artery on the individual tomograms. After stacking and interpolation the computer constructs a movie that gives the illusion of travelling through the artery. Using this technique van Ooijen et al were able to distinguish stenosed and calcified areas.[23]

CONCLUSION

Intravenous EBCT coronary angiography in conjunction with 3D reconstruction and rendering techniques is a promising imaging modality that allows for noninvasive visualization of the proximal and middle parts of the coronary arteries. Currently it is a reasonably robust technique for the visualization and assessment of the left main and left anterior descending coronary artery. An important problem at the moment is the rel-

atively high proportion of noninterpretable angiograms of the right and circumflex coronary artery. Active work is being conducted to improve in image acquisition and post-processing techniques. This is expected to improve visualization and diagnostic accuracy of the technique.

REFERENCES

1. Moshage WE, Achenbach S, Seese B, Bachmann K, Kirchgeorg M. Coronary artery stenoses: Three dimensional imaging with electrocardiographically triggered, contrast enhanced, electron beam CT. Radiology 1995;196:707-14
2. Schmermund A, Rensing BJ, Sheedy PF, Bell MR, Rumberger JA. Intravenous electron beam CT coronary angiography for segmental analysis of significant coronary artery stenoses: Feasibility and limitations. J Am Coll Cardiol 1998;31:1547-54
3. Rensing BJ, Bongaerts A, van Geuns RJ, van Ooijen P, Oudkerk M, de Feyter PJ. Intravenous coronary angiography by electron beam computed tomography. A clinical evaluation. Circulation 1998;98:2509-12
4. Achenbach S, Moshage W, Ropers D, Nossen J, Daniel WG. Value of electron-beam computed tomography for the noninvasive detection of high-grade coronary-artery stenoses and occlusions. N Engl J Med 1998;339:1964-71.
5. Nakanishi T, Ito K, Imazu M, Yamakido M. Evaluation of coronary artery stenoses using electron-beam CT and multiplanar reformation. J Comput Assist Tomogr 1997;21:121-27
6. Reddy PR, Chernoff DM, Adams JR, Higgins CB. Coronary artery stenoses: Assessment with contrast enhanced electron beam CT and axial reconstructions. Radiology 1998;208:167-72
7. Budoff MJ, Oudiz RJ, Zalace CP et al. Intravenous three-dimensional coronary angiography using contrast enhanced electron beam computed tomography. Am J cardiol 1999;83:840-845
8. Gould RG. Principles of ultrafast computed tomography: historical aspects, mechanisms and scanner characteristics. In: Stanford W, Rumberger JA, eds. Ultrafast computed tomography in cardiac imaging: principles and practice. Mt Kisco, NY: Futura, 1993:1-16
9. Assessment of the effective dose for routine protocols in conventional CT, electron beam CT and coronary angiography. Rofo Fortschr Geb Rontgenstr Neuen Bildgeb Verfahr 199;170:99-104
10. Janowitz WR, Agatston AS, Viamonte M. Comparison of serial quantitative evaluation of calcified coronary artery plaque by ultrafast computed tomography in persons with and without obstructive coronary artery disease. Am J Cardiol 1991;68:1-6
11. Stehling MK, von Smekal A, Reise M. MRI der Koronararterieen Moglichkeiten und Grenzen. Radiologe 1994;34:462-468.
12. Ney D, Fishman E, Magid D. volumetric rendering of computed tomography data: principles and techniques. Comput Graphics Applications 1990;10:24-32
13. McAlpine WA. Heart and coronary arteries. Heidelberg: Springer Verlag, 1975
14. Van Ooyen PMA, de Feyter PJ, Oudkerk M. An introduction to three dimensional cardiac image rendering and processing. Cardiologie 1997;4:312-19
15. Simons DB, Schwartz RS, Edwards WD, Sheedy PF, Breen JF, Rumberger JA. Noninvasive definition of anatomic coronary artery disease by Ultrafast computed tomographic scanning: a quantitative pathologic comparison study. J Am Coll Cardiol 1992;20:1118-1126
16. Mautner SL, Mautner GC, Froehlich J et al. Coronary artery calcification: assessment with electron beam CT and histomorphometric correlation. Radiology 1994;192:619-623
17. Stanford W, Brundage BH, Macmillan R, et al. Sensitivity and specificity of assessing coronary bypass graft patency with ultrafast computed tomography. J Am Coll Cardiol 1988;12:1-7
18. Bateman TM, Gray RJ, Whiting JS et al. Cine computed tomographic evaluation of aortocoronary bypass graft patency. J Am Coll Cardiol 1986;8:693-698.
19. Bateman TM, Gray RJ, Whiting JS et al. Prospective evaluation of ultrafast cardiac

computed tomography for determination of coronary artery bypass graft patency. Circulation 1987;75:1018-1024

20. Achenbach S, Moshage W, Ropers D, Nossen j, Bachman K. Non-invasive, three-dimensional visualization of coronary bypass grafts by electron beam tomography. Am J Cardiol 1997;79:856-851
21. Jong-Won H, seung-Yun C, Won-Heum S et al. Noninvasive evaluation of coronary artery bypass graft patency using three dimensional angiography obtained with contrast enhanced electron beam CT. AJR 1999;172:1055-1059
22. Thomas PJ, McCollough CH, Ritman EL. An electron-beam CT approach for transvenous coronary angiography. J Comput Assist Tomogr 1995;19:383-389
23. Van Ooijen PMA, de Feijter PJ, Oudkerk M. Virtual coronary angioscopy using electron beam computed tomography (abstract). Eur Radiol 1999;(suppl 1)9:S38

Chapter 14

In Vivo Assessment of Three Dimensional Coronary Anatomy using Electron Beam Computed Tomography after Intravenous Contrast Administration

B.J. Rensing, A.H.H. Bongaerts, R.J. van Geuns, P.M.A. van Ooijen,

M. Oudkerk, P.J. de Feyter

Published in Heart 1999;82:523-525

ABSTRACT

Intravenous coronary angiography with electron beam computed tomography (EBCT) allows for the non-invasive visualization of coronary arteries. With dedicated computer hardware and software, three dimensional renderings of the coronary arteries can be constructed, starting from the individual transaxial tomograms. This article describes image acquisition, postprocessing techniques, and the results of clinical studies. EBCT coronary angiography is a promising coronary artery imaging technique. Currently it is a reasonably robust technique for the visualisation and assessment of the left main and left anterior descending coronary artery. The right and circumflex coronary arteries can be visualised less consistently. Improvements in image acquisition and postprocessing techniques are expected to improve visualisation and diagnostic accuracy of the technique.

INTRODUCTION

Recently intravenous coronary angiography using electron beam computed tomography (EBCT) has emerged as a new coronary imaging technique.[1-7] By virtue of the absence of moving parts, EBCT can construct ECG triggered, high resolution tomograms in 100 ms. This is fast enough to reduce cardiac motion artefacts and produce high quality cardiac images,[8] especially when the acquisition window is set during diastasis. The scanner was originally designed in the 1980s for cardiac function studies and myocardial perfusion imaging.[8] Later it was applied for the accurate quantification of coronary calcification.[9]

TECHNIQUE

Image acquisition

Scanning is performed with the patient in the supine position. Contrast (iopromide 350 mg/ml) is injected through an antecubital vein to a total of 150 ml. Tomography starts just proximal to the left main coronary artery after an ECG trigger at 80% of the RR interval (diastasis). A tomogram thickness of 1.5 mm and a table increment after each tomogram of 1.5 mm results in contiguous non-overlapping slices. A total of 40-60 contrast enhanced tomograms are made during a single breath hold after intravenous contrast administration. Radiation exposure for a complete examination is estimated to be < 20 mGy.[3,9] This is approximately one fifth of the radiation exposure at coronary angiography.[10] It is our[3] and others'[11] experience that after instruction most patients are able to hold their breath for at least 35 seconds. The individual tomograms have a resolution of 4-6 linepairs/cm and the scanning time for each tomogram is 100 ms. The spatial resolution in the scanning direction is limited by the slice thickness of 1.5 mm. Very short lesions (< 3 mm long) in artery segments that are perpendicular to the scanning plane can therefore be missed. Although these specifications fall short of the spatial (5 linepairs/mm) and temporal resolution (up to 50 frames/s) of conventional cine coronary angiography, proximal and middle parts of the coronary arteries can be visualised with EBCT.

Three dimensional reconstruction

Two dimensional transaxial tomograms are transferred to a computer workstation where they are stacked and interpolated to form a three dimensional volume using specialised software. This process creates a database representation of a three dimensional object. With special rendering techniques this database representation of the three dimensional object can be visualised. Several three

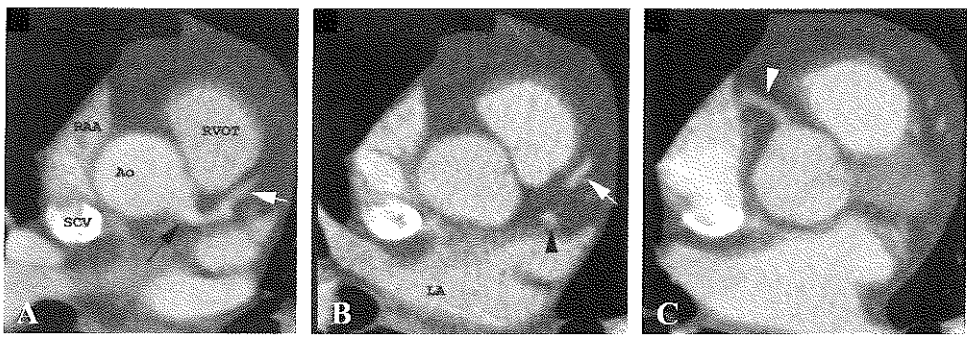

Figure 1 (A) *Transaxial tomogram after intravenous contrast injection. Ao, ascending aorta; RVOT, right ventricular outflow tract, RAA, right atrial appendage; black arrow, left main coronary artery; white arrow, proximal left anterior descending artery.* ***(B)*** *Transaxial tomogram at a lower level. LA, left atrium; black arrowhead, proximal circumflex artery cut perpendicular.* ***(C)*** *Transaxial tomogram at the level of origin of the right coronary artery (white arrowhead).*

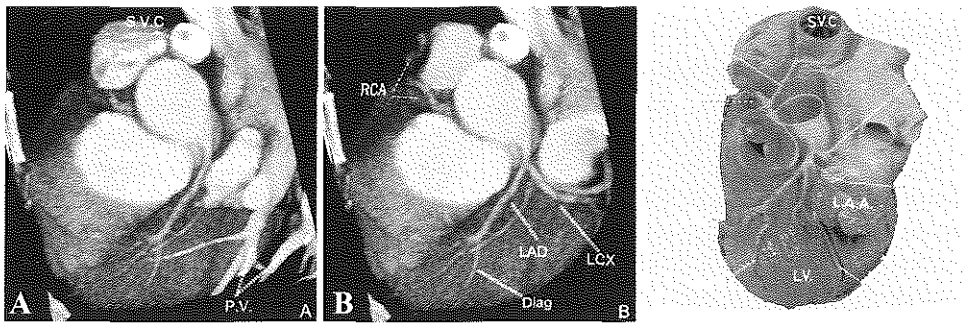

Figure 2. *Rendering of the left coronary artery before* ***(A)*** *and after* ***(B)*** *removal of the left atrial appendage (LAA). In* ***(A)*** *the left circumflex coronary artery (LCX) is hidden under the left atrial appendage. At the tomographic level the atrial appendage was removed manually on 15 levels before rendering* ***(B)*** *was made.* ***(C)*** *Pressure fixed anatomical specimen showing the relation between atrial appendage and circumflex artery. Diag, ramus diagonalis; LAD, left anterior descending coronary artery; PV, pulmonary veins; RAA, right atrial appendage; RCA, right coronary artery; RVOT, right ventricular outflow tract; SVC, superior vena cava. Reproduced from McAlpine[13] with permission of Springer Verlag.*

dimensional rendering techniques are available,[12] but we almost exclusively use volume rendering.[3] Volume rendering allows certain parts of the three dimensional object to be transparent so that structures behind these parts are still visible. By assigning the right colour and opacity values to different tissues, real anatomy is simulated in much the same way as pictures in an anatomic atlas (Figures 2, 3, and 4).[13]

CLINICAL PERFORMANCE

Several groups have compared intravenous EBCT coronary angiography to conventional angiography.[2-7] In all these studies both the original tomographic data and the three dimensional renderings were used to assess the coronary arteries. Overall, the technique allowed visualisation of the proximal and mid-coronary arteries in approximately 80% of cases. The left main coronary artery and proximal and middle parts of the left anterior descending coronary artery could gen-

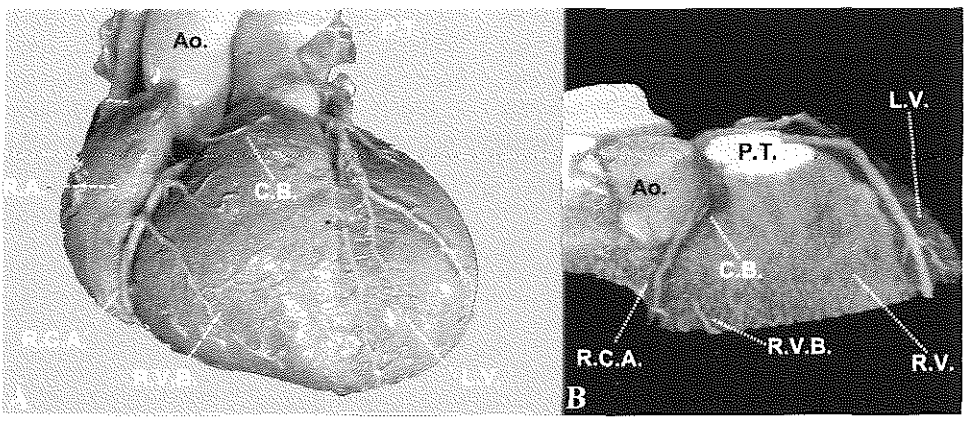

Figure 3. ***(A)*** *A pressure fixed anatomical specimen showing the proximal and middle right coronary artery (RCA) with its side branches (conus branch (CB) and right ventricular branch (RVB)). Reproduced from McAlpine [13] with permission of Springer Verlag.* ***(B)*** *A three dimensional rendering of the right coronary artery. Because of the small size, only the proximal part of the conus branch could be seen. The right ventricular branch has a stenosis in the proximal part. At the right side of the picture the left anterior descending coronary artery can be clearly seen. Ao, ascending aorta; PT, pulmonary trunk; LV, left ventricle; RV, right ventricle; RA, right atrium.*

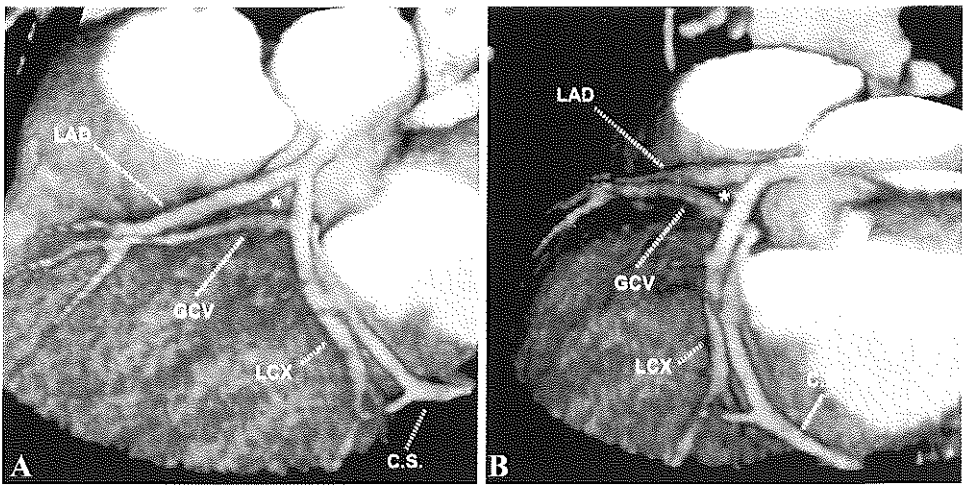

Figure 4. *Renderings of the left coronary arterial and venous systems.* ***(A)*** *Great cardiac vein (GVC) running parallel to the left anterior descending coronary artery (LAD), crossing under the circumflex artery (LCX) and entering the coronary sinus (CS). *Triangle of Brocq and Mouchet formed by the proximal left anterior descending coronary artery, the proximal circumflex coronary artery, and the great cardiac vein crossing from the anterior interventricular groove to the atrioventricular groove.* ***(B)*** *Three dimensional rendering of the same dataset offering a more lateral and posterior view of the heart, arteries, and veins. This clearly shows the possibility of the three dimensional rendering technique to view the object from any angle.*

erally be visualised and assessed in 90-100% of cases, with a sensitivity to detect a significant stenosis of 85-90% and a specificity of around 90%. Images of the right and circumflex coronary arteries were interpretable in only 75% of cases, with a little lower diagnostic accuracy in general. Major causes for non-assessability were cardiac motion artefacts, and the smaller size of the middle and distal parts of the right and circumflex arteries. Improvements in ECG triggering, shorter acquisition time (50 ms high resolution tomograms), and improved spatial resolution with a recently introduced new detector ring are expected to improve visualisation and diagnostic accuracy of the technique.

CONCLUSION

Intravenous EBCT coronary angiography is a promising imaging modality that allows for non-invasive visualisation of the proximal and middle parts of the coronary arteries.

REFERENCES

1 Moshage WE, Achenbach S, Seese B, et al. Coronary artery stenoses: three dimensional imaging with electrocardiographically triggered, contrast enhanced, electron beam CT. Radiology 1995;196:707-14.

2 Schmermund A, Rensing BJ, Sheedy PF, et al. Intravenous electron beam CT coronary angiography for segmental analysis of significant coronary artery stenoses: feasibility and limitations. J Am Coll Cardiol 1998;31:1547-54.

3 Rensing BJ, Bongaerts A, van Geuns RJ, et al. Intravenous coronary angiography by electron beam computed tomog-raphy. A clinical evaluation. Circulation 1998;98:2509-12.

4 Achenbach S, Moshage W, Ropers D, et al. Value of electron-beam computed tomography for the noninvasive detection of high-grade coronary-artery stenoses and occlusions. N Engl J Med 1998;339:1964-71.

5 Nakanishi T, Ito K, Imazu M, et al. Evaluation of coronary artery stenoses using electron-beam CT and multiplanar reformation. J

Comput Assist Tomogr 1997;21:121-7.
6 Reddy PR, Chernoff DM, Adams JR, et al. Coronary artery stenoses: assessment with contrast enhanced electron beam CT and axial reconstructions. Radiology 1998;208:167-72.
7 Budoff MJ, Oudiz RJ, Zalace CP et al. Intravenous three-dimensional coronary angiography using contrast enhanced electron beam computed tomography. Am J Cardiol 1999;83:840-5.
8 Stanford W, Rumberger JA. Ultrafast computed tomography in cardiac imaging: principles and practice. Mount Kisco, New York: Futura, 1993:1-16.
9 Wexler L, Brundage B, Crouse, J, et al. Coronary artery calcification: pathology, epidemiology, imaging methods, and clinical implications. A statement for health professionals from the American Heart Association. Circulation 1996; 94:1175-92.
10 Stehling MK, von Smekal A, Reise M. MRI der Koronararterieen Moglichkeiten und Grenzen. Radiologe 1994;34: 462-8.
11 Gay SB, Sistrom CL, Holder CA, et al. Breath-holding capability of adults. Implications for spiral computed tomography, fast acquisition magnetic resonance imaging, and angiography. Invest Radiol 1994;29:848-51.
12 Van Ooyen PMA, de Feyter PJ, Oudkerk M. An introduc-tion to three dimensional cardiac image rendering and processing. Cardiologic 1997;4:312-19.
13 McAlpine WA. Heart and coronary arteries. Heidelberg: Springer Verlag, 1975.

Chapter 15

Intravenous Coronary Angiography by Electron Beam Computed Tomography: A Clinical Evaluation

B.J. Rensing, R.J. van Geuns, A. Bongaerts, P. van Ooijen,

M. Oudkerk, P.J. de Feyter.

Published in Circulation 1998;98:2509-12

ABSTRACT

Background:
Noninvasive detection of coronary stenoses with electron beam CT (EBCT) after intravenous injection of contrast medium has recently emerged. We sought to determine the diagnostic accuracy of EBCT angiography in the clinical setting using conventional coronary angiography as the "gold standard."

Methods and Results:
Thirty-seven patients (30 men) were investigated. After intravenous injection of 150 mL of contrast medium, 40 to 60 consecutive transaxial tomograms, covering the proximal and middle parts of the coronary arteries, were obtained with ECG triggering at end diastole during breath-holding. Three-dimensional reconstructions of the proximal and middle parts of the arteries were compared with the conventional angiograms. Of the 259 proximal and middle coronary segments, 211 (81%) were analyzable by EBCT. Of the left anterior descending coronary artery (LAD) segments, 95% were assessable. Right coronary artery (RCA) and left circumflex artery (LCX) segments were assessable in 66% and 76%, respectively. Overall sensitivity and specificity to detect a >50% diameter stenosis were 77% and 94%, respectively. This was 82% and 92% for the LAD, 60% and 97% for the RCA, and 83% and 89% for the LCX (all figures based on assessable lesions).

Conclusions:
Intravenous EBCT coronary angiography is a promising coronary imaging technique. The technique is not yet robust enough to be an alternative to conventional coronary angiography. It can detect and rule out significant coronary artery disease of the left main proximal and mid portions of the LAD with good accuracy.

INTRODUCTION

Recently, electron beam CT (EBCT) has emerged as an imaging technique that allows visualization of epicardial coronary arteries after intravenous injection of contrast material.[1-5] Few data concerning the diagnostic accuracy of EBCT coronary angiography are available at the moment. The latest upgrading of the scanner allows improved resolution in the scanning direction. Slice thickness (collimation) and table feed after each scan can be decreased to 1.5 mm. The purpose of the present study was to compare noninvasive EBCT coronary angiography with conventional coronary angiography in the clinical setting and to determine the diagnostic accuracy of EBCT angiography.

METHODS

Thirty-seven patients who underwent diagnostic coronary angiography were asked to participate in the study and gave informed consent. The study was approved by the Institutional Review Board. Two patient slots per week for cardiac research were available at the EBCT site. Therefore, our patient population is not strictly consecutive. All patients who met the inclusion criteria were approached until the 2 slots for that week were filled. Exclusion criteria were previous bypass operation or stent implantation, severe lung disease or comorbidity that made breath-holding difficult, renal failure, nonsinus rhythm, and unstable clinical condition.

EBCT Angiography

The EBCT scanner (Siemens Evolution) allows the acquisition of high-resolution tomograms in 100 ms, which is fast enough to prevent cardiac motion artifacts. A description of scanner specifications can be found elsewhere.[6] Contrast transit time was determined by injection of 10 mL of contrast medium (Iopromide, Schering) at a rate of 4 mL/s through an antecubital vein and visualization of the passage of the contrast through the ascending aorta by 20 consecutive tomograms. The time from contrast injection to peak density of the aorta was considered the transit time. Image acquisition started with the injection of 150 mL contrast medium at 4 mL/s. At transit time, tomography commenced just proximal to the takeoff of the left main (LM) coronary artery after an ECG trigger at 80% of the RR interval. The table increment after each tomogram was 1.5 mm. A total of 40 to 60 tomograms were acquired. Because of patient limitations (maximal breath-hold time) and scanner limitations (1 scan per heart cycle and 1.5-mm tomogram thickness), only the proximal and middle parts of the coronary arteries could be visualized consistently. To decrease breath-holding time, atropine 0.5 to 1.0 mL was administered if heart rate was <60 bpm. Radiation dose was estimated to be <20 mGy.

Three-Dimensional Reconstruction

The 2-dimensional tomograms were transferred to a Silicon Graphics workstation, where they were stacked and interpolated to

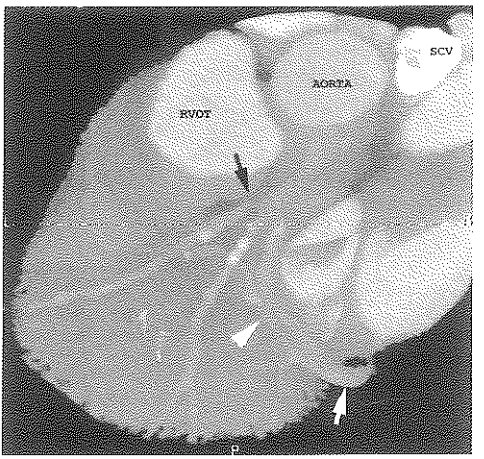

Figure 1. *3D rendering of left coronary artery. At trifurcation of LAD, intermediate branch, and LCX, stenosis in LAD can be seen (black arrow). Arrowhead indicates great cardiac vein on entering coronary sinus. Later, it blends with LCX (white arrow). RVOT indicates right ventricular outflow tract; SCV, superior caval vein.*

form a 3-dimensional (3D) volume by use of Voxel-View volume-rendering software. Postprocessing techniques were applied to better visualize the coronary arteries between the other contrast-enhanced cardiac structures.[7,8] Average postprocessing time was 15 to 20 minutes (Figure 1). To selectively visualize the coronary lumen, renderings were made with a lower threshold of 110 Hounsfield units. Two cardiologists unaware of the results of the selective coronary angiogram or the EBCT angiograms independently evaluated either EBCT angiograms (the 3D reconstructions and the individual tomograms) or the selective coronary angiograms. The coronary tree was divided into proximal, middle, and distal segments according to AHA guidelines.[9] The proximal and middle segments were graded as assessable or nonassessable. Then they were graded as having either no significant disease (<50% diameter stenosis) or significant disease (50% diameter stenosis). In case of disagreement, a third cardiologist decided.

Statistics

The selective angiogram served as the "gold standard" for determination of the diagnostic value of the noninvasive EBCT coronary angiogram. The diagnostic accuracy of EBCT angiography is expressed as sensitivity, specificity, and positive and negative predictive value.

RESULTS

Thirty-seven patients (30 men) underwent both conventional and EBCT coronary angiography. Mean age was 58±6 years (range, 42 to 82 years). Mean weight was 70±10 kg, and mean height was 171±12 cm. Mean time interval between both examinations was 10±13 days. At conventional angiography, 9 patients had no significant coronary stenosis, 12 had 1-vessel disease, 11 had 2-vessel disease, and 5 had 3-vessel disease. LM disease was present in 1 patient. Mean heart rate during the EBCT angiography was 72±10 bpm (60 to 105 bpm). Mean breath-holding time was 36 seconds. After mild hyperventilation and instruction, all patients were able to hold their breath for 40 tomograms. Atropine 0.5 to 1 mg was administered in 25 patients. Conventional angiography showed 1 significant LM lesion, 15 right coronary artery (RCA) lesions, 16 left anterior descending coronary artery (LAD) lesions, and 8 left circumflex (LCX) lesions in the proximal and middle portions of the coronary tree. Of the 259 proximal and middle coronary artery segments, 211 (81%) were assessable by EBCT angiography (Table 1). Five (33%) of the proximal and middle RCA lesions and 2 (25%) of the proximal and middle LCX lesions were located in segments deemed not assessable by EBCT angiography. Table 2

Table 1. No. of Segments Assessable

Segment	n (%)
RCA proximal	33 /37 (89)
RCA middle	16 /37 (43)
LM	36 /37 (97)
LAD proximal	35 /37 (95)
LAD middle	35 /37 (95)
LCX proximal	33 /37 (89)
LCX middle	23 /37 (62)
Total	211 /259

Table 2. Diagnostic Accuracy for Detection of a >50% Diameter Stenosis of EBCT Angiography[1]

	Total	LM	LAD	LCX	RCA
Sensitivity, %	77	100	82	83	60
Specificity, %	94	100	92	89	97
PPV, %	73	100	78	50	86
NPV, %	95	100	94	97	90

[1] Calculated for 211 assessable segments on a total of 259 proximal and middle coronary segments.PPV indicates positive predictive value; NPV, negative predictive value.

Table 3. Causes for Nonassessability of 48 Proximal and Middle Coronary Segments

	LAD, n (%)	LM, n (%)	RCA, n (%)	LCX n (%)
Scanning started below ostium	1 (25)	1 (100)	...	...
Circular calcification	2 (50)*	...	...	...
Cardiac motion artifacts	...	...	7 (28)	...
Breathing artifact	1 (25)	...	...	...
Blending with contrast-filled structures	...	...	5 (20)	4 (22)
Distal to total occlusion	...	...	3 (12)	1 (6)
Small vessel (<2 mm)	...	...	3 (12)	10 (56)
Poor distal opacification	...	...	3 (12)	3 (17)
Arrhythmia	...	...	3 (12)	...
Distal part not covered by tomograms	...	...	1 (4)	...

* *1 patient.*

summarizes diagnostic accuracy parameters of EBCT angiography. The causes for the inability to assess 46 proximal and middle coronary segments with EBCT are summarized in Table 3. The causes for false-negatives or false-positives are given in Table 4. The major cause of false-positive classification was poor opacification in small distal coronary arteries. Calcification of the vessel wall obscuring a luminal narrowing was the major cause of false-negative classification. The only reported side effect of atropine was oral dryness in 5 patients. Angina occurred once, with reversal after oral nitroglycerin.

DISCUSSION

Others[1-5] and we have shown that EBCT coronary angiography is feasible and safe. It allows visualization of the proximal and middle coronary arteries in a majority of patients. With special computer software, the individual tomograms can be stacked and 3D renderings of the coronary arteries constructed.[7,8]

Limitations of the Technique

The inability to assess coronary anatomy in a large proportion of mid RCA and LCX lesions requires further improvement of the technique. Conversely, all but 1 of the LM arteries and 95% of the proximal and mid LAD segments were assessable by current

Table 4. Reasons for Misclassification of Coronary Segments

	LAD, n	RCA, n	LCX, n
False positives			
Scanning started too low	2*	...	...
Premature atrial complex	1	...	...
Small distal artery (<2 mm)	1	...	5
Breathing artifact	...	1	...
False negatives			
Heavy calcification obscuring lumen	3#	2	...
Overlap with right auricle	...	1	...
Overlap with coronary sinus	...	...	1
Diastolic motion artifact	...	1	...

* *1 patient;*
\# *2 patients.*

Figure 2. *3D rendering of inferior side of heart after second contrast injection. Black arrowhead indicates middle cardiac vein entering coronary sinus (black arrow); white arrow, distal RCA; and white arrowhead, small posterior descending artery running parallel to vein. Discontinuity of RCA at crux cordis is caused by partial intramural course. On individual tomograms, absence of a stenosis could be observed.*

EBCT with a good diagnostic accuracy (Table 2). Breath-holding limitations and single tomogram acquisition per heart cycle restrict the volume of the heart that can be scanned during 1 contrast injection. Therefore, distal coronary arteries are only rarely visualized. Although one could argue whether stenoses in small distal coronary arteries have important symptomatic or prognostic meaning per se, visualization of the posterior descending artery is important and should be possible. A second contrast injection can visualize the distal part of the coronary trajectory, but at the expense of doubling the contrast volume (Figure 2). To accurately visualize coronary arteries <2 mm (the major cause of false-positive results and nonassessability), spatial resolution needs improvement.

Technical Improvements

A recently introduced new detector array is expected to improve in-plane resolution by 30%. This will probably increase assessability and diagnostic accuracy in small coronary vessels and might improve discrimination of overlapping contrast-filled structures. At the moment, the scanner can make only 1 tomogram per heart cycle. Ideally, the complete heart should be scanned within a few heartbeats, thereby shortening breath-holding time, decreasing the deleterious effect of arrhythmias on imaging, and reducing the total amount of contrast medium necessary for opacification. For this, the scanner has to be modified to allow acquisition of multiple simultaneous parallel tomograms and thus become more of a volume scanner. Finally, to prevent end-diastolic motion artifacts of the RCA, tomogram acquisition time <100 ms and true end-diastolic ECG (R-wave) triggering are necessary. A solution to the problem of circular calcification of the vessel wall (a major source of false-negatives) might be to visualize the coronary artery from the inside. A postprocessing technique called "fly-through" tracks the contrast-enhanced lumen of the artery on the individual tomograms. After stacking and interpolation, the computer constructs a movie that gives the illusion of traveling through the artery.

CONCLUSIONS

EBCT coronary angiography is a technique under development and is currently not an alternative to conventional coronary angiography. At the present time, it can detect and rule out significant coronary artery disease of the proximal and middle portions of the LAD with good accuracy and thus may provide us with important prognostic information.

REFERENCES

1. Moshage WE, Achenbach S, Seese B, Bachmann K, Kirchgeorg M. Coronary artery stenoses: three dimensional imaging with electrocardiographically triggered, contrast enhanced, electron beam CT. Radiology. 1995;196:707-714.

2. Schmermund A, Rensing BJ, Sheedy PF, Bell MR, Rumberger JA. Intravenous electron-beam computed tomographic coronary angiography for segmental analysis of coronary artery stenoses. J Am Coll Cardiol. 1998;31:1547-1554.
3. Achenbach S, Moshage W, Bachmann K. Detection of high-grade restenosis after PTCA using contrast-enhanced electron beam CT. Circulation. 1997;96:2785-2788.
4. Budoff MJ, Oudiz RJ, Zalace CP, Bakshesi H, Goldberg SL, Rami TG, Brundage BH. Intravenous three-dimensional coronary angiography using contrast enhanced electron beam computed tomography. J Am Coll Cardiol. 1997;29:393A. Abstract.
5. Chernoff DM, Ritchie CJ, Higgins CB. Evaluation of electron beam CT coronary angiography in healthy subjects. Am J Radiol. 1997;169:93-99.
6. Gould RG. Principles of ultrafast computed tomography: historical aspects, mechanisms and scanner characteristics. In: Stanford W, Rumberger JA, eds. Ultrafast Computed Tomography in Cardiac Imaging: Principles and Practice. Mt Kisco, NY: Futura; 1993:1-16.
7. Van Ooijen PMA, de Feyter PJ, Oudkerk M. An introduction to three dimensional cardiac image rendering and processing. Cardiology. 1997;4:312-319.
8. Ney D, Fishman E, Magid D. Volumetric rendering of computed tomography data: principles and techniques. Comput Graphics Applications. 1990;10:24-32.
9. American Heart Association Committee Report. A reporting system on patients evaluated for coronary artery disease. Circulation. 1975;51:7-34.

Chapter 16

Coronary Artery Fly-Through Using Electron Beam Computed Tomography

P.M.A. van Ooijen, M. Oudkerk, R.J.M. van Geuns,

B.J. Rensing, P.J. de Feyter.

Published in Circulation 2000;102:e6-e10

ABSTRACT

Background:

Virtual reality techniques have recently been introduced into clinical medicine. This study examines the possibility of coronary artery fly-through using a dataset obtained by noninvasive coronary angiography with contrast-enhanced electron-beam computed tomography.

Methods and Results:

Ten patients were examined, and 40 to 60 transaxial tomograms (thickness, 1.5 mm; in-plane pixel dimensions, 0.5×0.5 mm) were obtained after intravenous contrast injection. The datasets were processed on a graphics workstation using volume-rendering software. For fly-throughs, the contrast-enhanced lumen was made transparent and other tissue was made opaque. Then, key frames were selected in a path through the vessel, with software interpolation of frames between key frames. A typical movie contained 150 to 300 frames (10 to 15 key frames). Fly-throughs of coronary bypass grafts (n=3), left anterior descending arteries (LAD; n=6), and the intermediate branch (n=1) were reconstructed. Coronary calcifications were seen in 3 patients. The fly-through of the intermediate branch, the bypass grafts, and one of the LADs did not show any irregularities. In 2 cases, a stenosis was visible in the LAD; its presence was confirmed by conventional coronary angiography.

Conclusions:

Recent developments in fast-volume rendering using special-purpose hardware in combination with noninvasive coronary angiography with electron beam computed tomography have provided the possibility of performing coronary artery fly-throughs.

INTRODUCTION

Coronary angiography is the standard way of visualizing the coronary arteries. However, this method is invasive and, in a few cases, the procedure is associated with complications and has a small risk of mortality. Therefore, noninvasive methods to visualize the coronary arteries are currently under investigation; these include MRI[1,2] and electron-beam computed tomography (EBT).[3,4] Coronary angiography depicts the coronary artery as a planar silhouette (lumenogram) and, therefore, only detects a stenosis if the plaque obstructs the lumen; it also provides no information on the vessel wall. Coronary artery fly-through is another way to provide a comprehensive delineation of the lumen and the impact of vessel wall disease on the lumen. Some examples of fly-throughs of the coronary arteries with calcifications and stenoses are shown in this article.

METHODS

For this study, 10 patients were selected who had a noninvasive, contrast-enhanced EBT angiogram of adequate quality. The data acquisition was performed on an Evolution XP (Imatron) EBT scanner. The acquisition of the 3D dataset began with the injection of 120 to 180 mL of contrast medium at 3 to 4 mL/s through an antecubital vein. Scanning commenced just proximal to the left main coronary artery after an ECG trigger at 80% of the RR interval (diastasis). The tomogram (slice) thickness was set at 1.5 mm, and the table increment after each tomogram was set at 1.5 mm, which resulted in contiguous, nonoverlapping slices. A total of 40 to 60 transaxial tomograms were made during a single breath-hold. Breath-holding is necessary during data acquisition to avoid respiratory motion artifacts. Field-of-view size was generally set at 18 cm, with a matrix size of 512×512 pixels; this yielded a pixel size of 0.35×0.35 mm. The acquired data were then transferred to a special-purpose graphic workstation (Indigo2, Silicon Graphics, Inc) running VoxelView software (Vital Images) for volume rendering and processing.[5-8]

The volume dataset consisted of voxels (3D pixels), each of which had a certain value that was based on the tissue density value measured by the EBT scanner. Using these voxel values, several types of renderings can be performed. One of the possibilities is to construct a fly-through movie. A fly-through is similar in some ways to a flight-simulator. The surroundings in a flight-simulator are all virtually stored in a large computer database, and the image shown to the pilot is based on the position and direction of the virtual airplane in the virtual surroundings. By a fast and smooth replacement of the image of the virtual surroundings, the illusion of flying is created. In the case of a coronary artery fly-through, the surroundings are the scanned data, and the airplane can be thought of as a camera mounted on the tip of a catheter. The images shown are based on the position and direction of this catheter in the coronary artery. By displaying images at consecutive positions along a certain path through the coronary (the flight path), the illusion of moving through this artery is created.

To make a fly-through movie like this, the vessels must be "hollowed out" by assigning voxels representing contrast-media-rich blood an opacity of zero (full transparency) (Figure 1). Next, the viewpoint is moved inside the aorta or coronary artery; this will be the first key frame. After this, a number of viewpoints can be selected, which are positioned along the flight path as key frames for the movie (typically 10 to 15 key frames are selected). These key frames and the desired number of frames to be interpolated between the key frames are fed into the VoxelAnimator software, which is used to render the movie. From this information, the software interpolates a curve through the

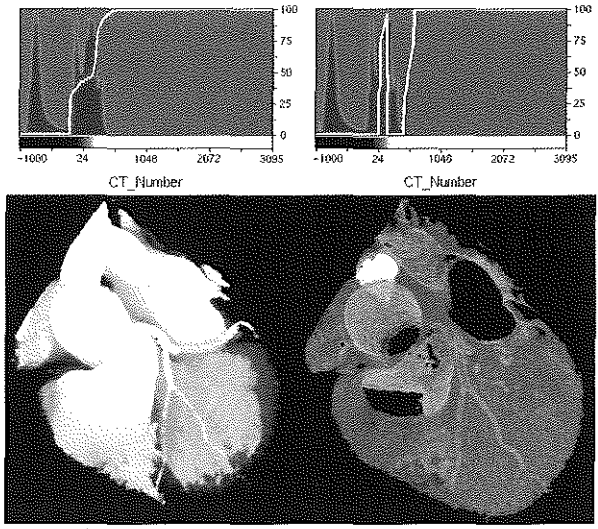

Figure 1. *Top, these graphs contain 2 types of information. The histogram shows the distribution of the voxel values. The x axis represents the voxel value, and the y axis, the number of voxels with this value. The line graph shows the opacity value assigned to a certain voxel value. The x axis again represents the voxel value, and now the y axis shows the opacity percentage (low value is transparent; high value is opaque). The images on the bottom demonstrate the effect of a change in opacity setting. The bottom left image shows the typical opacity setting used to depict the contrast-rich blood in the lumen of the vessel (maximum opacification), which is not necessarily an optimal setting for the depiction of the coronary arteries. In this case, the soft tissue and fat (with a lower voxel value) are transparent, and the contrast-enhanced blood (with a higher voxel value) is fully opaque. On the bottom right, the opacity for the soft tissue and fat is high (small peak in the yellow curve), and the voxel values corresponding to contrast-enhanced blood are fully transparent. As can be appreciated from the image shown, this type of setting hollows out the vessels, which enables flying through.*

defined key frames and renders the requested number of new frames between the key frames along this curve, which results in a 150- to 300-frame movie.

RESULTS

The 3D EBT datasets of 39 patients were evaluated, with special attention paid to interslice correlation quality, lack of artifacts, and slice image quality. The best 10 datasets were selected for coronary artery fly-throughs. From these 10 patients, fly-through movies of coronary artery bypass grafts (n=3), the left anterior descending artery (LAD; n=6), and the intermediate branch (n=1) were constructed. Typical examples from a bypass (Figure 2 and Movie I [Movies I to III can be found online at http://circ.ahajournals.org/

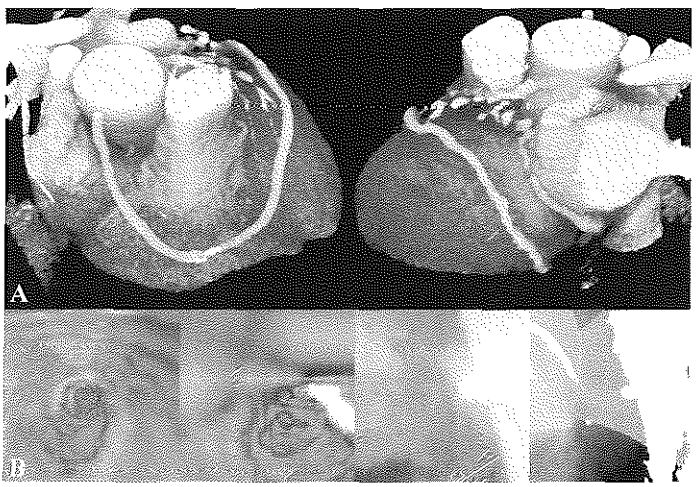

Figure 2. ***(A)*** *Volume renderings of a patient with a coronary artery bypass graft. The left image shows the artifact introduced by the segmentation of the sternum and sternal wires as a bright white portion of the bypass graft. Evaluating the patency of the graft at this particular point is difficult.* ***(B)*** *When flying through the vessel, it is clear from the first 2 images that the graft is patent. However, a possible calcified region shows up in the second image. By setting the opacity curves slightly differently (third and fourth images), the walls disappear and it becomes clear that this is not a calcified plaque, but an artifact from the sternum and the sternal wires. The actual fly-through is shown in Movie I.*

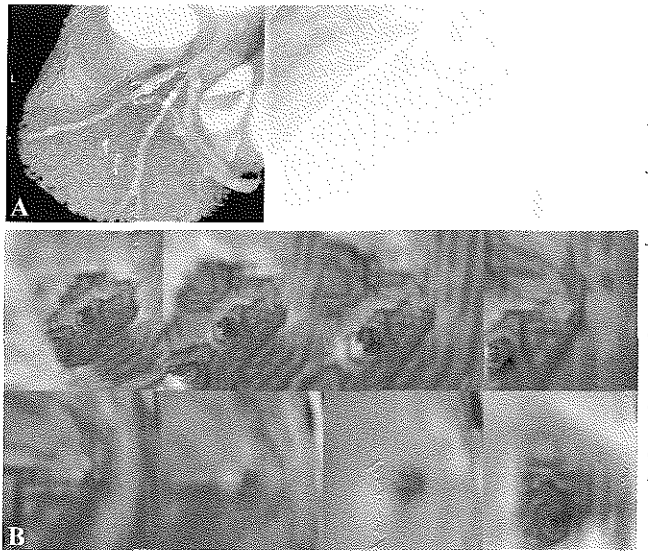

Figure 3. *(A) The left image shows a 3D volume rendering of the coronary arteries. The stenosis can be seen in the proximal part of the LAD right after the left main. This stenosis was confirmed using conventional coronary angiography shown on the right.* ***(B)*** *Some interesting frames from the fly-through. The trifurcation through the lumen is approached in frames 1 through 6, and movement is toward the stenosed origin of the LAD. Frame 7 shows the stenosis in close-up and, in frame 8, the stenosis has been crossed and the remaining part of the LAD is seen. The actual fly-through is shown in Movie II.*

cgi/content/full/102/1/DC1]) and from the LAD (Figures 3 and 4 and Movie II and III) are shown. Coronary calcifications were visible in 3 patients (eg, Figure 4 and Movie III), and a significant stenosis, which was confirmed by conventional diagnostic coronary angiography, was depicted in 2 patients (eg, Figure 3 and Movie II).

DISCUSSION

EBT coronary angiography has emerged as a potentially viable technique for noninvasive visualization of coronary arteries and coronary bypass grafts.[3,4] However, although the technique is reasonably robust, only 81% of the major coronary artery branches could be visualized with sufficient quality to assess patency, the presence of a severe stenosis, or total occlusion.[4] For the reconstruction of fly-through movies, the image quality of the 3D datasets must be perfect. Even small irregularities may hamper the successful construction of a coronary artery fly-through. Aquisition problems include the following. (1) Problems with breath-holding may reduce the continuation of a coronary artery from one slice to another. (2) Arrhythmia, or even a single premature complex, may lead to images that are triggered at a slightly different time in the heart cycle, resulting in a displacement of 1 to 2 mm of a single slice with respect to the other slices. This creates a discontinuation of the coronary arteries in 3D reconstructions. (3) Vessels with a diameter <1.75 mm (area, 5×5 pixels) will not provide a smooth coronary

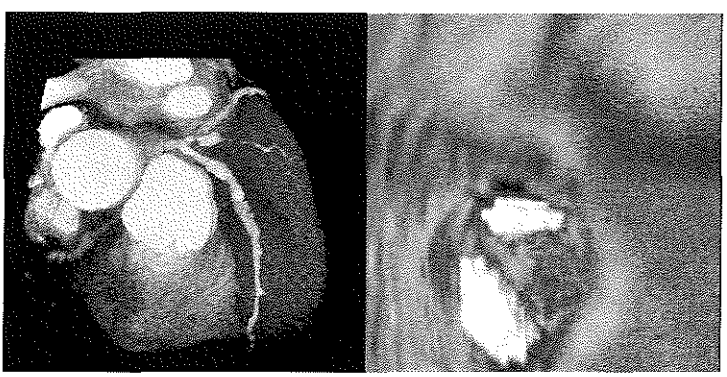

Figure 4. *When flying through a calcified LAD, the calcifications show up as white blobs floating inside the vessel. In this case, 3 big calcifications were passed on the fly-through of the LAD. The actual fly-through is shown in Movie III.*

fly-through. (4) Movement artifacts of the right coronary artery during the 100-ms image acquisition time hamper the construction of a fly-through movie of this artery.

In addition to these acquisition problems, the reconstruction of a coronary artery fly-through is very time-consuming; therefore, only the best quality datasets with a large vessel diameter were selected to undergo this procedure. For these reasons, a high-quality coronary artery fly-through was reconstructed in only 25% of the eligible patients. Much of the difficulties stated here can be overcome in the future by improvements in the spatial and temporal resolution of the EBT scanner. An update of the scanner is already available with a higher spatial resolution; this will increase the image quality and provide the possibility to display and fly-through smaller vessels. A reduction of slice acquisition time to below 100 ms will decrease the artifacts introduced by the movement of the right coronary artery. New scanning techniques that allow the acquisition of >1 slice during each heartbeat will shorten total scanning time and, thus, reduce the artifacts introduced by arrhythmias and breath-holding problems. Furthermore, the rapid development of both special-purpose rendering hardware and software will provide faster and more interactive ways to reconstruct fly-through movies.

Fly-through movies of venous bypass grafts are relatively easy to make because the vessel diameter is relatively large, and the cardiac motion of these vessels is limited. However, surgical clips or sternal wires may sometimes degrade the images because of the bright artifacts they cause (Figure 2 and Movie I). Calcifications of the vessel wall, which have a very high voxel value, are retained in the fly-throughs and are visible as white blobs floating in the artery (Figure 4 and Movie III).

These preliminary findings demonstrate the feasibility and potential of this method in coronary artery or bypass graft fly-through movies. The technique of coronary artery fly-through cannot be considered an alternative to traditional coronary angioscopy because it does not provide any information about the color of the lumen or its contents, such as plaque and thrombus. Coronary artery fly-through is an alternative way to evaluate non-invasive coronary angiography, and it has several advantages. (1) It provides a delineation of the "true" 3 dimensions of the vessel lumen, unlike diagnostic angiography (lumenography), which is limited by foreshortening and overlapping structures. (2) Fly-throughs may eliminate the time-consuming segmentation of overlapping, obscuring anatomical structures (left atrium, coronary sinus) that is needed to visualize the coronary arteries from the outside. (3) Fly-throughs may provide a more comprehensive delineation of bifurcation lesions or anastomoses of grafts on native vessels, which are sometimes difficult to asses, even with routine diagnostic angiography. Finally, fly-throughs may be helpful in assessing the remaining coronary lumen of a heavily calcified coronary plaque or stented segment, which may be invisible with traditional EBT-derived 3D rendering techniques.

CONCLUSIONS

A fly-through of coronary arteries and venous bypass grafts is feasible in clinical practice and may represent a future diagnostic technique that will allow comprehensive 3D delineation of the vessel lumen.

Footnotes

Movies I through III can be found at http://circ.ahajournals.org/cgi/content/full/102/1/DC1

REFERENCES

1. Manning WJ, Li W, Edelman RR. A pre-

liminary report comparing magnetic resonance coronary angiography with conventional angiography. N Engl J Med. 1993;328:828-832.
2. Van Geuns RJM, de Bruin HG, Rensing BJWM, et al. MRI of the coronary arteries: clinical results from three-dimensional evaluation of a respiratory gated technique. Heart.. 1999;82:515-519.
3. Moshage W, Achenbach S, Seese B, et al. Coronary artery stenoses: three-dimensional imaging with electrocardiographically triggered, contrast agent-enhanced, electron-beam CT. Radiology. 1995;196:707-714.
4. Rensing BJ, van Geuns RJM, Bongaerts AHH, et al. Intravenous coronary angiography using electron beam computed tomography, a viable alternative to conventional coronary angiography. Circulation.. 1998;98:2509-2512.
5. Ney DR, Fishman EK, Magid D, et al. Volumetric rendering of computed tomography data: principles and techniques. IEEE Computer Graphics Appl. 1990;10:24-32.
6. Fishman EK, Magid D, Ney DR, et al. Three-dimensional imaging: state of the art. Radiology. 1991;181:321-337.
7. Heath DG, Soyer PA, Kuszyk BS, et al. Three dimensional spiral CT during arterial portography: comparison of three rendering techniques. Radiographics. 1995;15:1001-1011.
8. Kuszyk BS, Heath DG, Ney DR, et al. CT angiography with volume rendering: imaging findings. AJR Am J Roentgenol. 1995;165:445-448.

Part 3

MRI versus EBT for Non-invasive Coronary Angiography

Chapter 17

Non-invasive Coronary Imaging: A Comparison Between MRI and EBT

R.J.M. van Geuns, M. Oudkerk, B.J.W.M. Rensing,

A.H.H. Bongaerts, H.G. de Bruin, P.A. Wielopolski,

P.M.A. van Ooijen, P.J. de Feyter, P.W. Serruys.

Submitted

ABSTRACT

Objectives:
To compare the diagnostic value of magnetic resonance imaging (MRI) and Electron beam computed tomography (EBT) using conventional coronary angiography as the "gold standard."

Background:
MRI and EBT have recently emerged as two modalities for non-invasive detection of coronary artery stenoses. A direct comparison between the both techniques has not been performed yet.

Methods:
Twenty-seven patients underwent coronary imaging with a contrast-enhanced ECG triggered breath-hold EBT protocol and a retrospective respiratory gated MRI protocol. Three-dimensional reconstructions of the 216 available proximal and middle parts of the coronary arteries were compared with the conventional angiograms.

Results:
EBT more frequently visualized the segments successfully compared to MRI (77% versus 69%, $p < 0.05$) which was mainly due to improved visualization of the LAD and LCX. Overall sensitivity and specificity for EBT to detect a 50% diameter stenosis were 70% and 95% respectively, while sensitivity and specificity for MRI were 46% and 90% respectively.

Conclusions:
Non-invasive coronary artery angiography with MRI and EBT are evolving techniques. At present EBT is slightly better than MRI to adequately visualize and detect a stenosis in the proximal and mid coronary artery segments, but the distal segments cannot be visualized by either technique.

INTRODUCTION

Recently two new non-invasive techniques for the detection of coronary artery disease have been introduced: Magnetic Resonance Imaging (MRI) and Electron Beam Tomography (EBT). MRI of the coronary arteries (MRCA) was first performed in 1993 with a single slice breathhold technique.[1-4] Non-invasive coronary imaging using EBT with intravenous administration of contrast agent was demonstrated by Moshage et al.[5,6] Both techniques have inherent problems to reliably visualize the coronary arteries due to the complex course and the small size of the coronaries, which is further complicated by the motion artifacts of cardiac contraction and respiration.

In this study we compared the current state of art techniques of MRI and EBT for the visualization and detection of stenoses in the proximal and mid segments of the coronary arteries.

METHODS

Patients

The study population consisted of 27 patients (11 women and 16 men ranging in age from 38 to 76 years) who were referred for elective coronary angiography. The patients were recruited from among those scheduled for outpatient coronary angiography. Exclusion criteria were previous coronary bypass operation, intracoronary stent implantation, artificial pacemaker, intracranial clips, claustrophobia, non-sinus rhythm, renal failure, allergy for contrast medium, unstable clinical condition and severe lung disease restricting breathholding capabilities to less than 30 seconds. Protocol approval was provided by the Hospital Committee on Clinical Investigation and informent consent was obtained from all patients.

MRI

Subjects were studied in a supine position, with a 4-channel quadrature body phased array coil placed over the thorax, in a 1.5T whole body MR imaging system (Vision; Siemens, Erlangen, Germany). Coronary artery imaging was performed using a standard Siemens 3D gradient echo sequence with retrospective respiratory gated technique described by Li et al.[7] A chemical shift fat suppression pulse was used to suppress the signal from the epicardial fat surrounding the coronary arteries. In our setup we used three slabs of 32 mm thickness with a 25% overlap and slice thickness was 2 mm. The matrix size was 128 × 256 with a Rectangular Field of View of 240 × 320 mm, resulting in an inplane resolution of 1.9 × 1.25 mm. The TR was 8 ms, the TE was 3 ms and the flip angle varied from 20° to 90°. The acquisition window (128 ms) was set from mid untill late diastole. Each slab was acquired in 8-12 minutes depending on the heart rated.

Retrospective respiratory gating was performed by a navigator echo created with two excitation bands placed to intersect at the dome of the right hemidiaphragm. Together, these two bands measure the diaphragmatic position before data acquisition. The most common position of the diaphragm is chosen as the gating center, commonly this is end-expiration. Each line of data was acquired five times to ensure end-expiration data collection. Data within a range of ± 1 mm from the gating center were used for image reconstruction. If none of the acquisitions of a certain data-lines were within the acceptance range, the acquisition obtained at diaphragm displacements closest to the gating center were used at image reconstruction. The total examination time for MR imaging of each subject including positioning of the patient, scout imaging, and setting up the navigator, was approximately 1 hour.

EBT

For non-invasive coronary angiography the

EBT scanner was operated in a 'high-resolution mode', which acquires a cross-section images in 100 ms with the acquisition window at end-diastole (80% of the RR interval). The matrix size was 512 × 512. Data were reconstructed using a 22-cm field of view (pixel size 0.43 × 0.43 mm). In-plane resolution was approximately seven line pairs per cm.

For the determination of contrast transit time 10cc's of isoosmolaar nonionic contrast (iopromide 350 mg/ml) was administered at a rate of 4 cc/sec through an antecubital vein. The passage of the contrast bolus through the ascending aorta was visualized by positioning the tomographic plane of the EBT scanner over this region. Contrast density within the ascending aorta in Hounsfield units was measured at several time intervals after contrast injection. The time from contrast bolus injection to peak intensity was assumed to be the contrast transit time.

For the acquisition of the non-invasive coronary angiogram 150 cc's of isoosmolar nonionic contrast medium was administered at a rate of 4 cc/second through an antecubital vein catheter. Forty to sixty transaxial tomograms starting just cranial of the left main coronary artery of 1.5mm thickness with 1.5mm table shift between each slice were acquired during a single breathhold. ECG triggering was performed at 80% of the RR interval. After mild hyperventilation the actual acquisition started at the determined contrast transit time with breathholding at inspiration.

Conventional Coronary angiography

All subjects underwent standard selective coronary artery angiography within 1 month of the MR and EBT examinations. Angiography was performed using the technique of Judkins.[8] The selective angiograms were jointly interpretated by two experienced cardiologists not familiar with the non-invasive results. The coronary tree was divided into proximal, mid and distal segments according to AHA guidelines.[9] These segments were graded as having either no significant disease (< 50% diameter stenosis) or significant disease (>50% diameter stenosis). In case of disagreement a final decision was made by a third cardiologist.

Interpretation of Non-invasive coronary angiograms

Both the EBT and MR datasets were transferred to a stand alone workstation (Indigo2, Silicon Graphics) and loaded into a post-processing program (VoxelView, Vital Images, Inc) for 3D evaluation with a volume rendering technique.[10-12] Within this program unwanted structures such as the thorax wall and lung vessels and overlapping structures as the left and right auricle were excluded from the datatsets. These prepared datasets could be rotated in every direction for optimal visualization of the major coronary artery branches. The 3D reconstructions together with the original axial slices were reviewed independently by a radiologist and a cardiologist. The left main, proximal and mid left anterior descending (LAD), proximal and mid left circumflex (LCX) and the proximal, mid and distal segments of the right coronary artery (RCA) were graded as assessable, non-assessable or outside the acquired volume. The assessable segments were graded as having either no significant or significant disease. In case of disagreement a third investigator made a final decision.

Statistics

The selective coronary angiogram served as the golden standard for determination of the diagnostic value of the non-invasive coronary angiogram. Diagnostic value of EBT and MR coronary angiography was expressed as sensitivity, specificity and accuracy. The McNemar test was used to compare differences between proportions.

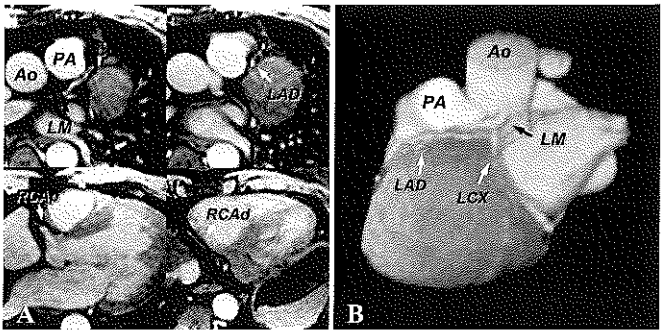

Figure 1. *Example of high quality MRI study.* ***(A)*** *Individual slices at different levels showing the left main coronary artery (LM), left anterior descending (LAD), proximal right coronary artery (RCAp), and distal right coronary artery (RCAd).* ***(B)*** *Three-dimensional interpretation of the whole volume using volume rendering software. Ao = Aorta, PA = pulmonary artery.*

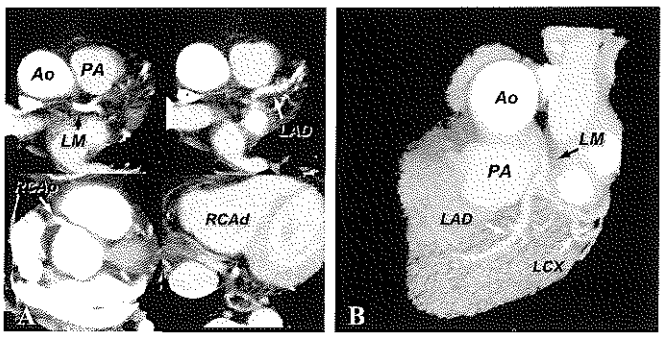

Figure 2. *Example of a high quality EBT study.* ***(A)*** *Individual slices at different levels showing the left main coronary artery (LM), left anterior descending (LAD), proximal right coronary artery (RCAp), and distal right coronary artery (RCAd).* ***(B)*** *Three-dimensional interpretation of the whole volume using volume rendering software. Ao = Aorta, PA = pulmonary artery.*

A p-value of < 0.05 was considered statically significant.

RESULTS

In 25 patients the MRI and EBT examinations were performed on the same day, in the other two patients the interval time was 7 days. The mean time interval between both examinations and conventional coronary angiography was 15 ± 7 days. Eight patients had no significant coronary stenosis in the major coronary arteries at selective angiography, 10 had 1-vessel disease, 6 had 2-vessel disease and 3 patients had 3-vessel disease. Overall 34 significant coronary artery stenoses were present in these patients (RCA: 16; LAD: 14; LCX: 4). Both techniques were able to obtain nearly motion free images (figure 1 and 2). Non-invasive visualization of the coronary artery was more frequently successful with EBT compared to MRI (77% versus 69%, $p < 0.05$) which was mainly due to improved visualization of the LAD and LCX (table 1). The RCA was more successful visualized with MRI, although this difference was not significant.

EBT showed a moderate sensitivity (70%) with a high specificity and accuracy (95% and 91% respectively), for the detection of significant coronary artery stenosis in assessable segments (figure 3). MRI showed a

Table 1. Assessability of different coronary artery segments by EBT and MRI.

Segment	CAG	EBT	MRI
RCA	74	41 (55.4%)	46 (62.2%)
1	27	24 (88.9%)	24 (88.9%)
2	24	13 (54.2%)	16 (66.7%)
3	23	4 (17.4%)	6 (26.1%)
LM + LAD	81	80 (98.8%)*	7 (87.7%)
5	27	27 (100.0%)	25 (92.6%)
6	27	26 (96.3%)	25 (92.6%)
7	27	27 (100.0%)*	21 (77.8%)
LCX	46	33 (71.7%)*	22 (47.8%)
11	21	17 (81.0%)*	10 (47.6%)
13	25	16 (64.0%)	12 (48.0%)
Total	201	154(76.6%)*	139 (69.2%)

** $p < 0.05$ compared to MRI*
RCA = right coronary artery, LM = left main artery, LAD = left anterior descending artery, LCX = left circumflex artery.

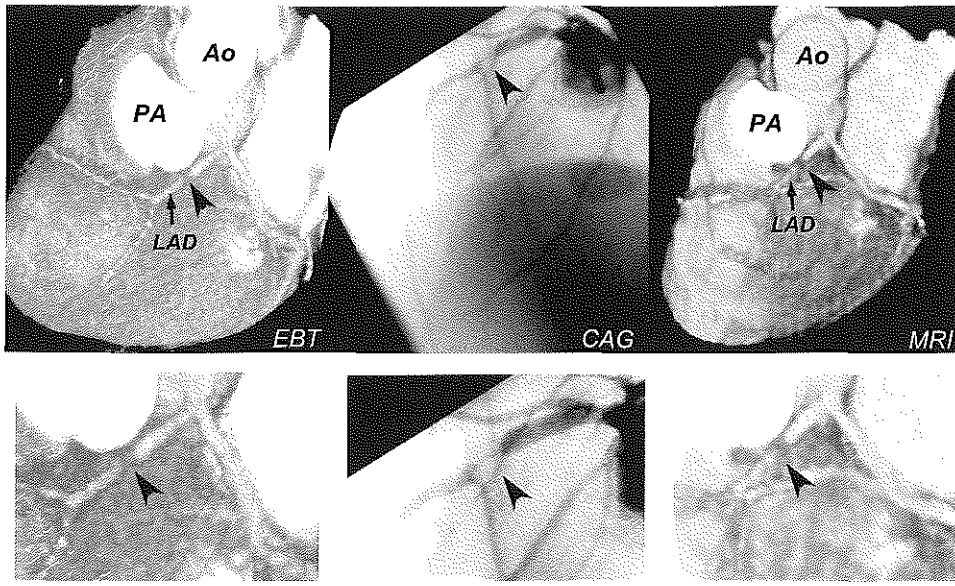

Figure 3. *Patient with a left anterior descending coronary artery LAD stenosis (arrow head) detected by conventional selective coronary angiography (middle image). Both EBT (left image) and MRI (right image) were able to detect this stenosis non-invasively. Ao = Aorta, PA = Pulmonary artery.*

Table 2. Diagnostic accuracy for the detection of a >50% diameter stenosis by non-invasive coronary angiography.

	EBT	MRI
All segments		
Sensitivity	69.9% (16/23)	46.2% (12/26)
Specificity	94.7% (124/131)	90.3% (102/113)
Accuracy	90.9% (140/154)	82.0% (114/139)
LAD/LM		
Sensitivity	57.1% (8/14)	75.0% (9/12)
Specificity	93.9% (62/66)	91.5% (54/59)
Accuracy	87.5% (70/80)	99.7% (63/71)
LCX		
Sensitivity	100% (3/3)	33.3% (1/3)
Specificity	93.3% (28/30)	94.7% (18/19)
Accuracy	93.9% (31/33)	86.4% (19/22)
RCA		
Sensitivity	83.3% (5/6)	18.2% (2/11)
Specificity	97.1% (34/35)	85.7% (30/35)
Accuracy	95.1% (39/41)	69.6% (32/46)

LAD = left anterior descending artery, LCX = left circumflex artery, LM = left main artery, RCA = right coronary artery.

lower sensitivity (46%) with a comparable specificity and accuracy (90% and 82% respectively) but these differences were not significant (table 2). Overall there was a moderate (93/122=76%) agreement between both methods in the interpretation of a particular segment. Figures 4 and 5 illustrate the different artifacts present in both techniques which limit the assessability of a segment or introduce false-negative and false-positive interpretations.

DISCUSSION

Although EBT and MRI are both non-invasive imaging technique there are major differences in acquisition strategies as breath-hold versus respiratory gated technique, slices acquisition versus true volume imaging, and contrast bolus versus non-contrast agent imaging (Table 3). These differences in acquisition strategy explain most of the artifacts present in each technique (Table 4).

Table 3. Acquisition characteristics	
EBT	MRI
Breath-hold	Respiratory gating
Stack of multiple 2D slice	3D (volume) acquisition
Contrast bolus	No contrast agent

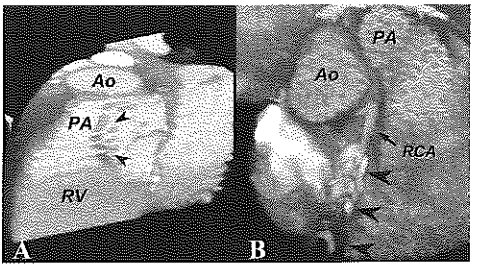

Figure 4. (A) *Example demonstrating the effects of arrhytmias on the correlation between individual slices in a EBT study. At the level of the pulmonary artery root (PA) three premature heart beats result in slice malpositioning (arrow heads). Ao = Aorta, RV = Right ventricle.* ***(B)*** *Patient with severe calcifications (arrow heads) in the right coronary artery (RCA) leading to severe artifacts in EBT. Ao = Aorta, PA = Pulmonary artery.*

EBT

Our results with EBT confirm earlier results from different groups for the possibility of EBT to detect significant stenoses in the proximal coronary arteries.[13-16]

Earlier we reported that artifacts in EBT which arise from involuntary patient motion and arrhythmias are the most frequent reasons for non-assessability of a particular coronary segment.[17] Arrhythmias will cause clear artifacts with odd correspondence between the individual slices of the dataset (figure 4A). Image quality in EBT can also be hampered by incorrect timing of the contrast agent bolus or low contrast enhanced at the last slices of the data set. Severe (circular) coronary artery calcification can obstruct the view on the vessel lumen introducing false negative results (Figure 4B). The contrast between the coronary vessel lumen and surrounding tissues can be improved by using a larger dose of contrast agent, or a more iodine containing contrast agent. To visualize the distal RCA a second breathhold with a new contrast bolus is necessary, which may be warranted with present safe contrast agents. Improvements in scanner design as higher inplane and/or z-axis resolution will improve image quality. A major improvement is the multislice computed tomography that acquires more slices (up to 4) per rotation, by which a complete volume can be scanned in a fraction of the scan time. This results also in a major improvement in terms of interslice correlation.

MRI

In this study we used a standard MR technique which is available on a modern MR scanner. The use of a single navigator signal from the diaphragm increases image quality of MRCA.[18] The value of this technique in the detection of coronary artery stenosis is still unsettled.[19-22] In this study the possibilities of this technique to detect significant coronary artery stenosis has been confirmed. Major reasons for insufficient image quality are residual respiratory blur depending on the gating window and respi-

Table 4. Artifacts in MRI and EBT		
	EBT	MRI
Arrhytmias	Single slice artifact	General blur
Respiration	Incorrect breathhold artifact	Residual respiratory blur
Contrast	Incorrect timing of contrast agent	General lower contrast
Vessel movement	++	++
Calcification	++	n.a.

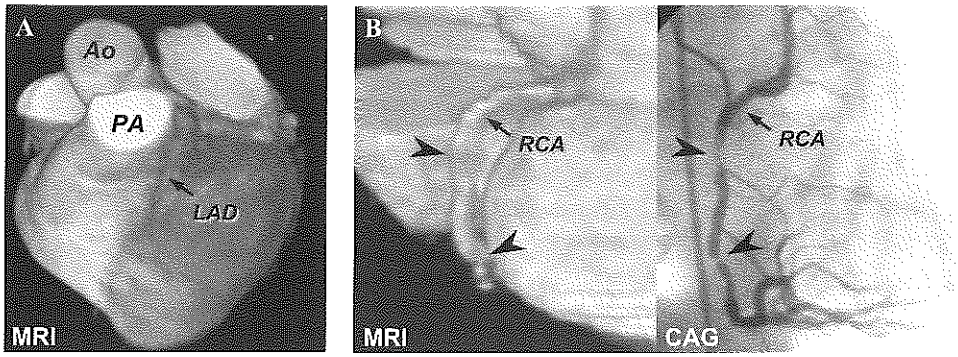

Figure 5. (A) *Patient with severe image blur in MRI due an irregular respiration pattern. The left anterior descending coronary artery (LAD) can hardly be differentiated from its surroundings. Ao = Aorta, PA = Pulmonary artery.* ***(B)*** *Example of false-negative interpretation of a diseased mid right coronary artery (RCA) segment. In the MRI image (left image) there is insufficient sharpness to detect the stenoses (arrow heads) visible in the conventional coronary angiogram (Right sided image)*

ration pattern (Figure 5A). False negative interpretations in respiratory MRCA are due to retrograde flow distal to complete occlusions, and volume averaging of vessels with adjacent structures (Figure 5B).[23] False positive interpretations arise from the low contrast between the coronary arteries and their surrounding tissue.

Respiratory gated MRCA may improve using prospective respiratory gating[24,25] where no data are acquired outside the gating window. This may include correction of image position with respiratory motion, where the imaging volume shift upwards during expiration and downwards during inspiration to improve scan efficiency.[26] Alternative MRI sequences acquire the central portion of k-space, which determines boundary sharpness, with a small respiratory gating window (e.g. 1 mm) while the data for the outer portions of k-space, determining image contrast, are scanned with increasingly coarser gating windows (e.g. 3 to 7 mm).[27]

Other possibilities in MRCA included new breathhold techniques with targeted volumes along the coronary arteries,[28] the use of intravascular MR contrast agents[29,30] or high field (3T) MR systems.

EBT versus MRI

Each technique has it advantages and disadvantages (Table 5). The higher resolution and faster acquisition of EBT compared to the selected MRI protocol will explain most of the differences found in this study. Both techniques have enough possibilities for improvement in the near future (table 6). The development in MRI will soon lead to the use of protocols with nearly the same resolution in considerably shorter imaging time,

Table 5. Advantages and disadvantages of EBT and MRI

EBT		MRI	
Advantages	Disadvantages	Advantages	Disadvantages
Fast	Sensitivity to arrhythmia	Repeatable	Low contrast
High in-plane resolution	Sensitivity to contrast timing	Covers whole volume of the heart	Interference on ECG
	Calcification artifacts		Claustrophobia
	Use of X-rays		
	Use of nefrotoxic contrast agents		

Table 6. Future improvements in MRI and EBT

EBT	MRI
Increased contrast dose	Prospective respiratory gating
Multi slice acquisition	Intravascular contrast agents
Higher in-plane resolution	High field systems (3T)

which will warrant new comparisons between both techniques.

CONCLUSION

Non-invasive coronary artery angiography with MRI and EBT are viable techniques. At the present state EBT is slightly better than MRI to adequately visualize proximal and mid coronary artery segments and to detect a stenosis in these segments. MRI has the advantages of a large coverage and the repeatability without hazards to the patient. Due to the limited acquisition speed both techniques are not yet an alternative to conventional coronary angiography.

REFERENCES

1. Manning WJ, Edelman RR. Magnetic resonance coronary angiography. Magn Reson Q 1993;9:131-51.
2. Manning WJ, Li W, Boyle NG, Edelman RR. Fat-suppressed breath-hold magnetic resonance coronary angiography. Circulation 1993;87:94-104.
3. Manning WJ, Li W, Edelman RR. A preliminary report comparing magnetic resonance coronary angiography with conventional angiography. N Engl J Med 1993;328:828-32.
4. Duerinckx AJ, Urman MK. Two-dimensional coronary MR angiography: analysis of initial clinical results. Radiology 1994;193:731-8.
5. Moshage WE, Achenbach S, Seese B, Bachmann K, Kirchgeorg M. Coronary artery stenoses: three-dimensional imaging with electrocardiographically triggered, contrast agent-enhanced, electron-beam CT. Radiology 1995;196:707-14.
6. Chernoff DM, Ritchie CJ, Higgins CB. Evaluation of electron beam CT coronary angiography in healthy subjects. AJR Am J Roentgenol 1997;169:93-9.
7. Li D, Kaushikkar S, Haacke EM, et al. Coronary arteries: three-dimensional MR imaging with retrospective respiratory gating. Radiology 1996;201:857-63.
8. Judkins MP. Selective coronary arteriography. I. A percutaneous transfemoral technic. Radiology 1967;89:815-24.
9. Austen WG, Edwards JE, Frye RL, et al. A reporting system on patients evaluated for coronary artery disease. Report of the Ad Hoc Committee for Grading of Coronary Artery Disease, Council on Cardiovascular Surgery, American Heart Association. Circulation 1975;51:5-40.
10. Ney D, Fishman E, Magid D. Volumetric rendering of computed tomography data: principles and techniques. Comput Graphics Applications 1990;10:24-32.
11. Rensing BJ, Bongaerts AH, van Geuns RJ, van Ooijen PM, Oudkerk M, de Feyter PJ. Intravenous coronary angiography using electron beam computed tomography. Prog Cardiovasc Dis 1999;42:139-48.
12. Johnson PT, Heath DG, Kuszyk BS, Fishman EK. CT angiography with volume rendering: advantages and applications in splanchnic vascular imaging. Radiology 1996;200:564-8.
13. Schmermund A, Rensing BJ, Sheedy PF, Bell MR, Rumberger JA. Intravenous electron-beam computed tomographic coronary angiography for segmental analysis of coronary artery stenoses. J Am Coll Cardiol 1998;31:1547-54.
14. Budoff M, Oudiz R, Zalace C, et al. Intravenous three-dimensional coronary angiography using contrast enhanced electron beam computed tomography. J Am Coll Cardiol 1997;29:393A.
15. Achenbach S, Moshage W, Bachmann K. Detection of high-grade restenosis after PTCA using contrast-enhanced electron beam CT. Circulation 1997;96:2785-8.
16. Achenbach S, Moshage W, Ropers D, Nossen J, Daniel WG. Value of electron-

beam computed tomography for the noninvasive detection of high-grade coronary-artery stenoses and occlusions. N Engl J Med 1998;339:1964-71.
17. Rensing BJ, Bongaerts A, van Geuns RJ, van Ooijen P, Oudkerk M, de Feyter PJ. Intravenous coronary angiography by electron beam computed tomography: a clinical evaluation. Circulation 1998;98:2509-12.
18. Wang Y, Rossman PJ, Grimm RC, Riederer SJ, Ehman RL. Navigator-echo-based real-time respiratory gating and triggering for reduction of respiration effects in three-dimensional coronary MR angiography. Radiology 1996;198:55-60.
19. Post JC, van Rossum AC, Hofman MB, Valk J, Visser CA. Three-dimensional respiratory-gated MR angiography of coronary arteries: comparison with conventional coronary angiography. AJR Am J Roentgenol 1996;166:1399-404.
20. Muller MF, Fleisch M, Kroeker R, Chatterjee T, Meier B, Vock P. Proximal coronary artery stenosis: three-dimensional MRI with fat saturation and navigator echo. J Magn Reson Imaging 1997;7:644-51.
21. Huber A, Nikolaou K, Gonschior P, Knez A, Stehling M, Reiser M. Navigator echo-based respiratory gating for three-dimensional MR coronary angiography: results from healthy volunteers and patients with proximal coronary artery stenoses. AJR Am J Roentgenol 1999;173:95-101.
22. Sandstede JJ, Pabst T, Beer M, et al. Three-dimensional MR coronary angiography using the navigator technique compared with conventional coronary angiography. AJR Am J Roentgenol 1999;172:135-9.
23. Woodard PK, Li D, Haacke EM, et al. Detection of coronary stenoses on source and projection images using three-dimensional MR angiography with retrospective respiratory gating: preliminary experience. AJR Am J Roentgenol 1998;170:883-8.
24. Stuber M, Botnar RM, Danias PG, et al. Double-oblique free-breathing high resolution three-dimensional coronary magnetic resonance angiography. J Am Coll Cardiol 1999;34:524-31.
25. Stuber M, Botnar RM, Danias PG, Kissinger KV, Manning WJ. Submillimeter three-dimensional coronary MR angiography with real-time navigator correction: comparison of navigator locations. Radiology 1999;212:579-87.
26. Danias PG, McConnell MV, Khasgiwala VC, Chuang ML, Edelman RR, Manning WJ. Prospective navigator correction of image position for coronary MR angiography. Radiology 1997;203:733-6.
27. Jhooti P, Wiesmann F, Taylor AM, et al. Hybrid ordered phase encoding (HOPE): an improved approach for respiratory artifact reduction. J Magn Reson Imaging 1998;8:968-80.
28. Wielopolski P, vanGeuns R, deFeyter P, Oudkerk M. Breath-hold Coronary MR Angiography with Volume Targeted Imaging. Radiology 1998;209:209-219.
29. Anzai Y, Prince MR, Chenevert TL, et al. MR angiography with an ultrasmall superparamagnetic iron oxide blood pool agent. J Magn Reson Imaging 1997;7:209-14.
30. Lauffer RB, Parmelee DJ, Dunham SU, et al. MS-325: albumin-targeted contrast agent for MR angiography. Radiology 1998;207:529-38.

Part 4

Supplement on MRI of the Thoracic Arteries

Chapter 18

Technical Aspects of Magnetic Resonance Imaging for Thoracic Aorta Disease

R.J.M. van Geuns, H.G. de Bruin, P.M.A. van Ooijen,

M. Oudkerk, P.J. de Feyter.

Submitted

ABSTRACT

Magnetic Resonance (MR) imaging is well suited for evaluation of the thoracic aorta. Although the initial techniques, spin-echo and gradient-echo imaging, produced relatively reliable images, second generation special MR angiography techniques, as time-of-flight and phase-contrast angiography, were developed but did not dramatically improve imaging of the thoracic aorta. Recently a new MR angiography technique, with intravenous injection of a MR contrast agent, has been introduced. This technique allows the acquisition of large, high resolution, three-dimensional (3D) volumes within 20-30 seconds during breath-holding. The 3D datasets acquired can be evaluated with different post processing techniques, as multiplanar reformatting (MPR), maximum intensity projection (MIP) and volume rendering (VR) techniques. The last two produce a 3D impression on 2D-surfaces. In this article we will review these techniques and their clinical applications on MR of the thoracic aorta.

INTRODUCTION

Magnetic Resonance (MR) imaging is well suited for the evaluation of the thoracic aorta. Aside from being noninvasive, MR imaging can provide large-field-of-view images in any number of planes for optimal evaluation of important anatomic relationships. Spin-echo and gradient-echo (cine) imaging are frequently used in the clinical setting. In general these are 2D techniques without background suppression and therefore not suited for evaluation with 3D post processing techniques. Special MR angiography techniques, as time-of-flight and phase-contrast angiography, have been developed but are not optimal for angiography of the thoracic aorta, due to long acquisition time and possible artifacts. Contrast-enhanced three-dimensional (3D) MR-angiography has been introduced recently for faster and less artifacted MR angiography. This technique is very well suited for postprocessing techniques including multiplanar reformatting (MPR), maximum intensity projection (MIP) and volume rendering (VR) for preparing 3D representations on a two-dimensional viewing surface. The combination of this new acquisition technique and special postprocessing techniques has shown to be able to diagnose aortic coarctation, aortic aneurysm and dissection.[1,2] In this article we will summarize present MR acquisition techniques and give an introduction to subsequent different postprocessing tools.

IMAGE ACQUISITION

T1- weighted spin-echo imaging or "Black blood imaging"

Spin-echo (SE) imaging was the first clinically used MR technique. After excitation by a 90° radiofrequency-pulse (RF-pulse) a 180° RF-pulse is applied to rephase the spinning atoms which will form the echo signal after a comparably long time (= echotime = TE) (figure 1). Because there is a certain time between the two RF-pulses, there will be a washout of flowing blood from the imaging plane and hence blood will appear black in the images. Slowly moving blood can be excited by both RF-pulses, thus producing an echo-signal, and hence be gray or white in the image (figure 2). The next signal can only be acquired after the atoms are realigned in their original position, depending on tissue characteristics, in cardiac imaging usually on the next RR interval (time of repetition (TR) = 1000 ms). For an image with 256 × 256 pixels, 256 heartbeats, approximately 3 minutes, are necessary. This sequence is still one of the most frequently used techniques because it provides excellent structural detail of the heart with high contrast between blood and surrounding tis-

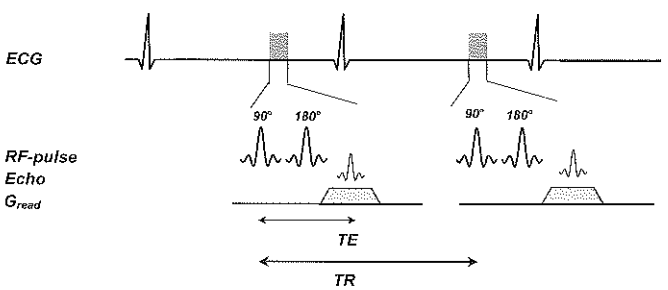

Figure 1. *In spin-echo imaging an echo signal is produced a short time (echotime (TE)) after the application of a 90° RF-pulse excitation by a 180° rephasing RF pulse. For cardiac spin-echo imaging every RR interval one echo is produced, an image with 256 lines will be collected in 256 heartbeats (3 minutes). TE = Echo Time, TR = Repetition Time. Gread = Gradients applied during acquisition of the echo signal for spatial encoding.*

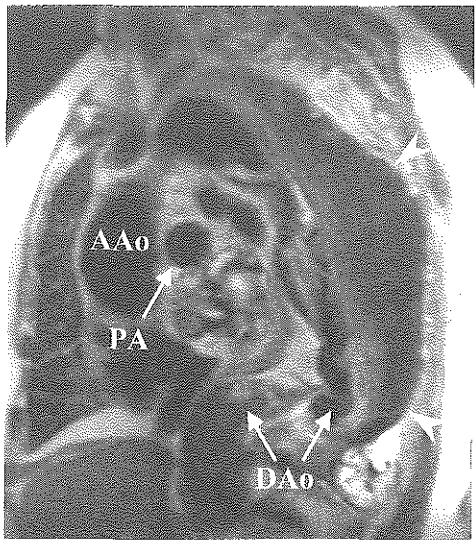

Figure 2. *Example of spin-echo MRI in patient with an aneurysm of the descending aorta (DAo). The normal flowing blood in the ascending aorta (AAo) and pulmonary artery (PA) is black, while the mural thrombus and slow flowing blood in the descending aorta produce some signal and therefore is gray in the image (arrow heads).*

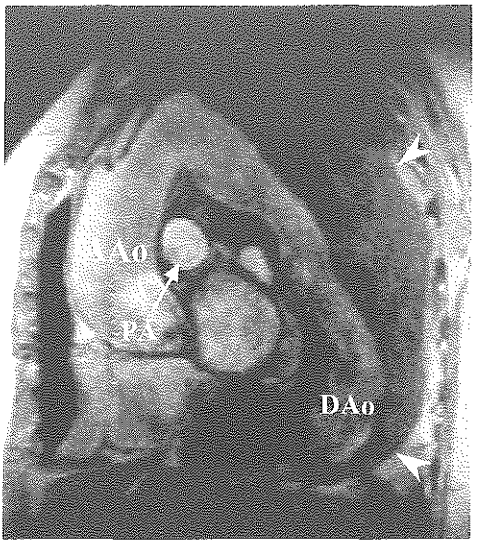

Figure 4. *Example of gradient echo MR imaging in patient with an aneurysm of the descending aorta (DAo). With this technique blood will appear bright in the images, although slow flowing blood may be saturated and have the same intensity as thrombus (arrowheads). Reviewing the images from different phases of the cardiac cycle allows differentiation of slow flowing blood from mural thrombus. Same patients as in figure 2, using a slightly different slice possition.*

sue as vascular wall and endocardial surface. It has a high sensitivity and specificity for the detection of aortic dissection.[3]

Cine MR techniques or Gradient echo sequences: "Bright blood imaging"

In gradient echo (GE) imaging the rephasing of the atoms is accomplished with a 180° switch of the magnetic gradients instead of a second RF-pulse (of 180°). In this technique the first RF-pulse is not necessarily a 90° pulse, but can be less, for example a flip angle of 15°. The atoms will then be realigned in their original position sooner, allowing faster repetition of the RF pulses. Frahm et al.[4,5] were able to collect an image

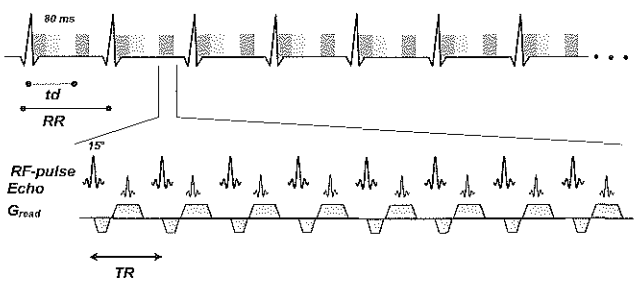

Figure 3. *In gradient echo MR imaging the echo is formed with the combination of a small (15°) flip angle excitation RF-pulse and a 180° switch of the magnetic gradient system (G_{read}). For the purpose of illustration only 4 different phases are acquired in the RR-interval in this example. During each phase 8 echo's are acquired in 80 ms by switching the gradient system shortly after a RF pulse. A maximum of 12 phases during one RR-interval can be acquired so that a complete dynamic image can be acquired within 16 heartbeats obtained during one breath-hold.*

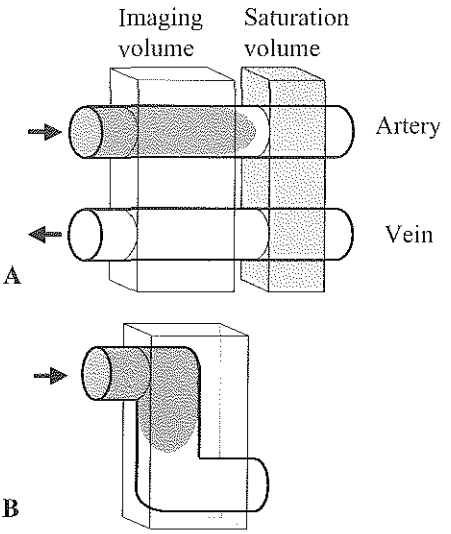

Figure 5. *(A) Time-of-Flight MR-angiography. The signal of blood will be bright as in any gradient echo sequence. With the use of short repetition and large flip angle signal from stationary tissue is suppressed while the signal from blood can be maintained by the inflow of unsaturated blood. The use of a saturation volume at the venous inflow site of the can be used to suppress venous signal.* ***(B)*** *ToF MR-angiography with inplane course of the vessel. Due to saturation now occurring the signal from blood loses its brightness.*

of 64 lines in 1.3s using a flip angle of 15° and a TR of 20 ms. They called this sequence: FLASH (Fast Low Angle Shot). The gradient switch will rephase all the atoms that have been excited by the RF-pulse, even moving blood, showing the vessels bright in distinction to SE-imaging. With the use of an even shorter TR of 10 ms 8 image lines can be acquired in 80 ms, so the RR interval, at heart rate of 60 bpm (RR interval = 1000 ms), can be divided in 12 different phases. The complete images (matrix 128 × 256) of these 12 phases can be acquired in 16 heartbeats (figure 3). Thus respiratory artifacts or degradation of image quality can be eliminated with this technique by breathholding. This technique is frequently applied for assessment of LV-function and the detection of valvular disease. In MR of the thoracic aorta cine MR imaging can demonstrate intravascular defects as thrombus (figure 4) and intimal tears more reliable than SE imaging[6,7]

Time of flight angiography

The basic idea of time-of-flight (ToF) MR-angiography depends on the inflow of blood into the image volume. Blood will be bright as in any gradient echo technique, but surrounding tissue can be suppressed (saturated) by a very rapid repetition of the RF-pulses, while the signal of blood will constantly be maintained by the inflow of new (unsaturated) blood (figure 5A). The flow signal from the veins can be sufficiently removed by the application of additional saturation pulses which are applied at the venous inflow site of the volume. The volume which can be visualized in one scan depends on several factors in which blood flow velocity is very important.

Artifacts may arise from slowly moving blood or an inplane course of the vessel (figure 5B). Acquisition time for a volume with ToF-angiography is dependent on many factors including TR. In ToF-angiography shortness of TR is limited because it leads to saturation of blood and thus rather long acquisition times are necessary. With long acquisition time this technique was mainly used in peripheral vascular disease.[8,9]

Phase contrast MR angiography

A different class of MR angiography techniques is based on the change in the phase of the rotation of the atoms around their axis. A phase shift occurs when the spinning atoms move along the magnetic field gradients (figure 6). These atoms can be differentiated from stationary tissue without a phase shift. The flow induced phase shift can be used for imaging and flow quantification techniques. To determine flow in all directions the sequence has to be repeated with gradients along the X-, Y- and Z-axis. This triples the acquisitions time, decreasing its

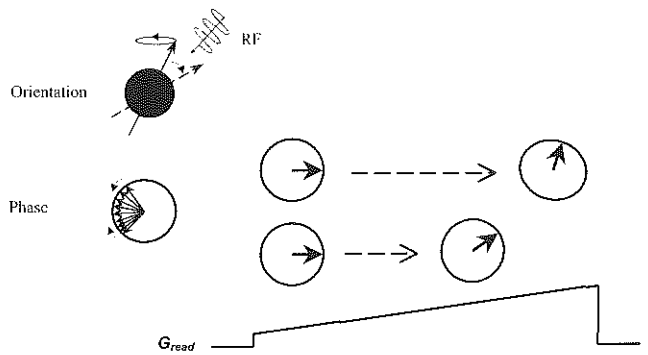

Figure 6. *Phase contrast angiography. A phase shift occurs when spinning atoms move along the magnetic field gradients. An image can be reconstructed in which the moving atoms are differentiated from stationary tissue without a phase-shift.*

use in clinical practice. This technique is insensitive to artifacts from inplane or slowly flowing blood such as known in ToF-angiography.[10]

Three-dimensional gadolinium enhanced MR-angiography (Contrast enhanced ToF-angiography)

With the use of a T1 shortening contrast agent (such as Gadolinium-DTPA) the rate of repetition of the RF pulses can be further increased without saturation of the blood. This also induces more saturation of the background signal, and thus the contrast-to-noise ratio is increased. With proper selection of the acquisition window the signal from the arterial phase can be selectively enhanced. The arterial phase is determined from the circulation time which is measured with a test injection of contrast agent. With the present MR hardware a volume of 40 × 45 × 15 cm, with a resolution 2.7 × 1.3 × 1.2mm can be acquired in 20 to 30 seconds.[11-14] This seems an ideal technique to cover the thoracic aorta over its full length in a single breathhold. This 3D dataset can be evaluated with different postprocesing techniques, including 3D reviewing techniques.

IMAGE EVALUATION

One of the main problems after acquisition of a 3D-data set is the presentation of the 3D content onto 2D display, without losing its 3D appearance. Several postprocessing techniques (rendering techniques) are available to evaluate 3D datasets on a viewing surface.

Multi Planar Reformatting (MPR)

The clinical technique most used is multiplanar reformatting (MPR) which resamples the volume data (usually along a plane) and displays the result in a separate image. In its simplest form, a single orthogonal section

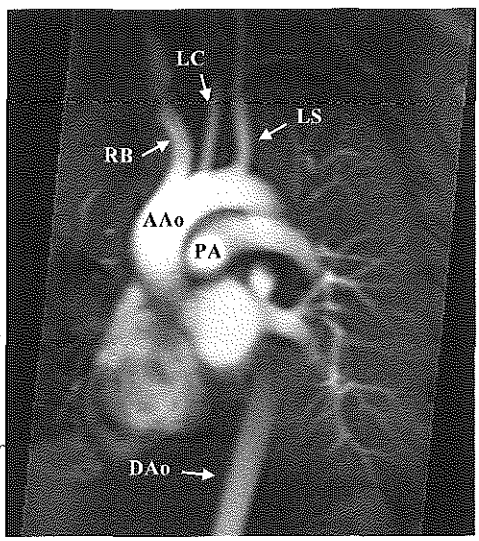

Figure 7. *Multi planar reconstruction (MPR) through the aortic arch from a dataset of 100 coronal slices. In this particula, thick slab, reconstruction the right brachiocephalic (RB), the left common carotid (LC) and the left subclavian (LS) artery can be displayed in a single image. However these vessels run out of the imaging plane after 3 cm of their origin and additional reconstructions are necessary to image these vessels in their distal course.*

through the volume is displayed. More advanced implementations which simultaneously show multiple orthogonal sections (coronal, sagittal, transversal), are able to display grey values along planes of arbitrary direction (oblique sectioning)(figure 7), or even along curved lines that can be interactively drawn. Due to the simplicity of these techniques, current workstation technology facilitates real-time display and manipulation of cut planes in volume data. MPR has proven to be useful in the detection of coarctation of the aorta with CT[15] and MR-techniques.[1] Although MPR will increase the anatomic information of the clinician the full possibilities of 3D datasets are not used. The major drawback of MPR is that only one vessel can be visualized in one image at a time and that tortuous and branching vessels are not depicted over their full length unless separate reconstructions are made for every branch. Some user interaction and care is necessary in the reconstruction process to avoid creating false-positive interpretation of the images.

Maximum Intensity Projection

In Maximum Intensity Projection (MIP) a 3D dataset is transformed to a shaded 2 dimensional projection on a viewing surface. This creates the illusion of "seeing" a 3D object. MIP is a technique which is widely used in both CT and MR angiography. In order to construct a MIP image, the volume element with the highest density value along a line extended from the viewpoint through the volume is selected to "construct" an image (figure 8). This assumes that the objects of interest have high intensities, which is not always the case. Advantages of MIP images for vascular imaging are that, in general, MIP images provide an excellent differentiation between vascular and non-vascular structures and the technique is fast compared to volume rendering (see later).

When MIP is used for vascular imaging sev-

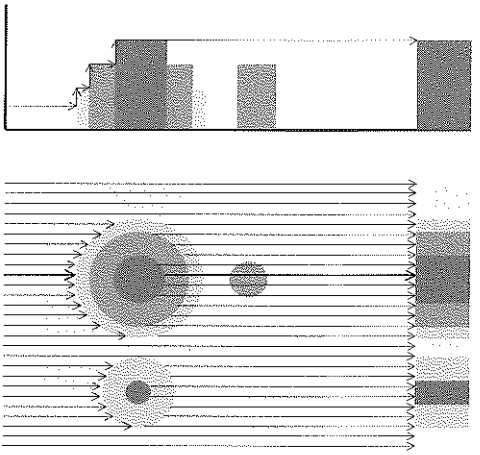

Figure 8. *Maximum intensity projection (MIP) algorithm. The brightest voxel encountered along a line from the viewer through the object is chosen as the displayed pixel value. Vessels on the same line with a lower intensity are "overruled" and thus are not imaged.*

eral artifacts may be introduced. First is the apparent reduction of vessel diameter. Because the flow of the blood is slower at the edges, the signal intensity will be decreased with flow dependent scanning techniques. Also partial volume effect at the edges of the vessels will decrease the intensity. In MIP images this may lead to the disappearing of the edge voxels due to background fluctuations. Overestimation of a stenosis can appear partly due to of local turbulence which is typical for a vascular stenosis. Small vessels may disappear completely or appear as a string of beads.

Second, the projectional nature of the MIP algorithm causes the resulting image to be three-dimensionally ambiguous, which means for instance that projections from anterior or posterior of a given volume will result in the same image. This causes loosing the sense of "depth" so that in crossing vessels no differentiation between crossing anterior or posterior can be made (figure 9). This lack of "depth" information can partially be compensated by volume rotation. The imaging object should be evaluated

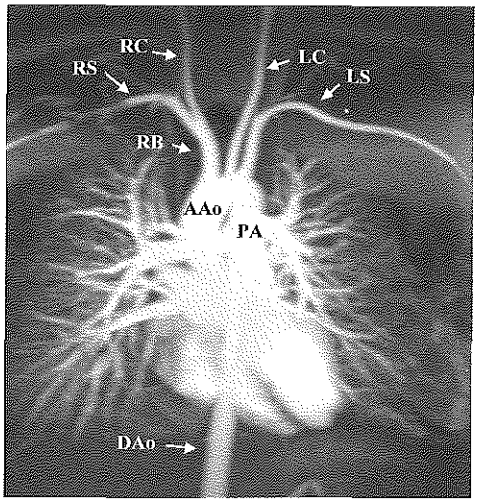

Figure 9. *Anterior view with maximum intensity projection (MIP) from the same dataset as in figure 7. The aortic arch branch vessels are now visualized over their full length within the imaging volume. In MIP no information on anterior and posterior is available. AAo = Ascending aorta, DAo = descending aorta, PA = pulmonary artery, RB = right brachiocephalic artery, RC right common cartid artery, RS = right subclavian artery, LC = left common carotid artery, LS = left subclavian artery.*

from different angles, like conventional angiography, which can easily be performed by putting together images from different orientations to create a rotating MIP movie (cine-loop).

If a higher intensity structure, for example the left ventricle, lies along the line of analysis, the resulting maximum-intensity pixel will contain no information from the contrast-enhanced vessel. These structures often need to be edited out by means of manual or automated methods.

Surface Rendering

Surface Rendering (SR) is capable of displaying three-dimensional reconstructions which can be computed on moderate computer systems (no special purpose hardware is required). Just like MIP, SR only uses about 10% of the image data to perform a 3D reconstruction. SR will, in contrary to MIP, display three-dimensional images with reasonable "depth" information, for instance clearly showing which vessel is in front and which is in the back.

With SR several preprocessing steps have to be taken to make the data ready for rendering. First, each voxel is classified as either belonging or not belonging to the object of interest. Using a threshold value all voxels below the threshold are discarded while only the voxels above are selected for the object (figure 10). This gives us an adequate description of the surface of the object of interest which is then modeled by the computer as a collection of geometric primitives (two-dimensional polygons, for example triangles or squares, used to approximate a three-dimensional surface). Only this collection of primitives is used for rendering, the rest of the data is discarded. Rendering the result can take a lot of processing time (in the order of minutes). However, after the rendering, interactive manipulation (rotation,

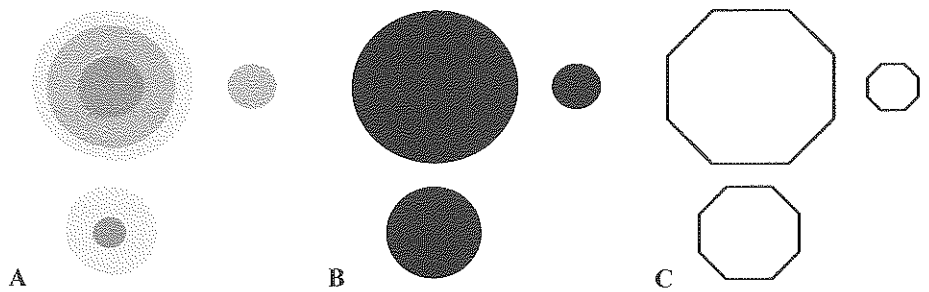

Figure 10. *Surface rendering algorithm. From the original dataset (A) the data desired are selected by thresholding (B). Using geometric primitives a simple model is created which can be visualized from different orientations*

translation, magnification) of the volume is possible. Often, a simulated light source is used to get some shading effect of the volume for a better 3D impression of the resulting image.

The downside of this method is that when the surface selection is changed, the time consuming preprocessing has to be repeated. Other limitations of surface rendering are the possible existence of false positive and/or false negative surface pieces, and the loss of minor detail due to the subdivision into surface primitives (voxels are assumed to contain only one tissue type and either belong to the object of interest or not), internal structures (like a thrombus within a vessel) cannot be displayed, and the determination of the optimal threshold is rather difficult and time-consuming. Incorrect setting of the threshold can lead to disconnected and floating vessels.

SR was the first three-dimensional rendering technique that was applied to medical images. It has frequently been used for CT-angiography.[16,17] In MR-angiography SR has been performed for the abdominal aorta and renal arteries.[18,19] Since the general use of surface coils, SR of MR-angiography is hampered by the difference of signal relating to the distance between the vessel and the surface coil. Due to this effect, the ideal threshold level is not uniform over the image.

Volume rendering

Volume rendering is a technique that retains all the voxels from the original 3D dataset during each rendering. Volume rendering algorithms sum the contributions of all voxels along a line that extends from the viewer's eye through the data volume (figure 11). This process is computationally intensive but has the advantage that no information gets lost during the process and that several additional image-processing techniques are still possible, without (unlike in SR) having to perform time consuming pre-processing

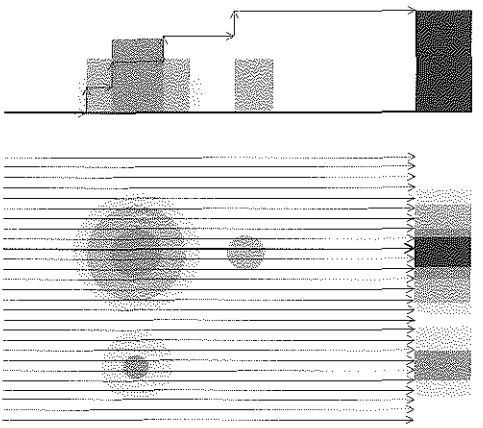

Figure 11. *Volume rendering algorithm. The values of all the voxels along a line that extends form the observer through the object of interest contribute to the resulting picture. Each tissue can be assigned a certain opacity, contributing to the total for the line.*

again. For instance each voxel can be assigned an opacity and color value. Based on these values, the intensity of each voxel is calculated and used for the display of the voxel. Volume rendering allows certain parts of the 3D object to be transparent so that structures behind it are still visible.

Volume rendering has a number of advantages over surface rendering and MIP. Because no distinct surfaces need be defined, this method is well suited for the demonstration of the ambiguous, volume-averaged edges that often appear in medical images. Because all of the data are used in the algorithm, the resulting images potentially contain more information than those created with surface rendering or MIP techniques. The ability to simultaneously display both superficial and deep structures in an image can be important in many applications. Volume rendering is often combined with depth and surface shading to give the image a very realistic sense of three-dimensionality. Volume rendered angiograms look much alike the images created with conventional catheter angiography, and may show vessel thickness,

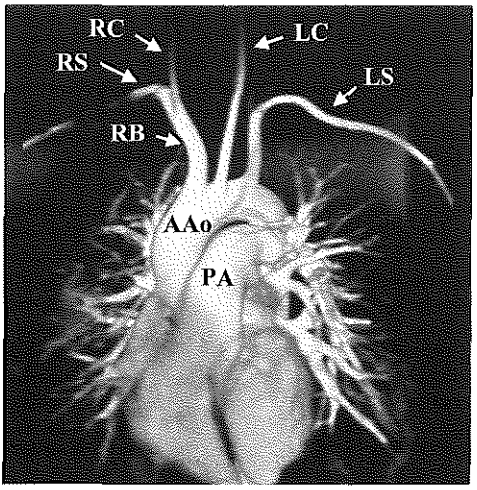

Figure 12. *Volume rendering of contrast enhanced MR-angiography from the same dataset as in figure 9. The volume rendering algorithm increases the "depth" information visible in the image. Aao = Ascending aorta, PA = pulmonary artery, RB = right brachiocephalic artery, RC right common cartid artery, RS = right subclavian artery, LC = left common carotid artery, LS = left subclavian artery.*

intraluminal features, and overlapping vasculature (figure 12). Finally, the volume-rendering algorithm itself is associated with few artifacts, although inaccurate classification of tissues before volume rendering can cause major artifacts.

Despite its numerous advantages, volume rendering also has important limitations. The final image quality depends on the segmentation of the data that are fed into the rendering algorithm. Segmentation is the process by which voxels are classified as belonging to specific objects with distinct features, such as individual organs or tumor. In volume rendering, both the segmentation and the rendering steps typically take much more computer power than either surface rendering or MIP. Very transparent volume renderings may not clearly depict distinct edges and may hinder measurements or other user interactivity such as surgical simulation programs.

CONCLUSIONS

The thoracic aorta can be evaluated with different non-invasive MR imaging techniques. Recent developments in MR technique and post-processing techniques have increased the clinical use of MR in assessing the thoracic aorta. The combination of 3D contrast enhanced MR-angiography with volume rendering as postprocessing technique gives unique detailed information of complex 3D structures such as aneurysms and dissections of the thoracic aorta.

REFERENCES

1. Krinsky GA, Rofsky NM, DeCorato DR, et al. Thoracic aorta: comparison of gadolinium-enhanced three-dimensional MR angiography with conventional MR imaging. Radiology. 1997;202:183-93.
2. Prince MR, Narasimham DL, Jacoby WT, et al. Three-dimensional gadolinium-enhanced MR angiography of the thoracic aorta. AJR Am J Roentgenol. 1996;166:1387-97.
3. Nienaber CA, von Kodolitsch Y, Nicolas V, et al. The diagnosis of thoracic aortic dissection by noninvasive imaging procedures. N Engl J Med. 1993;328:1-9.
4. Matthaei D, Frahm J, Haase A, et al. Regional physiological functions depicted by sequences of rapid magnetic resonance images [letter]. Lancet. 1985;2:893.
5. Frahm J, Haase A, Matthaei D. Rapid NMR imaging of dynamic processes using the FLASH technique. Magn Reson Med. 1986;3:321-7.
6. Hartnell GG, Finn JP, Zenni M, et al. MR imaging of the thoracic aorta: comparison of spin-echo, angiographic, and breath-hold techniques. Radiology. 1994;191:697-704.
7. Solomon SL, Brown JJ, Glazer HS, et al. Thoracic aortic dissection: pitfalls and artifacts in MR imaging. Radiology. 1990;177:223-8.
8. Bowen BC, Quencer RM, Margosian P, et al. MR angiography of occlusive disease of the arteries in the head and neck: current concepts [see comments]. AJR Am J Roentgenol. 1994;162:9-18.
9. Rofsky NM. MR angiography of the aortoiliac and femoropopliteal vessels. Magn

Reson Imaging Clin N Am. 1998;6:371-84.
10. Prince MR. Renal MR angiography: a comprehensive approach. J Magn Reson Imaging. 1998;8:511-6.
11. Leung DA, McKinnon GC, Davis CP, et al. Breath-hold, contrast-enhanced, three-dimensional MR angiography. Radiology. 1996;200:569-71.
12. Runge VM, Kirsch JE, Lee C. Contrast-enhanced MR angiography. J Magn Reson Imaging. 1993;3:233-9.
13. Revel D, Loubeyre P, Delignette A, et al. Contrast-enhanced magnetic resonance tomoangiography: a new imaging technique for studying thoracic great vessels. Magn Reson Imaging. 1993;11:1101-5.
14. Prince MR. Gadolinium-enhanced MR aortography. Radiology. 1994;191:155-64.
15. Sommer T, Fehske W, Holzknecht N, et al. Aortic dissection: a comparative study of diagnosis with spiral CT, multiplanar transesophageal echocardiography, and MR imaging [see comments]. Radiology. 1996;199:347-52.
16. Becker C, Soppa C, Fink U, et al. Spiral CT angiography and 3D reconstruction in patients with aortic coarctation. Eur Radiol. 1997;7:1473-7.
17. Zeman RK, Berman PM, Silverman PM, et al. Diagnosis of aortic dissection: value of helical CT with multiplanar reformation and three-dimensional rendering. AJR Am J Roentgenol. 1995;164:1375-80.
18. Hany TF, Schmidt M, Davis CP, et al. Diagnostic impact of four postprocessing techniques in evaluating contrast-enhanced three-dimensional MR angiography. AJR Am J Roentgenol. 1998;170:907-12.
19. Meyers SP, Talagala SL, Totterman S, et al. Evaluation of the renal arteries in kidney donors: value of three- dimensional phase-contrast MR angiography with maximum-intensity- projection or surface rendering. AJR Am J Roentgenol. 1995;164:117-21.

Chapter 19

Contrast Enhanced Three Dimensional Magnetic Resonance Angiography in Congenital and Acquired Disease of the Great Thoracic Vessels

R.J.M. van Geuns, H.G. de Bruin, P.M.A. van Ooijen, S.E. Spitaels,

A.J.J.C. Bogers, P.W. Serruys, M. Oudkerk, P.J. de Feyter.

Submitted

ABSTRACT

Background:

Nowadays two-dimensional magnetic resonance imaging (2D-MRI) has become a widely accepted tool for imaging of the great thoracic vessels. Recently intravenously contrast enhanced three-dimensional magnetic resonance angiography (3D-MRA) has been introduced to acquire large, high resolution, volumes of the aorta within 20-30 seconds. The objectives of this study were to determine both the diagnostic value of 3D-MRA and 3D postprocessing with volume rendering for the evaluation of congenital and acquired disease of the great thoracic vessels.

Methods and Results:

Nineteen patients were studied with conventional MR imaging techniques and contrast enhanced breath-hold 3D-MRA techniques using a three-dimensional turboFlash sequence with a resolution of $1.1 \times 1.2 \times 1.3$ mm. After manual segmentation the 3D-data sets of interest were evaluated with a volume rendering technique.

The signal-to-noise ratio (SNR) in the target vessel was significant higher compared to the systemic veins (515.1 versus 248.6, $p < 0.01$). No difference in SNR between the pulmonary arteries, pulmonary veins, and thoracic aorta was present. All the acquired and congenital abnormalities of the thoracic aorta including the main branches and the pulmonary artery and its branches were clearly visualized in the volume rendered images of the contrast enhanced 3D-MRA data. Identification of these abnormalities was confirmed by conventional imaging techniques or at surgery.

Conclusions:

Contrast enhanced 3D-MRA allows visualization of the thoracic aorta and pulmonary arteries. Evaluation with three-dimensional post-processing by volume rendering provides a unique three-dimensional insight into complex thoracic vascular structures.

INTRODUCTION

Magnetic Resonance (MR) imaging is a versatile technique characterized by its non-invasiveness, easily repeatability, large field of view and any plane imaging. Conventional two-dimensional (2D) MR imaging with spin-echo and gradient-echo techniques is a widely accepted accurate technique to assess thoracic aorta abnormalities.[1-3] However 2D-images are sometimes difficult to interpret in particular when the underlying vascular pathology is complex. Recently, upgraded faster MR-systems have made it possible to perform breath-hold three-dimensional magnetic resonance angiography (3D-MRA) without loss of spatial resolution. The acquired 3D-datasets are usually postprocessed with multiplanar reformatting (MPR) or maximum intensity projection (MIP). These techniques, although powerful, provide limited diagnostic information because they use only a part of the available information in the dataset and the 2D display of MIP and MPR makes the interpretation of complex anatomy often difficult. The recent introduction of volume rendering, a technique which uses all the information available in the 3D-dataset, allows a more comprehensive interpretation of complex 3D anatomy. The objectives of this study were to evaluate the diagnostic reliability of breath-hold contrast enhanced 3D-MRA and volume rendering for the assessment of congenital and acquired disease of the great thoracic vessels.

MATERIALS AND METHODS

The study population consisted of nineteen patients (8 males, 11 females; mean 37.0 years of age, range 17 to 76 years, 71.2 kg) who underwent evaluation of congenital or acquired disease of the great vessels with MR imaging. Eight patients were evaluated for a congenital abnormality of the aorta, four patients had prior surgery of the pulmonary artery to correct complex congenital disease. The remaining seven patients had acquired disease of the aorta including four aneurysms, one atherosclerotic stenosis, one Marfan's disease, one Ehlers-Danlos disease.

Subjects were studied in a supine position, with a four channel quadrature body phased array coil placed over the thorax, in a 1.5 T whole body MR imaging system (Vision; Siemens, Erlangen, Germany). Maximum gradient strength was 25 mT/m with a rise time of 300 ms.

Patients were not studied if they had an artificial pacemaker, intracranial clips or severe claustrophobia. The protocol was approved by our hospital committee of medical ethics and clinical investigation and informed consent was obtained before the examination.

Study protocol

After the patient was positioned with the aortic root in the isocenter of the magnet, scout views were obtained. Conventional 2D MR imaging was performed with both spin-echo techniques for black blood imaging and gradient-echo techniques for bright blood imaging prior to a contrast enhanced breath-hold 3D-MRA technique.

Black blood T1- weighted spin-echo imaging

In all patients axial ECG-triggered T1-weighted spin-echo MR images were obtained. In patients with aortic disease oblique fast spin-echo images were also acquired next. Typical imaging parameters for the axial ECG-triggered spin-echo MR imaging sequences were: TR equal to the RR interval, TE was 14 ms, matrix was 128-256 × 512 (phase encoding × frequency encoding) and a rectangular field of view with a maximum dimension of 30-40 cm was used to decrease acquisition time and preserve voxel size. A fast breath-hold spin-echo MR imaging sequence was used also with an

echo train length of nine and a matrix of 126 × 256. A single slice was obtained in fifteen heartbeats. Imaging parameters were: TR equal to the RR interval, TE was 32 msec. Section thickness varied from 5 to 10 mm in the axial plane and was 6 mm in the oblique sagittal or coronal plane.

Bright blood imaging cine gradient-echo imaging

Segmented k-space cine gradient-echo MR imaging without breath holding and triggered with ECG was performed with the following parameters: TR = 7.3 ms, TE = 6-8 ms, flip angle was 25-40, matrix was 128-200 × 256, field of view was rectangular with maximum dimension of 30-45 cm, three signals were acquired, and section thickness was 5 mm. Sagittal and coronal images were acquired as determined by the monitoring physician.

Contrast enhanced three-dimensional MR-angiography

Contrast enhanced 3D-MRA was performed by using an radiofrequency spoiled steady state T1-weighted 3D sequence. This sequence used asymmetric echo sampling (43%) an no flow compensation to minimize TE.

In the first 8 patients, the sequence parameter were TR/TE=4.6/1.8 ms, 30° flip angle, and 488 Hz per pixel bandwidth. Field of view was 200 × 400mm, matrix 165-195 × 512 with one signal acquired, which yielded an in-plane spatial resolution of 1.0 × 0.8 mm to 1.2 × 0.8 mm. The slab thickness was 13 cm using 32 partitions, 64 slices were reconstructed with zero filling which resulted in an effective section thickness of 2.0 mm.

In the latter 11 patients an improved sequence with the following parameter was used: TR/TE=3.65/1.60 ms, 25° flip angle, and 390 Hz per pixel bandwidth. Field of view 200 × 400 mm, matrix 180 × 512 with one signal acquired, which yielded an in-plane spatial resolution of 1.1 × 1.2 mm. The slab thickness was 13 cm with 44 partitions, the number of reconstructed sections varied between 80-100 by zero filling which yielded an effective section thickness of 1.3 to 1.6 mm. For these two sequences, k-space is acquired sequentially, which means that the central lines of k-space, which produce the contrast in the images, are acquired during the middle of the acquisition. The data sets on the aorta were acquired in sagittal direction, while the pulmonary artery images were acquired in the coronal direction

A contrast dose of 38 ml of Gadolinium-DTPA was delivered at a flow rate of 2 ml/sec intravenously with a MR-compatible power injector (Spectris; Medrad, Pittsburgh, PA, USA). The injection was flushed with 20 ml of saline solution. The time of arrival of contrast to the vessel of interest was adjusted depending on the circulation time. The circulation time was determined using a gradient-echo scan collecting 30 images at a one second interval. The power injector was used to administer a 2-mL test does of Gd-DTPA, which was immediately followed by 20 ml of saline. Gradient-echo scanning was initiated simultaneously at the onset of the test dose injection. The scans were obtained in the transversal plane through the aortic root and pulmonary artery. The image with maximal pulmonary or aortic enhancement was identified. The time between injection and peak enhancement was considered the patient's circulation time. The delay time (Tdelay) between initiation of contrast injection and initiation of scanning was calculated using a formula described by Prince et al.[4]:

$$T_{delay} = T_{circ} + T_{gad}/2 - T_{acq}/2$$

where T_{gad} is the duration of the contrast injection , and T_{acq} is the image acquisition time.

The total examination time to obtain all MR images of each subject, including positioning of the patient, scout imaging, conventional 2D and the contrast enhanced breathhold 3D-MRA was approximately one hour.

Image analysis

Source data were analyzed by a single reader, who drew regions of interest over the aortic root, ascending aorta, abdominal aorta, common pulmonary artery, superior caval vein, inferior caval vein, left atrium and noise outside the body to measure the mean and standard deviation (SD) of signal intensity. Signal-to-noise ratio (SNR) was defined as the ratio of mean signal in the vessel to the SD of signal in the air (noise) anterior to the chest. The target vessel was considered the aorta or the pulmonary artery, depending on the indication for the MR study. The non-targeted vessel was the pulmonary artery for aorta studies and the aorta in pulmonary artery studies.

Semi-quantitative evaluation was performed by two readers blinded to all clinical information in a joint session. For this part of this study, the aorta and pulmonary artery were divided into the following segments: aortic root, ascending aorta, aortic arch, abdominal aorta, common pulmonary artery, left pulmonary artery and right pulmonary artery. Motion and ghost artifacts were scored using the following scale: 0 = none, mild = 1, moderate = 2 and severe = 3. Aortic enhancement in each segment was graded using the following scale, excellent = 3, good = 2, some = 1, and none (similar to background) = 0. For comparison the enhancement of the superior and inferior caval vein was evaluated with the same scale.

Three-dimensional image evaluation

The contrast enhanced 3D-MRA studies were retrospectively evaluated in a joint session by a cardiologist and radiologist in a random order at least 2 months after the initial clinical evaluation of the conventional 2D techniques. The 3D-MRA data sets were transferred to a stand alone dedicated graphic workstation (Indigo2, Silicon Graphics, Mountain View, Calif, USA) for three dimensional evaluation with a volume rendering technique[5-7] using commercially available software (VoxelView, Vital Images Inc, Minneapolis, Minn, USA). The pulmonary vessels or the aorta were selected by manual segmentation, which required 10 to 15 minutes for each data set.

In the volume rendering technique, all image pixels are integrated to project a three dimensional data set as a single 2D-image. A certain opacity is assigned to every pixel based on its intensity value in the dataset. A projection line will pass through all the pixels from back to front and calculate a combined value of all intensities and opacities of the pixel on that line to project on the screen. The opacity for certain structures will improve the three dimensional impression of image. The datasets can be rotated in every direction for optimal visualization of the major thoracic vessels. The two readers reviewed the 3D reconstructions of the 3D-MRA studies together with the original axial slices of the 3D-MRA studies.

Confirmation of diagnosis

The 3D-MRA study diagnosis was correlated with either conventional imaging modalities or confirmation during actual surgery. Conventional imaging modalities included conventional angiography, CT angiography or conventional spin-echo and gradient-echo MR imaging.

Statistical analysis

All values are expressed as mean ± standard deviation. For continuous results the paired, two-tailed Student t-tests was calculated. For non-continuous results a nonparametric Wilcoxon's singed rank test for related samples was calculated using commercial-

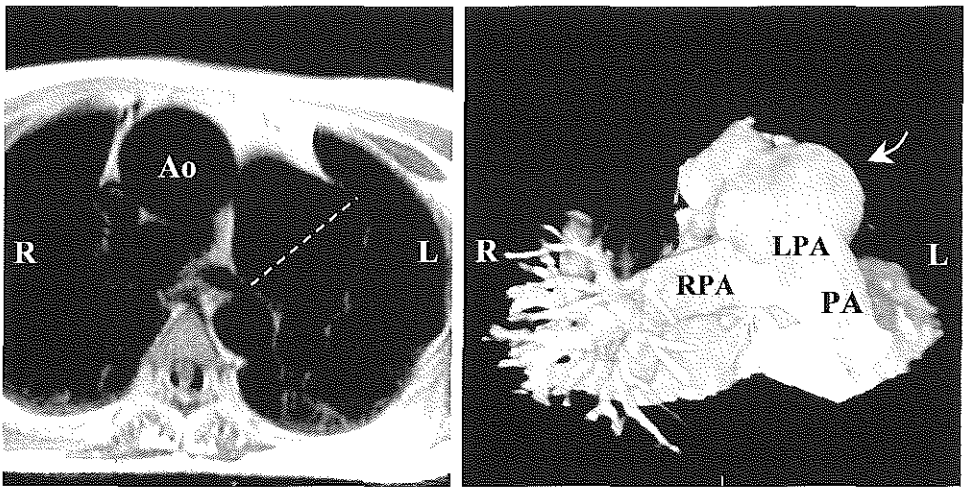

Figure 1. *(A) Conventional Spin-echo image of a patient with a Potts anastomosis between the aorta (Ao) and the left pulmonary artery (PA). Due to the turbulent flow through the anastomoses an aneurysm of 6 cm has developed in the left pulmonary artery.* ***(B)*** *Contrast enhanced 3D-MRA study of the same patient. In a single breath-hold a full 3D dataset of the pulmonary artery can be obtained. Besides the aneurysm (curved arrow) in the left pulmonary artery (LPA) a stenosis is visible in the proximal right pulmonary artery (RPA, straight arrow). For optimal visualization the aorta is removed by manual segmentation from the data set. Right anterior cranial view.*

ly available software (SPSS version 8.0, Statistical Package for the Social Sciences, Chicago , Il, USA). A threshold value of $p < 0.05$ was used to assign statistical significance.

RESULTS

Contrast timing for the pulmonary artery was 5.0 ± 1.9 sec and for the aorta 10.2 ± 3.1 sec. In patients with severe right to left shunt no difference was observed. In all patients the 3D-MRA was performed successfully. The mean acquisition time for the 3D-MRA study was 22.2 ± 3.3 seconds. Contrast enhancement was excellent or good in 18 of the 19 patients (excellent in 15, good in 3). In one patient contrast enhancement was only moderate due to an incorrect timing of the

Table 1. Quantitative and semi-quantitative image analysis.

	Artifacts	Enhancement	Signal intensity	Signal-to-noise ratio
Aortic root	0.95±0.78	2.79±0.42	475.5±403.1	43.4±23.8
Ascending aorta	0.26±0.45	2.74±0.56	506.5±476.1	45.6±26.1
Aortic arch	0.00±0.00	2.63±0.76	-	-
Descending aorta	0.11±0.32	2.89±0.32	488.7±471.3	42.3±23.1
Abdominal aorta	0.00±0.00	2.79±0.54	467.9±431.2	38.1±18.4
Pulmonary artery	0.47±0.51	2.63±0.76	471.8±450.2	41.9±26.1
Left Atrium	1.21±0.83	2.69±0.58	474.3±430.9	41.0±21.5
Superior caval vein	0.35±0.46	0.79±0.63	248.6±202.1	22.3±13.7
Inferior caval vein	0.56±0.51	0.68±0.58	230.4±206.4	18.6±10.6
Target vessel	0.32±0.48	2.79±0.54	515.1±456.8	47.5±28.8
Non-target vessel	0.42±0.51	2.58±0.77	514.5±479.9	46.9±28.0

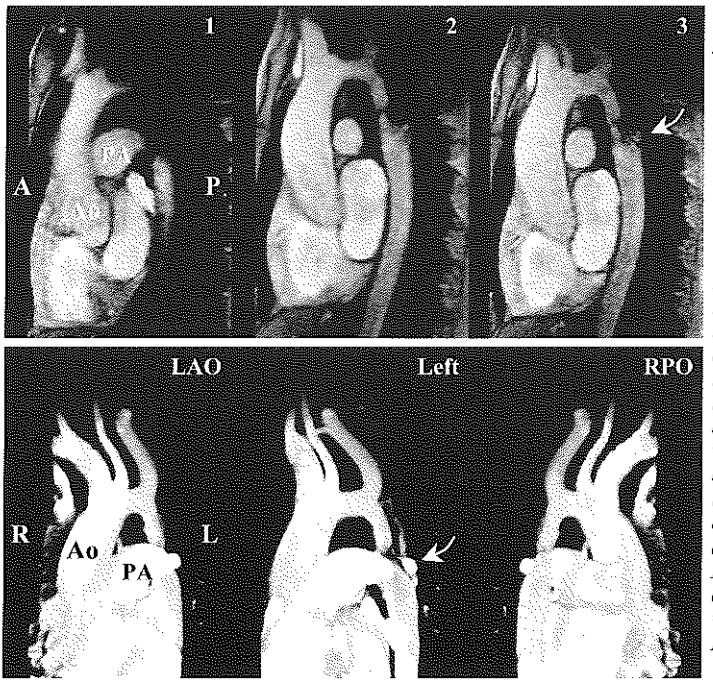

Figure 2. *Twenty-seven year old patient with prior surgery for coarctation of the aorta.* ***(A)*** *In conventional gradient-echo imaging, three parallel datasets are necessary to cover the complete coarctation site.* ***(B)*** *Contrast enhanced 3D-MRA covers the entire thoracic aorta in a single breathhold. With volume rendering this dataset can be reviewed off-line from different orientations and the coarctation site can be localized easily (straight arrow). In the left sided view (middle image) the collateral circulation (curved arrow) can be recognized easily. LAO = left anterior oblique view; RPO = right posterior oblique view; R = Right; L = Left; Ao = Aorta; PA = Pulmonary artery.*

contrast bolus. The use of a short contrast bolus resulted in only a moderate enhancement of the superior and inferior caval vein by the contrast agent (0.79 versus 2.74 for the ascending aorta, $p < 0.01$)(Table 1). Motion and ghost artifacts in the aortic root were larger compared to the ascending aorta (mean 0.95, versus 0.26, $p < 0.01$).

In the quantitative analysis the signal intensities and SNR of the blood in the aorta, pulmonary arteries and the left atrium were significant higher compared to the systemic veins. Between the different segments of the aorta and the pulmonary artery no significant difference in signal intensity and SNR was present. Although a shorter delay time was used for the targeted imaging of the pulmonary artery then for the aorta no significant difference in signal intensity and SNR between the target and non-target vessel was present in the data.

All acquired and congenital abnormalities of the thoracic aorta and pulmonary artery and its branches were clearly visualized with 3D-MRA. The diagnosis from 3D-MRA corresponded with the conventional imaging modalities or was confirmed during surgery. The results of all patients are listed in Table 2. The use of volume rendering to evaluate 3D-MRA studies of the aorta and pulmonary artery from different viewing angles is shown in Movie 1. Figure 1 and Movie 2 illustrate an example from the group of patients with congenital cardiac disease and prior surgery of the pulmonary artery. A typical example of a patient with a congenital aortic abnormality is shown in Figure 2. From the group of patients with acquired aortic disease an example is shown in Figure 3. Figure 4 illustrates the differences in post-processing with MPR, MIP and volume rendering. Figure 5 demonstrates the advantages of post-processing with volume rendering in congenital abnormalities of the aortic arch.

DISCUSSION

Contrast enhanced 3D-MRA acquisition

Conventional unenhanced MR imaging of the aorta performed with 2D spin-echo and

Table 2. Study population and results.

	Gender	Age	Diagnosis	Result	Confirmation
Pulmonary artery					
1	F	18	Fontan circulation	Normal pulmonary arteries	Conventional MR
2	M	17	Double outlet RV	Pulmonary artery stenosis	Surgery
3	M	40	Tetralogy of Fallot	Normal pulmonary vessels Mirror aortic arch	Conventional MR
4	F	57	Tetralogy of Fallot	Aneurysm left pulmonary artery, Ø 6 cm	Surgery
Congenital aortic abnormality					
5	M	29	Aortic coarctation?	No coarctation Tortuous aortic arch	Conventional MR
6	M	29	Aortic arch abnormality	Right sided aortic arch Aberrant left subclavian	Conventional MR
7	M	18	Aortic coarctation?	Severe coarctation Abundant collaterals	Surgery
8	M	37	Follow-up aortic coarctation	Long slight stenosis	Conventional MR
9	F	22	Follow-up aortic coarctation	Good post-operative result Cervical aortic arch	Conventional MR
10	F	27	Follow-up aortic coarctation	Restenosis, length 5 cm	Surgery
11	F	26	Follow-up aortic coarctation	Good post-operative result	Conventional MR
12	F	18	Follow-up aortic coarctation	Good post-operative result left subclavian from vertebral artery	Conventional MR
Acquired aortic disease					
13	F	61	Atherosclerotic aortic	Sever stenosis aortic arch arch stenosis	CT angio
14	F	64	Aneurysm ascending and descending aorta	Arch vessels not involved Ascending aorta: Ø 6.9 cm Aberrant right subclavian artery	Angio
15	F	29	Ehlers-Danlos	No aortic aneurysm	Conventional MR
16	F	25	Marfan's disease	Aneurysm non-coronary cusp	Angio
17	F	73	Aneurysm descending aorta	Arch vessels not involved, Ø 8 cm	Angio
18	M	76	Aneurysm aortic arch	Left carotid artery and subclavian from aneurysm Ø 9 × 7.7 cm	Angio
19	M	36	Aneurysm descending aorta	Arch vessels not involved, Ø 6 cm, mural thrombus	Angio

RV = Right Ventricle
MR = Magnetic Resonance
CT = Computed Tomography

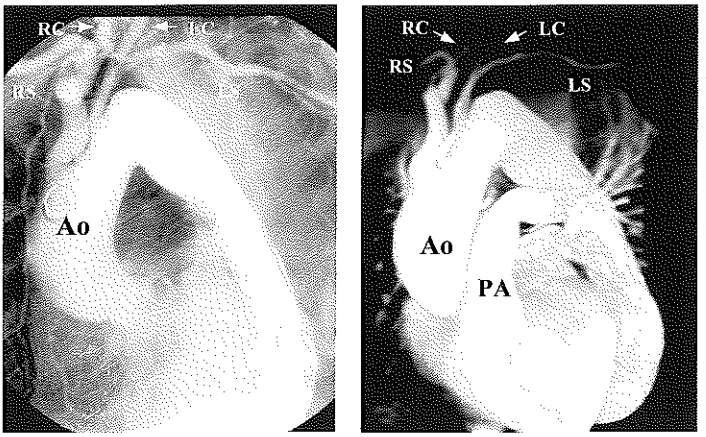

Figure 3. *(A) Conventional angiogram of a patient with an aneurysm of the ascending aorta.* ***(B)*** *Contrast enhanced 3D-MRA of the thoracic aorta (Ao) and pulmonary artery (PA). RC = Right common carotid artery, RS = Right subclavian artery, LC = Left common carotid artery, LS = Left subclavian artery.*

gradient-echo acquisitions has inherent limitations associated with the signal properties of flowing blood. In spin-echo imaging slow flow reduces the contrast between lumen and vessel wall thus underestimating real diameters, whereas in gradient-echo imaging blood flow turbulence due to a stenosis reduces the signal intensity thereby overestimating the severity of that stenosis. Contrast enhanced MRA overcomes these problems because the image contrast is predominantly derived from the T1-shortening effect of Gadolinium and therefore is only minimally degraded by flow-related artifacts. Initially contrast enhanced MRA required between two and three minutes for a 3D

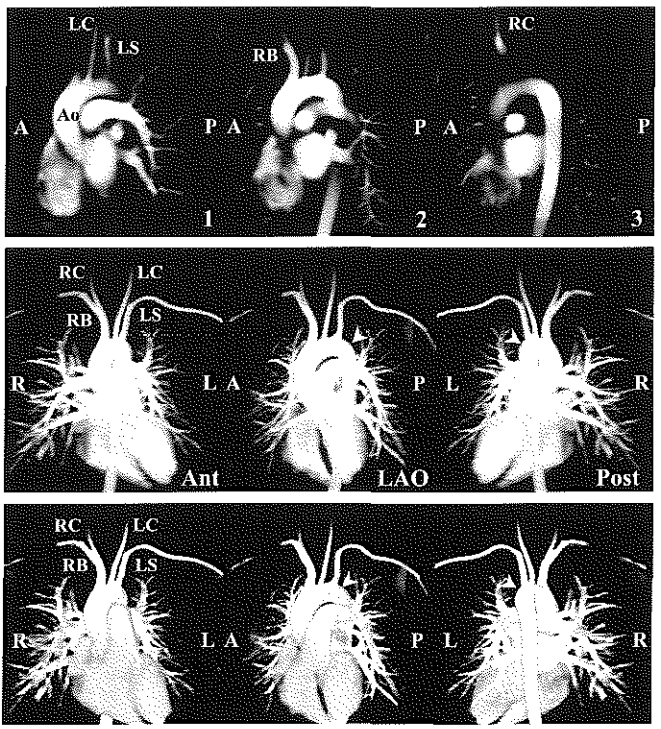

Figure 4. *Different post processing techniques for contrast enhanced 3D-MRA of a normal thoracic aorta.* ***(A)*** *Multiplanar reconstructions: multiple parallel slices are reconstructed to cover the whole aortic arch and it's branches. The left common carotid artery (LC) and left subclavian artery (LS) are best visualized in the first slice, the right brachiocephalic artery (RB) in the second and the right common carotid artery in the third slice.* ***(B)*** *Maximum intensity projection. Although the branch vessels can be visualized in a single image, due to the limited depth information the anterior (Ant) and posterior view (Post) of the same data set seem only mirrored images where the actual position of the descending aorta (arrow head) can not be determined.* ***(C)*** *Volume rendered image of the same patient illustrating the improved depth information compared to the MIP image. In these images the descending aorta can easily be recognized (arrow head).*

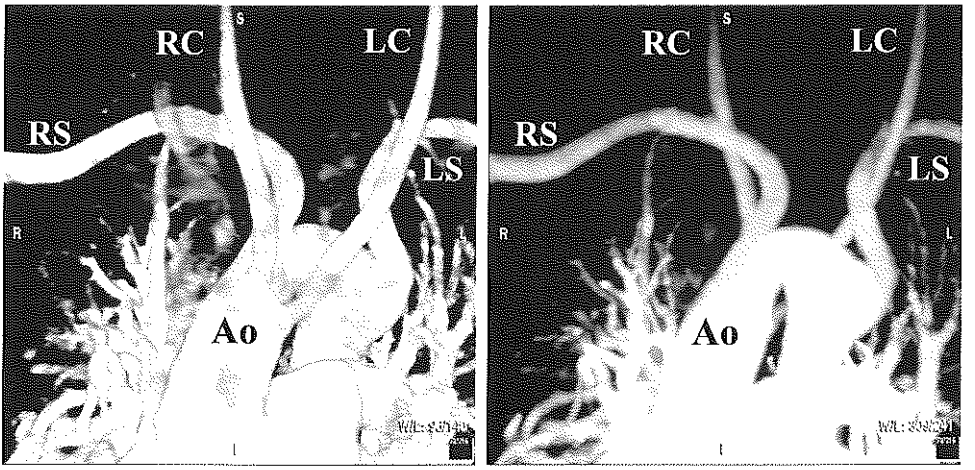

Figure 5. *Patient with a right sided aortic arch (Ao) with the left subclavian artery (LS) from the descending aorta. The volume rendered image* ***(A)*** *gives move depth information compared to the MIP image* ***(B)****. RS = Right subclavian artery, RC = Right common carotid artery, LC = Left common carotid artery.*

study with a continuous infusion of a contrast agent. Although only moderate enhancement was achieved and respiratory motion artifacts were present abdominal aneurysms, renal artery stenosis and thoracic artery disease were diagnosed. With present faster MR-systems a 3D study can be performed in 20 to 30 seconds which allows breath-holding to eliminate the respiratory motion artifacts. Now this technique is very useful for evaluation of a variety of pathology of the great thoracic vessels as shown in our patients. In addition contrast injection rates can be increased which results in an improvement of the SNR.[4,8]

Despite the advantages and possibilities of 3D-MRA some limitations should be mentioned. The contrast enhanced MRA was obtained without ECG-triggering. This allows also evaluation of patients with rhythm disturbances, but reduces the image quality of the aortic root and eliminates the ability to determine the functional impact of severe stenoses by the presence of turbulances and signal voids as present in gradient-echo imaging.

Exact timing of the contrast media arrival is crucial since sufficient T1 shortening of blood is achieved only during peak vascular concentration. Despite the use of a test bolus technique reduced enhancement of the desired vessel may appear when timing is not optimal. Real-time depiction of the bolus arrival[9] or multiphase acquisition strategies will diminish this problem.[10]

Three-dimensional image evaluation

Standard evaluation of 3D data sets is performed on the original source slices, either in sagittal or coronal direction, which requires a great amount of experience and knowledge of spatial anatomical relations in these directions, which may even be more problematic in congenital abnormalities.

Additionally new images can be reconstructed with multiplanar reformatting (MPR) which resamples the volume data (usually along a plane) and displays the result in a "new" separate image. In its simplest form, a single orthogonal section through the volume is displayed. More advanced implementations simultaneously show multiple orthogonal sections (coronal, sagittal, transversal), are able to display planes of arbitrary direction (oblique sectioning), or even along curved lines that can be interactively drawn.

Current workstation technology facilitates real-time display and manipulation of cut planes in volume data. The major drawback of MPR is that only a part of the dataset is used for a single image and only one image can be visualized at the same time so that tortuous and branching vessels are not depicted over their full length unless separate reconstruction's are made for every branch (Figure 4A). MIP is another algorithm which is widely used for both CT and MR angiography. MIP used for vascular imaging introduces several artifacts.[11-13] First, due to partial volume effects the value of the pixels at the edges of the vessel approximate the background noise which results in a reduction of vessel diameter and possible overestimation of stenosis. Second, because of the projectional nature of MIP three-dimensional ambiguous images are presented. This ambiguity can be perceived by displaying images from different view points for a dataset. After a rotation of 180° two seemingly mirrored images are obtained where the difference between anterior and posterior structures is lost (Figure 4B). This causes lack of depth in the images.

Volume rendering is an alternative 3D post-processing tool which is more computationally intensive and time consuming then MIP and MPR. However with present dedicated graphic workstations an image from any desired orientation can be computed within seconds. Volume rendering has a number of advantages over MIP. Because all the data in the 3D data set are used in the algorithm, the resulting images potentially contain more information than those created with MIP. The ability to simultaneously display both superficial and deep structures in an image creates "depth" in the image (Figure 4C). Volume rendering is often combined with depth and surface shading to give the view a very realistic sense of three-dimensionality which is an important issue in complex (congenital) aortic disease (Figure 5).

Volume rendered angiograms of MRA are much alike the images obtained with conventional catheter angiography (Figure 3) and may show vessel dimensions, intraluminal features, and overlapping vasculature. Despite its numerous advantages, volume rendering also has important limitations. The final image quality depends on the segmentations of the data that are fed to the rendering algorithm. Segmentation is the arbitrary user determined process by which voxels are classified as belonging to specific objects with distinct features, such as individual organs or tumor. The opacity settings for different tissues are arbitrary, and inappropriate use may introduce errors. Very opaque volume renderings may not clearly depict distinct edges, may hinder precise measurements, or may effect user interaction such as surgical simulation.

CONCLUSIONS

The combination of contrast enhanced 3D MRA with volume rendering as post processing technique gives unique information of complex 3D structures of the thoracic aorta. The technique is robust and may replace conventional angiography of the aorta and pulmonary artery.

REFERENCES

1. von Schulthess GK, Higashino SM, Higgins SS, et al. Coarctation of the aorta: MR imaging. Radiology. 1986;158:469-74.
2. Simpson IA, Chung KJ, Glass RF, et al. Cine magnetic resonance imaging for evaluation of anatomy and flow relations in infants and children with coarctation of the aorta. Circulation. 1988;78:142-8.
3. Nienaber CA, von Kodolitsch Y, Nicolas V, et al. The diagnosis of thoracic aortic dissection by noninvasive imaging procedures. N Engl J Med. 1993;328:1-9.
4. Prince MR, Narasimham DL, Stanley JC, et al. Breath-hold gadolinium-enhanced MR angiography of the abdominal aorta and its major branches. Radiology. 1995;197:785-92.

5. Ney D, Fishman E, Magid D. Volumetric rendering of computed tomography data: principles and techniques. Comput Graphics Applications. 1990;10:24-32.
6. Johnson PT, Heath DG, Kuszyk BS, et al. CT angiography with volume rendering: advantages and applications in splanchnic vascular imaging. Radiology. 1996;200:564-8.
7. Fishman EK, Magid D, Ney DR, et al. Three-dimensional imaging. Radiology. 1991;181:321-37.
8. Krinsky GA, Reuss PM, Lee VS, et al. Thoracic aorta: comparison of single-dose breath-hold and double-dose non-breath-hold gadolinium-enhanced three-dimensional MR angiography. Am J Roentgenol. 1999;173:145-50.
9. Wilman AH, Riederer SJ, King BF, et al. Fluoroscopically triggered contrast-enhanced three-dimensional MR angiography with elliptical centric view order: application to the renal arteries. Radiology. 1997;205:137-46.
10. Schoenberg SO, Bock M, Knopp MV, et al. Renal arteries: optimization of three-dimensional gadolinium-enhanced MR angiography with bolus-timing-independent fast multiphase acquisition in a single breath hold. Radiology. 1999;211:667-79.
11. Anderson CM, Saloner D, Tsuruda JS, et al. Artifacts in maximum-intensity-projection display of MR angiograms. Am J Roentgenol. 1990;154:623-9.
12. Marks MP, Napel S, Jordan JE, et al. Diagnosis of carotid artery disease: preliminary experience with maximum-intensity-projection spiral CT angiography. Am J Roentgenol. 1993;160:1267-71.
13. Heath DG, Soyer PA, Kuszyk BS, et al. Three-dimensional spiral CT during arterial portography: comparison of three rendering techniques. Radiographics. 1995;15:1001-11.

Part 5

Discussion, Conclusions and Summary

Chapter 20

General discussion and conclusions

R.J.M. van Geuns

INTRODUCTION

Cardiovascular disease remains the leading cause of death worldwide.[1-3] Conventional selective coronary angiography (CAG) is the gold standard for the assessment of the coronary artery anatomy.[4-6] However it is associated with significant radiation exposure and a small risk (1.7%) of serious complications.[7,8] Therefore non-invasive coronary angiography is highly desirable. In the development of non-invasive coronary angiography techniques the specifications of conventional selective coronary angiography have to be kept in mind. CAG is a projectional technique which covers the complex tortuous epicardial course of the coronary arteries with a high spatial resolution (up to 5 linepairs/mm, approximately 0.1 mm) and a high temporal resolution (up to 50 frames/sec). These specifications are almost unbeatable.

ACQUISITION STRATEGIES

In this thesis we studied two tomographic techniques which have the potential to visualize the coronary arteries non-invasively: electron beam computed tomography (EBT) and magnetic resonance imaging (MRI). Both do not achieve the acquisition speed possible with CAG, and therefore some trade off between resolution, coverage and image quality has to be made. With slower acquisition techniques cardiac motion related to respiration and cardiac contraction determine the major settings of all techniques. During cardiac contraction a acquisition window of less then 50 ms is highly desirable[9] but a window of approximately 100 ms during mid to late diastole, which does induce minimal image blur, must be accepted for current non-invasive techniques. Respiration related motion can be reduced with breath-hold or complicated respiratory gating techniques. In EBT breath-hold imaging is the only option and with a slice thickness of 1.5 mm a volume of 60 mm can be covered in approximately 30 seconds depending on the heartrate. MRI of the abdominal aorta and renal arteries using breath-hold contrast-enhanced magnetic resonance angiography, has been widely accepted for the diagnosis of atherosclerotic arterial disease. Magnetic resonance coronary angiography (MRCA) is more complex due to additional cardiac motion during the cardiac cycle. Using retrospective respiratory gated cardiac triggered MRCA we did not obtain sufficient image quality and diagnostic accuracy in a general patient population. This was mainly due to the large gating window necessary to obtain an acceptable acquisition time and the irregular breathing pattern frequently present in patients. With the introduction of faster MRI systems the possibil-

Tabel 1. Specification of non-invasive coronary angiography techniques compared with conventional invasive angiography.

	Invasive-CA	EBT-CA	MRCA-NAV	MRCA-BH (VCATS)
Resolution (mm)	0.1 x 0.1	0.7 x 0.7 x 1.5	1.9 x 1.25 x 2.0	1.9 x 1.25 x 1.5
Acquisition time	8 x 30 sec	2 x 30 sec	30 min	7 x 24 sec
Examination time	30 minutes	10 minutes	40 minutes	30 minutes
Acquisition window	Minimal 20 ms	100 ms	128 ms	110 ms
Contrast agent	Yes	Yes	No	No
Three-dimensional acquisition	Projectional	Stack of 2D	Real 3D	Real 3D

CA = coronary angiography, EBT = electron beam computed tomography, MRCA = magnetic resonance coronary angiography, NAV = Navigator free-breathing imaging, BH = Imaging during breath-holding.

ities of breath-hold MRCA are expected to increase, which may result in better image quality. For breath-hold MRCA we developed a new three-dimensional sequence which uses small targeted volumes to cover the major coronary artery branches is a few breath-holds. This sequence is known as VCATS (Volume Coronary Angiography using Targeted Scans). Table 1 compares the specifications of these non-invasive coronary angiography techniques with conventional selective coronary angiography.

In the first experiments the acquisition protocol of VCATS to visualize the major coronary artery branches proved to be robust in volunteers and patients (chapter 7). Additionally the length of the coronary arteries visualized was comparable to respiratory gated MRCA (chapter 8) while the image quality, and vessel delineation was even superior (chapter 9). These encouraging results prompted further studies to compare the capabilities of EBT and the two MRCA techniques for the detection of coronary artery stenosis. Table 2 compares the advantages and disadvantages of the two MRCA techniques with EBT.

IMAGE POSTPROCESSING

Both MRI and EBT may produce three-dimensional (3D) datasets while conventional CAG only provides projectional images. This may be an advantage in case of an eccentric atherosclerotic plaque which is a known problem in conventional CAG. To evaluate these 3D datasets using a two-dimensional surface as computer monitors, several postprocessing tools are available. During our research we experimented with multiplanar reconstruction (MPR), maximum intensity projection (MIP), surface rendering (SR) and volume rendering (VR) algorithms. Of these volume rendering has the largest potential, it is particular well suited to study complex three-dimensional structures as the aortic arch and coronary arteries. With volume rendering it is possible to produce both for MRI and EBT to produce nearly anatomical images (chapters 5 and 14). Additionally volume rendering includes the unique opportunity to provide a certain opacity to selected structures. The most striking example of this feature is the ability of make the blood in the coronary fully opaque and perform a fly-through of the coronary arteries which may look like a virtual angioscopy (chapter 16). It should be reminded that these images do not provide the same information about plaque composition as real coronary angioscopy. But they may be of value in patients with severe calcifications of the coronary artery wall or after coronary artery stent implantation where external visualization of the lumen is obstructed by high pixel intensities. Although with present computer systems volume ren-

Tabel 2. Advantages and disadvantages of different non-invasive coronary angiography techniques.

	EBT	MRCA-NAV	MRCA-BH (VCATS)
Advantages	· Fast	· Repeatable	· Repeatable
	· High in-plane resolution	· Covers whole volume of the heart	· Improved image quality
Disadvantages	· Sensitivity to arrhythmia	· Interference on ECG	· Interference on ECG
	· Calcification artefacts	· Claustrophobia	· Claustrophobia
	· Use of X-rays	· Low contrast	· Low contrast

EBT = electron beam computed tomography, MRCA = magnetic resonance coronary angiography, NAV = Navigator free-breathing imaging, BH = Imaging during breathholding.

dering it self may be a fast process, the selection of settings necessary to provide optimal images may be too cumbersome for routine clinical use. In studies comparing MRP, MIP and SR for MR and CT angiography of the renal arteries no additional benefits in diagnostic accuracy have been demonstrated.[10-12]

CLINICAL STUDIES

In the development of non-invasive coronary angiography many parameters to compare different techniques and sequences are used. Possibilities are vessel boundary sharpness, vessel diameter, vessel length visualized, signal-to-noise ratio, contrast-to-noise ratio and many others. However, these measurements should be considered as secondary endpoints. The final test is always the diagnostic accuracy of a technique in routine clinical practice. We performed these studies for the two different MRCA techniques and EBT and the results are listed in table 3.

Tabel 3. Non-invasive coronary angiography of the proximal and mid coronary segments

	EBT	MRCA-NAV	MRCA-BH (VCATS)
Visualization	81%	74%	69%
Sensitivity	77%	50%	68%
Specificity	94%	91%	97%
Accuracy	91%	84%	92%

From these results we concluded that breath-hold MRCA using VCATS is superior to retrospective respiratory gated MRCA. However EBT is superior to both with regard to the number of segments which could be visualized with an acceptable image quality (81% versus 69%, $p < 0.05$), while the diagnostic accuracy is comparable to VCATS (91% versus 92%, p = n.s).

FUTURE DEVELOPMENTS

Electron beam computed tomography

Since we performed our patient studies the inplane resolution of EBT has improved. The next generation EBT scanners will have a 50 ms acquisition window, which is an important improvement for the fast moving right coronary artery. The optimal delay time selected for cardiac triggering is still unresolved and may be different for the right coronary artery and the left anterior descending coronary artery. Repetitive imaging with different delay times, as in CAG, may be necessary to solve this issue. However the major limitation of EBT is that it only acquires a single slice in one heartbeat that limits the resolution in the z-axis or the coverage over the z-axis. A second contrast injection seems reasonable taking into account the present less toxic contrast media which may be used to increase the coverage. Implementation of a high-resolution double detector ring will be the awaited alternative technical development. In the same time the development of conventional CT is progressing fast. The fastest spiral CT-systems now in clinical use have a temporal resolution of 250 ms, which combined with a multi-slice detector and an ECG-gated reconstruction algorithm, are also able to produce images of the coronary arteries with acceptable image quality. In the future multislice spiral CT may proof to be the best alternative for non-invasive coronary angiography.

Magnetic resonance imaging

Possibilities to improve the signal-to-noise ratio

MRCA needs to be improved on several topics. Most importantly the resolution has to improve. For this the signal-to-noise ratio (SNR) is presently the limiting factor. MR contrast agents may be used for this purpose.

They boosted the implementation of MR angiography of the aorta and the peripheral vessels but did not yet provide the definite answer for MRCA. MRA of the aorta and the peripheral vessels does not require cardiac triggered scans, but uses continuous scanning. The tissues surrounding the vessels are then saturated while the blood remains unsaturated due to the presence of a strong T1 shortening contrast agent[13,14] which results in a high SNR and contrast-to-noise ratio (CNR). Standard, ECG triggered non-contrast enhanced MRCA sequences benefit from blood inflow effects between successive heartbeats making the signal amplitude of blood less dependent on the T1 relaxivity of blood and therefore SNR and CNR will improve less from present available MR contrast agents. Improvements have been envisioned only if the T1 of blood is reduced to values less then 50ms (or shorter T1s with the faster TRs possible in new MR gradient systems).[15] Gadolinium based agents used for contrast enhanced magnetic resonance angiography of the aorta and peripheral vessels are able to achieve this, but they are distributed initially within the intravascular compartment and diffuse rapidly throughout the extracellular (vascular plus interstitial) space. This limits their possible use in the long acquisition schemes frequently used in coronary imaging. Therefore intravascular MR contrast agents have been developed[16-19] but none is FDA approved yet. We demonstrated that with some presently available MR contrast agents SNR in MRCA can be improved using dedicated sequences. Alternative SNR ratio can be increased using higher field magnets (3T) in dedicated cardiac MRI systems. In the same time high gradients and short rise times may be used to reduce the acquisition time of MRCA which will result in less motion artifacts. Phase array body coils to improve SNR are now standard in cardiac imaging. Dedicated MRI systems will incorporate the spatial localization of coil reception pattern in the reconstruction algorithms as SMASH or SENSE to speed up the acquisition. Most of these newer MRI scanner are shorter and have a larger bore, which will reduce claustrofobia effects in patients.

Possibilities to improve cardiac triggering

The quality of the ECG is hindered by interference of the gradient systems so that precise cardiac triggering is difficult. One solution provided by some manufacturers is an ECG system in which one of the limb leads can be selected at will that produces the best ECG tracing. Nevertheless, this does not guarantee complete elimination of the interference created by the gradient switching and newly developed optical ECG devices have started to appear on the market 20. These devices amplify the ECG signal close to the reception electrodes and send the analog signal via fiber optics to the patient-monitoring unit. These devices are robust even with EPI acquisitions [21] and will be available with future cardiac-dedicated MRI units.

Possibilities to reduce respiratory motion artifacts

In our studies respiratory related coronary motion was better reduced with breath-hold imaging compared to retrospective respiratory gating. Prospective respiratory triggered techniques may also be an improvement. These may be combined with a tracking algorithm to shift the imaging volume with the craniocaudal motion of the heart during breathing. More sophisticated sequences in which the central portion of k-space is collected with a small respiratory gating window (e. g., ± 1 mm) while the data for the outer portions of k-space are scanned with increasingly coarser gating windows (e. g., ± 3, ± 5, and ± 7 mm) may even further reduces respiratory motion artifacts. It should be reminded that the craniocaudal

motion of the heart during breathing is different for the aortic root region and the apex of the heart and also varies for each patient. And in addition to the craniocaudal cardiac motion during respiration there is also significant anteriorposterior and left-right motion. Although these movements are small, they and the craniocaudal motion problems mentioned before, will limit the visualization of submillimeter details with respiratory gated MRCA.

THE ROLE OF MRCA IN CARDIOVASCULAR DISEASE

Although the results of MRCA are presently insufficient for routine clinical use, MRI of the coronary arteries may have some advantages over conventional selective coronary angiography and EBT or CT. In CAG little information regarding coronary artery blood flow is obtained and no functional significance of coronary lesions is obtained. Therefore intracoronary echo-doppler flow and pressure measurements have been developed. However, these are invasive and expensive. Velocity encoded phased-contrast MRI (PC-MRI) can been used to measure flow in a variety of vessels, including the coronary arteries. Studies comparing PC-MRI and intracoronary US measurements showed a good correlation between both techniques.[22] Clinically it has been used for the detection of restenosis after percutanous coronary intervention and coronary artery bypass graft patency.[23,24]

MRCA combined with additional MRI techniques may provide a full non-invasive cardiac evaluation. Wall motion and systolic wall thickening are now standard techniques in cardiac MRI examinations. Dobutamine Stress-Cine MRI has shown to be highly accurate to detect reliable myocardial ischaemia. Alternatively functional evaluation of coronary artery lesions may be performed with MR perfusion imaging which is now in the clinical phase evaluation. The most exciting new possibility of MRI is the ability to study non-invasively the components of the arterial wall. The composition of the atherosclerotic plaque, rather than the degree of vessel stenosis, is known to modulate the risk of rupture and subsequent intravascular thrombus. Superficial vessels such as the carotid and femoral arteries, using externally placed coils were studied, and to overcome the SNR barrier for deeper arteries intravascular catheter MR probes were used.[25] It appeared that it was possible to accurately characterize and quantify atherosclerotic lesions using T1-, proton density, and T2- weighted imaging sequences.[26-30] This technique may become a major tool to study more closely atherosclerosis.

Consequently MRI will be a significant tool in the evaluation of the full cardiovascular status of patients with atherosclerotic disease. This will include not only MRCA and determination of functional parameters as myocardial perfusion and systolic wall thickening but also angiography of the aorta, carotid and peripheral arteries.

CONCLUSIONS

MRI is a general accepted imaging technique to evaluate a wide range of diseases of the central and peripheral vasculature and is presently replacing conventional contrast angiography. Non-invasive coronary angiography is much more complex due to cardiac motion during respiration and the cardiac contraction cycles. Both EBT and MRI are presently insufficiently reliable to replace conventional selective coronary angiography but many new improvements are being developed. Eventually the technique may evolve into a reliable non-invasive coronary angiography technique.

REFERENCES

1. Cardiovascular disease statistics. In:: American Heart Association; 1998.
2. Hart en Vaatziekten in Nederland. Cijfers over ziekte en sterfte. In:: Nederlandse

Hartstichting; 1998.
3. Stone NJ. The clinical and economic significance of atherosclerosis. Am J Med. 1996;101:4A6S-9S.
4. Sones FJ, Shirey E. Cine coronary angiography. Mod Concepts Cardiovasc Dis. 1962;31:735-738.
5. Judkins MP. Selective coronary arteriography. I. A percutaneous transfemoral technic. Radiology. 1967;89:815-24.
6. Ross JR, Brandenburg RO, Dinsmore RE. Guidelines for coronary angiography. A report of the American College of Cardiology/American Heart Association Task Force on Assessment of Diagnostic and Therapeutic Cardiovascular Procedures (Subcommittee on Coronary Angiography). Circulation. 1987;76:963A-977A.
7. Johnson LW, Krone R. Cardiac catheterization 1991: a report of the Registry of the Society for Cardiac Angiography and Interventions (SCA&I). Cathet Cardiovasc Diagn. 1993;28:219-20.
8. Krone RJ, Johnson L, Noto T. Five year trends in cardiac catheterization: a report from the Registry of the Society for Cardiac Angiography and Interventions. Cathet Cardiovasc Diagn. 1996;39:31-5.
9. Hofman MB, van Rossum AC, Sprenger M, et al. Assessment of flow in the right human coronary artery by magnetic resonance phase contrast velocity measurement: effects of cardiac and respiratory motion. Magn Reson Med. 1996;35:521-31.
10. Rubin GD, Dake MD, Napel S, et al. Spiral CT of renal artery stenosis: comparison of three-dimensional rendering techniques. Radiology. 1994;190:181-9.
11. Johnson PT, Halpern EJ, Kuszyk BS, et al. Renal artery stenosis: CT angiography--comparison of real-time volume-rendering and maximum intensity projection algorithms. Radiology. 1999;211:337-43.
12. Hany TF, Schmidt M, Davis CP, et al. Diagnostic impact of four postprocessing techniques in evaluating contrast-enhanced three-dimensional MR angiography. AJR Am J Roentgenol. 1998;170:907-12.
13. Prince MR, Narasimham DL, Stanley JC, et al. Breath-hold gadolinium-enhanced MR angiography of the abdominal aorta and its major branches. Radiology. 1995;197:785-92.
14. Prince MR, Narasimham DL, Jacoby WT, et al. Three-dimensional gadolinium-enhanced MR angiography of the thoracic aorta. AJR Am J Roentgenol. 1996;166:1387-97.
15. Johansson LO, Fischer SE, Lorenz CH. Benefit of T1 reduction for magnetic resonance coronary angiography: a numerical simulation and phantom study. J Magn Reson Imaging. 1999;9:552-6.
16. Anzai Y, Prince MR, Chenevert TL, et al. MR angiography with an ultrasmall superparamagnetic iron oxide blood pool agent. J Magn Reson Imaging. 1997;7:209-14.
17. Lauffer RB, Parmelee DJ, Dunham SU, et al. MS-325: albumin-targeted contrast agent for MR angiography. Radiology. 1998;207:529-38.
18. Dong Q, Hurst DR, Weinmann HJ, et al. Magnetic resonance angiography with gadomer-17. An animal study original investigation. Invest Radiol. 1998;33:699-708.
19. Wagenseil JE, Johansson LOM, Lorenz CH. Characterization of T1 Relazation and Blood-Myocardial Contrast Enhancement of NC100150 Injection in Cardiac MRI. In: Proceedings of the Seventh Meeting of the International Society for Magnetic Resonance in Medicine. Philadelphia; 1999:1176.
20. Felblinger J, Lehmann C, Boesch C. Electrocardiogram acquisition during MR examinations for patient monitoring and sequence triggering. Magn Reson Med. 1994;32:523-9.
21. Felblinger J, Debatin JF, Boesch C, et al. Synchronization device for electrocardiography-gated echo-planar imaging. Radiology. 1995;197:311-3.
22. Hundley WG, Lange RA, Clarke GD, et al. Assessment of coronary arterial flow and flow reserve in humans with magnetic resonance imaging. Circulation. 1996;93:1502-8.
23. Galjee MA, van Rossum AC, Doesburg T, et al. Value of magnetic resonance imaging in assessing patency and function of coronary artery bypass grafts. An angiographically controlled study. Circulation. 1996;93:660-6.
24. Hundley WG, Hillis LD, Hamilton CA, et al. Assessment of coronary arterial restenosis

with phase-contrast magnetic resonance imaging measurements of coronary flow reserve. Circulation. 2000;101:2375-81.
25. Quick HH, Ladd ME, Zimmermann-Paul GG, et al. Single-loop coil concepts for intravascular magnetic resonance imaging. Magn Reson Med. 1999;41:751-8.
26. Worthley SG, Helft G, Fuster V, et al. Noninvasive In Vivo Magnetic Resonance Imaging of Experimental Coronary Artery Lesions in a Porcine Model. Circulation. 2000;101:2956-2961.
27. Worthley SG, Helft G, Fayad ZA, et al. Magnetic Resonance Imaging and Asymptomatic Aortic Dissection. Circulation. 2000;101:2771-2961.
28. Fayad ZA, Nahar T, Fallon JT, et al. In Vivo Magnetic Resonance Evaluation of Atherosclerotic Plaques in the Human Thoracic Aorta : A Comparison With Transesophageal Echocardiography. Circulation. 2000;101:2503-2961.
29. Worthley SG, Helft G, Fuster V, et al. Serial In Vivo MRI Documents Arterial Remodeling in Experimental Atherosclerosis. Circulation. 2000;101:586-2961.
30. Fayad ZA, Fallon JT, Shinnar M, et al. Noninvasive In Vivo High-Resolution Magnetic Resonance Imaging of Atherosclerotic Lesions in Genetically Engineered Mice. Circulation. 1998;98:1541-2961.

Chapter 21

Summary

This thesis investigates magnetic resonance imaging (MRI) and electron beam computed tomography (EBT) as two non-invasive alternatives for conventional angiography with a special focus on the coronary arteries.

The first part of this thesis provides an overview of the technical principles of MRI for non-invasive coronary angiography. Chapter one and two provide an introduction for cardiologist to the principles of magnetic resonance imaging and the special needs for magnetic resonance coronary angiography (MRCA). A technical paper (Chapter 3) which describes the difficulties of MRCA with more detail follows this. Chapter four provides a practical approach to obtain the different imaging planes necessary to study or evaluate the coronary arteries in non-invasive imaging. Chapter five provides an overview of the coronary artery anatomy in three-dimensional imaging by MRI. Chapter six evaluates standard cardiac triggered respiratory gated MRCA with for the detection of coronary artery disease. Chapter seven introduces a new strategy for MRCA using targeted volumes along the anatomical routes of the coronary arteries to optimize the resolution and the imaged volume within a 25 seconds breath-hold acquisition period. This strategy will be referred to as VCATS for volume coronary angiography with targeted scans. Chapter eight provides a first evaluation of MRCA with VCATS in patients. The robust of VCATS is confirmed and the visualized vessel length is sufficient for clinical use. To compare VCATS with earlier MRCA techniques chapter nine studies quantitatively image sharpness and vessel diameter in VCATS and respiratory gated MRCA. It concludes that in unselected patients breath-hold MRCA provides sharper vessel boundaries with a more realistic vessel diameter. In the next two chapters the possible clinical application of VCATS are explored. In chapter 10 the feasibility to detect coronary arteries stenoses is explored. In this study the obtained sensitivity and specificity is insufficient to warrant the use of this technique in a clinical setting. Nonetheless chapter 11 demonstrates that VCATS has a very high diagnostic accuracy to detect the patency of sequential venous coronary artery bypass grafts. The benefits of MR contrast agents to improve MRCA are evaluated in the last chapter of this part.

The second part of this thesis describes the principles of non-invasive coronary angiography with electron beam computed tomography in chapter 13. In chapter 14 and 15 the clinical results of EBT for the diagnosis of coronary artery disease are reported. Here it is shown that EBT is able to visualize > 70% of the major coronary arteries with a high image quality. Within these branches significant coronary arteries stenoses can be detected with a high degree of diagnostic accuracy. The use of the latest postprocessing tools to perform a virtual coronary angioscopy of the coronary arteries using data from EBT coronary angiography is illustrated in chapter 16.

The third part (chapter 17) gives a direct comparison between MRI and EBT as tools for detecting of significant coronary artery stenosis in patient referred for convention coronary angiography. It is concluded that EBT is presently slightly better than MRI to adequately visualize the proximal and mid coronary artery segments and detect stenoses in , these segments, but distal segments cannot be visualized by either technique.

Part 4 is a supplement on non-ECG-triggered magnetic resonance angiography of the thoracic arteries. Chapter 18 reviews the present MRI protocols for the thoracic arteries and

describes the advantages of breath-hold contrast enhanced magnetic resonance angiography. The value of contrast enhanced magnetic resonance angiography for the diagnosis of congenital and acquired disease of the aorta and pulmonary artery disease is studied in Chapter 19.

The last part of this thesis contains a general discussion on the present status of both techniques and their possible future developments for non-invasive angiography.

Samenvatting

Dit proefschrift behandelt magnetische resonantie beeldvorming (magnetic resonance imaging [MRI]) en elektronen bundel computer tomografie (EBT) als twee verschillende niet-invasieve alternatieven voor conventionele angiografie, met de nadruk op de afbeelding van de coronaire arteriën.

Het eerste deel van dit proefschrift geeft een overzicht van de technische principes van MRI voor niet-invasieve coronaire angiografie. Hoofdstukken 1 en 2 bevatten een inleiding tot de principes van magnetische resonantie coronaire angiografie (MRCA). Hierop volgt een technisch hoofdstuk (hoofdstuk 3) dat de problemen van MRCA meer gedetailleerd beschrijft. Aansluitend geeft hoofdstuk 4 een praktische werkwijze om de verschillende afbeeldingsvlakken te verkrijgen die nodig zijn om de coronaire arteriën niet-invasief te onderzoeken. Hoofdstuk 5 geeft een overzicht van de anatomie van de coronaire arteriën in drie-dimensionale afbeeldingen verkregen met MRI. Hoofdstuk 6 geeft een evaluatie van ECG-gestuurde en ademhaling-volgende MRCA voor het opsporen van coronaire arterie ziekten. Hoofdstuk 7 introduceert een nieuwe strategie voor MRCA met behulp van kleine doelgerichte volumes langs anatomische vlakken met data acquisities gedurende een adem-stilstand van 25 seconden. Deze strategie wordt aangeduid met VCATS (Volume Coronary Angiography with Targeted Scans). Hoofdstuk 8 geeft een eerste evaluatie van VCATS bij patiënten. De praktische uitvoerbaarheid van dit principe werd bevestigd en het afgebeeld gedeelte van de coronaire arteriën was van voldoende lengte voor klinisch gebruik. Om VCATS te vergelijken met eerder gebruikte MRCA technieken wordt in hoofdstuk 9 VCATS kwantitatief vergeleken met een ademhaling-volgende techniek voor afbeeldingsscherpte en bloedvatdiameter. Uit dit onderzoek bleek dat bij ongeselecteerde patiënten MRCA tijdens ademstilstand scherpere bloedvaten en een meer realistische bloedvatdiameter oplevert dan ademhaling-volgende technieken. In de volgende twee hoofdstukken worden twee mogelijke klinische toepassingen van VCATS onderzocht. In hoofdstuk 10 wordt de mogelijkheid om vernauwingen in de coronaire arteriën op te sporen geëvalueerd. Uit deze studie bleek dat de sensitiviteit en specificiteit onvoldoende waren om deze techniek in de praktijk toe te passen. Niettemin kan in hoofdstuk 11 worden aangetoond dat VCATS een zeer hoge sensitiviteit en specificiteit heeft voor het aantonen van de doorgankelijkheid van aorta-coronaire omleidingen. De mogelijkheden van MR-contrastmiddelen om MRCA te verbeteren worden onderzocht in het laatste hoofdstuk van dit gedeelte.

In het tweede gedeelte van dit proefschrift worden de principes van niet-invasieve coronaire angiografie met behulp van EBT beschreven in hoofdstuk 13. In de hoofdstukken 14 en 15 wordt gerapporteerd over twee klinische studies om met EBT de diagnose van coronaire arterie ziekten op te sporen. Hierin werd aangetoond dat EBT in staat is meer dan 70 % van de belangrijkste coronaire arteriën af te beelden met een uitstekende beeldkwaliteit. In deze vaten konden significante vernauwingen met een hoge graad van zekerheid worden opgespoord. Het gebruik van de nieuwste beeldbewerking computerprogramma's om een virtuele coronaire angioscopie te verrichten met behulp van data van EBT coronaire angiografie wordt in hoofdstuk 16 beschreven.

Het derde gedeelte (hoofdstuk 17) is een vergelijking tussen MRI en EBT als niet-invasieve technieken voor het opsporen van significante vernauwingen in de coronaire arteriën van patiënten, verwezen voor conventionele coronaire angiografie. Er kan worden geconcludeerd

dat EBT op dit moment enigszins beter is dan MRI voor het adequaat afbeelden en het opsporen van vernauwingen in de proximale en midden segmenten van de coronaire arteriën. Helaas konden distale segmenten door beide technieken onvoldoende worden afgebeeld.

Het vierde gedeelte van dit proefschrift betreft een supplement over niet-ECG-gestuurde magnetische resonantie angiografie van de thoracale arteriën. Hoofdstuk 18 geeft een overzicht van de verschillende MRI protocollen die thans in gebruik zijn om de thoracale arteriën af te beelden en beschrijft de voordelen van MR angiografie protocollen waarbij contrastmiddel wordt gebruikt. De waarde van MR angiografie waarbij contrastmiddel wordt gebruikt voor de diagnose van congenitale en verworven ziekten van de aorta en pulmonaal arteriën is het onderwerp van hoofdstuk 19.

Het laatste gedeelte van dit proefschrift bevat een algehele discussie over de huidige stand van zaken van beide technieken en de mogelijke toekomstige ontwikkelingen van niet-invasieve angiografie.

Dankwoord

Dit proefschrift zou niet tot stand zijn gekomen zonder de steun van velen. In de eerste plaats wil ik alle patiënten bedanken die zich belangeloos hebben "opgeofferd" om vaak lang in de MRI scanner te liggen. Op de tweede plaats wil ik alle cardiologen, arts-assistenten, secretariële stafleden, technici en verpleegkundigen van het catheterisatie laboratorium van het Thoraxcentrum en het ZuiderZiekenhuis bedanken voor ondersteuning van de voor dit proefschrift benodigde studies.

De volgende mensen wil ik persoonlijk noemen.
Allereerst wil ik mijn promotor, Prof. dr. P.W. Serruys, bedanken voor de mogelijkheden en vrijheid die hij mij geboden heeft in het Thoraxcentrum. Mijn co-promotor dr P.J. de Feyter. Beste Pim, jij hebt ervoor gezorgd dat ik drie jaar achter elkaar volledig aan dit onderzoek heb kunnen werken. Tevens was je de stuwende kracht achter alle artikelen, waarbij je onvermoeibaar iedere nieuwe versie hebt gelezen en becommentarieerd. Dit alles in een fantastisch vriendschappelijke sfeer. Dr. M. Oudkerk, mijn tweede co-promotor. Beste Matthijs, jou wil ik bedanken voor de mogelijkheden die je mij hebt geboden met de beste technische apparatuur te werken die nodig was voor dit onderzoek. Hierbij moet met name gedacht worden aan de energie die nodig was om alles goed met elkaar te laten communiceren in een computernetwerk.
Prof. dr. L. Jordaens, Prof. dr. E.E. van der Wall en Prof. dr. A.C. van Rossum wil ik bedanken voor het kritisch doorlezen van het manuscript en de gegeven opmerkingen, waarover wij nog wel vaker zullen discussiëren.
Piotr Wielopolski, mijn paranimf, wil ik speciaal bedanken. Zonder jou zou ik nooit met MRI een coronair gezien hebben. Ik zal nog lang terugdenken aan de vele uren die wij hebben zitten praten over jouw ideeën om MR coronaire angiografie op een totaal andere manier aan te pakken. Nog steeds kan ik jou in deze niet volledig volgen, en ben je vele anderen voor.
Peter van Ooijen is een van de andere mensen die hier een speciale vermelding verdient. Eerst heb je mij moeten uitleggen hoe beeldbewerkingsprogramma's werken, vervolgens heb je mij nog vele malen moeten helpen als ik een van de computers had laten vastlopen. Maar uiteindelijk zijn de fantastische plaatjes die hiervan het gevolg waren vaak de basis geweest voor acceptatie van een artikel. Veel dank ben ik ook aan Benno Rensing verschuldigd. Met jouw ervaring in wetenschappelijk onderzoek en het publiceren daarvan hebben we in korte tijd snel onze eerste ervaringen met EBT kunnen publiceren.
Marianne Eicholtz wil ik bedanken voor haar nuttige adviezen, de praktische hulp en ondersteuning bij het afhandelen van al die formele administratieve zaken.
Ook wil ik de medewerkers van de afdeling Radiologie van de Daniel den Hoedkliniek bedanken voor de gelegenheid en ondersteuning die ze me boden om naast (en tussendoor) de oncologische patiënten ook de "Harten" te doen. Twee zal ik er met naam noemen: Bart Schraa en Arie Munne, specialisten op het gebied van respectievelijk MRI en CT. Zonder deze twee schakels in de praktijk zou ik geen wetenschappelijk onderzoek hebben kunnen doen. In de Daniel den Hoed Kliniek wil ik nog apart Hein de Bruin bedanken voor zijn bijzondere interesse voor cardiale MRI en de snelle revisie van mijn manuscripten.
Buiten het ziekenhuis wil ik Robert Jan Dubbeldam, mijn andere paranimf, bedanken. Al sinds onze eerste dagen op Njord zijn wij bevriend en nog steeds vinden we tijd voor onze gezamenlijke hobby's. Als getuige bij mijn huwelijk en nu als paranimf heb ik een zware last op je schouders gelegd, maar die schouders bewijzen al jaren dat ze dat aankunnen.

Natuurlijk wil ik ook mijn ouders bedanken. Mede dankzij hun steun en meeleven heb ik kunnen studeren en is dit proefschrift tot stand gekomen.

Tenslotte gaat mijn grootste waardering uit naar mijn gezin. Dit dankwoord zou niet compleet zijn zonder Madeleine, Dorine en Emma te noemen. Ik hoop dat we nu meer tijd krijgen om met zijn allen bij elkaar te zijn.

Publications

1. Magnetic resonance imaging of the coronary arteries. R.J.M. van Geuns, P. Wielopolski, H. de Bruin, M. Oudkerk, P.M.A. van Ooijen, P.J. de Feyter
Cardiologie 1997;4:372-377.

2. Non-invasive coronary angiography using Electron Beam Tomography and Magnetic Resonance Imaging. A case report. B. Rensing, R.J. van Geuns, P. Wielopolski, M. Oudkerk, P. de Feyter
The Thoraxcentre Journal 1997;9/4:32-33.

3. Magnetic Resonance Imaging of the Coronary Arteries. R.J.M. van Geuns, P.A. Wielopolski, H.G. de Bruin, P.M.A van Ooijen, P.J. de Feyter, M.. Oudkerk
Imaging Decisions MRI 1997;(2):8-14.

4. Noninvasive coronary angiography using electron beam computed tomography. B.J.W.M. Rensing, R.J.M. van Geuns, P.M.A. van Ooijen, F. Bongaerts, M. Oudkerk, P.J. de Feyter
Cardiologie 1997;4:440-446.

5. Heart and Coronary Arteries. P.A. Wielopolski, R.J.M. van Geuns, P.J. de Feyter, M. Oudkerk.
Eur Radiol. 1998;(8):873-885.

6. VCATS, Magnetic Resonance Coronary Angiography with Breath-hold Volume Targeted Scans. P.A. Wielopolski, R.J.M. van Geuns, P.J. de Feyter, M.. Oudkerk.
Radiology 1998;209:209-219.

7. Breath-hold 3D MR coronary angiography (MRCA). P. Wielopolski, R. van Geuns, P. de Feyter, H. de Bruin, M.. Oudkerk.
In: High-power gradient MR-imaging. Advances in MRI II; Oudkerk M, Edelman R, eds. Berlin: Blackwell Wissenschaft, 1997:46-53.

8. Intravenous coronary angiography by electron beam computed tomography: a clinical evaluation. B.J. Rensing, R.J. van van Geuns, A. Bongaerts, P. van Ooijen, M Oudkerk, P.J de Feyter.
Circulation 1998;98:2509-12.

9. Magnetic resonance and electron beam tomography coronary angiography. P.J. de Feyter, R.J. van Geuns, P. van Ooijen, F. Bongaerts, B. Rensing, H. de Bruin, P. Wielopolski, M. Oudkerk.
In: What's New in Cardiovascular Imaging? J.H.C. Reiber and E.E. van der Wall. Kluwer, Dordrecht, The Netherlands. 1998:411-418.

10. Kernspintomografie van de coronaire arteriën / Imagerie des artères coronaires par résonance magnétique. R.J.M. van Geuns, P. Wielopolski, H. de Bruin, M. Oudkerk, P.M.A. van Ooijen, P.J. de Feyter.
Tijdschr Cardiol 1998;10(4):42-48 / J Cardiol 1998;10(4):42-48.

11. Images in Cardiology: Atrial Myxoma. W.R.M. Hermans, A. Dall'Agata, R.J. van Geuns, C. Breburda, J.R.T.C. Roelandt.
The Thoraxcentre Journal 1998:10(3);24.

12. Basic principles of magnetic resonance imaging. R.J.M. van Geuns, P.A. Wielopolski, H.G. de Bruin, B.J.W.M. Rensing, P.M.A. van Ooijen, M. Hulshoff, M. Oudkerk, P.J. de Feyter.
Progress in Cardiovascular Disease 1999,42(2):149-156.

13. Magnetic resonance Imaging of the Coronary Arteries: Techniques and results. R.J.M. van Geuns, P.A. Wielopolski, H.G. de Bruin, B.J.W.M. Rensing, P.M.A. van Ooijen, M. Hulshoff, M. Oudkerk, P.J. de Feyter.
Progress in Cardiovascular Disease 1999,42(2):156-166.

14. Magnetic resonance Imaging of the Coronary Arteries: Imaging planes and resulting anatomy in two-dimensional imaging. R.J.M. van Geuns, P.A. Wielopolski, H.G. de Bruin, B.J.W.M. Rensing, P.M.A. van Ooijen, M. Hulshoff, M. Oudkerk, P.J. de Feyter.
Coronary Artery Disease, 1999;10(7):525-31.

15. Magnetic Resonance Imaging of the Coronary Arteries: Anatomy of coronary arteries and veins in three-dimensional imaging. R.J.M. van Geuns, P.A. Wielopolski, H.G. de Bruin, B.J.W.M.. Rensing, P.M.A. van Ooijen, M. Hulshoff, M. Oudkerk, P.J. de Feyter.
Coronary Artery Disease 1999, 10:261-267.

16. MRI of the coronary arteries: clinical results from three-dimensional evaluation of a respiratory gated technique. R.J.M. van Geuns, H.G. de Bruin, B.J.W.M. Rensing, P.A. Wielopolski, M.D. Hulshoff, P.M.A. van Ooijen, M.. Oudkerk, P.J. de Feyter.
Heart 1999,82:515-519.

17. Intravenous coronary angiography using electron beam computed tomography. B.J. Rensing, A.H.H. Bongaerts, R.J. van Geuns, P. van Ooijen, M. Oudkerk, P.J de Feyter.
Progress in Cardiovascular disease 1999,42:139-148.

18. In vivo assessment of three-dimensional coronary anatomy using Electron Beam Computed Tomography after intravenous contrast administration. B.J. Rensing, A.H.H. Bongaerts, R.J. van Geuns, P. van Ooijen, M. Oudkerk, P.J. de Feyter.
Heart 1999;82:523-525.

19. MR Coronary Angiography with breath-hold targeted volumes: Preliminary clinical results. R.J.M. van Geuns, P.A. Wielopolski, H.G. de Bruin, B.J.W.M. Rensing, M. Hulshoff, P.M.A. van Ooijen, M. Oudkerk, P.J. de Feyter.
Radiology 2000;217:270-277.

20. Stentocarditis. B.J. Rensing, R.J. van Geuns, M. Janssen, M. Oudkerk, P.J. de Feyter.
Circulation 2000;101:e188.

21. Aberrant Right Subclavian Artery Mimics Aortic Dissection. M. Janssen, C.S. Breburda, R.J.M. van Geuns, W.R.M. Hermans, P. Klootwijk, J.A. Bekkers, J.R.T.C. Roelandt. *Circulation 2000 101: 459-460.*

22. Coronary Artery Fly-Through Using Electron Beam Computed Tomography. P.M.A. van Ooijen, M. Oudkerk, R.J.M. van Geuns, B.J. Rensing, and P.J. de Feyter *Circulation 2000;102:e6-e10.*

23. Non-invasive coronary angiography. R.J.M. van Geuns, P.J. de Feyter, M. Oudkerk. *Ned Ver voor Radiodiagnostiek, Edurad 2000.*

24. Magnetic resonance angiography of a pulmonary artery stenosis late after cardiac surgery. R.J.M. van Geuns, M. Oudkerk, P.J. de Feyter, S.E. Spitaels *Circulation 2000;102:e71-e72.*

25. Coronary arteries. P.A. Wielopolski , R.J.M. van Geuns , P.J. de Feyter, M. Oudkerk. *Eur Radiology 2000;10:12-35.*

Curriculum Vitae

Robert-Jan Matthijs van Geuns was born on May 14, 1966 in Son en Breugel, The Netherlands. He finished secondary school in 1984 at the "Gemeentelijke Scholengemeenschap Woensel" in Eindhoven. In the same year, he started his medical training at the University of Leiden. After graduation, he fulfilled his military service from April 1992 until July 1993 in the Royal Dutch Navy. Subsequently he worked as a house-officer at the department of Cardiothoracic Surgery of the University Hospital Leiden (Prof. Dr. H.A. Huysmans) and the department of cardiology, Thoraxcenter of the Erasmus University Rotterdam.

The work resulting in this thesis was started in 1996 as collaboration between the Catheterization Laboratory (Dr. P. de Feyter and Prof. dr. P.W. Serruys) of the Thoraxcenter and the department of Radiology (Dr. M. Oudkerk), Daniel den Hoedkliniek, both at the Erasmus University Rotterdam.

Currently, he fulfills residency in Internal Medicine in the Albert Schweitzer Ziekenhuis in Dordrecht, (Dr J. van der Meulen) part of his training as a cardiologist at the Thoraxcenter (Prof. dr. J.RT.C. Roelandt) of the Erasmus University Rotterdam.